

# Polymerisations in Supercritical Carbon Dioxide



The University of  
**Nottingham**

UNITED KINGDOM • CHINA • MALAYSIA

## Simon Bassett

Thesis submitted to the University of Nottingham for the degree of

Doctor of Philosophy, July 2015

### **Disclaimer**

All work presented in this Thesis is the original work of the author, with the exception of results referenced to other sources. It has not been submitted as part of any other degree or professional qualification.

Signed:.....

Date: .....

Simon Peter Bassett

## Acknowledgements

Firstly I would like to thank Professor Steve Howdle for giving me the opportunity to undertake my PhD in Nottingham, and for his help and support throughout. I must also thank Dr Derek Irvine for his co-supervision and advice throughout the duration of my PhD. Without Helen Carson I'm sure our group would fall apart so a special thank you must be saved for her!

I'm indebted to the guys in the workshop, in particular Mark Guyler, Martin Dellar, Pete Fields, Rich Wilson, and Dave Litchfield for their technical help and keeping all the equipment running and coming up with solutions to what seemed like an endless stream of problems!

Thank you to all of our collaborators; without whom this work would not have been possible. Wim Bras, Daniel Hermida-Merino, Guiseppe Portable and everyone from DUBBLE at the ESRF. Also the team from the University of Bath: Matthew Davidson, Matthew Jones, Tom Forder, and Paul McKeown.

There have been a vast number of other postdocs, PhD students, undergraduates and visitors who have worked in and around B10 during my time in Nottingham, all of which I'm grateful to for making my time so enjoyable! In particular Jaouad El harfi, Jianing Li, and James Jennings for their scientific advice, and the MSci students who have contributed results to this work; Lydika David, Anna Douglas and Katie Reynolds

I would like to thank my family for their help and support over the last 26 years. Without them I wouldn't be where I am today. Last but not least, I have to thank Han for her love and support and for putting up with me, especially during this writing up period, I couldn't have done any of this without her.

## Overview

This Thesis describes the synthesis of polymers utilising supercritical carbon dioxide as a reaction medium, and the development of a new high pressure cell for measuring small angle x-ray scattering *in situ*.

Chapter 2 details the high pressure equipment used for this body of work, as well as the analytical techniques employed. This includes equipment details for a new high pressure cell designed for measuring small angle x-ray scattering of polymers *in situ*.

Chapter 3 describes the homopolymerisation of both methyl methacrylate and styrene in a supercritical carbon dioxide expanded phase system. Effects of molecular weight and viscosity on the final reaction product are probed in order to ascertain the most suitable types of polymers to be synthesised by this method. This is then extended to create low molecular weight block copolymers in the absence of any volatile organic solvents, with comparable properties to those produced by conventional methods.

The development of the high pressure cell for measuring small angle x-ray scattering of block copolymers synthesised in a supercritical carbon dioxide dispersion polymerisation *in situ* is described in Chapter 4. Initial investigations showed problems with the synthesis in this new vessel, with different products obtained compared to a conventional autoclave. However, data is presented to display the suitability of certain aspects of the design and that scattering patterns can be acquire *in situ* during a polymerisation. Details of a second modified design are presented, with construction currently in progress.

Finally, a green synthetic route to producing renewable, biodegradable and biocompatible polymers is presented in Chapter 5. By using supercritical carbon dioxide to lower the melting temperatures of the monomers, polymerisations usually conducted at temperatures in excess of 130 °C were successfully conducted at 80 °C. Through the use of a novel zirconium catalyst the tacticity of poly(lactic acid) was controlled, opening up a route to functional materials.

## Abbreviations

% m/v	mass to volume percentage
% v/v	volume to volume percentage
(k)Da	(kilo) Daltons
$[M]_0$	concentration of monomer at time zero
$[M]_t$	concentration of monomer at time t
AIBN	2,2-azobis(2-methylpropionitrile)
ATRP	atom transfer radical polymerisation
BHA	butylated hydroxy anisole
BHT	butylated hydroxy toluene
2,2'-BPY	2,2'-bipyridine
BzMA	benzyl methacrylate
CCTP	catalytic chain transfer polymerisation
CO <sub>2</sub>	carbon dioxide
COPhBF	bis-[(difluoroboryl)diphenylglyoximato] cobalt (II)
CPBD	2-Cyanopropyl Benzodithioate
CPDT	2-Cyano-2-propyl dodecyl trithiocarbonate
CRP	controlled radical polymerisation
CTA	chain transfer agent
CXL	carbon dioxide expanded liquid
Đ	dispersity
DBU	1,8-diazabicyclo[5.4.0]undec-7-ene
DCM	Dichloromethane
DCP	Dicumyl Peroxide
DDMAT	2-(Dodecylthiocarbonothioylthio)-2-methylpropionic acid
DLA	D-lactide
DLLA	rac-lactide
DMA	N,N-dimethyl acrylamide
DMA	dynamic mechanical analysis
DMAEMA	N,N-dimethylaminoethyl methacrylate
DOT	disorder-order transition
DSC	differential scanning calorimetry
DUBBLE	Dutch-Belgian Beamline
EP	Expanded Phase

EPDM	Ethylene Propylene Diene Monomer
ESRF	European Synchrotron Radiation Facility
$\epsilon$ -CL	$\epsilon$ -caprolactone
f	initiator efficiency
$f_A$	volume fraction (of block A)
FRP	free radical polymerisation
G' (E')	storage modulus
G'' (E'')	loss modulus
GPC	gel permeation chromatography
GXL	gas expanded liquid
HEL	Homogenous Expansion Limit
HIP	High Pressure Equipment
HPLC	high pressure liquid chromatography
$J_{crit}$	Critical Molecular Weight
LDOT	lower disorder-order transition
LLA	L-lactide
MADIX	macromolecular design <i>via</i> the interchange of xanthates
MBP	Methyl 2-bromopropionate
$M_c$	Critical Molecular Weight
MMA	methyl methacrylate
$m_{monomer}$	monomer molecular weight
$M_n$	number average molecular weight
$M_n^{calc}$	calculated number average molecular weight
$M_n^{theo}$	theoretical number average molecular weight
$m_{polymer}$	polymer molecular weight
$m_{RAFT}$	RAFT agent molecular weight
$M_w$	weight average molecular weight
NMP	nitroxide mediated radical polymerisation
NMR	nuclear magnetic resonance spectroscopy
ODT	order-disorder transition
OOT	order-order transition
Pa·s	Pascal seconds
PAAc	poly(acrylic acid)
PBd	poly(butadiene)

$p_c$	critical pressure
PCL	poly( $\epsilon$ -caprolactone)
PDLA	poly(D-lactide)
PDLLA	poly(racemic-lactide)
PDMS	poly(dimethyl siloxane)
PDMS-Br	poly(dimethyl siloxane) bromide terminated
PDMS-MA	Poly(dimethyl siloxane monomethyl methacrylate)
PE	poly(ethylene)
PEG	poly(ethylene glycol)
PEO	poly(ethylene oxide)
PFOMA	poly(1,1'-dihydroperfluorooctyl methacrylate)
PIp	poly(isoprene)
PLA	poly(lactic acid)
PLLA	poly(L-lactide)
PMMA	poly(methyl methacrylate)
PMPCS	poly(2,5-bis[(4-methoxyphenyl)oxycarbonyl]styrene)
PnBMA	poly(n-butyl methacrylate)
PnHMA	poly(n-hexyl methacrylate)
PPG	poly(propylene glycol)
$P_r$	probability of heterotactic enchainment
PS	poly(styrene)
PVAc	poly(vinyl acetate)
PVPi	poly(vinyl pivalate)
RAFT	reversible addition fragmentation chain transfer
ROP	ring-opening polymerisation
$R_t$	rate of termination
SANS	small angle neutron scattering
SARM	solvent-absorbing/solvent-releasing
SAXS	small angle x-ray scattering
scCO <sub>2</sub>	supercritical carbon dioxide
SCF	supercritical fluid
SEC	size exclusion chromatography
SEM	scanning electron microscopy
SG-1	[ <i>tert</i> -butyl-N-[1-diethyl phosphono(2,2-dimethylpropyl)]oxy

Sn(Oct) <sub>2</sub> )	tin (II) octanoate
SORP	self-organised reprecipitation
s-PLA	stereocomplexed poly(lactic acid)
SS316	stainless steel 316
Tanδ	loss modulus/storage modulus
T <sub>c</sub>	critical temperature
TEM	transmission electron microscopy
TEMPO	(2,2,6,6-Tetramethylpiperidin-1-yl)oxy
T <sub>g</sub>	glass transition temperature
TGA	thermo-gravimetric analysis
THF	tetrahydrofuran
TIPNO	2,2,5-trimethyl-4-phenyl-3-azahexane-3-oxy
UODT	upper order-disorder transition
VAZO-88	1,1'-azobis(cyclohexanecarbonitrile)
VOC	volatile organic compound
WAXS	wide angle x-ray scattering
X <sub>c</sub>	weight fraction degree of crystallinity
X <sub>n</sub>	degree of polymerisation
Zr- <sup>t</sup> BuC <sub>3</sub>	zirconium trisphenolate complex
ΔH <sub>f</sub> (T <sub>m</sub> )	enthalpy of fusion (at the melting point)
ΔH <sub>f</sub> <sup>0</sup> (T <sub>m</sub> <sup>0</sup> )	enthalpy of fusion (for a 100% crystalline polymer)
η	viscosity
χ	Flory-Huggins interaction parameter

## Contents

Chapter 1 -Introduction .....	1
<b>1. Overview</b> .....	1
<b>1.1. Polymers</b> .....	2
<i>1.1.1. Polymer Structures</i> .....	2
<i>1.1.2. Molecular Weight</i> .....	2
<i>1.1.3. Polymer Synthesis</i> .....	3
<i>1.1.4. Free Radical Polymerisation</i> .....	4
<i>1.1.4.1. Initiation</i> .....	5
<i>1.1.4.2. Propagation</i> .....	6
<i>1.1.4.3. Termination</i> .....	6
<i>1.1.5. Controlled Radical Polymerisation</i> .....	8
<i>1.1.5.1. Nitroxide Mediated Radical Polymerisation</i> .....	9
<i>1.1.5.2. Atom-Transfer Radical Polymerisation</i> .....	10
<i>1.1.6. Reversible Addition Fragmentation Chain Transfer Polymerisation</i> .....	11
<i>1.1.7. CRP vs FRP</i> .....	15
<i>1.1.8. Ring Opening Polymerisation</i> .....	16
<b>1.2. Supercritical Fluids</b> .....	18
<i>1.2.1. Supercritical Carbon Dioxide</i> .....	19
<i>1.2.2. Polymer Properties in Supercritical Carbon Dioxide</i> .....	21
<i>1.2.3. Polymerisation in scCO<sub>2</sub></i> .....	23

<i>1.2.3.1. Precipitation Polymerisations</i> .....	23
<i>1.2.3.2. Dispersion Polymerisations</i> .....	24
<i>1.2.4. Controlled Radical Polymerisation in scCO<sub>2</sub></i> .....	25
<b>1.3. Summary and Thesis Aims</b> .....	28
<b>1.4. References</b> .....	30
Chapter 2 - Equipment and Characterisation .....	40
<b>2. Overview</b> .....	40
<b>2.1 High Pressure Equipment</b> .....	40
<i>2.1.1. CO<sub>2</sub> Pump</i> .....	40
<i>2.1.2. High Pressure Setup</i> .....	42
<i>2.1.3. MKIII Autoclave</i> .....	44
<i>2.1.4. In-situ Monomer Addition via HPLC Pump</i> .....	49
<i>2.1.5. High Pressure View Cell</i> .....	52
<i>2.1.6. Variable Volume High Pressure View Cell</i> .....	55
<i>2.1.7. X-ray Cell MKI</i> .....	56
<b>2.2. Analytical Techniques</b> .....	67
<i>2.2.1. Gel Permeation Chromatography</i> .....	67
<i>2.2.2. Nuclear Magnetic Resonance Spectroscopy</i> .....	68
<i>2.2.3. Scanning Electron Microscopy</i> .....	69
<i>2.2.4. Transmission Electron Microscopy</i> .....	69
<i>2.2.5. Small Angle X-ray Scattering</i> .....	70

2.2.6. <i>Differential Scanning Calorimetry</i> .....	70
2.2.7. <i>Dynamic Mechanical Analysis</i> .....	71
2.2.8. <i>Rheometer</i> .....	72
<b>2.3. References</b> .....	74
Chapter 3 - Expanded Phase Polymerisation .....	75
<b>3. Overview</b> .....	75
<b>3.1. Introduction</b> .....	76
3.1.1. <i>Gas-expanded liquids</i> .....	76
3.1.2. <i>Polymerisations in carbon dioxide expanded liquids</i> .....	77
3.1.3. <i>Controlled radical polymerisations in CXLs</i> .....	80
3.1.4. <i>Critical entanglement weight limits</i> .....	82
3.1.5. <i>Aims and objectives</i> .....	83
<b>3.2. Experimental</b> .....	83
3.2.1. <i>Materials</i> .....	83
3.2.2. <i>Bulk synthesis</i> .....	85
3.2.3. <i>Expanded phase synthesis</i> .....	85
3.2.4. <i>Block copolymer synthesis in bulk</i> .....	86
3.2.5. <i>Block copolymer synthesis in CO<sub>2</sub> expanded phase</i> .....	87
<b>3.3. Results and Discussion</b> .....	88
3.3.1. <i>Poly(styrene) homopolymerisation in CO<sub>2</sub> expanded phase</i> ..	88
3.3.2. <i>Targeting PMMA with M<sub>n</sub> values above the M<sub>c</sub></i> .....	101

3.3.3.	<i>High pressure rheology studies</i>	107
3.3.4.	<i>Low molecular weight block copolymers</i>	118
3.3.5.	<i>Supercritical Fluid Extraction of Residual Monomer</i>	127
<b>3.4.</b>	<b>Conclusions</b>	131
<b>3.5.</b>	<b>References</b>	133
Chapter 4 – Dispersion polymerisation in scCO <sub>2</sub>		138
<b>4.</b>	<b>Overview</b>	138
<b>4.1.</b>	<b>Introduction</b>	139
4.1.1.	<i>Block copolymer phase separation</i>	139
4.1.2.	<i>Phase separation in scCO<sub>2</sub></i>	141
4.1.3.	<i>Phase separation in scCO<sub>2</sub> – in situ studies</i>	143
4.1.4.	<i>Internally ordered block copolymer particles – indirect synthesis</i>	144
4.1.5.	<i>Internally ordered block copolymers particles – direct synthesis</i>	146
4.1.6.	<i>Cross-linking</i>	148
4.1.7.	<i>Cross-linking in scCO<sub>2</sub></i>	149
4.1.8.	<i>Aims and objectives</i>	151
<b>4.2.</b>	<b>Experimental</b>	152
4.2.1.	<i>Materials</i>	152
4.2.2.	<i>In-situ SAXS measurements</i>	152
4.2.3.	<i>MMA homopolymerisation</i>	153

4.2.4.	<i>One pot synthesis of block copolymers</i> .....	154
<b>4.3.</b>	<b>Results and Discussion</b> .....	155
4.3.1.	<i>New High Pressure Cell</i> .....	155
4.3.2.	<i>Reproducibility</i> .....	157
4.3.3.	<i>Block copolymer synthesis in the x-ray cell</i> .....	161
4.3.4.	<i>CO<sub>2</sub> Backgrounds</i> .....	163
4.3.5.	<i>Initial synthesis in situ</i> .....	167
4.3.6.	<i>X-ray cell MKII</i> .....	171
4.3.7.	<i>Modifications of copolymer particles</i> .....	175
4.3.8.	<i>Addition Order</i> .....	176
4.3.9.	<i>Solubility Studies</i> .....	180
4.3.10.	<i>Internal phase separation</i> .....	184
4.3.11.	<i>Thermal Properties</i> .....	186
4.3.12.	<i>Other monomers</i> .....	188
<b>4.4.</b>	<b>Conclusions</b> .....	191
<b>4.5.</b>	<b>References</b> .....	192
Chapter 5 - ROP of Renewable Monomers in scCO <sub>2</sub> .....		199
<b>5.</b>	<b>Overview</b> .....	199
<b>5.1.</b>	<b>Introduction</b> .....	201
5.1.1.	<i>Poly(lactic acid)</i> .....	201
5.1.2.	<i>Thermal properties of PLA</i> .....	203

5.1.3.	<i>Poly(<math>\epsilon</math>-caprolactone)</i> .....	204
5.1.4.	<i>Commercial ROP catalysts</i> .....	205
5.1.5.	<i>Novel ROP catalysts</i> .....	206
5.1.6.	<i>PLA and PCL properties in supercritical carbon dioxide</i> ....	208
5.1.7.	<i>ROP in supercritical carbon dioxide</i> .....	209
5.1.8.	<i>Aims and Objectives</i> .....	212
<b>5.2.</b>	<b>Experimental</b> .....	212
5.2.1.	<i>Materials</i> .....	212
5.2.2.	<i>View cell procedure</i> .....	213
5.2.3.	<i>Homopolymerisation procedure</i> .....	214
5.2.4.	<i>Block copolymerisation procedure</i> .....	214
<b>5.3.</b>	<b>Results and Discussion</b> .....	215
5.3.1.	<i>View cell experiments</i> .....	215
5.3.2.	<i>ROP of DLLA using Zr-<sup>t</sup>BuC<sub>3</sub> in scCO<sub>2</sub></i> .....	219
5.3.3.	<i>[M]:[I] ratio of 300:1</i> .....	226
5.3.4.	<i>Reaction Duration</i> .....	228
5.3.5.	<i>Chain Extensions</i> .....	234
5.3.6.	<i>ROP of <math>\epsilon</math>-caprolactone using Zr-<sup>t</sup>BuC<sub>3</sub> in scCO<sub>2</sub></i> .....	237
<b>5.4.</b>	<b>Conclusions</b> .....	239
<b>5.5.</b>	<b>References</b> .....	241
	Chapter 6 –Conclusions and Future Work .....	247

<b>6.</b>	<b>Overview</b> .....	247
<b>6.1.</b>	<b>Conclusions</b> .....	247
<b>6.2.</b>	<b>Future Work</b> .....	249
<b>6.3.</b>	<b>References</b> .....	251

# Chapter 1 -Introduction

---

## 1. Overview

Worldwide production of polymers is constantly growing as they can provide solutions to multiple applications. They are found in a vast range of products from packaging, coatings, and adhesives through to drug delivery vehicles and biomedical devices, with these only a few examples of many.<sup>1</sup> The versatility of polymers with regards to their structure, size, chemical composition, and material properties facilitates their applicability to such a breadth of products.

The drive to create novel products has prompted the research community to design new and improved ways to influence polymerisations. A variety of methods have been developed with controlled radical techniques perhaps the most successful.<sup>2</sup> The level of control that can be exerted upon the synthesis has enabled the production of many novel materials including monodisperse polymers, block copolymers and structures previously unobtainable. The advances in these techniques are introduced here moving from the original breakthroughs until the current cutting edge methods.

The huge amount of polymer based products manufactured annually has directed research towards greener solvents, with a particular example being supercritical fluids.<sup>3, 4</sup> An overview of these as reaction media is presented with a detailed review specifically concerning carbon dioxide, being the fluid of choice in this work. A summary of polymer synthesis and properties in supercritical fluids is included with specific examples given at the beginning of each relevant Chapter.

## 1.1. Polymers

### 1.1.1. Polymer Structures

Polymers can exist in a variety of structures dependent on the number and composition of the monomers used.<sup>1</sup> If one monomer is used then this is called a homopolymer, with copolymers consisting of one or more monomer units. If two or more monomer units are added together, the arrangement depends on their concentration and reactivity ratios leading to either random or alternating copolymers. Block copolymers are formed by first polymerising one monomer to completion followed by chain extension by a second monomer giving two distinct blocks. Branched or cross-linked polymers are synthesised using either multi-functional monomers or those with reactive pendant groups.

### 1.1.2. Molecular Weight

There are different ways of expressing the molecular weight of a polymer, with the two most common being the number average molecular weight ( $M_n$ ) and the weight average molecular weight ( $M_w$ ). These are defined in Equation 1-1 and Equation 1-2, with  $N_i$  being the total number of chains with  $X_n$ , degree of polymerisation of  $i$ , and  $M_i$  referring to the molecular weight of those chains.

$$M_n = \frac{\sum_i N_i M_i}{\sum_i N_i}$$

**Equation 1-1.**

$$M_w = \frac{\sum_i N_i M_i^2}{\sum_i N_i M_i}$$

**Equation 1-2.**

The relationship between the  $M_n$  and  $M_w$ , referred to as the dispersity<sup>5</sup> ( $\mathcal{D}$ ) (Equation 1-3), is the numerical value expressing the molecular weight distribution. Ideally the dispersity should equal one, as  $M_n = M_w$ , giving a monodisperse sample but due to the nature of polymerisation processes this is impossible to achieve.

$$\mathcal{D} = \frac{M_w}{M_n}$$

**Equation 1-3.**

### *1.1.3. Polymer Synthesis*

There are two main methods of synthesising polymers, chain-growth and step-growth, themselves split into further subsets.<sup>1</sup> Step-growth polymerisation requires two bi-functional monomers which combine through a condensation reaction often producing small molecules as by-products, typically water. Examples of polymers synthesised by this method are polyamides and polyesters. At the beginning of the reaction low molecular weight oligomeric products are generated which subsequently join together to form the high molecular weight polymer. This route often needs long reaction times to produce the high molecular weight products with removal of the by-products also important to drive the reaction forwards.

Chain-growth polymerisation is composed of several steps; initiation, propagation and termination. The first monomer units react with the initiator, including anions, cations, radicals or metal-based co-ordination compounds, followed by addition of multiple monomer steps during the propagation step. Finally the active chain end is terminated either inter- or intra-molecularly, preventing further growth. However, these termination steps can be suppressed

via the use of living polymerisation techniques allowing further chain extension to occur upon addition of monomer. Figure 1-1 depicts the general development throughout the polymerisations relating molecular weight to conversion. At low conversions chain-growth polymerisations produce high molecular weight polymer easily, compared to step-growth producing the oligomeric products discussed. Therefore even in relatively unsuccessful reactions long chain polymers can be generated. Living and controlled radical polymerisations will be discussed further in section 1.1.5.

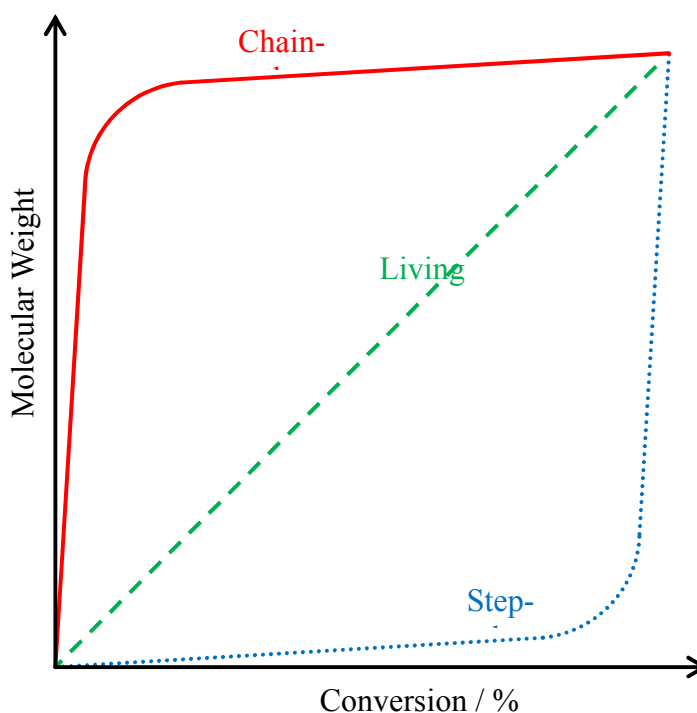


**Figure 1-1 Relationship between molecular weight and conversion for chain growth (solid, red), living (dashed, green) and step growth (dotted, blue) polymerisations**

#### 1.1.4. Free Radical Polymerisation

Free radical polymerisation (FRP) is probably the most widespread method for the synthesis of high molecular weight polymers owing to its ease

of use and applicability to multiple types of monomer, many of which are commercially available. It has a high tolerance for impurities meaning radical stabilisers used to prolong the shelf life of the monomer need not be removed, and other reactants do not need purifying. One particular benefit is the tolerance for a broad range of functional groups on the monomers, allowing for functional polymers to be synthesised easily. The main stages of FRP are as follows.

#### 1.1.4.1. Initiation

Initiation is composed of two steps. First, decomposition of an initiator into radical species, then these radicals add to the monomer in the actual initiation step. The decomposition of 2,2-azobis(2-methylpropionitrile) (AIBN) and initiation of methyl methacrylate (MMA) are shown in Figure 1-2. The driving force behind this reaction is the formation of two relatively stable 2-cyano-2-propyl radicals, an extremely strong  $\text{N}\equiv\text{N}$  triple bond with a bond dissociation energy of  $945 \text{ kJ mol}^{-1}$  and also the gain in entropy by forming the gaseous dinitrogen.<sup>6</sup>

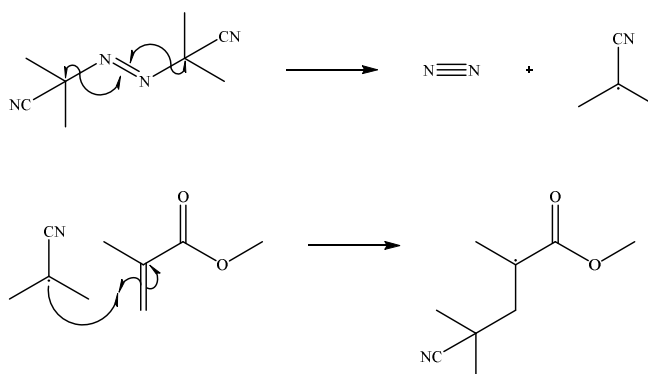


**Figure 1-2. (Top) Thermal decomposition of AIBN into two 2-cyano-2-propyl radicals and dinitrogen. (Bottom) Mechanism of initiation of MMA by the 2-cyano-2-propyl radical.**

#### 1.1.4.2. Propagation

The polymer chain is grown through the addition of further monomer units to the radical formed in the initiation step. The radical centre is transferred to the end of the chain in each case, retaining its high reactivity, forming high molecular weight polymer. An example again using MMA is shown in Figure 1-3.

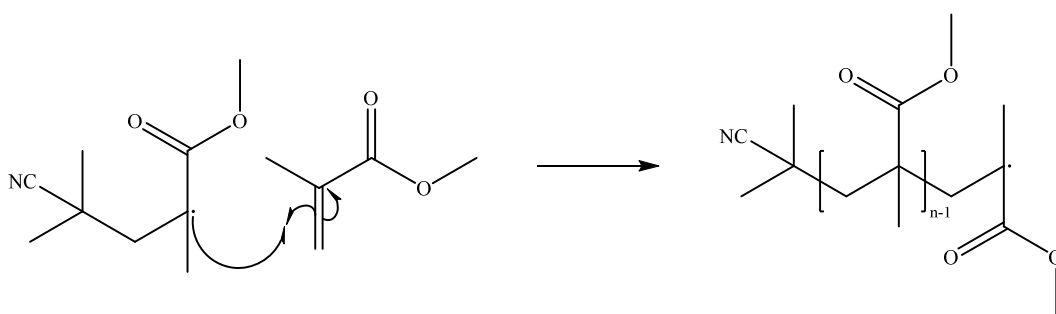


**Figure 1-3. Mechanism of propagation of MMA.**

#### 1.1.4.3. Termination

Termination is the process by which two radicals react, form covalent bonds, and therefore cease to propagate further. There are two routes through which this can occur. Combination is where two radicals join in a head to head manner to form a high molecular weight polymer. Disproportionation occurs when one growing chain abstracts a hydrogen from the end of another to form two separate polymer chains; one with a terminal hydrogen and the other with a double bond at the end of the chain. Figure 1-4 displays the two processes with regards to the termination of two PMMA polymeric radicals.

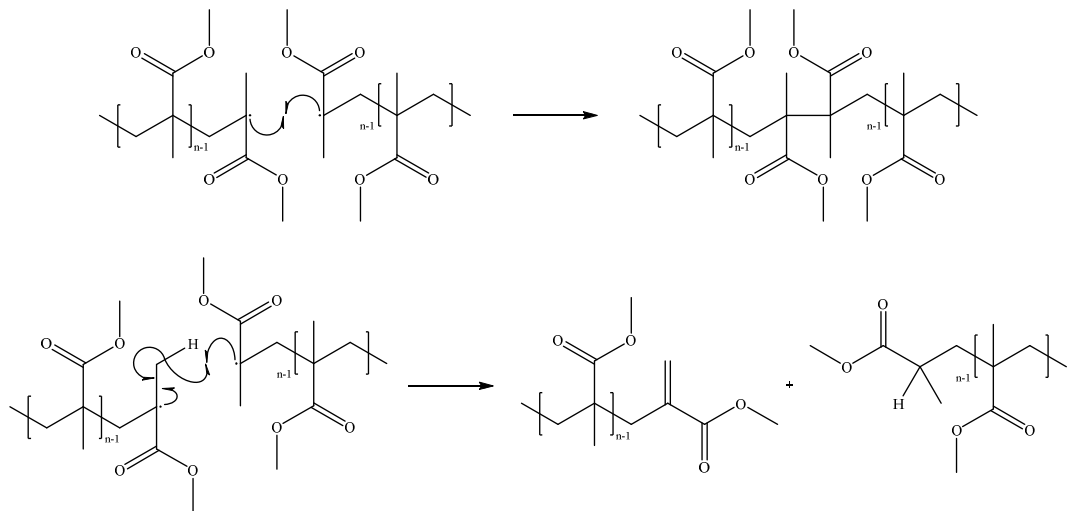


**Figure 1-4. Mechanism of chain termination of two PMMA radicals, (top) Combination, (bottom) Disproportionation.**

As mentioned, high molecular weight polymer is generated even at low conversions for FRP, even though the termination processes have the fastest rates. This is a result of the steady state conditions where the rate of initiation is equal to the rate of termination ( $R_i = R_t$ ). This means radicals are constantly being generated and new chains grow and terminate throughout the reaction.

One drawback is the lack of control over the polymer chain length, with broad dispersities a characteristic feature ( $\mathcal{D} > 2.0$ ), and as the majority of chains are irreversibly terminated, synthesising block copolymers is not possible. For this reason new techniques have been developed to control certain kinetic features of a radical polymerisation to ensure all the polymer chains are similar in length ( $\mathcal{D} < 1.5$ ) and end groups capable of being re-initiated are present.

### 1.1.5. Controlled Radical Polymerisation

FRP, although relatively simple to perform, is not particularly versatile with regards to synthesising polymer of varying composition and architecture. Living polymerisation, first discovered in 1956 by Szwarc *et al.*,<sup>7</sup> is an alternative route that enables control to be exerted; defined as “*chain polymerisation from which chain termination and irreversible chain transfer are absent*”.<sup>8</sup> Therefore in theory a polymerisation will propagate until complete consumption of monomer, with retention of a living end group. Upon addition of further monomer the chains can be extended by further propagation. Another characteristic of a living polymerisation is the linear increase of molecular weight with conversion, which allows chain lengths to be targeted and dispersities to remain narrow. It was here that living ionic polymerisation was born with many commercial products still synthesised by this method today, typically rubbers such as poly(butadiene) or poly(isoprene).<sup>1</sup>

Methods of imparting control over FRP have been investigated for a number of years, with this field known as Controlled Radical Polymerisation (CRP). This began with the use of chain transfer agents (CTAs), leading up to Catalytic Chain Transfer Polymerisation (CCTP)<sup>9</sup> where only parts per million levels of catalyst are required. It was the 1980s that CRP techniques with living characteristics were introduced, first with Iniferter Polymerisation,<sup>10</sup> then with Nitroxide-Mediated Radical Polymerisation (NMP).<sup>11</sup> The 1990s however was when the key discoveries including Atom Transfer Radical Polymerisation (ATRP)<sup>12, 13</sup> and Reversible Addition-Fragmentation Chain

Transfer Polymerisation (RAFT)<sup>14</sup> were made giving rise to the area of research that is commonplace today.

#### 1.1.5.1. Nitroxide Mediated Radical Polymerisation

NMP was first patented in 1985 by Solomon *et al.* but it was Georges *et al.* in the early 1990s that developed it into the process known today.<sup>15</sup> It is based upon reversible termination of the growing polymeric radical by a stable free radical species. (2,2,6,6-Tetramethylpiperidin-1-yl)oxy (TEMPO) was the first persistent radical to be implemented in as an NMP agent (Figure 1-5), with the rapid equilibrium between itself and the growing polymer chain sufficient to impart control over the kinetics.

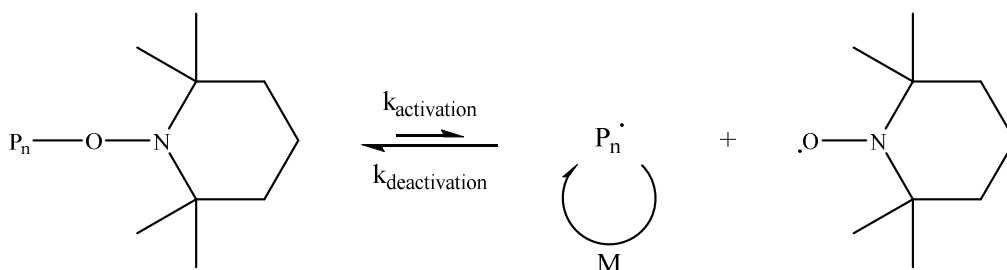


**Figure 1-5. Mechanism of NMP controlled using TEMPO.**

NMP has been well reviewed by Hawker *et al.*<sup>16</sup> Other NMP agents have been developed, most notably N-tert-butyl-N-[1-diethyl phosphono(2,2-dimethylpropyl)]oxy (SG-1),<sup>17</sup> with the aim to expand the number of monomers that can be controlled by this technique. However, the monomer set remains limited to styrenics and acrylates with only a handful of papers claiming control over methacrylates.<sup>18</sup> Coupled with the high temperatures often needed this makes NMP the least versatile of the main three techniques.

## 1.1.5.2. Atom-Transfer Radical Polymerisation

ATRP was simultaneously developed by Matyjaszewski<sup>12</sup> and Sawamoto<sup>13</sup> in 1995. As with NMP, the polymeric radical is reversibly capped, this time with a halogen. ATRP employs a metal complex, usually copper, with an organo halide with a weak C-X bond, often C-Cl or C-Br, as shown in Figure 1-6. Firstly, the organic halide initiator is activated by the copper complex ( $\text{Cu}^{\text{I}}\text{X}/\text{ligand}$ ), generating  $\text{R}\cdot$  and an oxidised copper complex ( $\text{Cu}^{\text{II}}\text{X}_2/\text{ligand}$ ).  $\text{R}\cdot$  can then initiate a polymer chain, creating a polymeric radical. A halogen from the  $\text{Cu}^{\text{II}}\text{X}_2/\text{ligand}$  complex is then exchanged with the polymeric radical, which is the beginning of the reversible activation/deactivation equilibrium. This equilibrium lies towards the deactivated species, reducing the number of radicals in the system, lowering the possibility of irreversible termination. In the active form monomer can add to the polymeric radical, but it should be noted that irreversible termination steps can occur here, so a truly living polymerisation is never fully established, which is the case for all CRP processes.

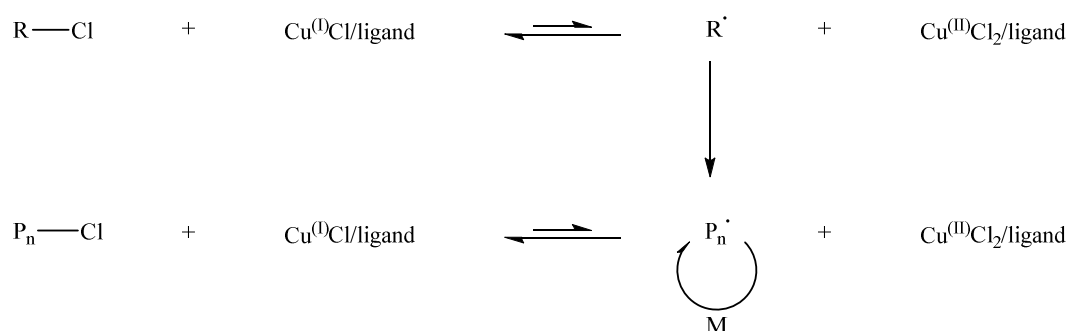


**Figure 1-6. Generic ATRP mechanism, with Cl as the halogen used in this case.**

ATRP is much more versatile than NMP and can be utilised with most conventional monomers such as methacrylate and styrenics,<sup>2</sup> although there are fewer reports of less active monomers such as vinyl acetate.<sup>19</sup> Another key benefit is many of the precursors, including the transition metals, ligands and alkyl halides, are commercially available.

#### *1.1.6. Reversible Addition Fragmentation Chain Transfer Polymerisation*

RAFT differs to NMP and ATRP as it is based upon a degenerative chain transfer process, although the same principles behind a controlled radical polymerisation must still be fulfilled. It was originally developed at CSIRO in 1998 by Chiefari *et al.*,<sup>14</sup> with a similar process known as macromolecular design *via* the interchange of xanthates (MADIX) patented by Rhodia in the same year.<sup>20</sup>

The process is similar to a typical free radical polymerisation with the addition of a thiocarbonyl RAFT agent.<sup>21</sup> This is composed of two key parts, the R group must be sufficiently labile to fragment and initiate a new polymer chain, whilst the Z group influences the reactivity of the C=S. There are several classes of RAFT agent including dithioesters, trithiocarbonates, xanthates<sup>22</sup> and dithiocarbamates, with the choice dependent upon the monomers used (Figure 1-7).<sup>23</sup>

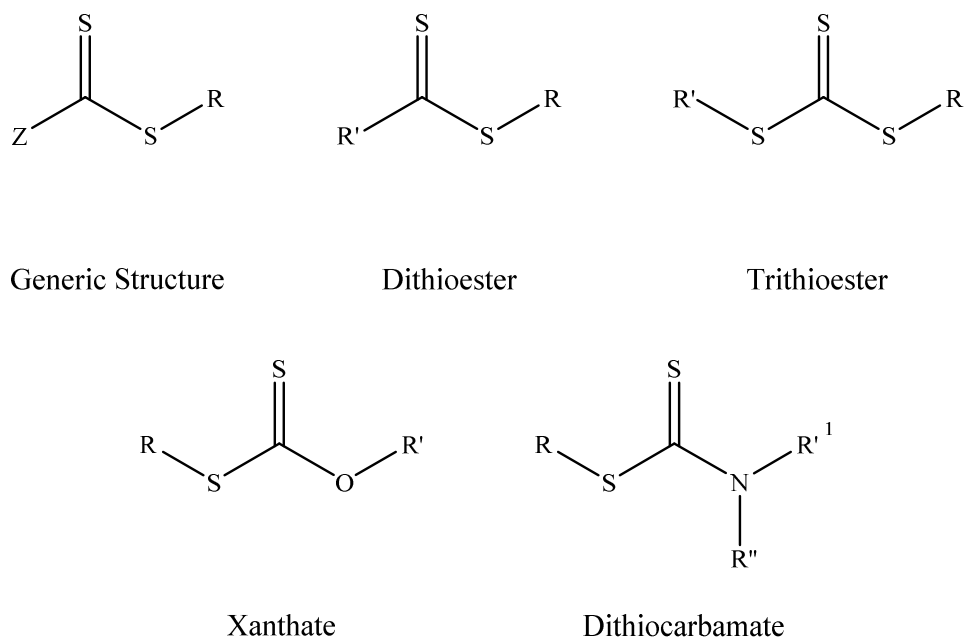


**Figure 1-7. RAFT agent structures. R group is the leaving group, with R' and R'' as carbon based functional groups.<sup>24</sup>**

The first steps follow the same mechanism of FRP; decomposition of an initiator, followed by addition to a monomer unit and propagation. At this point the polymeric radical can attack the RAFT agent (Figure 1-8, top), forming the intermediate thiocarbonyl radical species, stabilised by the Z group. Fragmentation of the weak S-R bond produces the RAFT agent terminated polymer and R· radical. This R· can initiate a new polymer chain, which can then attack further RAFT agents. An equilibrium is established where the polymeric radical species ( $P_n\cdot$ ) attacks a capped polymer, itself being deactivated (Figure 1-8, bottom). Another polymeric radical ( $P_m\cdot$ ) is reactivated and can propagate, before attacking the RAFT agent once again. Through this shuttling mechanism, all chains have an equal probability of growing at the same rate, controlling the molecular weight distribution.

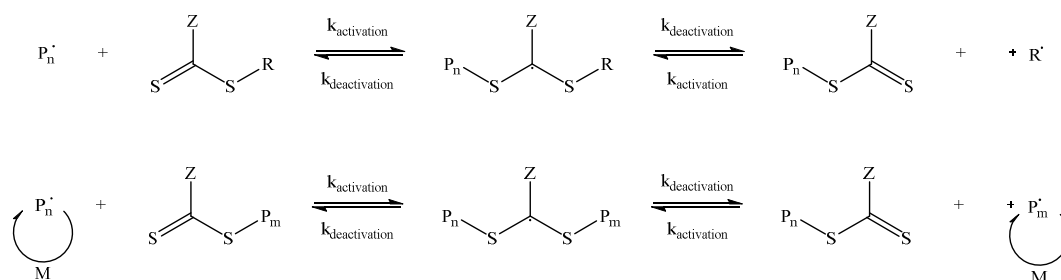


**Figure 1-8. (top) Attack of the polymeric radical, followed by fragmentation of the leaving group  $R^\bullet$  which proceeds to initiate a new polymer chain, (bottom) Generic RAFT equilibrium.**<sup>25, 26</sup>

The ability of the Z group to stabilise the intermediate radical is key to determining the reactivity of the RAFT agent.<sup>25</sup> A highly stabilised intermediate will fragment slowly causing retardation. The R group must be sufficiently weak to be able to fragment efficiently, but the radical formed must be able to re-initiate a new chain.<sup>26</sup> The broad choice of RAFT agents means it can be applied to most common monomers, and is probably the most versatile of all the CRP techniques. As most RAFT agents are organic compounds they are soluble in a variety of media, including standard solvents such as toluene,<sup>14</sup> aqueous systems,<sup>27</sup> ionic liquids,<sup>28</sup> and as will be discussed later, supercritical fluids.<sup>29, 30</sup>

Molecular weight control is determined by the initial concentrations of RAFT agent and monomer (Equation 1-4). The targeted molecular weight ( $M_n^{\text{theo}}$ ) is calculated based on the initial concentration of monomer ( $[M]_0$ ), and the final concentration ( $[M]_f$ ), the initial RAFT agent concentration ( $[RAFT]_0$ ) and the molar masses of the monomer and RAFT agent ( $m_{\text{monomer}}$  and  $m_{\text{RAFT}}$ ). There are some assumptions made, notably that the chains are only initiated by

the reinitiating R· group, and not by the radical initiator. Typically a [RAFT]:[initiator] ratio of 10:1 is used, therefore around 9% of chains will be initiated by the initiator.

$$M_n^{\text{theo}} = \frac{[M]_0 - [M]_t}{[\text{RAFT}]} \times m_{\text{monomer}} + m_{\text{RAFT}}$$

**Equation 1-4.**

Therefore to have a successful RAFT polymerisation fast initiation is required, and a low radical concentration throughout the reaction is also needed. As low a concentration of initiator as possible can help improve the living character and potential for chain extending.<sup>31</sup> This opens the possibility for synthesising block copolymers, although the RAFT agent must be compatible with both monomers.<sup>32</sup> More recently, pH switchable RAFT agents have been developed which can control polymerisation of both more activated monomers such as MMA, as well as less activated monomers such as vinyl acetate by protonation of the control agent.<sup>33-36</sup> Other complex architectures can also be created, including stars and hyperbranched polymers.<sup>37, 38</sup>

The main disadvantage of RAFT from a commercial standpoint is the cost and time required to synthesise the control agents, as well as the toxicity of the sulfur compounds, although the toxic nature is not necessarily transferred to the polymer.<sup>39</sup> The resulting sulfur based polymer end-groups are also responsible for colouring the polymers, often pink or yellow, making it difficult to enter medical markets where white products are often necessary to fit with consumer demand. Methods developed by Perrier *et al.* to easily

remove the colour and toxicity by reacting with excess AIBN offer a solution, with other organic modification possible also.<sup>40-44</sup>

### 1.1.7. CRP vs FRP

There are several important features that differentiate CRP reactions from typical FRP ones.<sup>2, 45</sup> Firstly, initiation must be fast in CRP to enable all of the chains to begin growing at the same time. In FRP, chains are initiated throughout the polymerisation, with excess initiator often remaining post-reaction. Polymer chains which would usually be initiated, propagate, and terminate in a matter of seconds in FRP have longer lifetimes in CRP, as they spend more time in the dormant state to keep the radical concentration low. This also impacts upon the polymerisation rate, with CRP typically much slower. A key difference is the amount of 'dead' polymer, with FRP having almost all chains terminated, whereas in a successful CRP reaction <10% of chains are typically dead.

The main difference is between the kinetic profiles, and the growth in molecular weight with conversion. Figure 1-1 shows the linear profile expected for a living polymerisation, with successful CRP reactions following a similar trend. In FRP the steady state radical concentration is when the rate of initiation is equal to the rate of termination. In CRP a steady radical concentration is dependent upon the rates of activation and deactivation, and the assumption that the rate of termination approaches zero, and the rate of initiation exceeds the rate of propagation, therefore the overall rate of polymerisation can be expressed as follows:

$$\ln([M]_0/[M]) = k_p [M^*]t$$

**Equation 1-5.**

Therefore, a plot of  $\ln([M]_0/[M])$  against time should give a straight line. This along with the linear growth of molecular weight with conversion, provides evidence of a controlled polymerisation.

1.1.8. *Ring Opening Polymerisation*

Ring opening polymerisation (ROP) is defined as “*Polymerization in which a cyclic monomer yields a monomeric unit that is either acyclic or contains fewer rings than the cyclic monomer*”.<sup>46</sup> ROP can proceed through enzymatic, radical, anionic and cationic mechanisms (Figure 1-9, Figure 1-10), with examples of polymers produced through this method including poly(esters), poly(dimethyl siloxanes), poly(amides) and poly(carbonates).<sup>47</sup> Cyclic monomers containing heteroatoms are often more susceptible to ring opening polymerisation as the heteroatom can coordinate to metal catalysts, and provide an active centre for electrophilic or nucleophilic attack.

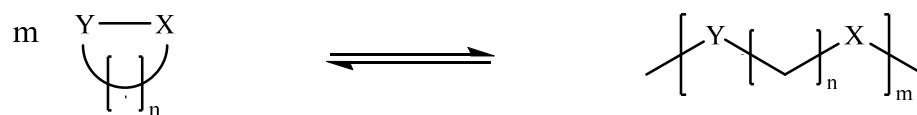


**Figure 1-9. Generic scheme for ring opening of a cyclic monomer. An initiator and/or catalyst are required to drive this reaction.**

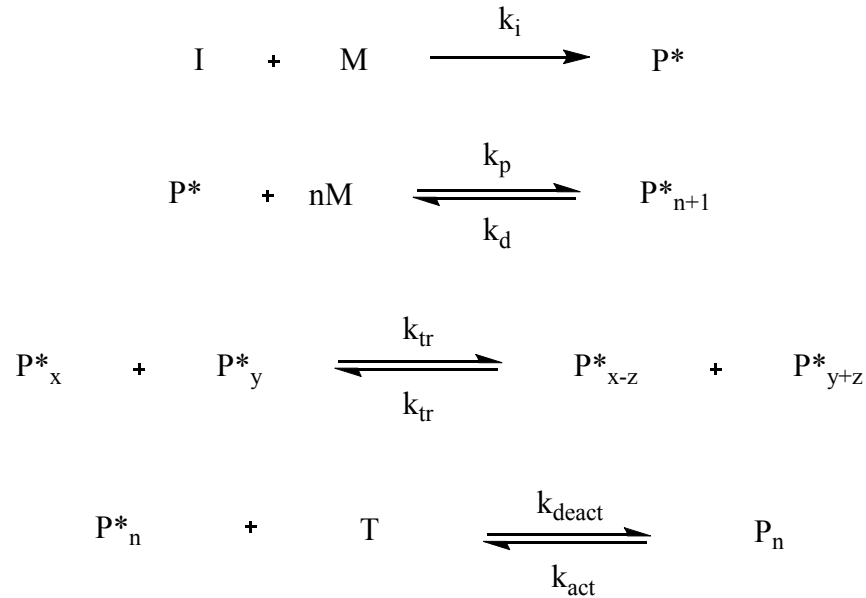


**Figure 1-10. Reaction scheme for pseudo-living ROP. Monomer (M) reacts with the initiating species (I) to form the opened/active polymer P\*. This attacks further monomer. Reversible reactions can deactivate the chains by either segmental exchange or temporary termination by transfer agent (T).**

In general, the initiating species will ring open the first monomer unit and create an active centre. This will attack further monomer units, transferring the active centre to the end of the polymer. As with CRP, if initiation is rapid, all the chains will begin to grow at the same time. This leads to a linear increase of molecular weight with conversion, as described by Equation 1-6. If side reactions do occur, they do so at a rate slower than the rate of polymerisation, and the process still follows pseudo-living kinetic behaviour.

$$R_p = -\frac{d[M]}{dt} = k_p \sum [P_n^*] [M] - k_d \sum [P_n^*]$$

But as  $k_p \gg k_d$  it can be assumed  $k_d = 0$

$$\text{Integrating: } \ln \frac{[M]_0 - [M]_{eq}}{[M] - [M]_{eq}} = k_p \Sigma [P_n^*] t$$

$$\text{Simplified: } \ln \frac{[M]_0}{[M]} = k_p [P_n^*] t$$

**Equation 1-6.**

Therefore plotting  $\ln([M]_0/[M])$  against time should give a linear fit . However, when initiation is slow, trans-esterification processes become dominant, leading to a loss of control. This also happens at low monomer concentration, therefore trans-esterification often occurs a high conversion. Further details can be found in Chapter 5, which will focus on metal alkoxide catalysed ROP *via* a coordination/insertion mechanism to form poly(esters).

## 1.2. Supercritical Fluids

Supercritical fluids (SCFs) have gained much attention as alternative reaction solvents, in particular from a green chemistry perspective.<sup>48, 49</sup> They are defined as a fluid above both its critical temperature ( $T_c$ ) and critical pressure ( $p_c$ ), known as the critical point.<sup>3, 4</sup> SCFs have several benefits compared to volatile organic solvents (VOCs), the most important of which are the gas-like diffusivities, as well as liquid-like densities. The density can easily be varied by small changes in the temperature or pressure, enabling the solvating power of the SCF to be tuned, especially when close to the critical point (Figure 1-11).

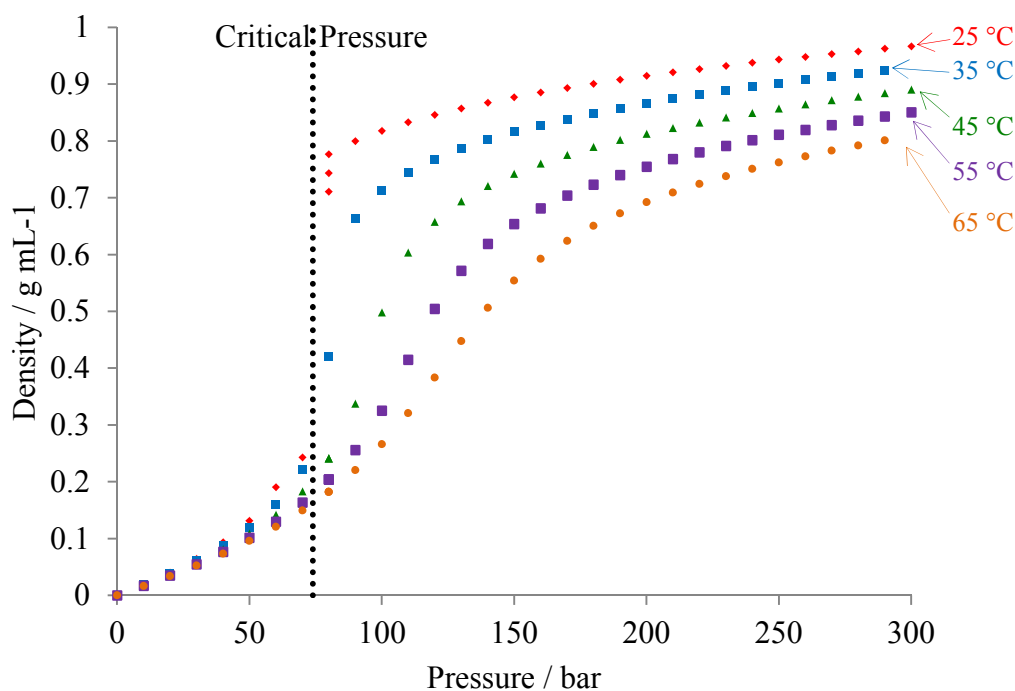


**Figure 1-11. Isothermal change in density with pressure for carbon dioxide at five different temperatures. The largest variations in density occur around the critical pressure of 73.8 bar. All values taken from the NIST webbook.<sup>50</sup>**

### 1.2.1. Supercritical Carbon Dioxide

Supercritical Carbon Dioxide (scCO<sub>2</sub>) is non-toxic and non-flammable with a relatively accessible critical point ( $T_c = 31.1\text{ }^\circ\text{C}$ ,  $p_c = 73.8\text{ bar}$ , Figure 1-12).<sup>51, 52</sup> CO<sub>2</sub> presents many advantages over VOCs with regards to its “green” characteristics, fulfilling several of the 12 principles of green chemistry.<sup>53</sup> (1) prevention, (4) safer chemicals, (5) safer solvents, (7) use of renewable feedstocks. For example, if a toxic VOC is replaced with CO<sub>2</sub>, the emissions are reduced, CO<sub>2</sub> is less toxic and it is often obtained as a by-product from other industrial processes and recycled. However, these benefits are highly dependent on the process as a whole, with certain principles violated; for example the energy efficiency can be poorer compared to traditional

processes owing to the high pressure equipment and compression of the gas, as well as the cost of chilling the carbon dioxide to ensure it remains in the liquid phase to allow pumping.

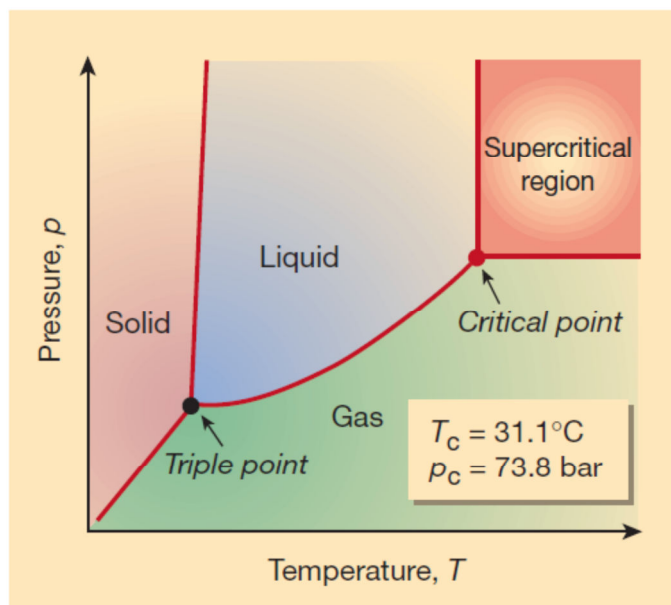


**Figure 1-12. Phase diagram for carbon dioxide<sup>51</sup>**

The ability to tune the density, and subsequently the solvating power, makes scCO<sub>2</sub> an attractive medium for chemical reactions, ranging from organic synthesis to polymerisations. The moderate conditions needed as well as being both naturally abundant and produced as a by-product of many industrial processes, make reactions in scCO<sub>2</sub> a viable option for use on an industrial scale.<sup>54</sup> The ease of solvent removal is another particularly appealing prospect, as upon releasing the pressure the CO<sub>2</sub> can escape as a gas. This reduces the often time-consuming and energy-intensive purification methods employed industrially with VOCs, with the CO<sub>2</sub> able to be recycled post-reaction. For example, scCO<sub>2</sub> is used in applications including the decaffeination of coffee,<sup>55</sup> as well as dry cleaning.<sup>56</sup>

### 1.2.2. Polymer Properties in Supercritical Carbon Dioxide

In general, CO<sub>2</sub> is a poor solvent for most polymers, although exceptions to this include fluorinated and siloxane based polymers. Favourable interactions between CO<sub>2</sub> and the C-F bonds or the –Si – O – Si – backbone help to solubilise these polymers compared to fully hydrocarbon polymers.<sup>52</sup> CO<sub>2</sub> is able to penetrate these already flexible polymers well and reduce polymer-polymer interactions. The solubility of polymers in CO<sub>2</sub> can be improved by adding fluorinated groups or through copolymerising with fluorinated monomers.<sup>57</sup>

Lewis acid-Lewis base interactions between polymers containing certain functional groups enhances their solubility in CO<sub>2</sub>; also the solubility of CO<sub>2</sub> in the polymers.<sup>58-60</sup> For example, poly(ethylene) (PE), with no functionality, has been shown to be insoluble at extreme conditions of over 270 °C and 2750 bar. By contrast, recent studies have shown poly(vinyl acetate) (PVAc) and poly(vinyl pivalate) (PVPi) exhibiting a moderately high solubility in scCO<sub>2</sub>, due to favourable interactions between CO<sub>2</sub> with the acetate/pivalate carbonyls.<sup>61, 62</sup> For example, a PVAc sample with an M<sub>n</sub> of 9.6 kDa becomes soluble at 35 °C and 243.1 bar, whereas PVPi of M<sub>n</sub> 10.0 kDa becomes soluble at 174.7 bar at the same temperature of 35 °C. Other polymers with carbonyl side groups such as PMMA, also exhibit similarly favourable interactions, although this is exhibited by lowering of the glass transition temperature with the polymer not dissolving in CO<sub>2</sub>.<sup>52 63</sup>

It is sorption of CO<sub>2</sub> into polymers that has a pronounced effect on their mechanical and physical properties, as it penetrates between the polymer chains and causes swelling. One property that is influenced is the glass

transition temperature (T<sub>g</sub>); the temperature at which an amorphous or semi-crystalline polymer changes from a glassy solid to a rubber. Below the T<sub>g</sub> the chains are rigid, but above the T<sub>g</sub> the polymer backbones are able to move due to an increase in the free volume. CO<sub>2</sub> is able to depress the T<sub>g</sub> of a polymer, as it can penetrate between the chains, increasing the free volume, allowing the chains to move more freely. Therefore, through the addition of CO<sub>2</sub> the processing temperatures can be lowered, which will reduce the processing costs.<sup>64</sup> The extent to which a polymer is plasticised is dependent upon the amount of CO<sub>2</sub> that it can absorb, with carbonyl containing polymers often exhibiting large depressions from the Lewis-acid Lewis-base interactions. Several methods exist for quantifying T<sub>g</sub> depressions in CO<sub>2</sub>, including high pressure differential scanning calorimetry, high pressure rheology and through visual inspection.<sup>65-67</sup>

The addition of CO<sub>2</sub> can also heavily reduce the viscosity of a polymer by penetrating between the polymer chains, lowering the polymer-polymer interactions thus allows the chains to move more freely.<sup>68</sup> This can be useful for blending two polymers together without the use of high temperatures or VOCs. Medical applications are one area of current interest, where biodegradable polymers such as PLA can be liquefied below body temperature (37 °C) enabling drugs to be blended in, without losing their activity.<sup>69-71</sup> Upon removal of the CO<sub>2</sub> the polymer solidifies, and the drug can be fully encapsulated in a polymer matrix.

### 1.2.3. Polymerisation in *scCO*<sub>2</sub>

Although most polymers are insoluble in *scCO*<sub>2</sub>, many monomers, initiators and control agents are, therefore heterogeneous polymerisation techniques are often employed.<sup>72</sup> There are some exceptions, including fluorinated polymers, which can proceed through more traditional homogeneous solution polymerisations.<sup>73</sup> The difference in solubility between the monomer and polymers is beneficial for purification, as during depressurisation unreacted monomer can be removed through a supercritical fluid extraction process, leaving the pure polymer product in the reactor. A number of heterogeneous techniques have been employed, with the focus on precipitation and dispersion polymerisations, although examples of suspension and emulsion polymerisation have been reported.<sup>74</sup>

Many polymerisation processes have also been employed, including radical, ring-opening, cationic and condensation.<sup>4</sup> The following examples will have an emphasis on free radical polymerisations, with examples of ROP detailed in the suspension polymerisation section. *scCO*<sub>2</sub> is an ideal solvent for radical polymerisations as it is unreactive to radicals, therefore no chain-transfer to solvent occurs as with some commonly used VOCs such as toluene. However, initiator decomposition<sup>75</sup> and polymerisation rates can be significantly altered in *scCO*<sub>2</sub>.

#### 1.2.3.1. Precipitation Polymerisations

The difference in solubility of most monomers and polymers make precipitation polymerisation an ideal technique to employ. At the beginning of the reaction the monomer, initiator, *CO*<sub>2</sub> and any control agents form a

homogeneous mixture. As the polymer chains form, they precipitate out, forming a separate polymer phase. The first free radical precipitation polymerisations in scCO<sub>2</sub> were reported during the 1960s, with several patents issued.<sup>4</sup> It was not until the 1990s when research into polymer synthesis in scCO<sub>2</sub> began to gain more attention, with polymers such as PMMA, PS, and poly(acrylic acid) (PAAc)<sup>76-79</sup> being produced *via* precipitation processes. DeSimone *et al.* have since shown that polymerisation occurs in the continuous CO<sub>2</sub> phase, as well as polymer phase, whilst studying the precipitation polymerisation of PAAc.<sup>80</sup> In general, precipitation polymerisations have mainly been exploited to clean, dry, powdered products, in the absence of VOCs, although not with much functionality. This has been extended to semi-continuous processes, again synthesising PAAc, through the use of a continuous stirred tank reactor.<sup>79, 81</sup> As the polymerisation proceeded, the PAAc precipitated and was extracted from the bottom of the reactor, with new monomer and initiator injected in through the top of the vessel.

#### 1.2.3.2. *Dispersion Polymerisations*

Dispersion polymerisations are similar to precipitation polymerisations, except for the addition of a colloidal stabiliser, usually with CO<sub>2</sub>-philic and polymer-philic sections. Initially all the reagents (including the stabiliser) form a homogeneous mixture, but once the oligomeric radicals reach a critical molecular weight ( $M_c$ ) they separate from the continuous phase. The stabiliser then either adsorbs or chemically attaches to the polymer, preventing agglomeration, thus creating polymer particles in a continuous phase of CO<sub>2</sub>. The stabilisers usually work *via* a steric stabilisation, owing to the low

dielectric constant of CO<sub>2</sub>, and are often fluorinated or siloxane based polymers. Stabilisers with a terminal initiating group have also been implemented, with the 'inistab' acting as the initiator and stabiliser simultaneously.<sup>82</sup> The high cost and toxicity of these stabilisers has created a need for newer fully hydrocarbon alternatives, with recent examples based on PVAc and PVPi showing promise owing to their enhanced solubility discussed in section 1.2.2.<sup>61, 62, 83</sup> If a successful dispersion has been maintained, then upon depressurisation, discrete spherical polymer particles remain, typically between 100 nm to 10 µm in size.

DeSimone *et al.* first reported the free radical dispersion polymerisation of MMA in 1994, utilising a fluorinated poly(1,1-dihydroperfluorooctylacrylate) stabiliser<sup>84</sup>, with others reporting similar syntheses with different stabilisers and conditions.<sup>85-88</sup> Since then a vast number of monomers have been polymerised in free radical dispersion polymerisation processes, including styrene,<sup>89</sup> divinyl benzene,<sup>90, 91</sup> and a variety of different other methacrylates.<sup>92-94</sup> The introduction of CRP methods has further increased the use of radical based dispersion polymerisations in scCO<sub>2</sub>; discussed in section 1.2.4.

#### 1.2.4. Controlled Radical Polymerisation in scCO<sub>2</sub>

The invention of CRP methods has enabled a range of polymer structures, including blocks and stars to be formed, as well controlling the chain length and dispersity. Applying these techniques in the heterogeneous polymerisation in scCO<sub>2</sub> offers a green synthetic route to producing functional materials. All three of the main CRP techniques (NMP, ATRP, RAFT)

described earlier have been performed in scCO<sub>2</sub>, in both precipitation and dispersion reactions.<sup>95</sup>

Precipitation NMP in scCO<sub>2</sub> has been investigated for the polymerisation of styrene and *tert*-butyl acrylate; these reports will be discussed in depth in Chapter 3. Briefly, control over the molecular weight and dispersity could be achieved at high monomer loadings of around 70 v/v%.<sup>96</sup> At loadings of 40 v/v%, precipitation occurred at lower conversions, and the nitroxide partitioned into the CO<sub>2</sub> phase more easily, preventing it from controlling the polymerisation.<sup>97</sup>

PS has also been synthesised in scCO<sub>2</sub> dispersion polymerisations by Okubo *et al.* using a PS-*b*-PDMS alkoxyamine, which acts as both the initiator and stabiliser.<sup>95, 98</sup> It was observed that the  $M_n > M_n^{\text{theo}}$  for most cases, with some control over the dispersity noted ( $\approx 1.5$ ). However, a successful dispersion was not maintained, leading to aggregated particles, attributed to either poor stabilisation or the high temperatures (110 °C) plasticising the polymer. Their following paper enabled higher conversions (>85%) to be achieved, producing spherical particles, indicating a successful dispersion. Partitioning of the SG-1 nitroxide into the continuous phase was again observed, with an excess of SG-1 required to maintain control.<sup>99</sup>

Limited studies of ATRP in precipitation have been reported, with MMA the only monomer investigated. DeSimone *et al.* investigated the effect of the copper complex ligand on the polymerisation, comparing the bpy ligand to a fluorinated analogue (Figure 1-13, a and c respectively), with MBP as the initiating group (Figure 1-13, b). The increased solubility of the fluorinated analogue in scCO<sub>2</sub> led to an improvement in control.<sup>100</sup>

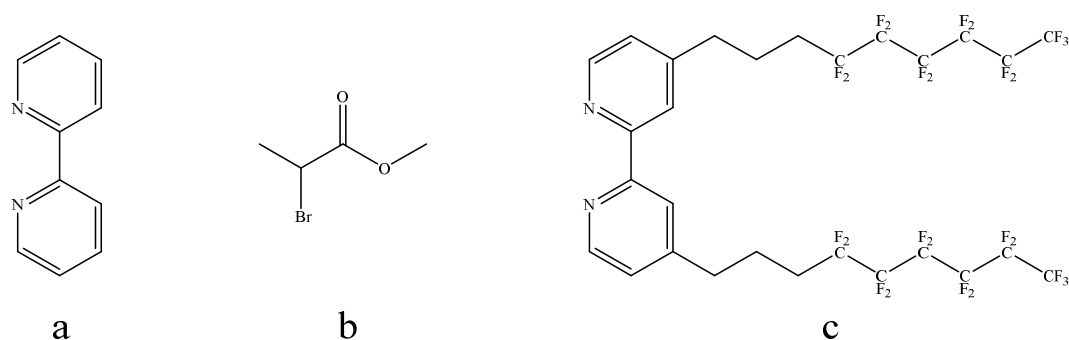


**Figure 1-13. (a) 2,2'-BPY ligand, (b) MBP as the initiating group, (c)**

### **Fluorinated BPY derivative for performing ATRP in $\text{scCO}_2$**

Dispersion polymerisations have been more successful, with several reports of free flowing powders being produced, with  $M_n \approx M_n^{\text{theo}}$  and narrow dispersities. Okubo *et al.* used an inistab method, with a halogen terminated PDMS-Br macro-initiator, showing good control over the polymerisation ( $\bar{D} \approx 1.25$ ).<sup>101</sup>

Grignard and co-workers have published several reports of dispersion ATRP in  $\text{scCO}_2$  with MMA, and styrene,<sup>102, 103</sup> then a functional methacrylate based polymer.<sup>104</sup> In these studies a polymeric ligand to solubilise the copper complex, whilst also stabilising the dispersion was used. The copolymer stabiliser was prepared *via* RAFT, with the  $\text{CO}_2$ -philic portion provided by a heptafluorodecyl acrylate monomer, with the copper complexing section a tetraethyldiethylenetriamine capped 2-hydroxyethyl acrylate monomer. Spherical PMMA microspheres were produced, with narrow dispersities ( $\approx 1.2$ ), although one drawback was the  $M_n > M_n^{\text{theo}}$ . PS was more successful with regards to the polymerisation ( $M_n \approx M_n^{\text{theo}}$ ), although in this case the dispersion was poor and non-uniform particles were produced.

Arita *et al.* studied the precipitation homopolymerisation of styrene and methyl acrylate using cumyl dithiobenzoate as the RAFT agent at 80 °C and 300 bar.<sup>105, 106</sup> Control was maintained, with results similar to the analogous reactions in toluene. The only other published report of a RAFT precipitation in scCO<sub>2</sub> was by Gregory *et al.*, achieving a low conversion compared to the same polymerisation in a dispersion process.<sup>30</sup>

RAFT controlled scCO<sub>2</sub> dispersion polymerisation was first performed by Thurecht *et al.* with MMA, and subsequent chain extension with styrene.<sup>29</sup> A high [RAFT]:[initiator] ratio of 1:1 was used, although no detrimental effects were observed, attributed to the slower AIBN decomposition in scCO<sub>2</sub>.<sup>75</sup> Powdered polymer was obtained with  $M_n \approx M_n^{\text{theo}}$  and  $\text{Đ} < 1.5$ . A more comprehensive study using several RAFT agents followed with good control and living behaviour for each of the four used.<sup>30</sup> The success of RAFT in scCO<sub>2</sub> is partly due to the lack of control agent partitioning seen with ATRP and NMP. Once the equilibrium is established the RAFT agent remains attached to a polymer chain at all times, which prevents it from dissolving in the continuous CO<sub>2</sub> phase.

### 1.3. Summary and Thesis Aims

This Chapter has introduced the fundamentals behind both radical and ring-opening polymerisation, with a focus on performing these reactions using scCO<sub>2</sub> as a solvent. The requirement for industrially applicable synthetic procedures using greener solvents and methodologies is growing, with scCO<sub>2</sub> a solvent that offers a viable solution to VOCs.<sup>109</sup>

Chapter 2 outlines the high pressure equipment and analytical techniques used throughout this Thesis. The development of a new high pressure X-ray sample cell for conducting *in situ* time-resolved X-ray scattering experiments in the pressure and temperature regime required (pressures up to 210 bar and temperatures up to 120 °C) is also described.

Although CO<sub>2</sub> itself is highly abundant from a number of natural and recycled sources, the cost of compressing a large quantity of the gas can be high. The majority of precipitation reactions utilise fairly low monomer loadings, typically between 10 -30 % v/v, therefore a high proportion of the reactor volume is composed of CO<sub>2</sub>. Chapter 3 details a synthetic method using a much higher monomer loading of 70% v/v, thus a far lower amount of CO<sub>2</sub>; this is known as scCO<sub>2</sub> expanded phase polymerisation.<sup>110</sup> The implementation of RAFT polymerisation into such a system is described, first for homopolymerisations, then onto the synthesis of oligomeric block copolymers. The aim is to completely remove the use of volatile organic solvents from these syntheses, whilst also removing the need for toxic and expensive stabilisers required in dispersion CO<sub>2</sub> systems.

Block copolymer micro-particles have been synthesised in a RAFT controlled scCO<sub>2</sub> dispersion polymerisation, with internal micro-phase separation.<sup>107, 108</sup> Preferential CO<sub>2</sub> interactions with certain blocks have been shown to alter the phase behaviour compared to conventionally produced micro-particles. Chapter 4 investigates the synthesis of these micro-particles in the new high pressure X-ray sample cell, with *in situ* scattering experiments used to determine how and when phase separation occurs. The results of

adding a cross-linking agent into this reaction are then presented, with the aim of retaining these structures upon thermal or solvent treatment.

Finally, the synthesis of PLA using stereoselective initiators is hindered by the high temperatures required to perform a melt polymerisation (>130 °C), with a loss of stereoselective control. CO<sub>2</sub> is known to plasticise this polymer, significantly lowering the temperature at which it liquefies.<sup>70</sup> Chapter 5 details the stereoselective synthesis of PLA in scCO<sub>2</sub>, with the objective to reduce the reaction temperature, whilst retaining the same activity and selectivity. This is then extended to the synthesis of PCL, opening up the possibility of creating biodegradable copolymers with targeted thermal and mechanical properties.

#### 1.4. References

1. C. E. Carraher, *Carraher's Polymer Chemistry*, Ninth edn., CRC Press, Taylor & Francis Group, 2014.
2. W. A. Braunecker and K. Matyjaszewski, *Progress in Polymer Science*, 2007, **32**, 93-146.
3. A. I. Cooper and J. M. DeSimone, *Current Opinion in Solid State & Materials Science*, 1996, **1**, 761-768.
4. J. L. Kendall, D. A. Canelas, J. L. Young and J. M. DeSimone, *Chemical Reviews*, 1999, **99**, 543-563.
5. R. F. T. Stepto, *Polymer International*, 2010, **59**, 23-24.
6. A. F. Parsons, *An Introduction to Free Radical Chemistry*, Blackwell Science, 2000.
7. M. Szwarc, *Nature*, 1956, **178**, 1168-1169.

8. A. D. Jenkins, R. G. Jones and G. Moad, *Pure and Applied Chemistry*, 2010, **82**, 483-491.
9. A. A. Gridnev and S. D. Ittel, *Chemical Reviews*, 2001, **101**, 3611-3659.
10. T. Otsu, *Journal of Polymer Science Part a-Polymer Chemistry*, 2000, **38**, 2121-2136.
11. P. Cacioli, E. Rizzardo and D. H. Solomon, *European Patent 135280*, 1985.
12. J. S. Wang and K. Matyjaszewski, *Journal of the American Chemical Society*, 1995, **117**, 5614-5615.
13. M. Kato, M. Kamigaito, M. Sawamoto and T. Higashimura, *Macromolecules*, 1995, **28**, 1721-1723.
14. J. Chiefari, Y. K. Chong, F. Ercole, J. Krstina, J. Jeffery, T. P. T. Le, R. T. A. Mayadunne, G. F. Meijs, C. L. Moad, G. Moad, E. Rizzardo and S. H. Thang, *Macromolecules*, 1998, **31**, 5559-5562.
15. R. P. N. Veregin, M. K. Georges, P. M. Kazmaier and G. K. Hamer, *Macromolecules*, 1993, **26**, 5316-5320.
16. C. J. Hawker, A. W. Bosman and E. Harth, *Chemical Reviews*, 2001, **101**, 3661-3688.
17. S. Grimaldi, J. P. Finet, F. Le Moigne, A. Zeghdaoui, P. Tordo, D. Benoit, M. Fontanille and Y. Gnanou, *Macromolecules*, 2000, **33**, 1141-1147.
18. Y. Guillaneuf, D. Gigmes, S. R. A. Marque, P. Astolfi, L. Greci, P. Tordo and D. Bertin, *Macromolecules*, 2007, **40**, 3108-3114.

19. H. D. Tang, M. Radosz and Y. Q. Shen, *Aiche Journal*, 2009, **55**, 737-746.
20. P. Corpart, D. Charmot, T. Biadatti, S. Zard and D. Michelet, *WIPO Patent WO/1998/058974*, 1998.
21. C. Barner-Kowollik and S. Perrier, *Journal of Polymer Science Part a-Polymer Chemistry*, 2008, **46**, 5715-5723.
22. S. Perrier and P. Takolpuckdee, *Journal of Polymer Science Part a-Polymer Chemistry*, 2005, **43**, 5347-5393.
23. C. Barner-Kowollik, *Handbook of RAFT Polymerisation*, Wiley-VCH, 2008.
24. G. Moad, E. Rizzardo and S. H. Thang, *Polymer*, 2008, **49**, 1079-1131.
25. J. Chiefari, R. T. A. Mayadunne, C. L. Moad, G. Moad, E. Rizzardo, A. Postma, M. A. Skidmore and S. H. Thang, *Macromolecules*, 2003, **36**, 2273-2283.
26. Y. K. Chong, J. Krstina, T. P. T. Le, G. Moad, A. Postma, E. Rizzardo and S. H. Thang, *Macromolecules*, 2003, **36**, 2256-2272.
27. A. B. Lowe and C. L. McCormick, *Progress in Polymer Science*, 2007, **32**, 283-351.
28. S. Perrier, T. P. Davis, A. J. Carmichael and D. M. Haddleton, *Chemical Communications*, 2002, 2226-2227.
29. K. J. Thurecht, A. M. Gregory, W. Wang and S. M. Howdle, *Macromolecules*, 2007, **40**, 2965-2967.
30. A. M. Gregory, K. J. Thurecht and S. M. Howdle, *Macromolecules*, 2008, **41**, 1215-1222.

31. G. Moad, J. Chiefari, Y. K. Chong, J. Krstina, R. T. A. Mayadunne, A. Postma, E. Rizzardo and S. H. Thang, *Polymer International*, 2000, **49**, 993-1001.
32. Y. K. Chong, T. P. T. Le, G. Moad, E. Rizzardo and S. H. Thang, *Macromolecules*, 1999, **32**, 2071-2074.
33. M. Benaglia, M. Chen, Y. K. Chong, G. Moad, E. Rizzardo and S. H. Thang, *Macromolecules*, 2009, **42**, 9384-9386.
34. M. Benaglia, J. Chiefari, Y. K. Chong, G. Moad, E. Rizzardo and S. H. Thang, *Journal of the American Chemical Society*, 2009, **131**, 6914-6915.
35. D. J. Keddie, C. Guerrero-Sanchez, G. Moad, E. Rizzardo and S. H. Thang, *Macromolecules*, 2011, **44**, 6738-6745.
36. D. J. Keddie, C. Guerrero-Sanchez, G. Moad, R. J. Mulder, E. Rizzardo and S. H. Thang, *Macromolecules*, 2012, **45**, 4205-4215.
37. G. Moad, E. Rizzardo and S. H. Thang, *Australian Journal of Chemistry*, 2005, **58**, 379-410.
38. A. Gregory and M. H. Stenzel, *Progress in Polymer Science*, 2012, **37**, 38-105.
39. D. Pissuwan, C. Boyer, K. Gunasekaran, T. P. Davis and V. Bulmus, *Biomacromolecules*, 2010, **11**, 412-420.
40. S. Perrier, P. Takolpuckdee and C. A. Mars, *Macromolecules*, 2005, **38**, 2033-2036.
41. H. Willcock and R. K. O'Reilly, *Polymer Chemistry*, 2010, **1**, 149-157.
42. G. Moad, E. Rizzardo and S. H. Thang, *Polymer International*, 2011, **60**, 9-25.

43. G. Moad, Y. K. Chong, A. Postma, E. Rizzardo and S. H. Thang, *Polymer*, 2005, **46**, 8458-8468.
44. M. Chen, G. Moad and E. Rizzardo, *Journal of Polymer Science Part a-Polymer Chemistry*, 2009, **47**, 6704-6714.
45. A. Goto and T. Fukuda, *Progress in Polymer Science*, 2004, **29**, 329-385.
46. S. Penczek and G. Moad, *Pure and Applied Chemistry*, 2008, **80**, 2163-2193.
47. P. Dubois, O. Coulembier and J.-M. Raquez, *Handbook of Ring-Opening Polymerization*, Wiley-VHC, Weinheim, 2009.
48. C. A. Eckert, B. L. Knutson and P. G. Debenedetti, *Nature*, 1996, **383**, 313-318.
49. J. M. DeSimone, *Science*, 2002, **297**, 799-803.
50. <http://webbook.nist.gov/chemistry/fluid/>, Accessed 16 February 2015.
51. W. Leitner, *Nature*, 2000, **405**, 129-130.
52. M. F. Kemmere and T. Meyer, *Supercritical Carbon Dioxide in Polymer Reaction Engineering*, Wiley-VCH, 2005.
53. E. J. Beckman, *Journal of Supercritical Fluids*, 2004, **28**, 121-191.
54. J. G. Stevens, P. Gomez, R. A. Bourne, T. C. Drage, M. W. George and M. Poliakoff, *Green Chemistry*, 2011, **13**, 2727-2733.
55. C. A. Eckert, J. G. Vanalsten and T. Stoicos, *Environmental Science & Technology*, 1986, **20**, 319-325.
56. J. M. DeSimone and W. Tumas, *Green Chemistry Using Liquid and Supercritical Carbon Dioxide*, Oxford University Press, 2003.

57. E. Girard, T. Tassaing, S. Camy, J. S. Condoret, J. D. Marty and M. Destarac, *Journal of the American Chemical Society*, 2012, **134**, 11920-11923.
58. S. G. Kazarian, M. F. Vincent, F. V. Bright, C. L. Liotta and C. A. Eckert, *Journal of the American Chemical Society*, 1996, **118**, 1729-1736.
59. T. Sarbu, T. Styranec and E. J. Beckman, *Nature*, 2000, **405**, 165-168.
60. B. Tan, H. M. Woods, P. Licence, S. M. Howdle and A. I. Cooper, *Macromolecules*, 2005, **38**, 1691-1698.
61. N. A. Birkin, N. J. Arrowsmith, E. J. Park, A. P. Richez and S. M. Howdle, *Polymer Chemistry*, 2011, **2**, 1293-1299.
62. E. J. Park, A. P. Richez, N. A. Birkin, H. Lee, N. Arrowsmith, K. J. Thurecht and S. M. Howdle, *Polymer*, 2011, **52**, 5403-5409.
63. F. Rindfleisch, T. P. DiNoia and M. A. McHugh, *Journal of Physical Chemistry*, 1996, **100**, 15581-15587.
64. A. I. Cooper, *Journal of Materials Chemistry*, 2000, **10**, 207-234.
65. T. Banerjee and G. C. Lipscomb, *Journal of Applied Polymer Science*, 1998, **68**, 1441-1449.
66. P. Alessi, A. Cortesi, I. Kikic and F. Vecchione, *Journal of Applied Polymer Science*, 2003, **88**, 2189-2193.
67. I. Kikic, F. Vecchione, P. Alessi, A. Cortesi, F. Eva and N. Elvassore, *Industrial & Engineering Chemistry Research*, 2003, **42**, 3022-3029.
68. D. L. Tomasko, H. B. Li, D. H. Liu, X. M. Han, M. J. Wingert, L. J. Lee and K. W. Koelling, *Industrial & Engineering Chemistry Research*, 2003, **42**, 6431-6456.

69. E. Tayton, S. Fahmy, M. Purcell, A. Aarvold, J. O. Smith, S. Kalra, A. Briscoe, S. Lanham, S. Howdle, K. Shakesheff, D. G. Dunlop and R. O. C. Oreffo, *Journal of Biomedical Materials Research Part A*, 2012, **100A**, 3211-3219.
70. E. Tayton, M. Purcell, A. Aarvold, J. O. Smith, S. Kalra, A. Briscoe, K. Shakesheff, S. M. Howdle, D. G. Dunlop and R. O. C. Oreffo, *Acta Biomaterialia*, 2012, **8**, 1918-1927.
71. M. Tang, M. Purcell, J. A. M. Steele, K. Y. Lee, S. McCullen, K. M. Shakesheff, A. Bismarck, M. M. Stevens, S. M. Howdle and C. K. Williams, *Macromolecules*, 2013, **46**, 8136-8143.
72. C. D. Wood, A. I. Cooper and J. M. DeSimone, *Current Opinion in Solid State & Materials Science*, 2004, **8**, 325-331.
73. J. M. DeSimone, Z. Guan and C. S. Elsbernd, *Science*, 1992, **257**, 945-947.
74. F. A. Adamsky and E. J. Beckman, *Macromolecules*, 1994, **27**, 312-314.
75. Z. B. Guan, J. R. Combes, Y. Z. Menciloglu and J. M. Desimone, *Macromolecules*, 1993, **26**, 2663-2669.
76. T. J. Romack, E. E. Maury and J. M. DeSimone, *Macromolecules*, 1995, **28**, 912-915.
77. T. Liu, J. M. DeSimone and G. W. Roberts, *Journal of Polymer Science Part a-Polymer Chemistry*, 2005, **43**, 2546-2555.
78. T. Liu, J. M. DeSimone and G. W. Roberts, *Polymer*, 2006, **47**, 4276-4281.

79. T. Liu, P. Garner, J. M. DeSimone, G. W. Roberts and G. D. Bothun, *Macromolecules*, 2006, **39**, 6489-6494.
80. T. Liu, J. M. DeSimone and G. W. Roberts, *Chemical Engineering Science*, 2006, **61**, 3129-3139.
81. P. A. Charpentier, K. A. Kennedy, J. M. DeSimone and G. W. Roberts, *Macromolecules*, 1999, **32**, 5973-5975.
82. M. Okubo, S. Fujii, H. Maenaka and H. Minami, *Colloid and Polymer Science*, 2002, **280**, 183-187.
83. H. Lee, E. Terry, M. Zong, N. Arrowsmith, S. Perrier, K. J. Thurecht and S. M. Howdle, *Journal of the American Chemical Society*, 2008, **130**, 12242-12243.
84. J. M. Desimone, E. E. Maury, Y. Z. Menciloglu, J. B. McClain, T. J. Romack and J. R. Combes, *Science*, 1994, **265**, 356-359.
85. H. S. Hwang, Y. S. Gal, K. P. Johnston and K. T. Lim, *Macromolecular Rapid Communications*, 2006, **27**, 121-125.
86. H. S. Hwang and K. T. Lim, *Macromolecular Rapid Communications*, 2006, **27**, 722-726.
87. H. Yuvaraj, H. S. Hwang, W. S. Kim, H. G. Kim, E. D. Jeong and K. T. Lim, *European Polymer Journal*, 2008, **44**, 2253-2261.
88. W. X. Wang, A. Naylor and S. M. Howdle, *Macromolecules*, 2003, **36**, 5424-5427.
89. D. A. Canelas, D. E. Betts and J. M. DeSimone, *Macromolecules*, 1996, **29**, 2818-2821.
90. A. I. Cooper, W. P. Hems and A. B. Holmes, *Macromolecular Rapid Communications*, 1998, **19**, 353-357.

91. A. I. Cooper, W. P. Hems and A. B. Holmes, *Macromolecules*, 1999, **32**, 2156-2166.
92. M. R. Giles, R. M. T. Griffiths, D. J. Irvine and S. M. Howdle, *European Polymer Journal*, 2003, **39**, 1785-1790.
93. T. Casimiro, A. M. Banet-Osuna, A. M. Ramos, M. N. da Ponte and A. Aguiar-Ricardo, *European Polymer Journal*, 2005, **41**, 1947-1953.
94. W. X. Wang, M. R. Giles, D. Bratton, D. J. Irvine, S. P. Armes, J. V. W. Weaver and S. M. Howdle, *Polymer*, 2003, **44**, 3803-3809.
95. P. B. Zetterlund, F. Aldabbagh and M. Okubo, *Journal of Polymer Science Part a-Polymer Chemistry*, 2009, **47**, 3711-3728.
96. F. Aldabbagh, P. B. Zetterlund and M. Okubo, *European Polymer Journal*, 2008, **44**, 4037-4046.
97. P. O'Connor, P. B. Zetterlund and F. Aldabbagh, *Macromolecules*, 2010, **43**, 914-919.
98. J. Ryan, F. Aldabbagh, P. B. Zetterlund and M. Okubo, *Polymer*, 2005, **46**, 9769-9777.
99. R. McHale, F. Aldabbagh, P. B. Zetterlund, H. Minami and M. Okubo, *Macromolecules*, 2006, **39**, 6853-6860.
100. J. H. Xia, T. Johnson, S. G. Gaynor, K. Matyjaszewski and J. DeSimone, *Macromolecules*, 1999, **32**, 4802-4805.
101. H. Minami, Y. Kagawa, S. Kuwahara, J. Shigematsu, S. Fujii and M. Okubo, *Designed Monomers and Polymers*, 2004, **7**, 553-562.
102. B. Grignard, C. Calberg, C. Jerome, W. X. Wang, S. Howdle and C. Detrembleur, *Chemical Communications*, 2008, 5803-5805.

103. B. Grignard, C. Jerome, C. Calberg, R. Jerome, W. X. Wang, S. M. Howdle and C. Detrembleur, *Macromolecules*, 2008, **41**, 8575-8583.
104. B. Grignard, C. Calberg, C. Jerome and C. Detrembleur, *Journal of Supercritical Fluids*, 2010, **53**, 151-155.
105. T. Arita, S. Beuermann, M. Buback and P. Vana, *E-Polymers*, 2004.
106. T. Arita, S. Beuermann, M. Buback and P. Vana, *Macromolecular Materials and Engineering*, 2005, **290**, 283-293.
107. J. Jennings, M. Beija, A. P. Richez, S. D. Cooper, P. E. Mignot, K. J. Thurecht, K. S. Jack and S. M. Howdle, *Journal of the American Chemical Society*, 2012, **134**, 4772-4781.
108. J. Jennings, M. Beija, J. T. Kennon, H. Willcock, R. K. O'Reilly, S. Rimmer and S. M. Howdle, *Macromolecules*, 2013, **46**, 6843-6851.
109. F. Picchioni, *Polymer International*, 2014, **63**, 1394-1399.
110. K. Adlington, A. Green, W. X. Wang, S. M. Howdle and D. J. Irvine, *Dalton Transactions*, 2013, **42**, 127-136.

## Chapter 2 - Equipment and Characterisation

---

### 2. Overview

This Chapter describes the experimental apparatus used throughout this Thesis. The first section outlines the high pressure equipment including the stainless steel clamp-sealed autoclaves and high pressure monomer addition system *via* the attached HPLC pump. Experimental procedures are then summarised covering the standard operating procedures for all equipment used. Two view cells are then introduced; used to study the phase behaviour and effect of CO<sub>2</sub> under high pressure conditions. Further details related to specific reactions can be found in the individual Chapters. The second section focusses on the analytical techniques used to characterise all products in this Thesis.

### 2.1 High Pressure Equipment

#### 2.1.1. CO<sub>2</sub> Pump

For all high pressure experiments the CO<sub>2</sub> was delivered by a PM-101 high pressure pump (New Ways of Analytics, Germany), with a schematic shown in Figure 2-1. The CO<sub>2</sub> is introduced from a cylinder at ~ 55 bar, monitored by the first pressure dial, through a refrigerated condenser to ensure liquid phase CO<sub>2</sub> fills the pump. The dual piston pump is driven by compressed air at 3 – 5 bar which compresses the CO<sub>2</sub> to the required reaction pressure, usually 300 bar, monitored by the second pressure dial. By opening, HIP (b) (Figure 2-1) the CO<sub>2</sub> can be distributed to individual fume hoods.

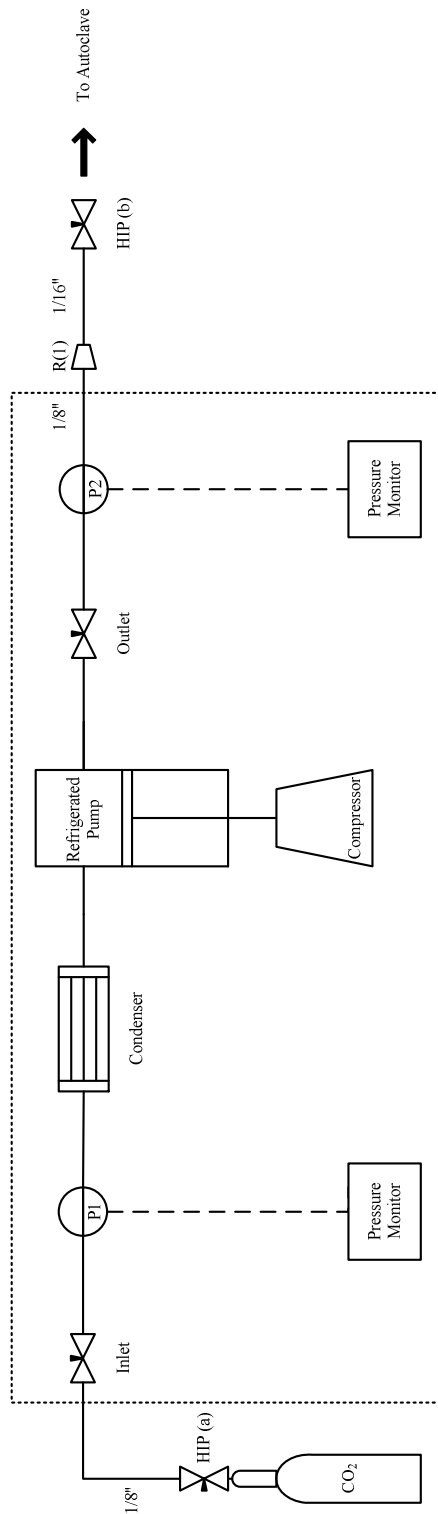


Figure 2-1. High pressure pump schematic.

*2.1.2. High Pressure Setup*

Each setup consists of the pump, an autoclave, associated pipe work and electronics. Figure 2-2 is a simplified schematic showing the pump system linked to the autoclave. All pipes are Swagelok SS316, with taps purchased from HIP (High Pressure Equipment) to control the CO<sub>2</sub> flow. Non-return valves are placed before each autoclave to prevent reagents flowing back into the pump.

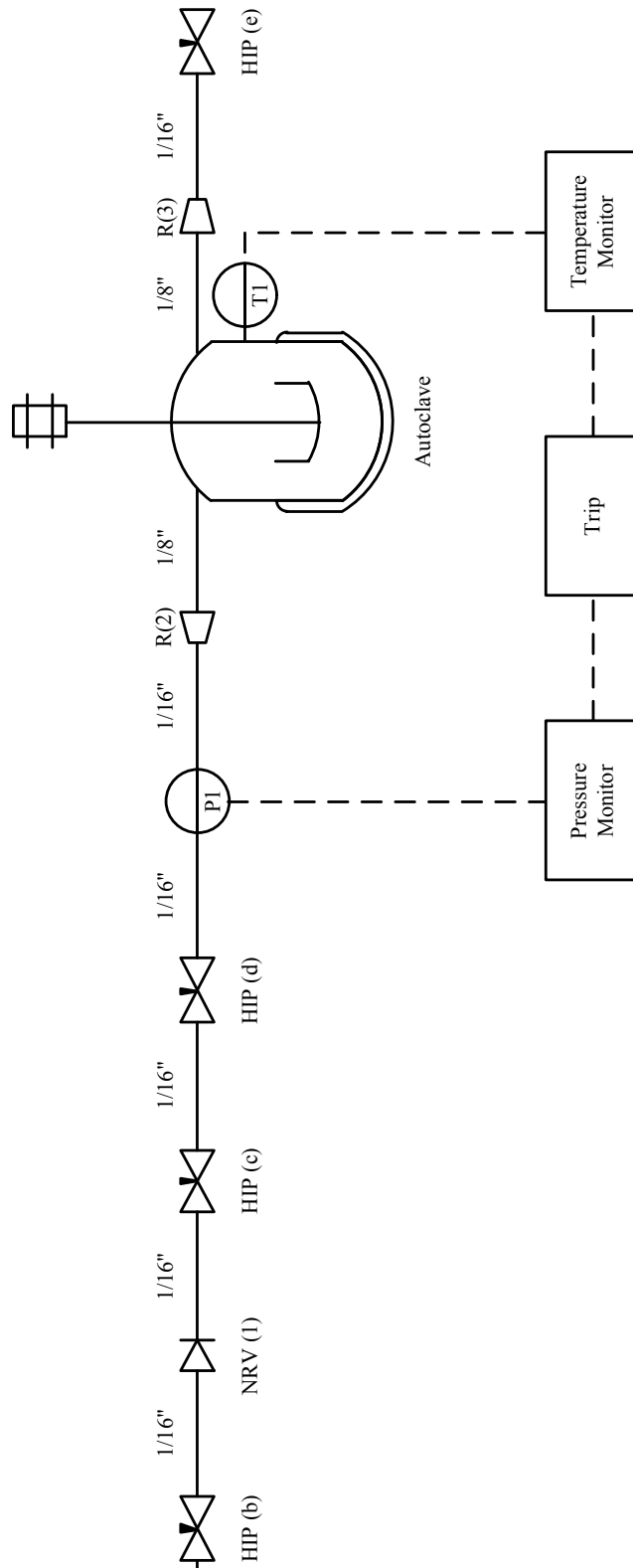
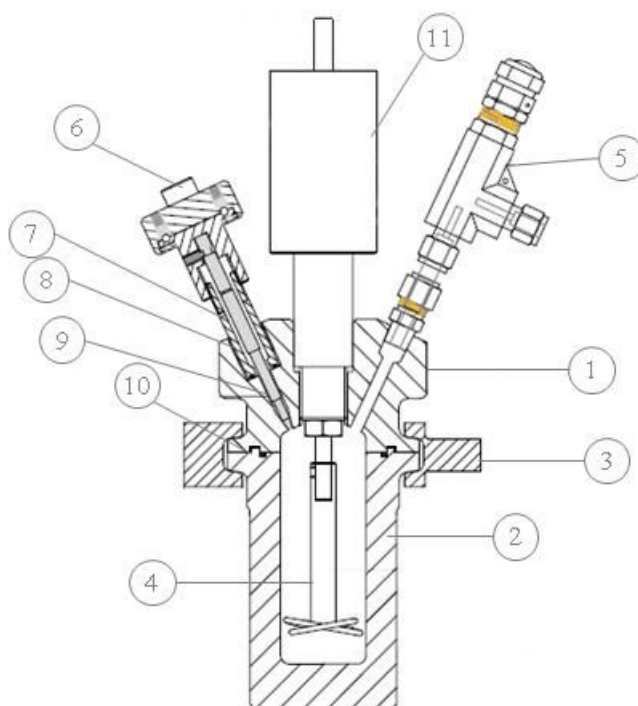


Figure 2-2 Schematic diagram for an individual high pressure setup.

HIP (b) connects to the pump setup

## 2.1.3. MKIII Autoclave

High pressure autoclaves, developed at The University of Nottingham, were used for polymerisations in supercritical carbon dioxide (scCO<sub>2</sub>). A schematic is shown in Figure 2-3, with images in Figure 2-4. The maximum working pressure is 300 bar (4350 psi) at 300 °C.



**Figure 2-3. Schematic representation of a 60 mL clamp-sealed stainless steel autoclave. (1) Head, (2) Cell Body, (3) Clamp, (4) Stirrer Blade, (5) Spring Loaded Pressure Relief Valve, (6) Torque Thumbwheel, (7) Vent Hole, (8) Screw Insert, (9) Safety Needle, (10) EPDM O-ring, (11) Magnetically Coupled Overhead Stirrer.**

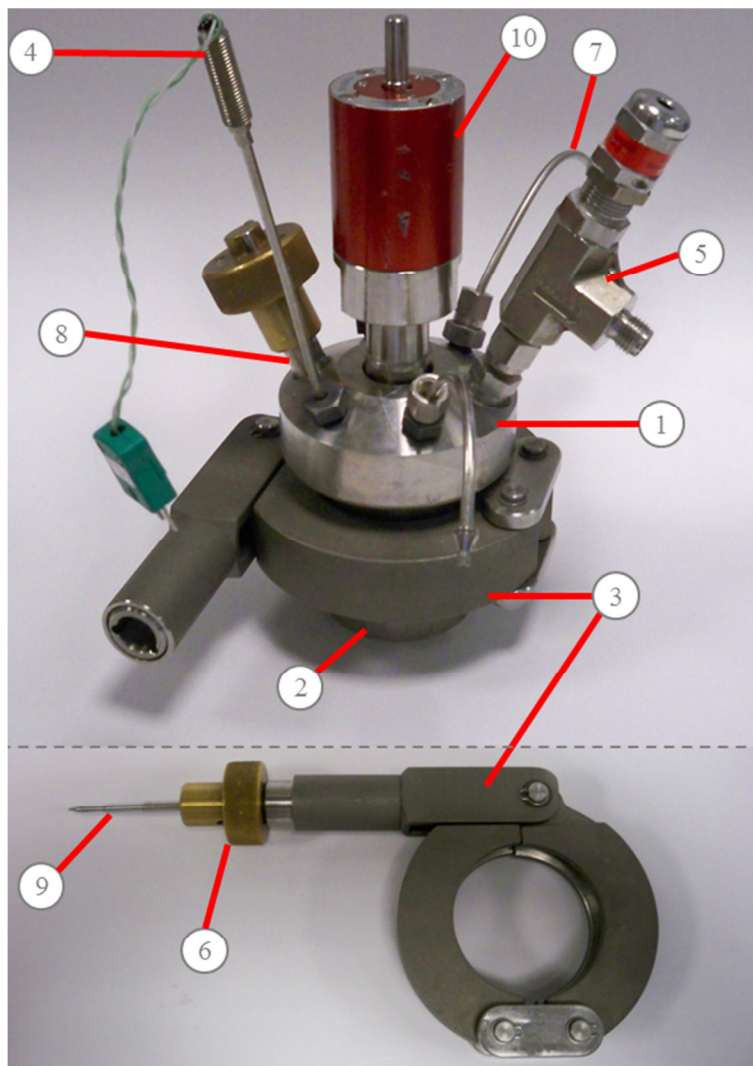


**Figure 2-4. 20 mL clamp-sealed stainless steel autoclave. (1) Head, (2) Cell Body, (3) Clamp, (4) Thermocouple, (5) Spring Loaded Pressure Relief Valve, (6) Torque Thumbwheel, (7) 1/8" SS316 tubing, (8) Screw Insert, (9) Safety Needle, (10) Magnetically Coupled Overhead Stirrer.**

Each autoclave consists of two main sections, the head and the body. The autoclave head contains the required ports for addition of reagents and monitoring purposes, with the heated body providing the bulk volume of the reactor. The two parts are sealed by an O-ring placed between matching faces on the head and body. Typically Ethylene Propylene Diene Monomer (EPDM) O-rings are used. This limits the autoclave for safe operating use between -55 and 150 °C, although typically a maximum temperature of 130 °C is used in case of over temperature. A stainless steel clamp holds the two parts together which is secured by a screw mechanism, tightened with a unique key. This key is located on the safety needle assembly, which is screwed into the autoclave head to create a final seal before pressurising. A torque thumbwheel (Figure 2-3 (6)) is employed to prevent over-tightening of the key, potential damage to the fragile safety needle and subsequent problems with leaks. Two safety features arise from this assembly, firstly that the clamp cannot be undone whilst the autoclave is still under pressure. Secondly, in the event of a valve blockage during the venting process the key can be loosened slowly with the residual pressure being released *via* the vent hole (Figure 2-3, (7)). 1/8" Swagelok SS316 pipe is used for both the CO<sub>2</sub> inlet and outlet vent lines, secured in place using brass nuts and ferrules (Autoclave Engineers). An internal thermocouple (SS316 sheathed K-type, RS Components, Ø = 1.5 mm) is used to control the reaction temperature. The thermocouple is connected to an external heating jacket (Watlow) controlled to ± 1 °C using a Cal 3200 digital heating controller (RS, UK). The pressure is monitored with a quartz piezoelectric transducer (345 bar (5000 psi) RDP Electronics). A digital read out is generated by an electrical current emitted when the quartz crystal

experiences strain under pressure, displayed in pounds-per-square-inch on an in-house manufactured monitor. In the event of the pressure exceeding the 300 bar (4350 psi) maximum an electrical trip is incorporated which disconnects power to the heating jacket, reducing the temperature and subsequently the pressure.

The operational integrity of the cell is protected by a spring loaded pressure relief valve (Swagelok SS-4R3A, maximum pressure 300 bar), connected to the head through a 1/8" NPT fitting (S-400-1-2) and 1/4" SS316 pipe. If the pressure exceeds the maximum the valve is forced open to relieve the pressure, and once below this level the valve re-seals and the reaction can proceed.

A magnetically coupled stirrer (Figure 2-3, (11)) is located in the centre of the autoclave head, extending into the body. A number of different stirrer blades can be attached to the shaft depending on the size of the autoclave and also the type of mixing required. The stirrer is driven by a motor (IKA Eurostar Digital) at between 50 - 2000 rpm, with a typical reaction at 300 rpm.

A standard procedure was used for all reactions in MKIII autoclaves, with some modifications to the methods depending on the type of reaction required. All taps and pipes in the following procedure relate to Figure 2-2, with the taps associated with the pump (HIP (a) and (b)) remaining open for the duration of the experiment.

1. An EPDM o-ring was placed in the body, then the head and body clamped together. The clamp was tightened using the safety key which was then screwed into the head. The inlet and outlet pipes were attached and tightened (reducing unions R2 and R3), then the heating jacket was secured around the body.
2. The setup was leak tested by pressurising to  $\sim 138$  bar (2000 psi) by opening HIP (c) and (d), keeping HIP (e) closed. All fittings were checked for leaks with 'Snoop' (Sigma Aldrich).
3. If required, the autoclave was vented to ambient pressure through HIP (e) and any leaking fittings adjusted. (Fittings were never tightened under pressure).
4. Steps 2 and 3 were repeated until no leaks were visible then any remaining gas was vented until the autoclave was at atmospheric pressure.
5. In order to remove residual oxygen the key was removed, HIP (e) closed and CO<sub>2</sub> flowed through the open key hole at  $\sim 2$  bar (30 psi) for 30 minutes (HIP (c) and (d) partially open).
6. A monomer solution was added through the open key hole with the positive pressure of CO<sub>2</sub> to ensure no oxygen entered the vessel. The key was then screwed in and the pressure was raised to  $\sim 50$  bar (725 psi).
7. The stirrer was switched on, set to 300 rpm, and the CO<sub>2</sub>/monomer solution mixed for 10 minutes.
8. The internal thermocouple and heating band were connected to the control box and set to the desired temperature with the pressure monitored throughout.

9. The autoclave was allowed to reach its final temperature and the pressure increased to 276 bar (4000 psi) by slow addition of CO<sub>2</sub>. Note that this process caused the cell to cool slightly, so the temperature was allowed to stabilise after each addition of CO<sub>2</sub>.
10. After the desired reaction time, the autoclave was quenched by switching off and removing the heating band allowing the temperature to cool to ambient. This was accelerated by placing the vessel in a dry ice/acetone bath.
11. Once at ambient, the CO<sub>2</sub> was vented into the fume hood by opening HIP (e). Generally this was over a 30 minute period.
12. Once at ambient temperature and pressure, the safety key was removed, reducing unions R2 and R3 disconnected, the clamp opened and the product collected.

#### *2.1.4. In-situ Monomer Addition via HPLC Pump*

A modified autoclave has also been developed at The University of Nottingham with the option to add liquid reagents whilst still under pressure. An extra port has been added in the head with a 1/8" to 1/16" union screwed into this to connect the autoclave to the HPLC pump. An HIP tap is inserted to separate the pump setup from the vessel and enable the reagent addition. A pipe schematic is shown in Figure 2-5 with a schematic of the modified head in Figure 2-6. The SOP for this modified head is identical to a standard MKIII autoclave with the addition of attaching the 1/8" to 1/16" reducer in the top and the HIP tap, both of which were leak tested prior to use. Two separate HPLC pumps have been used for this work; the first a Gilson 305 and the second a

Jasco PU980. The following standard operating procedure was identical for both pumps.

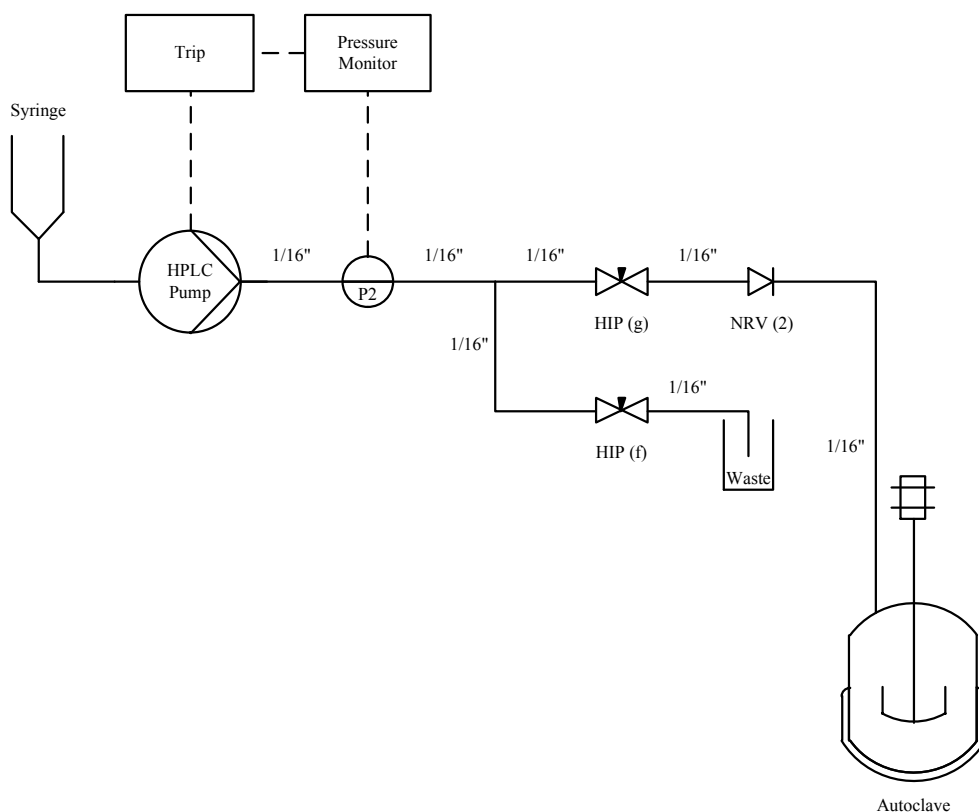


**Figure 2-5. HPLC schematic**

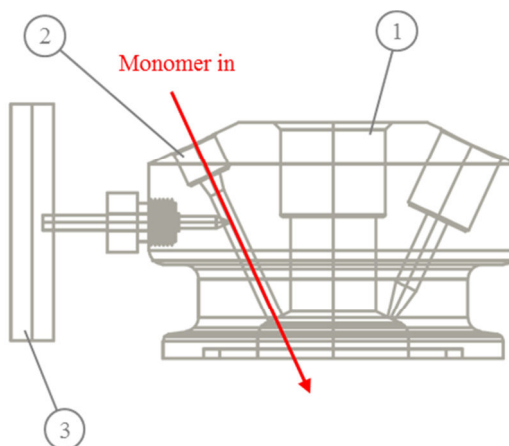


**Figure 2-6. Schematic representation of a modified MKIII head to include an HIP tap for monomer addition under high pressure. (1) Head, (2) 1/8" Swagelok port to connect to HPLC setup, (3) Built-in HIP tap.**

1. The first block was left at 276 bar (4000 psi) and 65 °C for the desired reaction time, following the procedure in section 0.
2. The autoclave was vented to ~ 200 bar (2900 psi) by opening HIP (e). This enabled space to be created for the addition of the second monomer which would have increased the pressure above the 300 bar safety limit.
3. The HPLC setup was connected to the 1/8" to 1/16" reducing union in the autoclave head (Figure 2-6).
4. The degassed monomer/initiator solution was transferred to the syringe attached to HPLC inlet.
5. The pump was primed by opening HIP (f), ensuring taps leading to the autoclave (HIP (g)) were closed. Monomer solution was then flowed through the line for a few seconds.
6. HIP (f) was closed and the built-in tap on the autoclave opened.
7. HIP (g) was opened with an increase in back pressure monitored through the pressure monitor connected to P2.
8. The monomer solution was pumped at 3 mL min<sup>-1</sup> until the pressure of the pump was equal to the pressure inside the autoclave.
9. The monomer level in the syringe was noted and the desired amount of solution added, taking into account dead volume between the entry pipe and the autoclave head (taken to be 1 mL). The autoclave pressure was monitored throughout.
10. The pump was stopped and the built-in tap closed.
11. The HPLC setup was detached by removing the 1/16" fitting. Some monomer solution remained in the pipe so this was opened slowly to release residual pressure.

12. To clean the HPLC setup HIP (f) and (g) were opened and solvent flushed through the pipes.

13. If the pressure of the autoclave was not at 276 bar then more CO<sub>2</sub> was added to raise it back to this level.

#### 2.1.5. High Pressure View Cell

To study the behaviour of the reagents and resulting polymers under high pressure conditions two view cells have been utilised. The first is a fixed volume view cell with a volume of ~ 100 mL. The basic design is identical to the MKIII autoclave, consisting of a heated body attached to two heads utilising the same key and clamp system (Figure 2-7). The autoclave itself is attached with the same inlet and outlet 1/8" SS316 tubing through the side of the body, connected to the high pressure line as with the MKIII vessel. The standard operation procedure was as follows:

1. The two heads were assembled:
  - a. Teflon spacers were placed in the crevice.
  - b. EPDM o-rings were fitted around the sapphire window.
  - c. The head was laid onto a level surface and the sapphire window inserted, kept straight at all times.
2. An o-ring was placed in the body at the rear end, then the back head and body clamped together. The clamp was tightened using the safety key. The body was positioned on a purpose-built stand and secured in place. The inlet and outlet pipes were attached and tightened (reducing unions R2 and R3), then the heating cartridges were slotted into the body.

3. An o-ring was placed in the front end of the body, then the front head and body clamped together. The clamp was tightened using the safety key which was then screwed into the body as shown in Figure 2-7.
4. The safety screen was position in front of the window, removing only when at ambient pressure.
5. The setup was leak tested by pressurising to ~ 100 bar (1450 psi) by opening HIP (c) and (d), keeping HIP (e) closed. All fittings were checked for leaks with 'Snoop' (Sigma Aldrich).
6. If required, the autoclave was vented to ambient pressure through HIP (e) and any leaking fittings adjusted. (Fittings were never tightened under pressure).
7. Steps 5 and 6 were repeated until no leaks were visible then any remaining gas was vented until the autoclave was at atmospheric pressure.
8. The key was removed, the front end opened. Solid materials contained in an open glass vial were placed inside. The front end was then re-sealed.
9. If removal of residual oxygen was required, HIP (e) was closed and CO<sub>2</sub> flowed through the open key hole at ~ 2 bar (30 psi) for 30 minutes (HIP (c) and (d) partially open).
10. If liquid reactants were required they were added by injecting through the still open safety valve. . The key was then screwed in and the pressure increased to ~ 50 bar (725 psi).
11. The safety screen was positioned in front of the window.
12. The internal and external thermocouples and heating cartridges were connected to the control box and set to the desired temperature with the pressure monitored throughout. A lag was observed between the internal and

external thermocouple due to the increased wall thickness relative to the MKIII autoclave.

13. The autoclave was heated to its target temperature and the pressure increased to the experimental conditions by slow addition of CO<sub>2</sub>.

14. Temperature and pressure were then varied dependent on the experiment.

15. Once complete, the autoclave was quenched by switching off the heating cartridges, allowing the temperature to cool to ambient.

16. The CO<sub>2</sub> was vented into the fume hood by opening HIP (e). Generally this was over a 30 minute period.

17. Once at ambient temperature and pressure, the safety key was removed, reducing unions R2 and R3 disconnected, the front end clamp opened and the product collected.

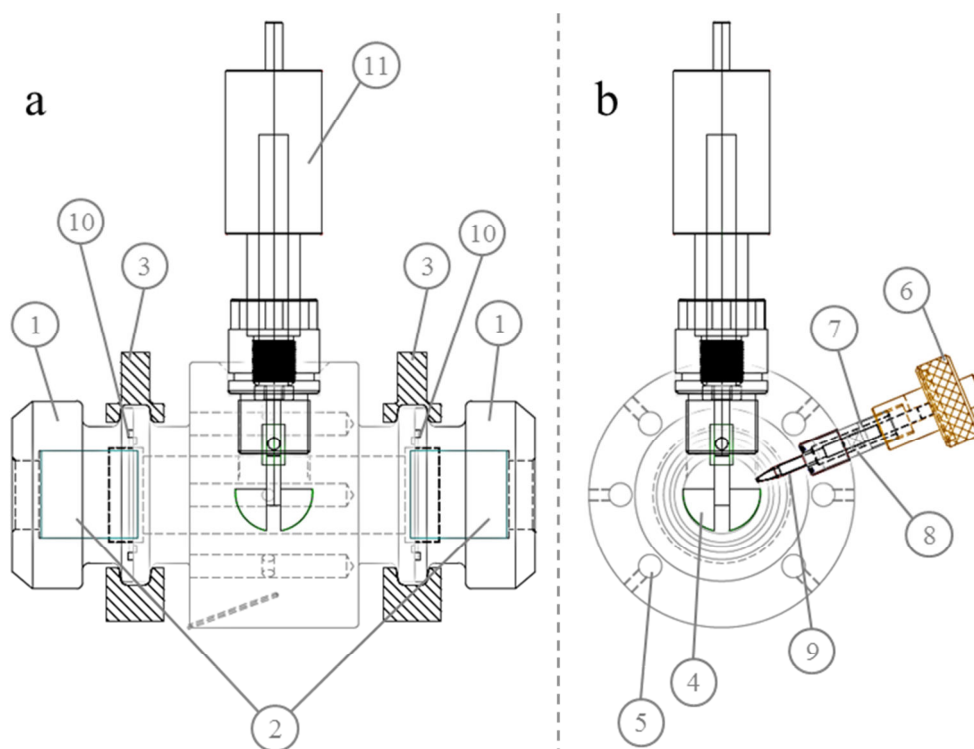


**Figure 2-7. Schematic representation of a 100 mL clamp-sealed stainless steel autoclave with dual viewing ports (a) side view, (b) front-end view.**

**Labels as follows: (1) Head, (2) Sapphire Windows, (3) Clamp, (4) Stirrer Blade, (5) Heating Cartridges, (6) Torque Thumbwheel, (7) Vent Hole, (8) Screw Insert, (9) Safety Needle, (10) EPDM O-ring, (11) Magnetically Coupled Overhead Stirrer.**

#### *2.1.6. Variable Volume High Pressure View Cell*

The variable volume view cell is similar to the fixed volume equivalent; the body has six cartridge heaters to vary temperature and two clamp-sealed heads housing sapphire windows. In this case a magnetic stirrer bar inside the cell is used to mix reagents. The setup for delivery CO<sub>2</sub> and changing pressure however is vastly different, and has been described elsewhere (Figure 2-8).<sup>1</sup>

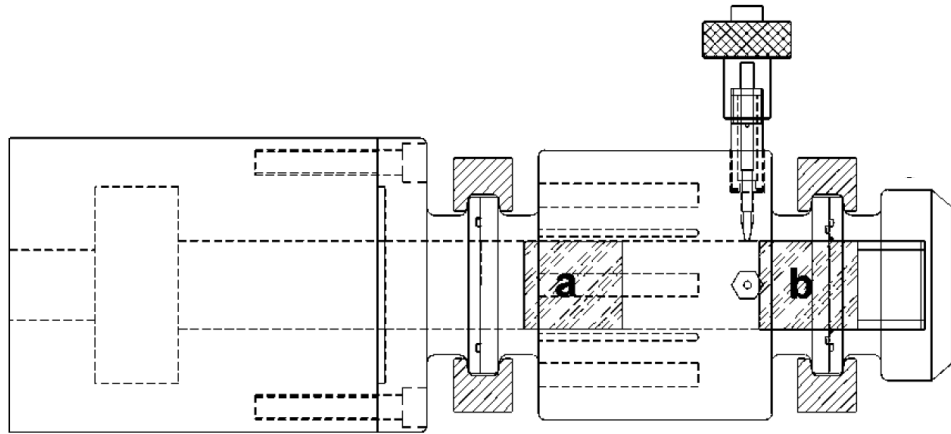


**Figure 2-8. Variable volume view cell as described by Licence *et al.*<sup>1</sup> (a) sapphire piston (b) static sapphire window**

Briefly, a hollow hydraulic ram is connected to the back window enabling the volume of the cell to be varied, which can increase or decrease the pressure. The CO<sub>2</sub> is initially delivered from a high pressure bomb, filling the cell to approximately 60 bar (870 psi) and the effect of heating and lowering the volumes allows the temperature and pressure to be raised to supercritical conditions.

#### 2.1.7. X-ray Cell MKI

A high pressure cell suitable to be operated at 210 bar and 120 °C has been constructed from AISI 316/316L EN1.4401/4404 certified stainless steel. The design is based on the MKIII high pressure autoclave introduced in 2.1.3. with the key difference being the addition of two diamond windows housed in the body of the vessel. These windows are interchangeable allowing difference path lengths to be utilised depending upon the desired experiment, with the diamonds suitable for both x-ray and neutron scattering experiments. As with

MKIII, the cell is split into several components, mainly the head and body as detailed in Figure 2-9.

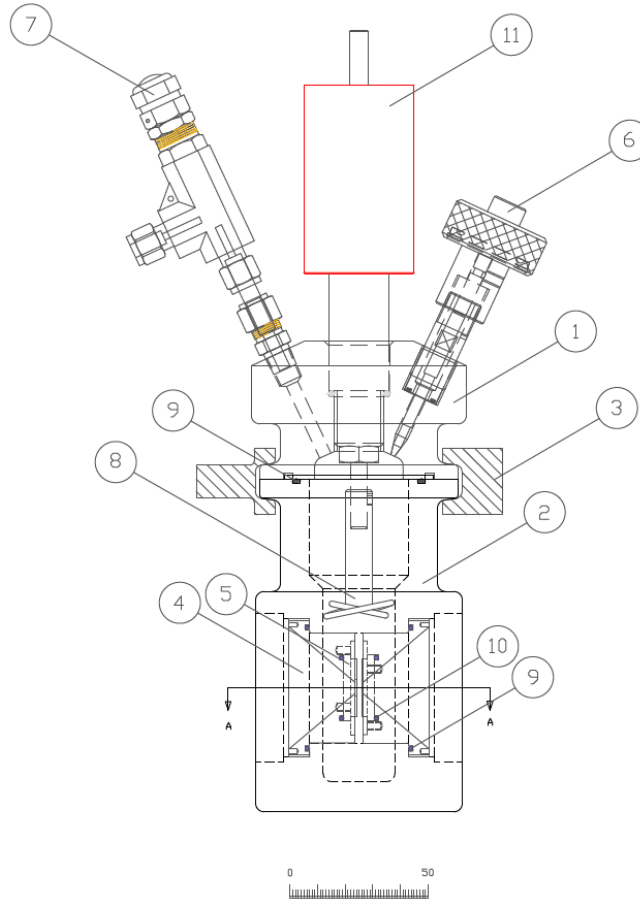


**Figure 2-9. Engineering drawing showing details of the high pressure X-ray scattering cell (units in mm) consisting of (1) Head, (2) Cell Body, (3) Clamp, (4) Screwed Window Holder, (5) Carbide Window Holder, (6) Safety Needle Assembly, (7) Swagelok Blow Off Valve, (8) Paddle Stirrer, (9) O-ring (EPDM 42 mm x 2 mm), (10) O-ring (BS019 EPDM 35 mm x 1.78 mm) and (11) Overhead Magnetic Stirrer.**

The head section contains the connections for the required services such as gas inlets and outlets, stirring, and over pressure safety devices. The head is joined to the body *via* the same clamping mechanism as with the MKIII cell,

utilising a safety key to prevent the cell being opened whilst still under pressure. The versatile head design would allow further auxiliary techniques such as a Differential Scanning Calorimetry (DSC), FT-IR, or Raman spectroscopy to be added to the head or body in the future.

The body is where the main modifications have been made; containing two threaded mounts to house the diamond windows. The opening angle for the windows is  $40^\circ$  which allows simultaneous SAXS/WAXS experiments and the optical pathway is set to 2.5 mm to optimise both transmission and representative sampling (Figure 2-10, Figure 2-11). The windows are made of a synthetic single crystal diamond type III supplied by Element 6. The window dimensions are 6 mm in diameter with 4 mm clear optical aperture and the thickness is  $0.4 \text{ mm} \pm 0.05 \text{ mm}$ . The diamond windows are coated with Au/Sn (80/20) on the 2 mm external diameter. The window mount is manufactured from 6% cobalt tungsten carbide which provides a thermal expansion coefficient matched with diamond. The soldering material (Ti-60 nm/Pt-120/Au-1000 nm) has been coated on the mount and brazed to the windows at  $280^\circ\text{C}$  (melting point).

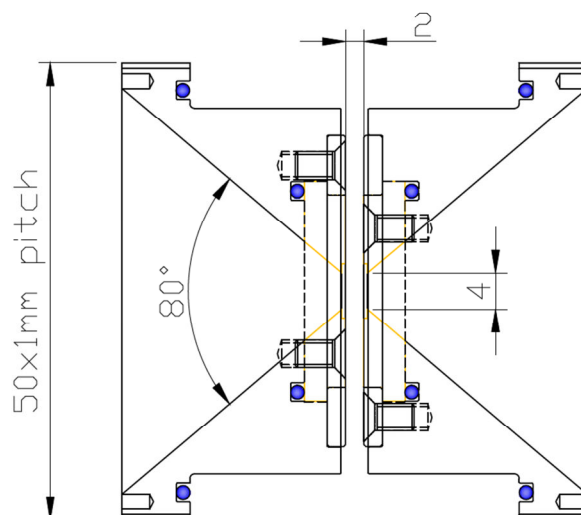


**Figure 2-10. Diamond window inserts showing the 40° clear optical aperture for collecting simultaneous SAXS-WAXS. The free window diameter is 4 mm and the exit opening angle is 40°. All values on the diagram are in mm.**

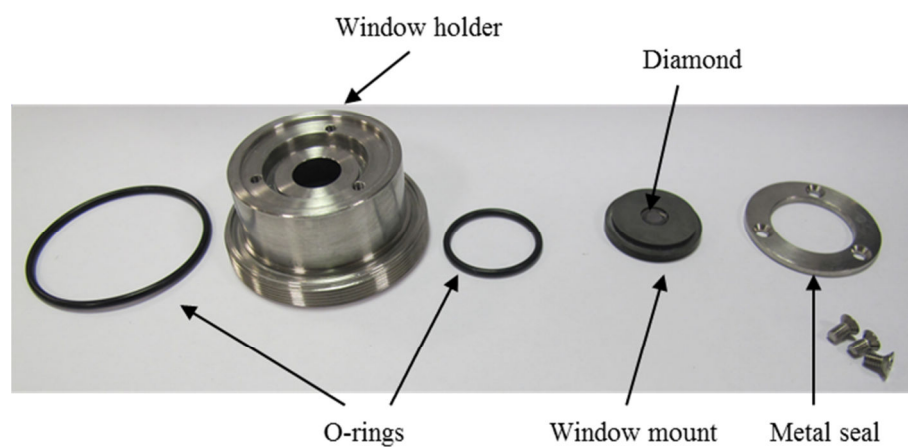


**Figure 2-11. Images of a window holder broken down into its component parts.**

The distance between the windows can be varied by interchanging the threaded mounts to create a different optical path length for different experiments. This is required to be able to optimise the X-ray path length as a function of scattering density contrast and wavelength versus absorption.

The temperature within the autoclave is regulated by means of an external heating jacket controlled to  $\pm 1$  °C using a Cal 3200 digital heating controller (RS, UK). The reaction conditions are monitored *via* an internal thermocouple (RS, 316 stainless steel sheathed K-type thermocouple,  $\text{Ø} = 1.5$  mm) and external pressure transducers (RDP Electronics type A-105 transducer, 690 bar maximum). HIP high pressure valves and Swagelok tubing and fittings were adopted to connect the system to the pump. A high pressure PM101 pump (New Ways of Analytics, Lörrach (Baden-Württemberg), Germany) was used to charge CO<sub>2</sub> into the autoclave. An HPLC pump (JASCO PU-980) can be connected for the addition of the second monomer. The pumps and controllers are housed on a trolley for mobility between laboratories. Finally an insulating cell holder has been designed to place the cell on the centre of mass of the sample pillar of BM26-b @ ESRF to assist in the alignment process (Figure 2-13). Figure 2-13 shows the schematic diagram of the pipe set up including where the HPLC pump can be attached when required.

The operational integrity of the cell is protected by two devices, Safety 1 and 2. Safety 1 (Figure 2-9, Label (7)) is a preset spring loaded proportional relief valve, set to 240 bar to protect the working integrity of the cell. Safety 2 is a 310 bar rupture disc to protect the structural integrity of the cell. The elastomeric seals are Ethylene Propylene Diene Monomer (EPDM, -55 to 150 °C), although these can be changed dependent on which reaction is under study. The cell has an estimated safe life time of 1000 cycles.



**Figure 2-12(Left) High pressure cell with pump and control box. (Right) Cell aligned in the beamline with SAXS and WAXS detectors.**

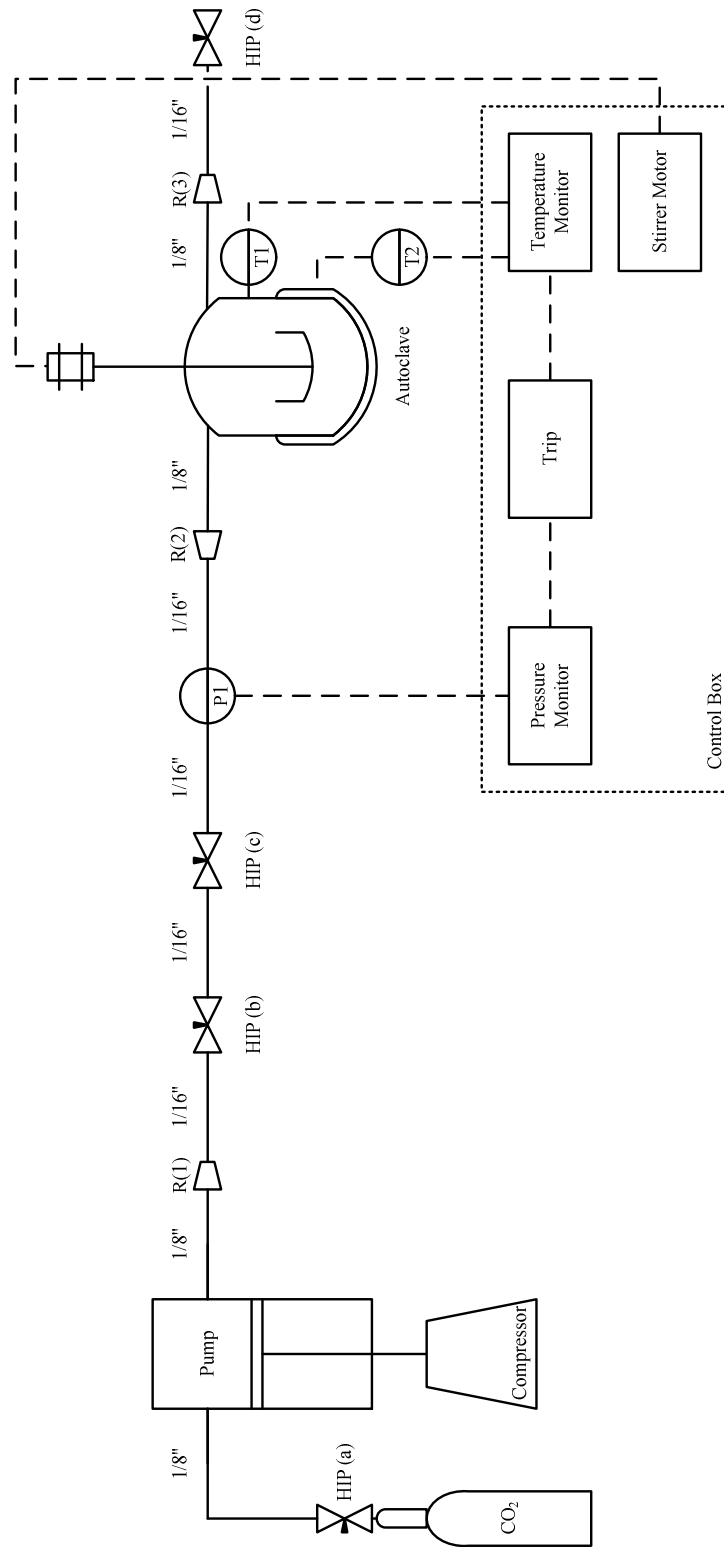


**Figure 2-13. Pipe and Engineering Drawings for the X-ray Scattering Cell. PM101 pump is used to introduce CO<sub>2</sub> into the system.**

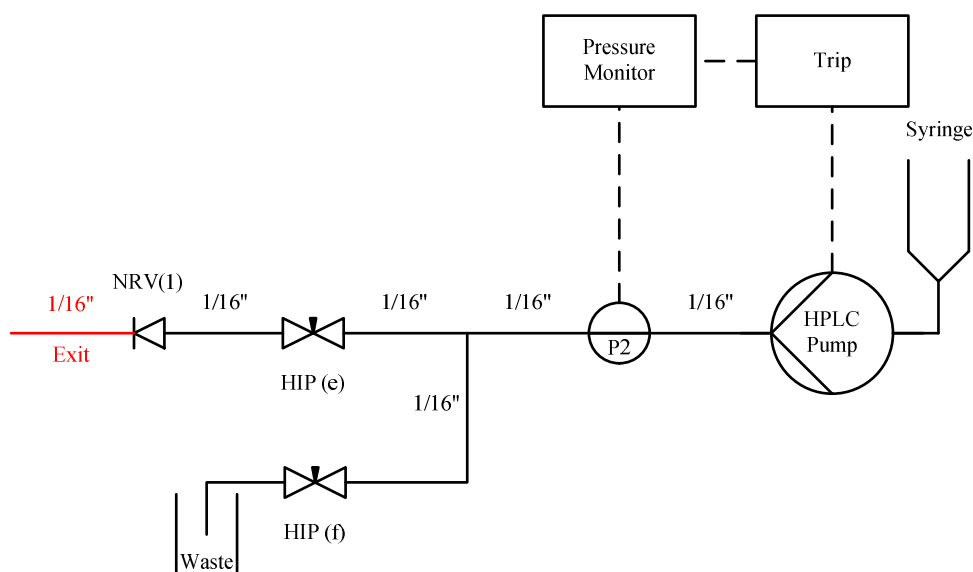


**Figure 2-14. HPLC schematic for the X-ray scattering cell autoclave. The 1/16" exit pipe connects to HIP (d) in Figure 2-13.**

Reactions were performed in the same way as for a standard MKIII, following the same SOP, autoclave although differences in the heating must be noted. The temperature control is based upon the external heating jacket therefore this must be set higher than the desired 65 °C to ensure the internal temperature reaches this. The heating step took approximately twice as long as for a MKII owing to the increased wall thickness and the inability of the heating jacket to cover the entire base. As mentioned, the second monomer is not added through the top but through the exit line (Figure 2-13, HIP(d)).

For reactions monitored by SAXS the first block was polymerised offline, not in the beamline, and the cell moved into the beam prior to addition of the second monomer.

1. The window holders were assembled with two o-rings, the window mount containing the diamond windows, and secured using the metal seal. These were both screwed into the body.
2. An o-ring was placed in the body, then the head and body clamped together. The clamp was tightened using the safety key which was then screwed into the head. The inlet and outlet pipes were attached and tightened (reducing unions R2 and R3), then the heating jacket was secured around the body.
3. The setup was leak tested by pressurising to  $\sim 138$  bar (2000 psi) by opening HIP (b) and (d), keeping HIP (c) closed. All fittings were checked for leaks with 'Snoop' (Sigma Aldrich).
4. If required, the autoclave was vented to ambient pressure through HIP (d) and any leaking fittings adjusted. (Fittings were never tightened under pressure).
5. Steps 2 and 3 were repeated until no leaks were visible then any remaining gas was vented until the autoclave was at atmospheric pressure.
6. In order to remove residual oxygen the key was removed, HIP (d) closed and CO<sub>2</sub> flowed through the open key hole at  $\sim 2$  bar (30 psi) for 30 minutes (HIP (b) and (c) partially open).
7. A monomer solution was added through the open key hole with the positive pressure of CO<sub>2</sub> to ensure no oxygen entered the vessel. The key was then screwed in and the pressure was raised to  $\sim 50$  bar (725 psi).
8. The stirrer was switched on, and the CO<sub>2</sub>/monomer solution mixed for 10 minutes.

9. Both the thermocouples and heating band were connected to the control box and set to the desired temperature with the pressure monitored throughout.
10. The autoclave was allowed to reach its final temperature and the pressure increased to 200 bar (2900 psi) by slow addition of CO<sub>2</sub>. Note that this process caused the cell to cool slightly, so the temperature was allowed to stabilise after each addition of CO<sub>2</sub>.

*For HPLC addition:*

- a) *The first block was left at 200 bar (2900 psi) and 65 °C for the desired reaction time.*
- b) *The autoclave was vented to ~ 140 bar (2000 psi) by opening HIP (d). This enabled space to be created for the addition of the second monomer which would have increased the pressure above the 200 bar safety limit.*
- c) *The HPLC setup was connected to HIP (d)*
- d) *The degassed monomer/initiator solution was transferred to the syringe attached to HPLC inlet.*
- e) *The pump was primed by opening HIP (f), ensuring taps leading to the autoclave (HIP (e)) were closed. Monomer solution was then flowed through the line for a few seconds.*
- f) *HIP (f) was closed and HIP (d) opened.*
- g) *HIP (e) was opened with an increase in back pressure monitored through the pressure monitor connected to P2.*
- h) *The monomer solution was pumped at 3 mL min<sup>-1</sup> until the pressure of the pump was equal to the pressure inside the autoclave.*

- i) The monomer level in the syringe was noted and the desired amount of solution added, taking into account dead volume between the entry pipe and the autoclave head (taken to be 1 mL). The autoclave pressure was monitored throughout.*
- j) The pump was stopped and the built-in tap closed.*
- k) The HPLC setup was detached by removing the 1/16" fitting from HIP (d). Some monomer solution remained in the pipe so this was opened slowly to release residual pressure.*
- l) To clean the HPLC setup HIP (f) and (e) were opened and solvent flushed through the pipes.*
- m) If the pressure of the autoclave was not at 200 bar then more CO<sub>2</sub> was added to raise it back to this level.*

11. After the desired reaction time, the autoclave was quenched by switching off and removing the heating band allowing the temperature to cool to ambient.
12. Once at ambient, the CO<sub>2</sub> was vented into the fume hood by opening HIP (d). Generally this was over a 30 minute period.
13. Once at ambient temperature and pressure, the safety key was removed, reducing unions R2 and R3 disconnected, the clamp opened and the product collected.

## 2.2. Analytical Techniques

### 2.2.1. Gel Permeation Chromatography

For polymers the molecular weight and molecular weight distribution, as introduced in Chapter 1, are key for the analysis. Gel Permeation Chromatography (GPC), otherwise known as Size-Exclusion Chromatography (SEC), is a vital tool. The sample is dissolved in a suitable solvent and passed through a column filled with porous beads. Polymers are separated based on their hydrodynamic volume in the chosen solvent; larger molecules elute first as they cannot fit into many pores and take a more direct path towards the end of the column. Smaller molecules will pass through more pores, taking longer to filter through leading to longer elution times. Many detectors are available, with refractive index (RI) the most commonly used. The difference in the refractive index of the polymer solution relative to pure solvent enables signals to be generated and plotted. The elution times are then referenced to standards, usually near-monodisperse PMMA or PS giving a value for the molecular weight. For polymers with vastly different structures to the standards these values are only approximations. Different columns are available depending on the molecular weight range with common solvents including THF, Chloroform and DMF as well as aqueous systems.

In this Thesis, GPC analysis was carried out on either a Polymer Laboratories (PL) GPC-120 or GPC-50 equipped with a refractive index detector with THF (HPLC grade, Fisher) as the eluent at a flow rate of 1 mL min<sup>-1</sup>, at 40°C with a guard column and two PL PolarGel-M columns in series. Molecular weight and dispersity data was obtained relative to PS or PMMA narrow standards. Samples were dissolved in THF at approximately 10 – 20 g

mL<sup>-1</sup> and filtered prior to injection through 0.2 µm filters (Whatman). Crude data is shown for all figures unless stated.

### 2.2.2. Nuclear Magnetic Resonance Spectroscopy

NMR is a particularly useful tool for confirming the identity of a compound containing any NMR active nuclei. These nuclei have a spin which can interact with a magnetic field generate by an NMR spectrometer. For this work <sup>1</sup>H and <sup>13</sup>C are the most applicable, both having a nuclear spin quantum number (I) = ½. The interactions are measured as chemical shifts (δ) and plotted relative to a standard, often tetramethylsilane which has 12 protons defined at δ = 0 ppm, or the solvent itself. Different chemical environments give characteristic shifts, meaning the chemical structure can be deduced. For <sup>1</sup>H NMR a proton close to an area of high electron density will be shifted downfield towards a higher δ value, whereas one that is shielded will be further upfield at lower δ values. Interactions between nuclei in different environments but separated by only a few bonds are known as coupling interactions, producing characteristic splitting patterns. This is another useful factor in identifying a molecule. Intensity is also relative to the number of protons for each signal for many NMR active nuclei, giving integration values. Conversion of monomer to polymer for example can be calculated from the ratios of the respective signal integrations.

In this Thesis, <sup>1</sup>H NMR data were obtained from a Bruker 300 MHz NMR spectrometer using CDCl<sub>3</sub> as the solvent at ambient temperature.

### 2.2.3. Scanning Electron Microscopy

Particle morphology has been investigated using Scanning Electron Microscopy (SEM), in particular for polymers produced *via* scCO<sub>2</sub> dispersion polymerisations. A focussed electron beam is fired at the sample in an ultrahigh vacuum chamber; this prevents electron scattering from particles in the air. Combinations of secondary and back-scattered electrons are emitted from the sample, hit a detector and are translated into an electrical signal. This signal is then amplified and converted into the images presented. Typical length scales used between 10s of nanometres to micrometres.

Polymer samples were mounted on aluminium stubs with sticky carbon tabs and sputter coated with gold (Leica EM SCD005) prior to analysis. This helped to prevent charge build up; a common problem for polymers. Imaging was performed on a JEOL JSM 6060LV SEM at a range of magnifications.

### 2.2.4. Transmission Electron Microscopy

TEM is a technique used for imaging at the atomic level, enabling phase separation in block copolymers to be observed, although only a small sample is studied and may not be representative of the bulk (see SAXS). Thin sections of polymer are probed (<100 nm), through solvent-evaporation then cutting slices with a microtome. The sample is held in a vacuum then electrons are fired at it and transmitted through to the detectors. The interactions of the electrons as they pass through the sample generate information about the phase separated structures.

Particles were embedded in a medium epoxy resin (Agar 100) and set at 35 °C before being ultra-microtomed at room temperature to ~100 nm slices with a

diamond knife (Leica Diatome Ultra 45°) and collected on copper grids. Sections of PMMA-*b*-PBzMA were stained with RuO<sub>4</sub>, which adsorbed selectively to PBzMA domains, for ~1 h. PMMA-*b*-PS particles were stained prior to resin embedding with OsO<sub>4</sub> for 24 h, which adsorbed selectively to PS. Imaging of particle samples took place on a FEI Tecnai microscope.

### 2.2.5. Small Angle X-ray Scattering

Small and wide angle x-ray scattering (SAXS/WAXS) is a vital tool for investigating phase separation of block copolymers on the 1-100 nanometre scale.<sup>2</sup> Unlike TEM which focusses on a small area, SAXS analyses the bulk material to assess the persistence of morphology throughout. A high intensity beam allows probing of block copolymers where there is an electron density difference between the respective blocks. The development of synchrotron x-ray sources has enabled this, with time resolved measurements now possible. In general, a monochromatic x-ray beam is fired at the sample, with the majority of the x-rays passing through the sample; the x-rays that do interact however are scattered dependent on the sample structure. The scattering pattern generated can then be analysed to determine morphologies, presented as a function of the scattering vector,  $q$ . Further details of the specific analyses is in Chapter 4.

### 2.2.6. Differential Scanning Calorimetry

Thermal properties of polymers are measured using Differential Scanning Calorimetry (DSC), including melting points, crystallisations and glass transition temperatures. The technique is based upon the amount of

energy required to maintain the temperature of a pan containing the sample relative to an empty reference pan during heating and cooling. The energy difference measured is indicative of transitions of the material, both endo and exothermic. Several heating and cooling cycles are used, typically the first to delete the thermal history of the sample and further cycles to measure the values themselves.

The specific DSC used in this work is a TA Instruments Q2000, equipped with an auto-sampler, suitable for use from -90 to 300 °C using indium standards. Tzero aluminium pans (TA instruments) were used for all samples and pressed prior to use. Samples were run at a heating/cooling rate of 10 °C min<sup>-1</sup> in a nitrogen atmosphere. Data was analysed with Universal Analysis software.

### 2.2.7. Dynamic Mechanical Analysis

Similar to the DSC, dynamic mechanical analysis (DMA) can yield information concerning the T<sub>g</sub> of a material, measured *via* the mechanical properties of the sample. The technique relies on the temperature dependence of two properties; the storage modulus (E') concerning the elastic properties, and the loss modulus (E'') representing the viscous nature of the material. The relationship between the two, tanδ (Equation 2-1.) is indicative of a transition; the temperature at which tanδ reaches a maximum related to the T<sub>g</sub>.

$$\tan\delta = \frac{E''}{E'}$$

**Equation 2-1.**

A typical method is a temperature sweep where the stress and strain of the material is measured at a constant frequency. A constant stress is applied to the material and the response monitored during the temperature sweep. As the material becomes more rubbery there is an increase in the elastic modulus and a decrease in the storage modulus leading to the peak in a trace of  $\tan\delta$  versus temperature.

Analysis was carried out using a TT DMA (Mettler Toledo, formerly Triton Technology) with samples held in aluminium powder pockets. Operating temperatures were between room temperature to 200 °C in an air atmosphere, with the setup for the single cantilever bending mode at a frequencies of 1 and 10 Hz. Samples were rapidly heated at a rate of 10 °C  $\text{min}^{-1}$  until above the expected  $T_g$ , monitored at the  $\tan\delta$  maximum, and tightened to ensure good contact between the sample and powder pocket. Once cooled the measurements were taken at a ramp rate of 2 °C  $\text{min}^{-1}$ .

#### 2.2.8. Rheometer

Rheology is the study of how a material flows under certain conditions, particularly important for polymers. Rotational rheometers are used to generate data regarding shear stress and strain, similar to a DMA. In general, a spindle in contact with the sample is rotated at a known shear rate, with the force generated to maintain this shear rate, i.e. the torque, giving information about the sample (Figure 2-15). Storage modulus ( $G'$ ) data can be generated by looking at oscillating motion at a constant shear rate, with a temperature sweep changing the behaviour of the polymer. Upon heating the polymer becomes more rubbery, thus  $G'$  will decrease, indicative of the  $T_g$ .

Polymers are non-Newtonian fluids, the majority being shear thinning, and therefore as the shear rate is increased, the viscosity will decrease. There are three distinct behaviours: the first is the zero shear plateau where the viscosity is unaffected by shear rate, typically at low shear rates. A linear relationship between the decrease of the log of the viscosity as the log of shear stress is increased can then be observed as the polymer chains become less entangled. Once all the chains align no further shear thinning behaviour is observed, reaching an infinite viscosity plateau.

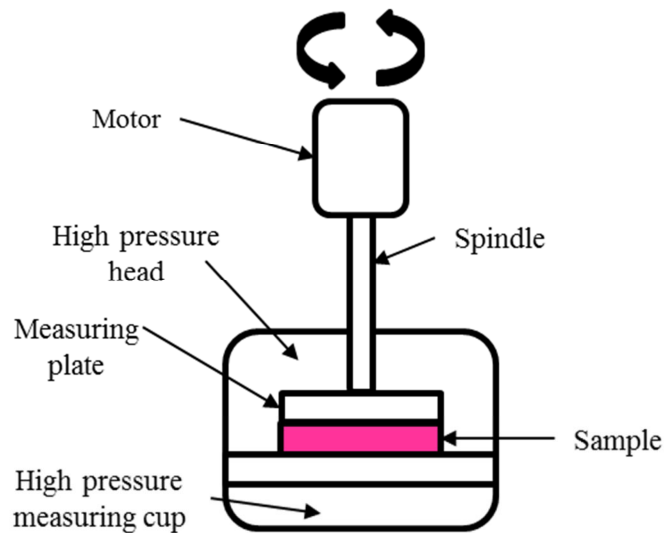


**Figure 2-15. Schematic of the rheometer setup. The sample is held in a high pressure measuring cup between the base and the measuring plate. A motor drives a spindle at a known torque, rotating the measuring plate, with viscosity measured relative to shear stress.**

A Physica MCR301 rheometer (Anton Paar, Austria) equipped with a high-pressure cell and parallel plate geometry of diameter 20 mm and gap of 1 mm. 800 mg of polymer sample was added to the cup of the HP rheometer. For

ambient pressure samples, the cell was heated at a rate of  $1\text{ }^{\circ}\text{C min}^{-1}$  to  $150\text{ }^{\circ}\text{C}$  to create a polymer disk, which ensured an even sample was being measured by the spindle. For the viscosity measurements the rheometer was set to rotational mode at constant temperature, and the shear rate increased on a log scale from  $10^{-3}$  to  $10^3\text{ s}^{-1}$ .

Prior to pressurising, the sample was cooled to room temperature, the cell was sealed and  $\text{CO}_2$  was added through a 260D syringe pump (Teledyne Isco, USA) to a pressure of 120 bar, then left to soak for 30 minutes. The cell was again heated at a rate of  $1\text{ }^{\circ}\text{C min}^{-1}$  to  $150\text{ }^{\circ}\text{C}$  to create a homogeneous sample contact with the spindle. The measurement temperature was set, and viscosity measurements taken at the same shear rates as before.

### 2.3. References

1. P. Licence, M. P. Dellar, R. G. M. Wilson, P. A. Fields, D. Litchfield, H. M. Woods, M. Poliakoff and S. M. Howdle, *Review of Scientific Instruments*, 2004, **75**, 3233-3236.
2. I. W. Hamley, *The Physics of Block Copolymers*, Oxford University Press, 1998.

## Chapter 3 - Expanded Phase Polymerisation

---

### 3. Overview

The need to create new methods of synthesising polymers on a large scale whilst adhering to regulations regarding volatile organic solvents has seen an increase in research concerning alternative “Green” solvents. Supercritical fluids, specifically supercritical carbon dioxide, have been shown to act as a good medium for polymerisations.<sup>1</sup> A high proportion of polymers synthesised in scCO<sub>2</sub> are through dispersion processes as this gives control over particle size and morphology. A key disadvantage is the typically high ratio of CO<sub>2</sub> to polymer product, which will potentially have major financial implications; typical monomer loadings are between 10-30% v/v. New systems increasing the monomer loading, thus producing more product per batch, have been investigated.<sup>2, 3</sup> These systems typically look at using higher monomer loadings between 50-80% v/v, with the monomer itself acting as a co-solvent. This also removes the need for costly surfactants, often fluorinated or siloxane-based polymers, which are also required to maintain a stable dispersion, and therefore a successful polymerisation. This has been termed CO<sub>2</sub> expanded phase polymerisation.<sup>4</sup> One disadvantage is the product morphology on the micron-scale. In dispersion polymerisations monodisperse spherical particles can be produced, whereas expanded phase polymerisations create particles with no defined structure.

As the initial capital costs of setting up a high pressure plant can be high, polymerisations in scCO<sub>2</sub> are expected to be only suitable for high value products with targeted properties.<sup>5</sup> Another important development in polymer science, controlled radical polymerisation, offers routes to create customisable

polymers of defined molecular weight and dispersity. This Chapter will discuss free radical polymerisations and the implementation of CCTP, NMP and RAFT in CO<sub>2</sub> expanded phase systems.

### 3.1. Introduction

#### 3.1.1. Gas-expanded liquids

The low solubility of many products has hindered the wider use of supercritical fluids as reaction media. For example in organic synthesis many common pharmaceuticals are strongly basic and do not interact well with CO<sub>2</sub> in particular. Interesting properties have been exploited by combining regular volatile organic solvents with high pressure gases, known as Gas-Expanded Liquids (GXLs) with the simple definition as follows: “A GXL is a liquid the volume of which is increased when pressurised with a condensable gas such as CO<sub>2</sub>”.<sup>6</sup> CO<sub>2</sub>-Expanded Liquids (CXLs) are one of the most common types of GXL owing to the moderately low pressures needed, the critical pressure for CO<sub>2</sub> is only 73.8 bar compared with water at 221 bar, and ease of separation upon reaction completion. GXLs can be assigned to one of three classes, first proposed by Jessop *et al.*, dependent upon the solubility of the condensable gas in the liquid. The following examples use carbon dioxide to illustrate the classes.<sup>7</sup>

Class I liquids have a low solubility of the gas in the liquid and thus limited expansion, for example CO<sub>2</sub> in water. Therefore there are no significant changes in properties with pressurisation.

Class II liquids are able to dissolve a high amount of the condensable gas and have a significant expansion affecting many physical properties of the

liquids. These include many organic solvents such as hexane and tetrahydrofuran but most importantly the monomers used in this Chapter.

Finally Class III liquids dissolve moderate amounts of CO<sub>2</sub> leading to a small volume expansion and some change in physical properties such as viscosity. Typical examples include ionic liquids and liquid polymers. Organic syntheses in GXLs have been comprehensively reviewed elsewhere.<sup>6, 7</sup> This Chapter will focus exclusively on reviewing polymerisations in CXLs and detailing the progression made in developing the use of controlled radical polymerisation techniques in CXLs.

### 3.1.2. *Polymerisations in carbon dioxide expanded liquids*

Dispersion polymerisations in CXLs have enabled control over particle size and molecular weight. One recent example by Zetterlund and co-workers attributed the variations between products to the relative polarity of the solvents and monomer partitioning.<sup>8</sup> In the absence of stabiliser, free radical polymerisations of common monomers in scCO<sub>2</sub> proceed *via* a precipitation process. It is often beneficial for the reaction to remain homogeneous to improve diffusivity of reactants and prevent partitioning of reactants into either a monomer-rich or polymer-rich phase.<sup>3</sup> Localised concentration differences can lead to molecular weight differences between areas as the ratio of control agent and initiator to monomer will vary. Less control agent or initiator leads to higher molecular weight products, and more of either leads to lower molecular weight products. Polymers tend to display good solubility in GXLs where the liquid component is a good polymer solvent that prevents

precipitation, maintaining a homogeneous reaction mixture and retaining an element of control.<sup>9, 10</sup>

Initial studies by Han *et al.* focussed on the use of CO<sub>2</sub> to expand mixtures of monomers and conventional organic solvents.<sup>11-14</sup> Styrene and THF at a 1:1 ratio was first investigated over a range of pressures (0-60 bar). An inverse relationship between pressure and  $M_n$  was observed at a 33% monomer loading, higher pressures led to lowering of the molecular weight, although this was accompanied by a reduction in yield. This was attributed to a change in solvent power upon increasing the pressure, with CO<sub>2</sub> being the anti-solvent and inducing precipitation.

A similar system with MMA and THF also found a comparable decrease in molecular weight with pressure.<sup>14</sup> Increasing the pressure reduced the overall monomer concentration, which in a conventional free radical polymerisation leads to lowering of the molecular weight. The decomposition of the AIBN was also affected, with a faster decomposition rate upon increasing pressure. It is known that by increasing the amount of radicals in a system a reduction  $M_n$  is expected, with this system following this rule.  $R_d$  increased from  $4.47 \times 10^{-6} \text{ s}^{-1}$  to  $6.24 \times 10^{-6} \text{ s}^{-1}$  over the pressure range 40 – 85 bar. Guan *et al.* also saw an increase in decomposition rate with pressure over this range, also reporting an increase in  $k_d$  in THF/CO<sub>2</sub> mixtures compared with pure CO<sub>2</sub>.<sup>15</sup> Addition of THF in this case, increases the dielectric constant of the solvent system, which increases the decomposition rate. A disadvantage of these systems is that VOCs were still necessary for achieving control. Although these are easily removed with supercritical fluid extraction it still requires an extra processing step

Subsequent studies have focussed on using the monomers themselves as a reaction solvent, more appropriately compared to a bulk polymerisation. Zwolak *et al.* reported the Catalytic Chain Transfer polymerisation (CCTP) of MMA with bis-[(difluoroboryl)diphenylglyoximato]cobalt(II) (COPhBF) and AIBN in an expanded monomer system at a 33% v/v monomer loading in dense CO<sub>2</sub> (60 bar). An enhanced chain transfer constant was attributed to the increased diffusivity.<sup>16-18</sup> Investigations into the homogeneous expansion limit (HEL), the pressure at which phase separation between the polymer and CO<sub>2</sub> occurs, found that for this system pressures of 60 bar were above the HEL. This enabled studies concerning the benefit of maintaining a homogeneous mixture to be undertaken. At 50 bar, below the HEL, a single phase is sustained, thus the  $M_n$  and dispersity are as expected. Above the HEL however, a bimodal molecular weight distribution and loss of control was observed. Two loci of polymerisation were observed in a CO<sub>2</sub>-rich phase and polymer-rich phase, with the difference in monomer, COPhBF and AIBN concentrations affecting the molecular weights.

*In-situ* formation of catalytic chain transfer species were investigated by Adlington *et al.* at a monomer loading of 83% v/v and pressures of 276 bar.<sup>4</sup> Compared with bulk analogues, polymerisations in the expanded phase system produced polymers of similar molecular weight indicating that the catalyst efficiency is not diminished in CO<sub>2</sub>. Unlike Zwolak *et al.* the authors did not witness an increased chain transfer constant with the improved diffusion, although here the amount of CO<sub>2</sub> utilised was almost four times lower (17 v/v% CO<sub>2</sub> versus 67 v/v%). The viscosity reduction may be enough to see

processing improvements but not enough to significantly affect the chain transfer mechanism. In bulk the reactions were stopped at around 80% conversion as they became too viscous, but by using CO<sub>2</sub> conversions >90% were reported owing to this viscosity reduction. The ease of purification post-reaction was demonstrated with a fine powdery product compared with a solid mass for the conventional bulk polymerisations.

### 3.1.3. Controlled radical polymerisations in CXLs

Investigations using controlled radical polymerisation techniques have demonstrated additional benefits of using expanded monomers compared to a precipitation process and conventional solvents.

NMP has been successfully implemented in CO<sub>2</sub> expanded phase systems by Aldabbagh *et al.* for the polymerisation of styrene and *tert*-butyl acrylate.<sup>3, 9, 10, 19</sup> Two nitroxides were used, 2,2,5-trimethyl-4-phenyl-3-azahexane-3-nitroxide (TIPNO) and N-*tert*-butyl-N-[1-diethylphosphono-(2,2-dimethylpropyl)] (SG-1), with white powdered PS obtained at monomer loadings of around 75%, and conversions above 65%. One disadvantage of the mechanism of NMP is that during the activation step the nitroxide is separated from the polymer chain, and being small molecules, exhibit a moderately high CO<sub>2</sub> solubility. The nitroxide can therefore partition into the CO<sub>2</sub> phase, away from the locus of polymerisation in and on the surface of the particles, reducing its ability to control the reaction. This partitioning is more evident for TIPNO than SG-1. The organic TIPNO has a higher CO<sub>2</sub> solubility than the partly inorganic SG-1, therefore during the reaction the TIPNO is more likely

to be in the CO<sub>2</sub> phase, shown by low molecular weight shoulders in the GPC traces and broader dispersities.

The conversion at which the polymer precipitates from solution ( $J_{\text{crit}}$ ) is important for understanding when the reaction mixture is no longer homogeneous, as this is when reactant partitioning can occur.  $J_{\text{crit}}$  has been determined over a range of conditions in the NMP system, with only selected reactions allowed to proceed to high conversion.  $J_{\text{crit}}$  was seen to increase with monomer loading as the polymers studied are soluble in their monomer. For example, at conditions of 300 bar and 110 °C, a loading of 70% mass/volume (m/v) leads to a  $J_{\text{crit}}$  occurring at a conversion of 22%, whereas at a loading of 30% m/v  $J_{\text{crit}}$  is at 1%. Increasing the pressure also increased  $J_{\text{crit}}$  as the PS is more soluble in scCO<sub>2</sub> at higher pressures; a 70% m/v loading at 110 °C at 100 bar had a  $J_{\text{crit}}$  at 17% conversion.

Styrene has been polymerised *via* RAFT (Beuermann *et al.*) using cumyl dithiobenzoate as the control agent at a monomer loading of 78% v/v in both toluene and CO<sub>2</sub>.<sup>2, 20</sup> Enhanced termination in CO<sub>2</sub> was again observed compared with the analogous toluene polymerisations attributed to improved diffusivity of reagents in the CXL. These reactions were halted after predetermined times, which corresponded to conversions below 25%. This meant a high proportion of monomer still remained to help solubilise the polymer, and it is likely that the polymerisation was stopped below or near the  $J_{\text{crit}}$  conversion value.

MMA was first polymerised by RAFT in CO<sub>2</sub> dispersion polymerisation by Gregory *et al.*, using surfactants to stabilise the polymer particles. In the absence of stabiliser, which is then a precipitation polymerisation, very low

conversion (24%) was achieved, accompanied with a broadening of the molecular weight distribution ( $\bar{D} = 1.49$ ). These studies were performed at a low monomer loading of 17% v/v, which would lead to rapid precipitation of the polymer, and prevent further monomer addition.

### 3.1.4. Critical entanglement weight limits

In a following study by the same group, the volume fraction of monomer relative to the carbon dioxide, again without stabiliser, was increased for the 2-cyano-prop-2-yl dithiobenzoate controlled polymerisation of MMA.<sup>21</sup> At a loading of 70% v/v good control could be maintained over both molecular weight and dispersity. A key drawback was an apparent molecular weight limit above the critical entanglement weight ( $M_c$ ) of the polymer; for PMMA this is 27 kDa. Viscosity is known to increase proportionally to molecular weight (Figure 3-1), but when the molecular weight reaches the  $M_c$ , the viscosity increases as the entangled changes reduce the polymers ability to flow.

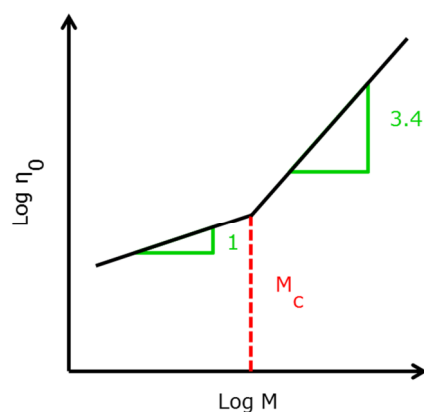


**Figure 3-1. Theoretical plot of the  $\log \eta_0$  ( $\eta_0$  = viscosity) against  $\log M$  ( $M$  = molecular weight).**

When the molecular weight targets were above this value, a broadening of the dispersity was seen, coupled with a vast difference between the  $M_n$  of samples taken from different parts of the autoclave. For example, when targeting a molecular weight of 50 kDa, the polymer at the top of the autoclave proceeded by a free radical polymerisation mechanism ( $M_n = 215$  kDa,  $\mathcal{D} = 2.38$ ), whereas the sample from the bottom of the autoclave still appeared to be well controlled by the RAFT agent ( $M_n = 38$  kDa,  $\mathcal{D} = 1.19$ ).

### 3.1.5. Aims and objectives

Investigations into CO<sub>2</sub> expanded phase polymerisations are described to further probe the molecular weight limit for MMA. These studies are extended to the controlled homopolymerisation of styrene *via* RAFT in the CO<sub>2</sub> expanded phase. Block copolymers synthesised by sequential RAFT polymerisations in bulk require toxic organic solvents for extraction of the product from reactors, and subsequent precipitation into anti-solvents or lengthy drying steps. By using a CO<sub>2</sub> expanded phase system, the aim is to synthesise block copolymers powders without using these purification steps, thus minimising the use of solvents or energy intensive and costly drying processes.

## 3.2. Experimental

### 3.2.1. Materials

Methyl Methacrylate (MMA, 99%) and Styrene (S, 99%) were obtained from Acros. Inhibitors were removed from both monomers prior to use by passing through a column of neutral aluminium oxide. Monomers were then

deoxygenated by bubbling with argon for 45 minutes and before storing in the freezer. 2,2'-Azobis(2-methylpropionitrile) (AIBN, 98%) was purchased from Sigma-Aldrich and purified by recrystallizing twice in methanol. 1,1'-Azobis(cyclohexanecarbonitrile) (VAZO-88, 98%) and Dicumyl Peroxide (DCP, 97%) were obtained from Sigma-Aldrich and used as received. 2-(Dodecylthiocarbonothioylthio)-2-methylpropionic acid (DDMAT) was synthesised following literature procedures.<sup>22</sup> 2-Cyano-2-propyl dodecyl trithiocarbonate (CPDT, 97%) and 2-Cyanopropyl Benzodithioate (CPBD, 97%) were purchased from Sigma-Aldrich and used as received. Tetrahydrofuran (THF, HPLC grade, 99.9%), Tetrahydrofuran (THF, laboratory reagent grade, 99.5%), Dichloromethane (DCM, analytical reagent grade, 99.99%), Hexane (laboratory reagent grade) and Methanol (laboratory reagent grade) were purchased from Fisher. Dry CO<sub>2</sub> (SFC grade, 99.99%) was purchased from BOC.

As CO<sub>2</sub> is known for its ability to dissolve small molecules and extract them from a mixture, it was decided that using conversions by NMR would be unreliable. For this reason, all reactions are compared using gravimetric yields obtained by dissolving the product in either DCM or THF, and precipitating into a poor polymer solvent (hexane or methanol). The DCM or THF along with any unreacted monomer remains in the poor solvent and a polymer powder is obtained.

### 3.2.2. Bulk synthesis

A typical bulk homopolymerisation of styrene was as follows. VAZO-88 (0.334 g, 1.37 mmol), DDMAT (0.998 g, 2.74 mmol) and a magnetic flea were charged into a Schlenk tube, sealed and degassed with argon for 30 minutes. Degassed styrene (14 mL, 122 mmol) was added to the Schlenk tube *via* a glass syringe and stirred at 700 rpm. Once homogeneous, the mixture was immersed in an oil bath and heated at 90 °C for between 24-72 hours. At the end of the reaction the Schlenk tube was removed from the oil bath and small samples were taken for GPC. Once cooled, the mixture was dissolved in DCM ( $\approx$  100 mL) and precipitated into excess methanol (2000 mL). The precipitated product was filtered and dried *in vacuo* at room temperature for 72 hours to remove residual solvent. Yields were determined gravimetrically, and were typically >80% for successful polymerisations.

### 3.2.3. Expanded phase synthesis

A typical CO<sub>2</sub> expanded phase polymerisation was conducted in an in-house designed 20 mL stainless steel autoclave as introduced in Chapter 2 (section 2.2). The reactor was sealed and leak tested up to 138 bar (2000 psi) with CO<sub>2</sub>. Once vented, the key was removed and the reactor was purged of oxygen with a flow of CO<sub>2</sub> at 2 bar (30 psi) for 20 minutes. VAZO-88 (0.334g, 1.37 mmol), DDMAT (0.998 g, 2.74 mmol) and a magnetic flea were charged into a round bottom flask, sealed and degassed with argon for 30 minutes. Degassed styrene (14 mL, 122 mmol) was added to the round bottom flask *via* a glass syringe and stirred until homogeneous. The monomer solution was transferred to the autoclave *via* a glass syringe through the keyhole. The

autoclave was then sealed and CO<sub>2</sub> added until a pressure of 48 bar (700 psi) was reached. The overhead stirrer was set to 300 rpm and the solution agitated for 10 minutes to ensure efficient mixing had taken place. The vessel was heated to 90 °C and once at the reaction temperature the pressure was raised to 276 bar (4000 psi). The reaction was left for between 24-72 hours at which time the heating and stirring was stopped. The vessel was quenched to -40 °C in a dry ice/acetone mixture then the CO<sub>2</sub> was vented slowly. After depressurisation the vessel was allowed to warm to room temperature, opened and samples were taken for GPC. The product appearance was noted, then the product was collected and dissolved in THF (≈100 ml). The polymer was purified by precipitation in excess methanol (2000 mL), filtered and dried *in vacuo* at room temperature for 72 hours to remove residual solvent. Yields were determined gravimetrically, typically >80%.

#### 3.2.4. Block copolymer synthesis in bulk

A typical bulk block co-polymerisation of styrene was as follows. AIBN (1.33 mmol), PMMA-macroRAFT (0.71 mmol) and a magnetic flea were charged into a Schlenk tube, sealed and degassed with argon for 30 minutes. Degassed styrene (8 mL, 70 mmol) was added to the Schlenk tube *via* a glass syringe and stirred at 700 rpm. Once homogeneous, the mixture was immersed in an oil bath and heated at 65 °C for between 24-72 hours. At the end of the reaction the Schlenk tube was removed from the oil bath and small samples were taken for GPC. Once cooled, the mixture was dissolved in DCM (≈ 100 mL) and precipitated into excess methanol (2000 mL). The precipitated product was filtered and dried *in vacuo* at room temperature for 72 hours to

remove residual solvent. Yields were determined gravimetrically and were typically >80%.

### 3.2.5. Block copolymer synthesis in CO<sub>2</sub> expanded phase

The autoclave was setup using the same procedure as section 3.2.3. AIBN (0.218 g, 1.33 mmol), PMMA-macroRAFT (5 g, 0.71 mmol) and a magnetic flea were charged into a round bottom flask, sealed and degassed with argon for 30 minutes. Degassed styrene (8 mL, 70 mmol) was added to the round bottom flask *via* a glass syringe and stirred until homogeneous. The monomer solution was transferred to the autoclave *via* a glass syringe through the keyhole. The autoclave was then sealed and CO<sub>2</sub> added until a pressure of 48 bar (700 psi) was reached. The overhead stirrer was set to 300 rpm and the solution was agitated for 10 minutes to ensure efficient mixing had taken place. The vessel was heated to 90 °C and once at the reaction temperature the pressure was raised to 276 bar (4000 psi). The reaction was left for between 24-72 hours at which time the heating and stirring was stopped. The autoclave was quenched to -40 °C in a dry ice/acetone mixture then the CO<sub>2</sub> was slowly vented. After depressurisation the vessel was allowed to warm to room temperature, opened and samples were taken for GPC. The product appearance was noted then the product was collected and dissolved in THF (≈ 100 mL). The polymer was purified by precipitation in excess methanol (2000 mL), filtered and dried *in vacuo* at room temperature for 72 hours to remove residual solvent. Yields were determined gravimetrically, and were lower than in bulk at between 40 – 78%.

### 3.3. Results and Discussion

#### 3.3.1. Poly(styrene) homopolymerisation in CO<sub>2</sub> expanded phase

To the best of the author's knowledge there are no reported studies taking the RAFT homopolymerisation of styrene to high conversion. The only reported studies by Arita *et al.* halted their reactions at 25% conversion as they were investigating kinetic data at the beginning of the reaction. Therefore PS was synthesised in CO<sub>2</sub> expanded phase (EP) with the aim to reach as high a conversion as possible to give an efficient process. 2-(Dodecylthiocarbonothioylthio)-2-methylpropionic acid (DDMAT) was chosen as the RAFT agent as it is well known to control styrene polymerisation in both conventional solvents and also scCO<sub>2</sub>.<sup>23</sup> Typically RAFT polymerisation uses a [RAFT]:[initiator] ratio of 10:1 to minimise the number of radicals in the system, aiding controlled growth by reducing the number of initiator derived chains. However, as AIBN has been shown to have a lower rate of decomposition in scCO<sub>2</sub> than conventional solvents such as benzene, a [RAFT]:[initiator] ratio of 2:1 is typically used to ensure enough radicals were present at the beginning of the reaction so a fast initiation step is still maintained.<sup>15</sup> The reaction scheme is shown in Figure 3-2.

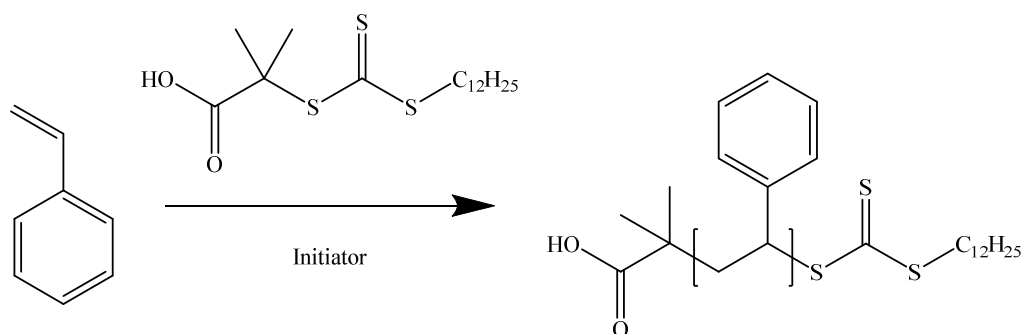


**Figure 3-2. Homopolymerisation of styrene using DDMAT as the control agent.**

### 3.3.1.1. Effect of reaction temperature

Initially, temperature was studied using three different initiators, all at their respective ten hour half-lives (Table 3-1), structures shown in Figure 3-1. This allowed a wide range of temperatures to be studied (AIBN at 65 °C, V-88 at 90 °C and DCP at 115 °C), whilst maintaining a similar number of initiator derived radicals in the systems. A molecular weight target of 18 kDa was chosen as this is below the reported  $M_c$  of styrene (31-36 kDa) to prevent any issues with control.<sup>24, 25</sup>

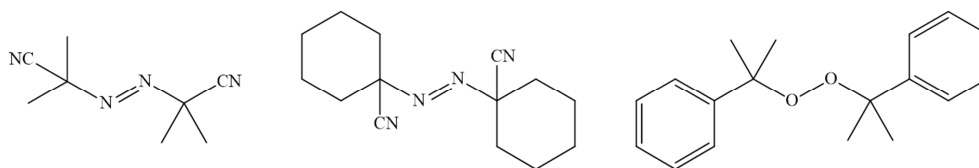


**Figure 3-3. Initiator structures (left) AIBN, (centre) V-88, (right) DCP**

**Table 3-1. Effect of reaction temperature on CO<sub>2</sub> expanded phase polymerisation of styrene<sup>a</sup>**

Entry	Initiator	Temp / °C <sup>b</sup>	Yield / % <sup>c</sup>	M <sub>n</sub> <sup>calc</sup> / Da <sup>d</sup>	M <sub>n</sub> / Da <sup>e</sup>	D <sup>e</sup>
1	AIBN	65	51	9200	8600	1.27
2	V-88	90	82	14800	11700	1.39
3	DCP	115	95	17200	15900	1.43

<sup>a</sup> All reactions were carried out in a 20 mL autoclave with 14 mL styrene at 276 bar for 72 h with M<sub>n</sub><sup>theo</sup> of 18 kDa at 100% conversion, S:DDMAT:initiator molar ratio of 345:2:1; <sup>b</sup> Polymerisation temperature; <sup>c</sup> Determined gravimetrically after precipitation into excess methanol and dried in-vacuo at room temperature for 72 h; <sup>d</sup> M<sub>n</sub><sup>calc</sup> = 18000 ×  $\frac{\text{yield}}{100}$ ; <sup>e</sup> Determined by GPC in THF relative to PS standards.

As expected, an increase in yield was observed as the temperature was raised for the same reaction duration. Comparisons between the theoretical and observed molecular weights show that a good degree of control was maintained, indicating that the RAFT process was not hindered by the CO<sub>2</sub>. A linear relationship between M<sub>n</sub> and conversion is necessary for a successful RAFT polymerisation, therefore at higher yields, a higher M<sub>n</sub> should be seen. As the reaction temperature is raised, the yield increases, subsequently a higher molecular weight polymer is obtained.

A broadening of the molecular weight distribution at higher temperatures was noted, caused by a greater amount of termination, as also seen by Arita *et al.*<sup>2</sup> The higher temperatures give the polymers more movement increasing the likelihood that chain ends meet. Styrene-based polymers terminate by combination as there are no labile hydrogens that can be extracted in a

disproportionation reaction, with a high molecular weight shoulder apparent in the GPC traces and broadening of the dispersity. This will not be the case for all monomers, including MMA, as termination by disproportionation leads to both dead chains having similar molecular weights. The product appearance upon opening the autoclave however was the key aspect when deciding which temperature to use for future reactions. At lower yields a high percentage of monomer remained in the vessel, solubilising the polymer and leaving a viscous liquid-like product. This is consistent with Arita *et al.* who obtained liquid products in a similar system (78% v/v monomer loading, 25% conversion). At higher conversions less monomer remained and a solid product was left, which is a key benefit of using the CO<sub>2</sub> expanded phase technique. For this reason AIBN was not used for further styrene homopolymerisation with the focus on VAZO-88 and DCP.

#### 3.3.1.2. Targeting $M_n$ values below the Critical Molecular Weight ( $M_c$ )

One of the disadvantages with RAFT polymerisation is the colouring of the products, typically pink or yellow depending on the control agent. At low molecular weights this is a particular problem, as the high concentration of RAFT agent required leads to intense colouring. This limits the uses in applications such as personal care products where white polymers are desired. However, from the work of Li,<sup>26</sup> targeting lower molecular weights was key to producing a well-controlled polymer product. An initial test was performed targeting only 5 kDa to confirm the RAFT mechanism was working consistently (Table 3-2). V-88 was chosen as the initiator as in the previous

section (Table 3-1), it gave a compromise of a lower yield compared to DCP, but a lower dispersity, thus better RAFT control.

**Table 3-2. Low molecular weight PS comparison <sup>a</sup>**

Entry	Media	Yield / % <sup>d</sup>	$M_n^{calc} / Da$ <sup>e</sup>	$M_n / Da$ <sup>f</sup>	$\bar{D}$ <sup>f</sup>
1	Bulk <sup>b</sup>	95	4800	4800	1.31
2	EP <sup>c</sup>	91	4600	3800	1.37

<sup>a</sup> All reactions were carried out at 90 °C for 24 h with  $M_n^{theo}$  of 5 kDa at 100% conversion, S:DDMAT:V-88 molar ratio of 90:2:1; <sup>b</sup> Schlenk tube immersed in an oil bath; <sup>c</sup> In a 20 mL autoclave with 14 mL styrene at 276 bar; <sup>d</sup> Determined gravimetrically after precipitation into excess methanol and dried in-vacuo at room temperature for 72 h; <sup>e</sup>  $M_n^{calc} = 5000 \times \frac{yield}{100}$ ; <sup>f</sup> Determined by GPC in THF relative to PS standards.

At these targets the synthesis was completed within 24 hours, producing polymer at the expected  $M_n$  with narrow dispersities. The difference between the bulk and expanded phase was minimal with the  $M_n$  of the expanded phase slightly lower.  $J_{crit}$  values were not able to be estimated as the autoclaves used did not have viewing ports, although this was expected to be an explanation for the similarity in the results. Lower molecular weight PS will have a higher solubility in the monomer/CO<sub>2</sub> mixture, therefore  $J_{crit}$  will not occur until higher conversions such as in the high weight systems by Aldabbagh *et al.*<sup>19</sup> For example, with an  $M_n^{theo}$  of 40 kDa, when decreasing the monomer loadings from 80 m/v% to 30 m/v%,  $J_{crit}$  occurred at conversions of 32.8% and 0.9% respectively. By delaying precipitation, the polymerisation will progress more

like the bulk reaction ensuring the control is maintained, and leading to similar polymer.

### 3.3.1.3. *Kinetic study below the critical molecular weight ( $M_c$ )*

As in Section 3.3.1.1 a target  $M_n$  of 18 kDa was then probed to investigate the kinetics of the polymerisations. This allowed more accurate GPC data to be obtained as even at low conversions the molecular weight distribution would be above the low limit of the PS standards used (around 500 Da). A temperature of 115 °C was chosen to ensure the highest conversion could be reached in both bulk and CO<sub>2</sub> expanded phase. Previously, work in the group by Li had indicated an issue with sampling directly from the high pressure autoclave using a modified sampling port (Figure 3-4).<sup>26</sup> As the polymer precipitates during the reaction, it can sink to the bottom of the vessel, therefore the sample collected may not be fully representative of the whole reaction. For this reason, reactions using the same reagent ratio were performed for different durations with results given in Table 3-3, Figure 3-5 and Figure 3-6.

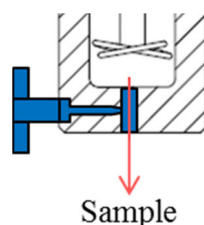


**Figure 3-4. Simplified schematic of a modified autoclave base to house a sampling port. Upon opening the HIP tap the polymer is forced out and collected for analysis.**

**Table 3-3. Kinetic experiments for styrene synthesis below the  $M_c$ <sup>a</sup>**

Entry	Media <sup>b</sup>	Time / h	Yield / % <sup>c</sup>	$M_n^{calc} / Da$ <sup>d</sup>	$M_n / Da$ <sup>e</sup>	$\bar{D}$ <sup>e</sup>
1	Bulk	1	30	5400	5100	1.19
2	Bulk	2	52	9400	8200	1.16
3	Bulk	5	93	16700	14200	1.16
4	Bulk	12	92	16600	15800	1.18
5	EP	1	15	2700	3300	1.54
6	EP	2	24	4300	5100	1.31
7	EP	5	52	9400	12000	1.22
8	EP	18	92	16600	15600	1.38

<sup>a</sup> All reactions were carried out at 115 °C with  $M_n^{theo}$  of 18 kDa at 100% conversion; <sup>b</sup> Bulk: Schlenk tube immersed in an oil bath, EP: 14 mL styrene in 20 mL autoclave at 276 bar; <sup>c</sup> Determined gravimetrically after precipitation into excess methanol and dried in-vacuo at room temperature for 72 h; <sup>d</sup>  $M_n^{calc} = 18000 \times \frac{yield}{100}$ ; <sup>e</sup> Determined by GPC in THF relative to PS standards.

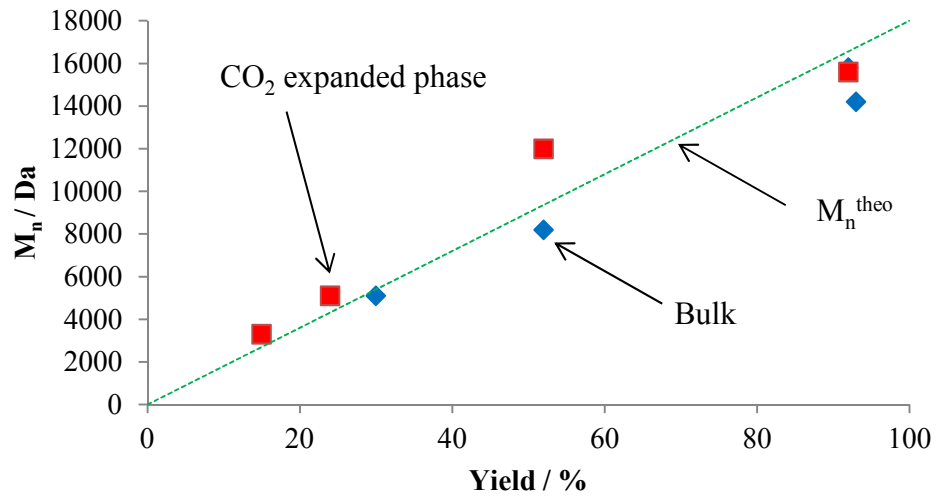


Figure 3-5. Plot of  $M_n$  vs. yield for the DDMAT controlled synthesis of PS.  $M_n^{\text{theo}}$  of 18 kDa at 100% conversion using DCP at 115 °C from Table 3-3.

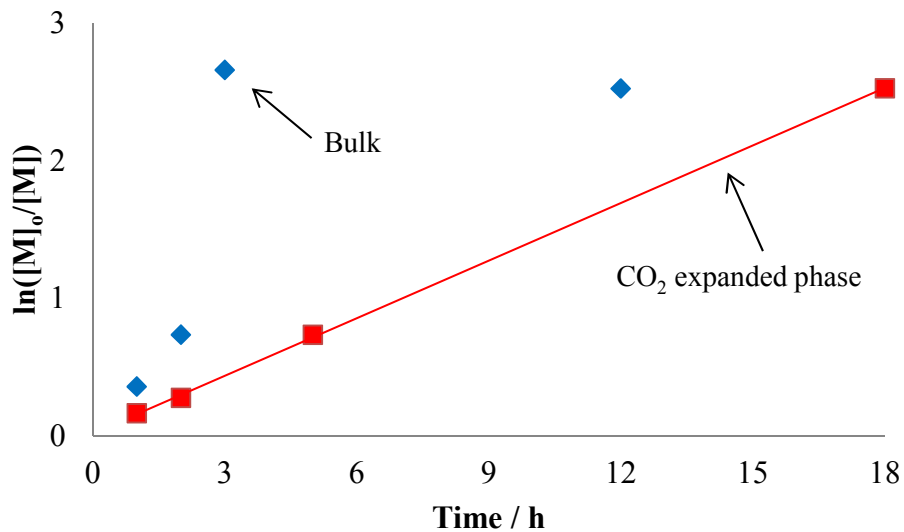


Figure 3-6. Pseudo-first order kinetic plot for the DDMAT controlled synthesis of PS.  $M_n^{\text{theo}}$  of 18 kDa at 100% conversion using DCP at 115 °C from Table 3-3.

Figure 3-5 clearly shows a linear increase of molecular weight with conversion for both the bulk and CO<sub>2</sub> expanded phase polymerisations, indicative of a controlled radical polymerisation.  $M_n$  values are also close to the theoretical weights demonstrating that DDMAT is a suitable RAFT agent for the polymerisation of styrene under these conditions. In the bulk, the yield is 93% after only 5 hours (Table 3-3, Entry 3), but leaving the reaction for 12 hours did not see an improvement in yield (92%, Table 3-3, Entry 4).

In all the bulk reactions, the reaction mixture solidified in the bottom of the Schlenk tube, requiring the addition of solvent to extract this fully. For the CO<sub>2</sub> expanded phase polymerisations viscous liquids were obtained at low conversion (Table 3-3, Entries 5-7). This is attributed to the residual monomer left in the autoclave, consistent with other literature studies in both precipitation<sup>3</sup> and dispersion polymerisations.<sup>27</sup> However, the final reaction (Table 3-3, Entry 8) yielded a free flowing, dry polymer powder which could be extracted easily, and was only dissolved and precipitated for means of calculating a gravimetric yield.

The plot of  $\ln([M]_0/[M])$  against time is useful for determining if the Trommsdorff Effect is occurring, as a sudden increase in rate would be observed. As a polymerisation progresses and the viscosity increases, the poor heat transfer causes an exotherm, which in turn increases the rate. The slope on this curve will have an inflection around this point, where the rate suddenly increases. This has been seen by Li *et al* in the bulk polymerisation of PMMA, but in a CO<sub>2</sub> expanded phase system this was suppressed and the rate remained generally constant throughout the polymerisation.<sup>26</sup> Typically a decrease in rate for polymerisations in CO<sub>2</sub> is expected for both RAFT<sup>26</sup> and NMP.<sup>28</sup>

Figure 3-6 compares the bulk and CO<sub>2</sub> expanded phase reactions with reaction rate differences clearly shown. The bulk reaction proceeds quicker most likely from two effects. Firstly the slower rate of initiator decomposition in CO<sub>2</sub>.<sup>15</sup> The generation of more radicals in the bulk in a given time will cause more chains to be initiated simultaneously causing the conversion to be higher. This also aids the RAFT mechanism where rapid initiation is a benefit to ensure all the chains grow at the same rate (Table 3-3, Entries 1-5). Secondly, the higher viscosity in bulk compared to the scCO<sub>2</sub> will reduce the diffusion inside the vessel thus reducing termination. Narrower dispersities are seen for the bulk indicating a more controlled product.

Both plots for the two synthetic methods follow linear trends. However, no Trommsdorff Effect is apparent for the bulk reaction; there are two potential explanations for this. The scale of the reaction (14 mL, 70 % v/v) may not be high enough to generate a sufficient exotherm to noticeably affect the reaction kinetics. On an industrial scale poor heat transfer and inefficient mixing are common issues where this may become more evident and potentially dangerous. Secondly the reaction temperature being above the T<sub>g</sub> of the material may enable relaxation of the polymer chains thus better diffusion of monomer evenly throughout the Schlenk tube. In the studies by Li *et al.* PMMA was synthesised at 65 °C, below its T<sub>g</sub> (around 120 °C), thus the viscosity of the reaction mixture will be much higher. The Trommsdorff Effect will therefore be more pronounced for PMMA than PS as seen in the kinetic plots.

In the expanded phase, CO<sub>2</sub> is able to reduce the viscosity allowing better heat transfer and circulation of reagents. One downside is the increase of

termination, which is a diffusion controlled reaction, causing a slight broadening of the molecular weight distribution. The hypothesis is that the PS/styrene/CO<sub>2</sub> mixture at 115 °C is more liquid-like than the PMMA/MMA/CO<sub>2</sub> mixture at 65 °C, increasing the diffusivity of reactants and polymer mobility allowing a controlled reaction to proceed. The limits of this system were then probed by synthesising higher molecular weight PS.

3.3.1.4. *Targeting  $M_n$  values above the critical molecular weight ( $M_c$ )*

Section 3.1.4 introduced the problems previously been encountered when synthesising PMMA above its critical entanglement molecular weight ( $M_c$ ) in the CO<sub>2</sub> expanded phase.<sup>26</sup> Two phases of polymerisation were observed, an upper, uncontrolled layer proceeding through a free radical polymerisation mechanism, and a lower, RAFT-controlled layer. Polymerisations of styrene above its  $M_c$  (31-36 kDa) were undertaken to investigate whether the same problems would extend to other monomers. To begin with a temperature of 90 °C was used, employing V-88 as the initiator, as this is below the T<sub>g</sub> of the polymer at ambient pressures (around 100 °C), whilst giving a high enough conversion to obtain powder (Table 3-4).

**Table 3-4. Homopolymerisation of styrene above its  $M_c$  with V-88<sup>a</sup>**

Entry	Media	Yield / % <sup>d</sup>	$M_n^{calc} / Da$ <sup>e</sup>	$M_n / Da$ <sup>f</sup>	$\bar{D}$ <sup>f</sup>
1	Bulk <sup>b</sup>	73	39200	39300	1.15
2	EP <sup>c</sup>	54	29200	23800	1.27

<sup>a</sup> All reactions were carried out at 90 °C for 72 h with  $M_n^{theo}$  of 54 kDa at 100% conversion, S:DDMAT:V-88 molar ratio of 1035:2:1; <sup>b</sup> Schlenk tube immersed in an oil bath; <sup>c</sup> In a 20 mL autoclave with 14 mL styrene at 276 bar; <sup>d</sup> Determined gravimetrically after precipitation into excess methanol and dried in-vacuo at room temperature for 72 h; <sup>e</sup>  $M_n^{calc} = 54000 \times \frac{yield}{100}$ ; <sup>f</sup> Determined by GPC in THF relative to PS standards.

A noticeable decrease in yield was observed when compared with the results at molecular weights below the  $M_c$  (Table 3-2). This was for both the bulk and the expanded phase, although the expanded phase was affected significantly more. As with previous results at low conversion, the product morphology was compromised by the excess monomer yielding viscous liquids as opposed to powdered solids. Although the  $M_n$  and dispersity were well controlled, it was decided that reactions longer than 72 hours would not be viable, therefore V-88 was replaced by DCP and reactions performed at 115 °C. This would have the benefit of a faster reaction rate as well as lowering the viscosity.

**Table 3-5. Homopolymerisation of styrene above its  $M_c$  with DCP <sup>a</sup>**

Entry	Media	$M_n^{theo} / kDa$ <sup>d</sup>	Yield / % <sup>e</sup>	$M_n^{calc} / Da$ <sup>f</sup>	$M_n / Da$ <sup>g</sup>	$\bar{D}$ <sup>g</sup>
1	Bulk <sup>b</sup>	54	90	48600	42700	1.22
2	EP <sup>c</sup>	54	82	44300	36900	1.44
3	Bulk <sup>b</sup>	100	88	88000	60300	1.32
4	EP <sup>c</sup>	100	75	75000	55800	1.61

<sup>a</sup> All reactions were carried out at 115 °C for 72 h, S:DDMAT:DCP molar ratio of 1035:2:1; <sup>b</sup> Schlenk tube immersed in an oil bath; <sup>c</sup> In a 20 mL autoclave with 14 mL styrene at 276 bar; <sup>d</sup> At 100% conversion, <sup>e</sup> Determined gravimetrically after precipitation into excess methanol and dried in-vacuo at room temperature for 72 h; <sup>f</sup>  $M_n^{calc} = M_n^{theo} \times \frac{yield}{100}$ ; <sup>g</sup> Determined by GPC in THF relative to PS standards.

Yields increased dramatically compared with V-88, also bridging the gap between the bulk and expanded phase results. Once again the increased temperature and higher diffusivity from the CO<sub>2</sub> broadened the dispersity but it still remained at an acceptable level for a controlled radical polymerisation. Consequently, the molecular weights were less controlled with  $M_n < M_n^{calc}$  in all cases. In particular the highest target weights were retarded the most which is often a disadvantage of RAFT polymerisation. This is not in agreement with previous issues encountered for PMMA synthesised in CO<sub>2</sub> expanded phase, where a dispersities  $> 2$  were routinely seen, as well as observed molecular weight (215 kDa) far exceeding the target (50 kDa).<sup>26</sup> Performing these reactions above the polymer Tg appears to be the route to successfully obtain higher molecular weight products. The next step was to synthesise PMMA in the same CO<sub>2</sub> system at elevated temperatures to determine if this would allow

higher molecular weight polymer to be formed whilst maintaining control over the dispersity.

### 3.3.2. Targeting PMMA with $M_n$ values above the $M_c$

RAFT agents are often chosen based on their ability to control different monomers.<sup>29, 30</sup> 2-cyano-2-propyl dithiobenzoate (CPDB) is known to have better compatibility with MMA than DDMAT used with styrene in the earlier results (Figure 3-7).

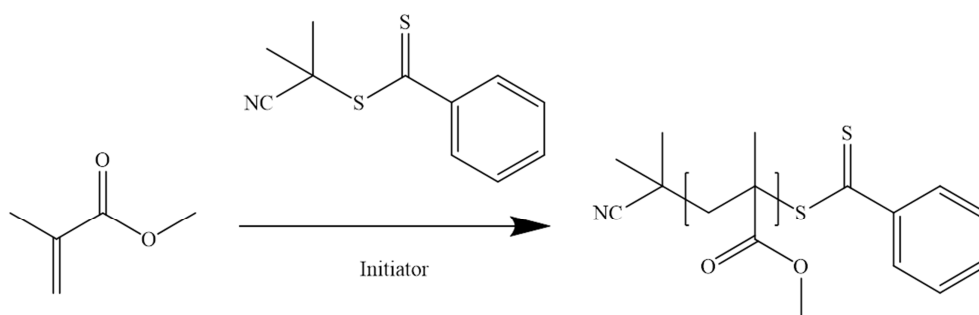


**Figure 3-7. Homopolymerisation of MMA using CPDB as the control agent**

#### 3.3.2.1. Effect of reaction temperature

MMA was polymerised using the same initiators as previously performed with styrene in section 3.3.1.1 (Table 3-6). This was expected to increase the polymerisation rate, but more importantly the viscosity will be lower at higher temperatures, thus better diffusion of reactants was anticipated. A  $M_n^{\text{theo}}$  of 55 kDa was selected as this is much higher than the reported  $M_c$  of MMA at 27 kDa. As MMA has a boiling point of around 100 °C, compared to styrene at around 145 °C, the bulk analogues could not be performed in Schlenk tubes. Although the autoclaves could withstand any pressure

generated, the heat transfer would be different to the glassware, thus the focus is solely on the CO<sub>2</sub> expanded phase system.

**Table 3-6. Effect of reaction temperature on MMA homopolymerisation <sup>a</sup>**

Entry	Initiator	Temp / °C <sup>b</sup>	Yield <sub>c</sub> / %	M <sub>n</sub> <sup>calc</sup> / Da <sup>d</sup>	M <sub>n</sub> / Da <sup>e</sup>	Đ <sup>e</sup>
1	AIBN	65	78	42900	32900	1.51
2	V-88	90	59	32500	31600	1.32
3	DCP	115	>99	68200	59100	1.19

<sup>a</sup> All reactions were carried out in a 20 mL autoclave with 14 mL MMA at 276 bar for 24 h with M<sub>n</sub><sup>theo</sup> of 55 kDa at 100% conversion, MMA:CPDB:initiator molar ratio of 1100:2:1; <sup>b</sup> 10 h half-life; <sup>c</sup> Determined gravimetrically after precipitation into excess hexane and dried in-vacuo at room temperature for 72 h; <sup>d</sup> M<sub>n</sub><sup>calc</sup> = 55000 ×  $\frac{\text{yield}}{100}$ ; <sup>e</sup> Determined by GPC in THF relative to PMMA standards.

Polymerisation using AIBN (Table 3-6, Entry 1) gave a relatively high yield of 78% with a slight broadening of the molecular weight distribution. The broadening is attributed to a loss of control as the viscosity is higher and limits the ability of the monomer to find the RAFT-capped chain ends. Increasing the temperature did not improve the yield but there was an improvement in control, with M<sub>n</sub> ≈ M<sub>n</sub><sup>calc</sup> and a narrower molecular weight distribution (Table 3-6, Entry 2). At 90 °C it is likely that the PMMA is sufficiently plasticised to enable good diffusion of both the monomer and polymer throughout the vessel, allowing controlled growth thus a narrower dispersity. With DCP however, a vast improvement was seen with near complete conversion, and a very narrow dispersity (1.19) (Table 3-6, Entry 3). Most importantly, the M<sub>n</sub> for this sample

(51 kDa) far exceeds the  $M_c$  (27 kDa), without affecting the polymer quality. This further supports the hypothesis that performing reactions above the  $T_g$  of the polymer in  $CO_2$  expanded phase is key for a successful reaction.

It was noted in all the above polymerisations that the stirring was maintained for the entire duration of the reaction which would account for all three reactions remaining relatively controlled. For the PMMA syntheses by Li,<sup>26</sup> that as the reaction progressed the stirrer ceased to work.<sup>26</sup> Magnetically-coupled stirrers are used for all autoclaves (Figure 3-8), therefore if the reaction mixture becomes too viscous the magnetic coupling can disconnect and the stirring will stop. This prevents a uniform reaction mixture being maintained and could potentially explain the observed loss of control.

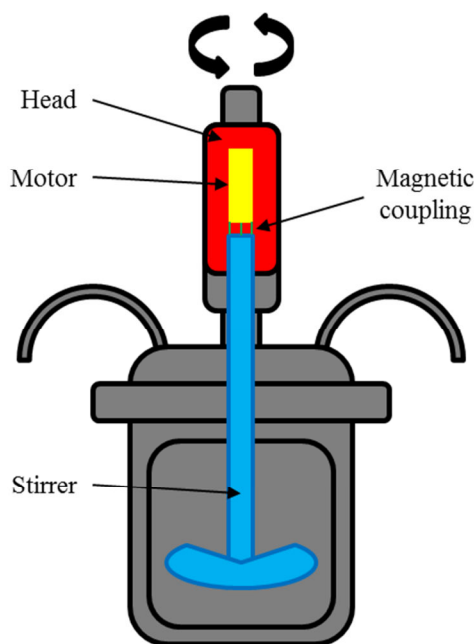


**Figure 3-8. Simplified schematic of a magnetically coupled stirrer. The head unit (red) contains a motor (yellow), which drives the stirrer. The shaft (blue) is magnetically coupled, with no physical linkages.**

3.3.2.2. *Agitation Efficiency*

In this set of experiments, for all cases, the stirring was observed to continue for the entire reaction duration. No loss of control was noted either, with experimental  $M_n$  values in good agreement with theory, as well as narrow molecular weight distributions. To determine the influence of the stirring, PMMA was again synthesised under the same conditions with the same 55 kDa target. However, after 4 hours the stirrer was manually stopped, and the reaction left at 65 °C and 276 bar for the remaining 20 hours (Table 3-7). Two samples were taken for GPC from each reaction, one from the top and one from the bottom, to see if there was a molecular weight gradient throughout the process.

**Table 3-7. Effect of agitation on reaction products <sup>a</sup>**

Entry	Stirring	Yield / % <sup>b</sup>	$M_n^{theo} / Da$ <sup>c</sup>	$M_n / Da$ <sup>d</sup>	$\bar{D}$ <sup>d</sup>
1	24 h	65	35800	47500/32200	1.19/1.17
2 <sup>c</sup>	4 h	100	55000	90700/16200	3.48/1.11

<sup>a</sup> All reactions were carried out in a 20 mL autoclave with 14 mL MMA at 65 °C and 276 bar for 24 h with  $M_n^{theo}$  of 55 kDa at 100% conversion, MMA:CPDB:AIBN molar ratio of 1100:2:1; <sup>b</sup> Determined gravimetrically after precipitation into excess hexane and dried in-vacuo at room temperature for 72 h; <sup>c</sup>  $M_n^{calc} = 55000 \times \frac{yield}{100}$ ; <sup>d</sup> Determined by GPC in THF relative to PMMA standards. Samples taken from the top/bottom of the autoclave.

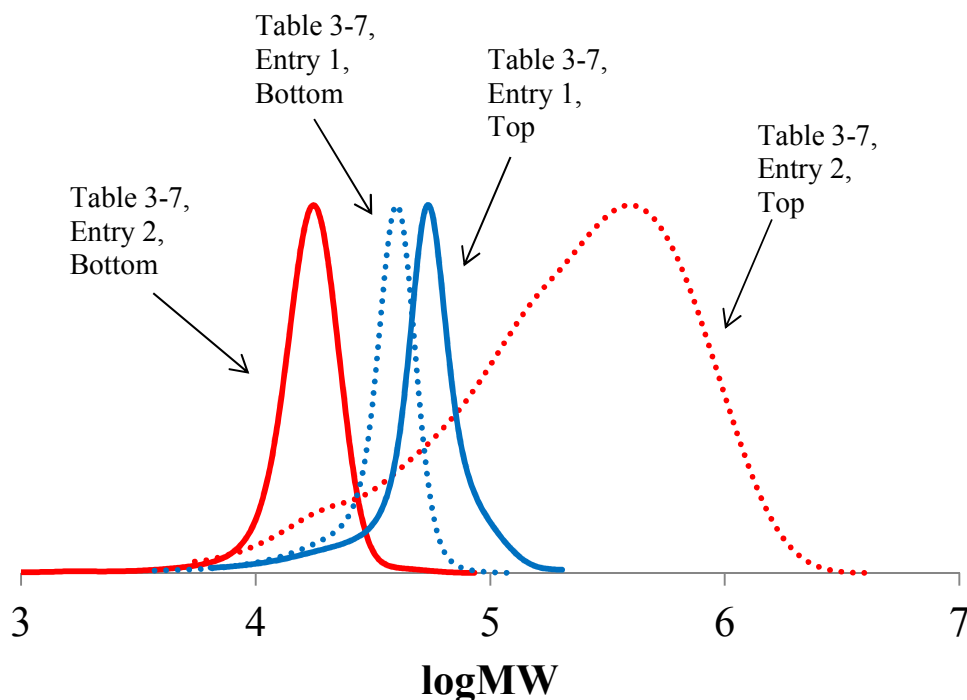


**Figure 3-9. Normalised GPC traces of samples from Table 3-7. Traces from Entry 1 are similar, but for Entry 2 there is a clear difference in molecular weight between the top and bottom samples.**

With stirring (Table 3-7, Entry 1) the reaction proceeded as expected, although an  $M_n$  difference of 15 kDa between the samples taken from the top and bottom was recorded. During the polymerisation the polymer will precipitate and as the viscosity increases can sink to the bottom of the vessel and not create a homogeneous reaction mixture. A more monomer rich phase will be formed nearer the top of the vessel allowing further propagation and the higher molecular weight polymer to be formed. However, when the stirring was stopped (Table 3-7, Entry 2) a much more substantial  $M_n$  difference between the top and bottom appeared. This is much clearer in Figure 3-9 with a vast difference in the traces from the sample taken at the top compared with the bottom. The dispersity was broader for the top layer indicative of a free

radical polymerisation mechanism. This was further reinforced by the visual appearance of the polymer with the top layer clear and the bottom, more controlled layer, being pink in colour (Figure 3-10 and Figure 3-11). Usually the colourisation of products from a RAFT polymerisation is considered a disadvantage, for example in medical applications many consumers prefer white tablets. However in this case it was an indicator for the problem, with the clear layer containing less RAFT agent, thus proceeding through an uncontrolled free radical type process. This is consistent with previous studies where the RAFT-terminated polymer is unable to diffuse through the viscous medium leaving a monomer-rich phase with only AIBN available to react and no control agent to cap the chain ends. The lack of efficient mixing is therefore a significant hindrance for the development of an industrial process based on CO<sub>2</sub> expanded phase polymerisations.

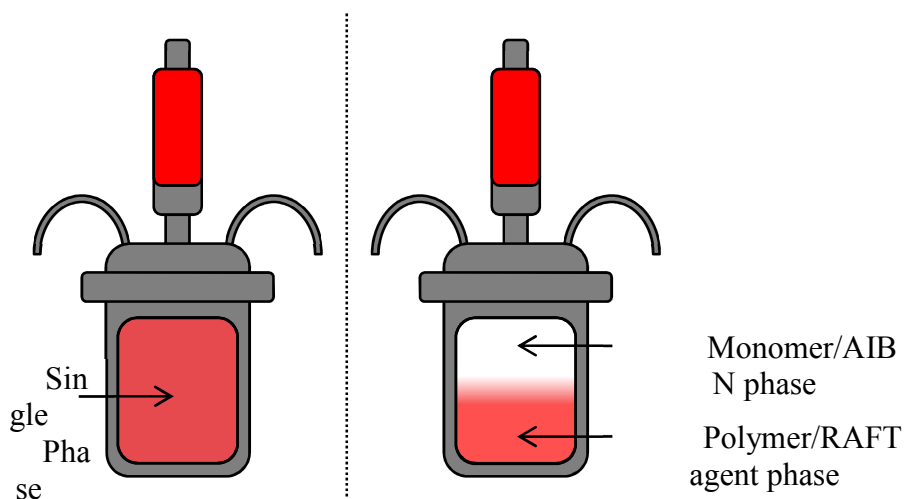


**Figure 3-10. Schematic diagram of expanded phase polymerisations (left) with stirring, (right) without stirring.**

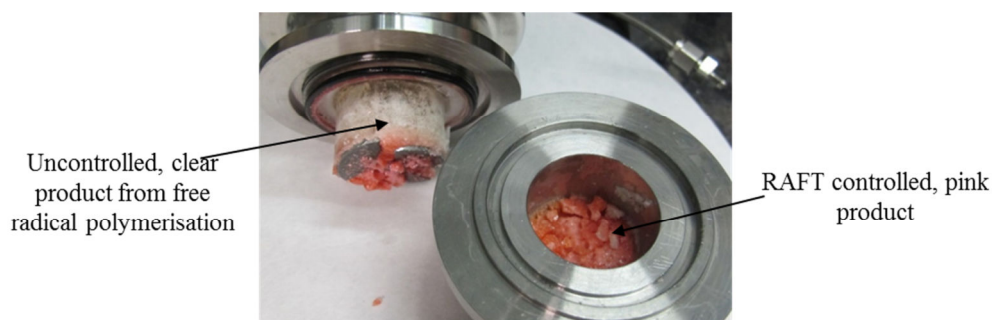


**Figure 3-11. Images of Table 3-7, Entry 2 after opening the autoclave.**

**Two layers clearly visible.**

Results thus far indicate that for successful CO<sub>2</sub> expanded phase polymerisations either molecular weights below the M<sub>c</sub> of the polymer must be targeted, or higher temperatures used for the synthesis to plasticise the polymers and reduce their viscosity. Further understanding the rheological behaviour of these polymers would offer quantitative data for comparing the different syntheses, particularly in CO<sub>2</sub>. A high pressure rheometer was used to investigate the polymers at both ambient and supercritical conditions.

### 3.3.3. High pressure rheology studies

The effect of CO<sub>2</sub> on polymers is well known but actually measuring reduction in T<sub>g</sub> and viscosity *in situ* during a reaction can be difficult, although measurements of pre-made polymers have been made.<sup>31-33</sup> For example, Royer *et al.* studied the change in viscosity of a poly(dimethyl siloxane) (PDMS) sample with CO<sub>2</sub> addition.<sup>34</sup> This polymer is known for having good CO<sub>2</sub> solubility, and is often used as a stabiliser in scCO<sub>2</sub> dispersion polymerisations (see Chapter 4). At conditions of around 200 bar and 30 °C, viscosity reductions of two orders of magnitude were observed. The same group also investigated some less CO<sub>2</sub>-philic polymers, including PMMA and

poly(propylene).<sup>31</sup> With PMMA, 6 wt% CO<sub>2</sub> was able to reduce the viscosity by 80% relative to ambient pressures.

To understand the effect of CO<sub>2</sub> in this system several measurements were taken using a high pressure rheometer (experimental details in Chapter 2) on the resulting polymer products. Two PMMA and two PS samples were chosen, one below their respective  $M_c$  values and one above (Table 3-8).

**Table 3-8. Molecular weight data for PMMA and PS samples**

Entry	Polymer	$M_c / \text{Da}^a$	$M_n / \text{Da}^b$
1	PMMA <sub>5 kDa</sub>	27000	5400
2	PMMA <sub>46 kDa</sub>	27000	45600
3	PS <sub>18 kDa</sub>	36000	17500
4	PS <sub>45 kDa</sub>	36000	44600

<sup>a</sup> From literature data; <sup>b</sup> Determined by GPC in THF relative to PMMA or PS standards;

Viscosity data were measured at both atmospheric pressure and 120 bar of CO<sub>2</sub>; the maximum for the rheometer used in this study. Although reactions are actually performed at 276 bar, other studies show the Tg depression plateaus on increasing pressure.<sup>35</sup>

For example, the Tg of PMMA has been reported to be lower than 30 °C when under CO<sub>2</sub> pressure, relating to a decrease of around 70 – 80 °C.<sup>36</sup> The Tg of PS has also been reported to be as low as 34 °C when treated with CO<sub>2</sub> under the correct conditions, relating to a depression of around 60 °C.<sup>35, 37, 38</sup> A sharp decline in Tg is observed at lower pressures, but as the CO<sub>2</sub> pressure approaches around 50 bar, the decrease is less pronounced, eventually beginning to plateau at pressures close to 200 bar (Figure 3-12). Therefore it

can be assumed that the polymers are all at temperatures above their respective glass transition temperatures when the viscosity measurements were made.

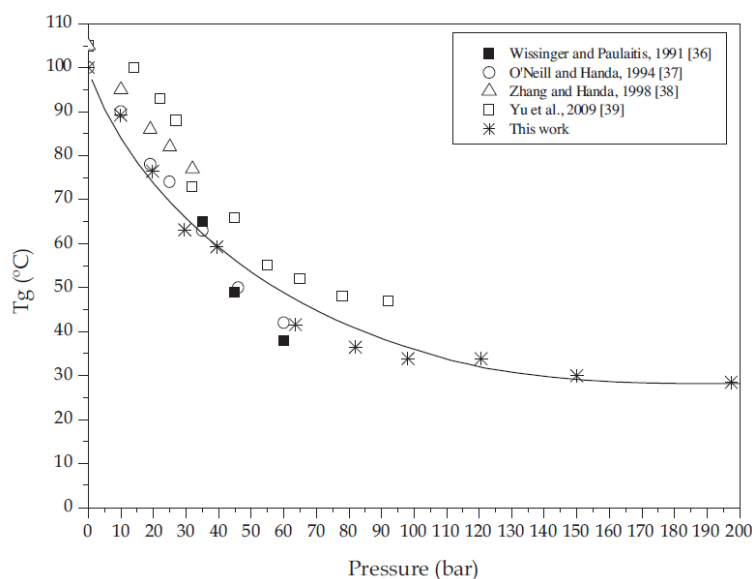


**Figure 3-12. Depression of the glass transition temperature of PS with increasing pressure of CO<sub>2</sub>. Reproduced from C. Gutiérrez *et al. J. of Supercritical Fluids* 2013, 76, 126– 134, with the (\*) labelled from their data.<sup>37</sup>**

As seen from the reactions with and without agitation, viscosity is likely to play an important role in determining if the reaction will be successful or not. A Physica MCR301 rheometer (Anton Paar, Austria) equipped with a high-pressure cell and parallel plate geometry of diameter 20 mm and gap of 1 mm was used to measure the viscosity of the samples. 800 mg of polymer sample was added to the cup of the HP rheometer. For ambient pressure samples, the cell was heated at a rate of 1 °C min<sup>-1</sup> to 150 °C to create a polymer disk, which ensured an even sample was being measured by the spindle. For the viscosity measurements the rheometer was set to rotational mode at constant temperature, and the shear rate increased on a log scale from

$10^{-3}$  to  $10^3 \text{ s}^{-1}$ . Three measurements were taken for each sample. The sample was cooled to room temperature, the cell was sealed and  $\text{CO}_2$  was added through a 260D syringe pump (Teledyne Isco, USA) to a pressure of 120 bar, then left to soak for 30 minutes. The cell was again heated at a rate of  $1 \text{ }^\circ\text{C min}^{-1}$  to  $150 \text{ }^\circ\text{C}$  to create a homogeneous sample contact with the spindle and to aid mixing of the  $\text{CO}_2$  with the polymer. The measurement temperature was set, and viscosity measurements taken at the same shear rates as before, again three measurements on each polymer were taken.

One point of note is that viscosity data at  $65 \text{ }^\circ\text{C}$  could not be obtained for either PS sample as the values indicated a solid sample was present at all shear rates. The data in Figure 3-13 are for both PS samples at  $115 \text{ }^\circ\text{C}$ , at both ambient pressure and 120 bar of  $\text{CO}_2$ .

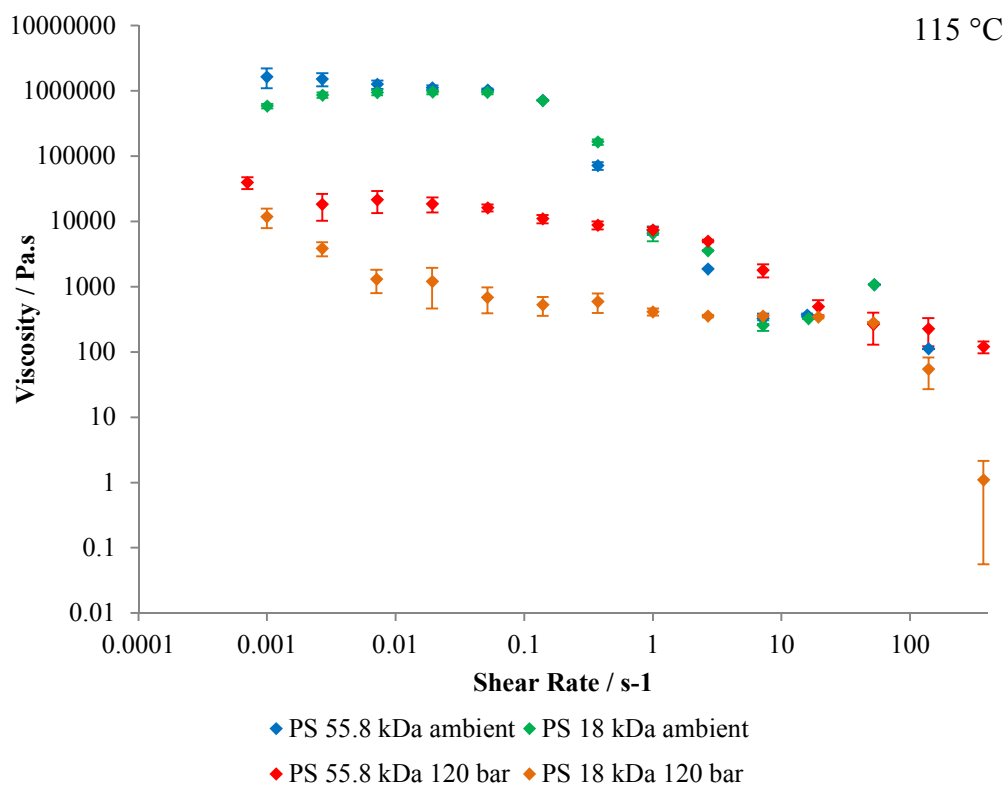


**Figure 3-13. Viscosity data for PS samples at 115 °C, at either ambient pressure or 120 bar CO<sub>2</sub>. Error bars are ± 0.5 standard deviation from the mean.**

Both PS samples have similar viscosities at ambient pressure and 115 °C. When CO<sub>2</sub> was added a decrease in viscosity was observed for both samples, but the sample with  $M_n < M_c$  showed a larger drop, indicating that the CO<sub>2</sub> can penetrate and swell the chains to a larger extent.

In all cases, the polymers display non-Newtonian behaviour, specifically they are all shear thinning, as seen for many amorphous polymers. Kelly *et al.* studied the reduction in viscosity upon pressurising poly(lactic acid) with CO<sub>2</sub>, observing a shear thinning effect attributing this to the long, entangled polymer chains becoming more disentangled and align in the direction of the shear.<sup>39</sup> The same paper also describes the reason why the different samples have a

different shear thinning behaviour, thus why the traces cross at higher shear rates. This is owing to the relaxation behaviour, with samples beginning at lower zero shear viscosities having an increased free volume, therefore a reduction in the relaxation time between measurements.

A slightly different order is seen for PMMA at 115 °C (Figure 3-14). Although both polymers show a reduction in viscosity with addition of CO<sub>2</sub>, the sample above the M<sub>c</sub> of PMMA has a higher viscosity at 120 bar than the lower M<sub>n</sub> sample at ambient conditions. At this pressure and 115 °C, the CO<sub>2</sub> density is only 0.23 g ml<sup>-1</sup> so potentially it will be unable to reduce the viscosity of the longer chains as effectively.

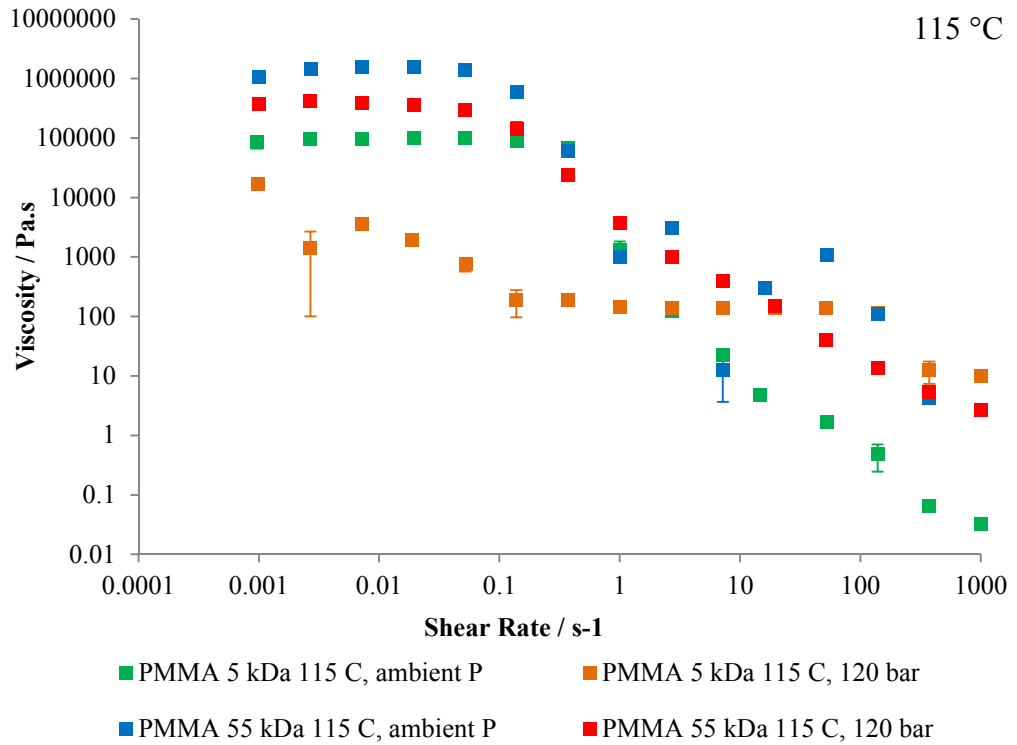


**Figure 3-14. Viscosity data for PMMA samples at 115 °C, at either ambient pressure or 120 bar CO<sub>2</sub>. Error bars are ± 0.5 standard deviation from the mean.**

Measurements taken at 65 °C for the PMMA samples showed the same trend as the PS samples at 115 °C (Figure 3-15). In general the viscosity values proceed in the order high MW > low MW > high MW with CO<sub>2</sub> > low MW with CO<sub>2</sub>.

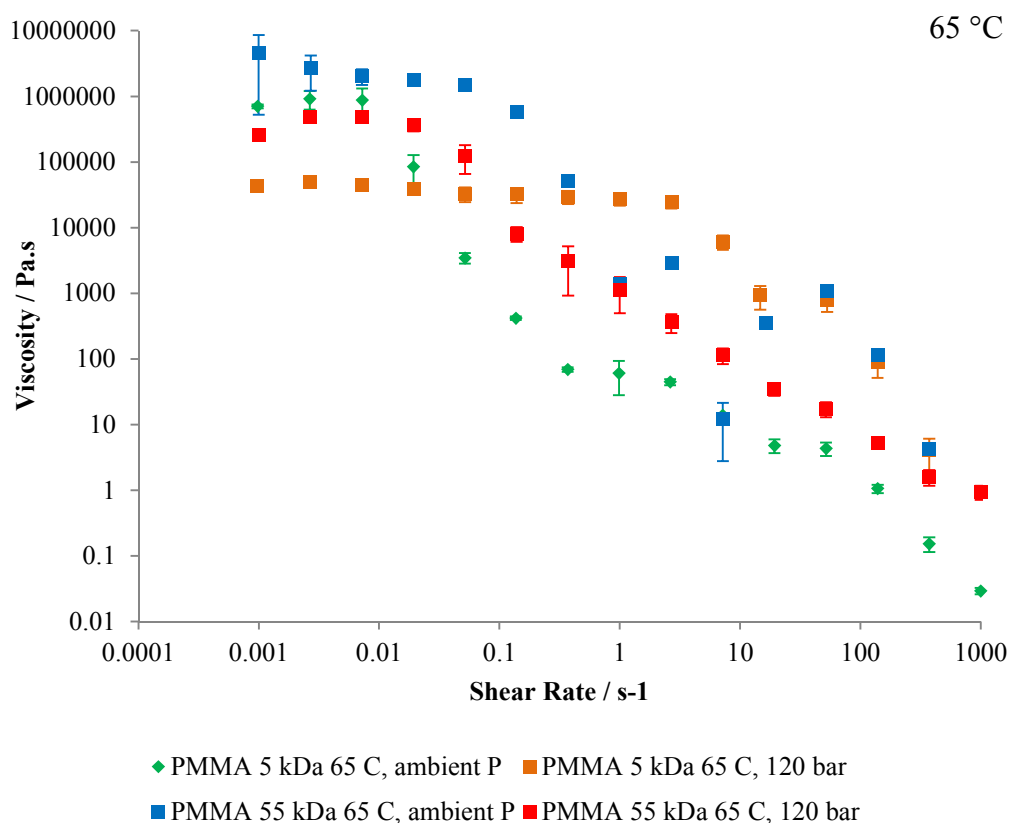


**Figure 3-15. Viscosity data for PMMA samples at 65 °C, at either ambient pressure of 120 bar CO<sub>2</sub>. Error bars are ± 0.5 standard deviation from the mean.**

Generally, the shorter chains will be less entangled than their higher molecular weight counterparts enabling the CO<sub>2</sub> to penetrate more easily thus producing the lowest viscosity readings. Lowering the viscosity helps to reduce the Trommsdorff effect, allowing better heat transfer and improved diffusion of reactants. This gives the polymer chains more mobility, enabling the RAFT end groups to react more easily, imparting better control. Higher molecular weight polymers are more viscous, therefore only the monomer can diffuse well, leading to a Trommsdorff effect, creating the monomer-rich phases seen in Figure 3-10 and Figure 3-11.

By studying the zero shear viscosities (the viscosity when the polymer is at rest and in the absence of any shear thinning effects), the differences between the PS and PMMA syntheses can be studied. Figure 3-16 compares the viscosity between the ambient pressure samples and when 120 bar of CO<sub>2</sub> is introduced. The values are given in Table 3-9, with the change in viscosity represented in percentage terms.

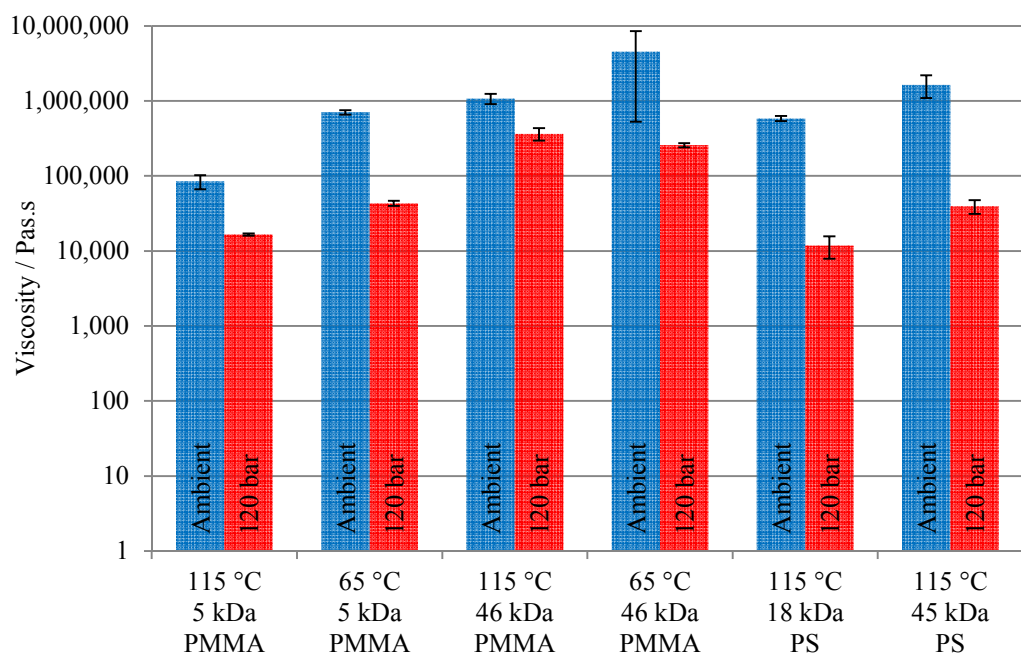


**Figure 3-16. Comparison of zero shear viscosities for the four polymer samples at both ambient pressure and 120 bar of CO<sub>2</sub>. PMMA samples were taken at 65 °C and 115 °C, whilst the PS was only measured at 115 °C. Error bars are ± 0.5 standard deviation from the mean.**

**Table 3-9. Comparison of the change in viscosity with CO<sub>2</sub> addition**

Entry	Polymer <sup>a</sup>	T / °C <sup>b</sup>	Average $\eta$ / Pa·s	Average $\eta$ at 120 bar / Pa·s	$\eta$ reduction / % <sup>c</sup>
1	PMMA <sub>5</sub> kDa	115	84,527	16,615	80
2	PMMA <sub>5</sub> kDa	65	703,650	43,313	94
3	PMMA <sub>46</sub> kDa	115	1,075,700	364,700	66
4	PMMA <sub>46</sub> kDa	65	4,535,725	258,267	94
5	PS <sub>18</sub> kDa	115	582,350	11,792	98
6	PS <sub>45</sub> kDa	115	1,640,133	39,468	98

<sup>a</sup> Determined by GPC in THF relative to PMMA or PS standards; <sup>b</sup>

Temperature at which viscosity data was obtained; <sup>c</sup> Percentage viscosity

$$\text{reduction} = \frac{\text{Average } \eta - \text{Average } \eta \text{ at 120 bar}}{\text{Average } \eta} \times 100$$

In all cases the decrease in viscosity upon adding CO<sub>2</sub> is clearly visible (Figure 3-16), although to differing degrees (Table 3-9). Gourgouillon *et al.* studied PEG/CO<sub>2</sub> mixtures, comparing samples at different temperatures in percentage terms.<sup>40</sup> They found that as the measurement temperature was increased, the effect of adding CO<sub>2</sub> to the polymer was reduced.

PS has the greatest percentage decrease in viscosity at 98%, as the PS is already above its T<sub>g</sub> and the CO<sub>2</sub> is able to penetrate into the polymer well. This helps to explain why the PS syntheses were successful, retaining good control in all cases, even above the M<sub>c</sub>.

This is followed by the PMMA samples at 65 °C at 94%, with the PMMA samples at 115 °C being the least affected (80% for lower molecular weight PMMA, and 66% for the higher molecular weight sample). This is probably due to a combination of effects. The CO<sub>2</sub> density at 65 °C and 120 bar is almost double that when at 115 °C and 120 bar (0.39 g ml<sup>-1</sup> compared with 0.23 g ml<sup>-1</sup>), meaning the CO<sub>2</sub> is able to swell the polymer to a higher degree at lower temperatures, reducing the viscosity more. However, looking

at the absolute viscosities, PMMA has a lower viscosity at 115 °C compared to 65 °C, which explains why the syntheses at the higher temperature prove more successful.

In absolute terms, two lower molecular weight samples have the lowest viscosities throughout, further indicating that synthesising low molecular weight polymers will be beneficial from a processing perspective. The anomaly is the high molecular weight PMMA. Intuitively, at higher temperatures the viscosity should decrease, which is the case for the ambient pressure samples (Table 3-9, Entries 3 and 4). However, when pressurised with 120 bar of CO<sub>2</sub> the viscosity at 115 °C is higher than at 65 °C. Kelly *et al.* observed the same effect for PLA, with their higher temperature samples having higher viscosities when pressurised with CO<sub>2</sub>. This was attributed to poorer CO<sub>2</sub> diffusion, and increased pressure effects.<sup>41</sup> As mentioned, the density is much lower at higher temperature and constant pressure, thus less CO<sub>2</sub> available to modify the viscosity.

The application of the CO<sub>2</sub> expanded phase will therefore be most appropriate for the synthesis of low molecular weight polymers as the percentage viscosity reduction with adding CO<sub>2</sub> is largest for these samples. This will suppress the Trommsdorff Effect, coupled with the better diffusion of monomer throughout the vessel, enabling a more controlled polymerisation thus higher quality product (narrower dispersity). Although higher temperatures can be utilised to drive the synthesis of higher T<sub>g</sub> polymers forward, this would be a significant obstacle for use on an industrial scale. Significant energy costs are associated with high temperature reactions,

particularly on large scales, further advocating the use of CO<sub>2</sub> expanded phase for oligomeric products.

#### 3.3.4. Low molecular weight block copolymers

The above data concludes that low molecular weight polymers are the most suitable for CO<sub>2</sub> expanded phase polymerisations. With this, oligomeric block copolymers were chosen as a field where a vast range of products exist with greener synthetic routes required. In particular amphiphilic block copolymers such as poly(acrylic acid)-*block*-poly(styrene) (PAAc-*b*-PS) can be used as surfactants and drug delivery agents.<sup>42</sup> Another example, oligomeric poly(bis(4-methoxyphenyl)-4-vinylphenylamine)-*block*-poly(neopentyl styrene sulfonate), has been synthesised by RAFT.<sup>43</sup> M<sub>n</sub> values of around 10 kDa and dispersities below 1.4 were reported, with applications as semi-conductors in solar cells.

To test the applicability of the CO<sub>2</sub> expanded phase system for oligomeric block copolymers the synthesis of a well-researched model system, poly(methyl methacrylate)-*block*-poly(styrene), was investigated *via* sequential polymerisations (Figure 3-17).

**Step 1.** Polymerise MMA *via* RAFT



**Step 2.** Collected product, precipitate into excess hexane to remove monomer and low molecular weight fractions.

**Step 3.** Chain extend the PMMA macro-RAFT agent with styrene monomer in a clean autoclave. Any ‘dead’ initiator terminated chains remaining will not polymerise further.

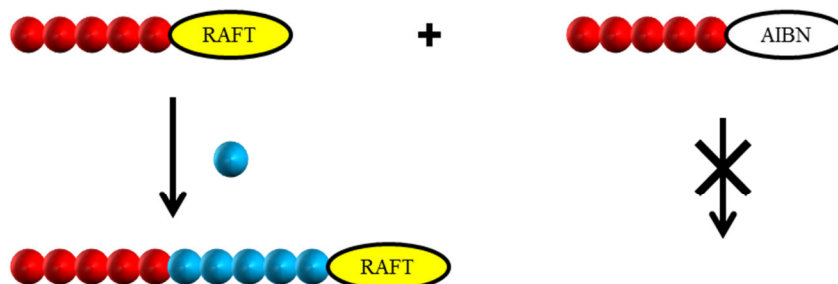


**Figure 3-17.** Schematic showing the polymerisation process to form a **PMMA-*b*-PS block copolymer**

#### 3.3.4.1. Choice of RAFT agent

Although both considered more activated monomers, MMA and styrene have differing reactivities with RAFT agents. Traditionally dithioesters are

used for MMA and trithiocarbonates used for styrenic systems, with a number of review articles indicating the best choices.<sup>29, 30, 44-46</sup> The homopolymerisation of MMA, the first block, was investigated using three different RAFT agents (Figure 3-18) in both bulk and CO<sub>2</sub> expanded phase conditions.

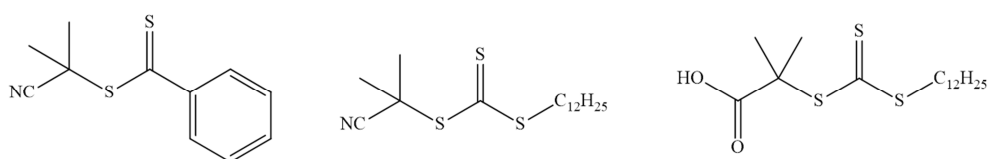


**Figure 3-18. RAFT agents (left) 2-cyano-2-propyl dithiobenzoate (CPDB), (centre) 2-cyano-2-propyl dodecyl trithiocarbonate (CPDT), (right) 2-(Dodecylthiocarbonothioylthio)-2-methylpropionic acid (DDMAT)**

**Table 3-10. RAFT agent comparison in CO<sub>2</sub> expanded phase <sup>a</sup>**

Entry	CTA	MMA:CPDB:AIBN	Yield / % <sup>b</sup>	$M_n^{calc} / Da$ <sup>c</sup>	$M_n / Da$ <sup>d</sup>	$\bar{D}$ <sup>d</sup>
1	CPDB	500:10:1	82	4100	4900	1.14
2	DDMAT	500:10:5	88	4400	6100	1.80
3	CPDT	500:10:1	87	4400	5100	1.33

<sup>a</sup> All reactions were carried out in a 20 mL autoclave with 14 mL MMA at

65 °C and 276 bar for 24 h with  $M_n^{theo}$  of 5 kDa at 100% conversion; <sup>b</sup>

Determined gravimetrically after precipitation into excess hexane and dried

in-vacuo at room temperature for 72 h; <sup>c</sup>  $M_n^{calc} = 5000 \times \frac{yield}{100}$ ; <sup>d</sup> Determined

by GPC in THF relative to PMMA standards.

DDMAT, although shown to work successfully for MMA in scCO<sub>2</sub> dispersion polymerisations,<sup>23</sup> proved to exhibit the least amount of control with

MMA in the CO<sub>2</sub> expanded phase, giving products with broader dispersities and  $M_n > M_n^{\text{calc}}$  (Table 3-10, Entry 2). This may be attributed to the excess initiator which was required to give a high enough conversion for fair comparison. For this reason no further work was performed using this RAFT agent. The other two options, CPDB and CPDT both yielded polymer of controlled  $M_n$  with narrow molecular weight distributions. Both of these were taken forward for chain extensions with styrene.

### 3.3.4.2. Block copolymers

Although AIBN was shown to be a poor initiator for the homopolymerisation of styrene at 65 °C this factor was used as an advantage to lower the amount of initiator derived chain and aid block formation. CPDT terminated PMMA was first to be chain extended with the trithiocarbonate moiety expected to react effectively with styrene (Figure 3-19). Three different PMMA samples were used for the regrowth experiments with the polymers detailed in Table 3-11.

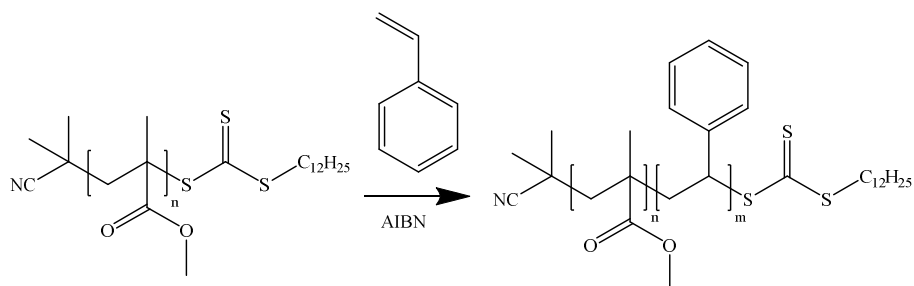


**Figure 3-19. Chain extension of PMMA-CPDT with styrene.**

**Table 3-11. CPDT terminated PMMA for chain extensions <sup>a</sup>**

Entry	Media <sup>b</sup>	Yield / % <sup>c</sup>	$M_n^{calc}$ / Da <sup>d</sup>	Crude Product		Pure Product	
				$M_n^{crude}$ / Da <sup>e</sup>	$\bar{D}$ <sup>e</sup>	$M_n^{pure}$ / Da <sup>e, f</sup>	$\bar{D}$ <sup>e, f</sup>
1	Bulk	90	4500	4700	1.72	6900	1.25
2	EP	76	3800	6400	1.22	6700	1.16
3	EP	87	4400	5100	1.33	6500	1.16

<sup>a</sup> All reactions were carried out at 65 °C for 24 h with  $M_n^{theo}$  of 5 kDa at 100% conversion; <sup>b</sup> Bulk: Schlenk tube immersed in an oil bath, EP: 14 mL MMA in 20 mL autoclave at 276 bar; <sup>c</sup> Determined gravimetrically after precipitation into excess methanol and dried in-vacuo at room temperature for 72 h; <sup>d</sup>  $M_n^{calc} = 5000 \times \frac{yield}{100}$ ; <sup>e</sup> Determined by GPC in THF relative to PMMA standards; <sup>f</sup> After precipitation.

PMMA synthesised in bulk (Table 3-11) produced a high yield of polymer, with the  $M_n$  close to the calculated value at that yield. The dispersity was quite broad (1.72) owing to a low molecular weight tail in the GPC trace (Figure 3-20). At high conversions the concentration of monomer is very low, but AIBN radicals are still being generated. Instead of monomer adding to the RAFT end group, initiator derived chains become more likely. These ‘dead’ chains do not chain extend as they proceed through a free radical mechanism and are irreversibly terminated. However, as can be seen in the GPC trace, after precipitation into excess methanol these low molecular weight fractions were removed, narrowing the molecular weight distribution.

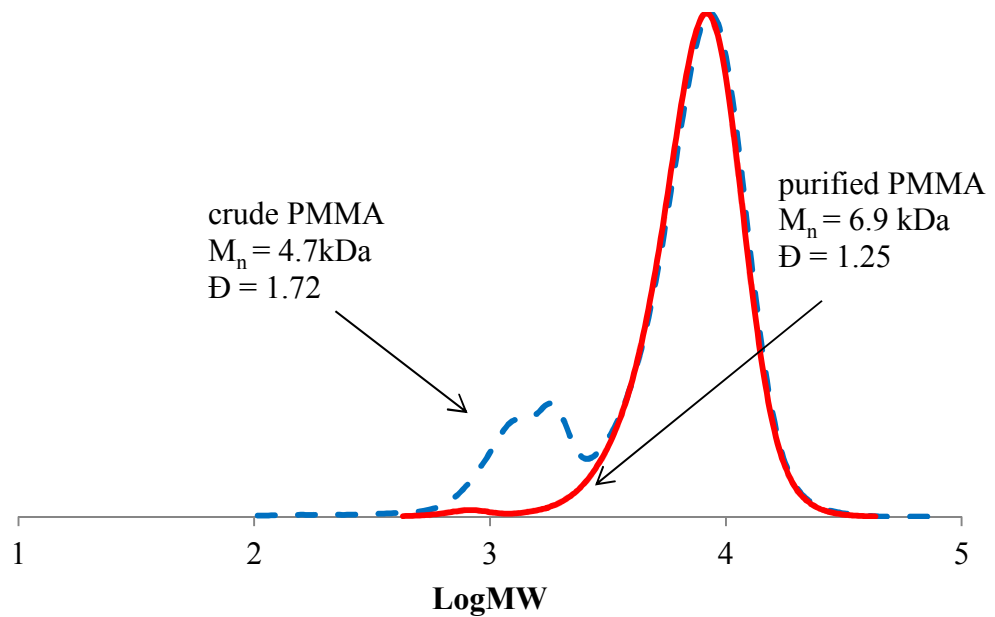


**Figure 3-20. Normalised GPC traces showing PMMA before and after precipitation into excess hexane. Removal of lower molecular weight fractions is observed by the dashed blue peak at LogMW of around 3 disappearing.**

After precipitation, all three polymers had similar molecular weights and narrow dispersities. The purified  $M_n$  values are all close to 7 kDa therefore the targeted overall  $M_n$  for the chain extensions was set to 21 kDa (1:2, PMMA:PS) to allow good separation by GPC.

**Table 3-12. Chain extension of CPDT terminated PMMA with styrene to produce polymers with  $M_n^{\text{theo}}$  of 21 kDa<sup>a</sup>**

Entry	Media <sup>b</sup>	PMMA <sup>c</sup>	[RAFT]:[AIBN]	Yield / % <sup>d</sup>	$M_n^{\text{calc}} / \text{Da}$ <sup>e</sup>	$M_n / \text{Da}$ <sup>f</sup>	$\bar{D}$ <sup>f</sup>
1	Bulk	Entry 1	5:1	84	17600	17800	1.27
2	EP 8 mL	Entry 2	5:1	44	9200	12500	1.16
3	Bulk	Entry 3	2:1	91	19100	24400	1.28
4	EP 8 mL	Entry 1	2:1	55	11600	16000	1.28
5	EP 10 mL	Entry 3	2:1	75	15800	16000	1.24

<sup>a</sup> All reactions were carried out at 65 °C for 48 h; <sup>b</sup> Bulk: Schlenk tube immersed in an oil bath, EP: 20 mL autoclave at 276 bar, the number denotes the amount of styrene used, with the [S]:[RAFT] kept constant; <sup>c</sup> Macro-RAFT agents from Table 3-11; <sup>d</sup> Determined gravimetrically after precipitation into excess methanol and dried in-vacuo at room temperature for 72 h; <sup>e</sup>  $M_n^{\text{calc}} = 21000 \times \frac{\text{yield}}{100}$ ; <sup>f</sup> Determined by GPC in THF relative to PMMA standard.

Several bulk reactions were performed to confirm that growth in CO<sub>2</sub> expanded phase followed that of conventional methods. A [RAFT]:[AIBN] ratio of 10:1 was used for the homopolymerisation of MMA, however styrene is known to polymerise at a slower rate therefore the initiator concentration was increased ([RAFT]:[AIBN] of 5:1). In the bulk polymerisation (Table 3-12, Entry 1) good chain extension was seen with a high yield of 84% and  $M_n \approx M_n^{\text{calc}}$ . For the first expanded phase chain extension, the mass/volume ratio of reactants was the same as for the homopolymer synthesis for consistency. This relates to a total mass of reactants of 13.104 g (the mass of 14 mL of MMA); corresponding to 7.248 g of styrene and 5.856 g of PMMA (Table 3-12, Entry 2). At this ratio limited growth was observed with a yield of only

44% obtained. To increase the rate of polymerisation more AIBN was used ([RAFT]:[AIBN] ratio of 2:1). A higher yield of 91% was obtained in the bulk, yet with the expanded phase only an 11 % increase was seen (Table 3-12, Entry 4).

Literature studies suggest that the volume of monomer is one of the largest contributing factors for a successful reaction. Aldabbagh *et al.* observed conversions of 27% and 45% at monomer loadings of 22% v/v and 45% v/v respectively, as the polymer precipitates at an early stage of the reaction and does not undergo further growth. At loadings of 66% v/v, conversions up to 95% were obtained as the reaction mixture remains homogeneous for longer.<sup>9</sup> The volume of reactants in the autoclave was therefore increased. PMMA and styrene were mixed in the same ratio and the volume found to be around 10 mL in total, which would lead to a 50% v/v ratio in the autoclave. Using 10 mL styrene, at the same PMMA:styrene ratio as before gave a volume of around 13 mL (Table 3-12, Entry 5). A much better growth was observed here, confirming volume was likely the main issue. This is similar to the styrene homopolymerisations at higher temperatures where the reaction was able to remain homogeneous, meaning it would be similar to a bulk reaction for longer.

To illustrate the growth a GPC trace is included (Figure 3-21), depicting the PMMA synthesised in a CO<sub>2</sub> expanded phase reaction, purified by precipitation and subsequently chain extended in both bulk and CO<sub>2</sub>. A clear shift is observed to higher molecular weights for both the bulk and expanded phase processes, indicative of a chain extension. Promisingly, little

homopolymer appears to remain in the block copolymer samples, suggesting a high degree of living character.

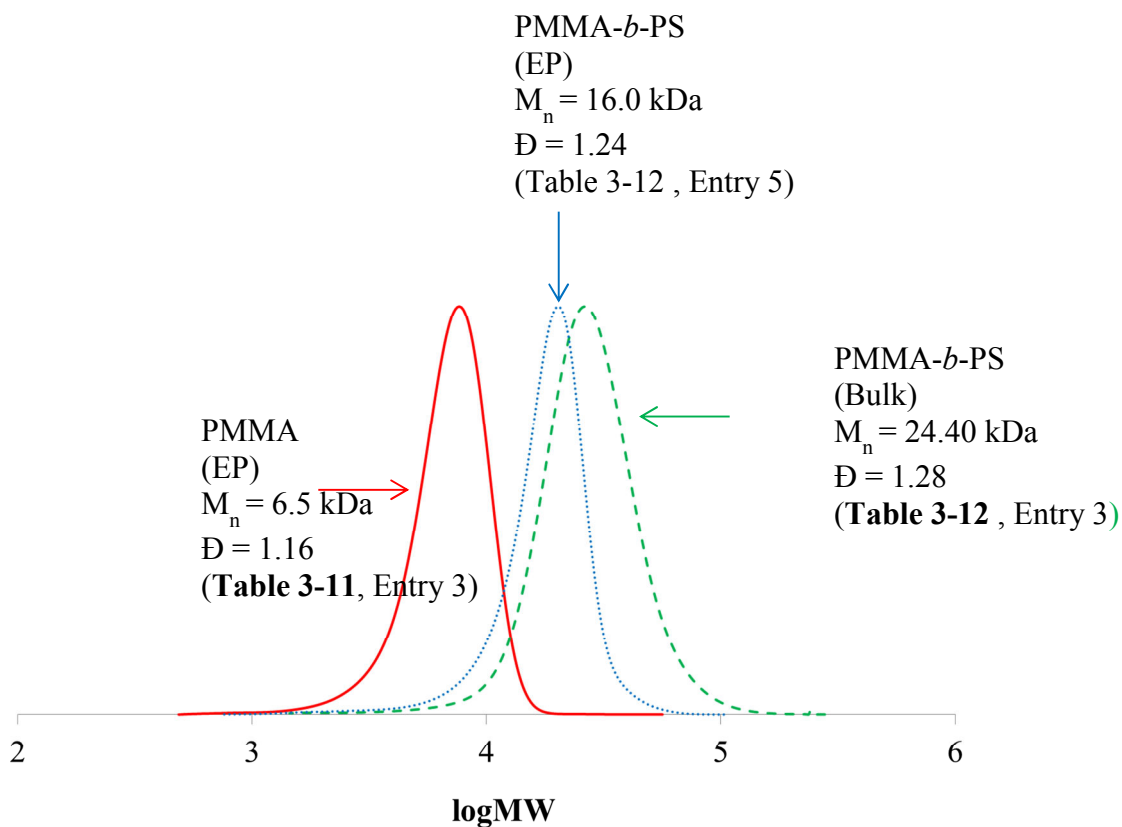


**Figure 3-21. Normalised GPC traces illustrating the shift in molecular weight after chain extension of CPDT-terminated PMMA with styrene in both bulk and CO<sub>2</sub> expanded phase.**

As CPDB mediated PMMA led to the most controlled polymer, chain extension with styrene was then attempted (Figure 3-22). There are literature examples of styrene having been homopolymerised using CPDB as the control agent, although in that system low conversions were reached and therefore a liquid product was obtained.<sup>20</sup> The same was observed here with liquid products which would display poor chain extension. This is most likely from

poor addition of styrene to the polymeric PMMA radical, causing retardation. The dithioester moiety on the CPDB RAFT agent is more stable than the trithiocarbonate group on CPDT so addition of further monomer is less likely. Styrenic radicals also have delocalisation around the ring which slows down the rate of addition. Both of these factors combine to prevent good addition of monomer to the RAFT terminated polymer. As the key aim was to produce solid powdered products CPDB controlled polymerisation was not suitable.

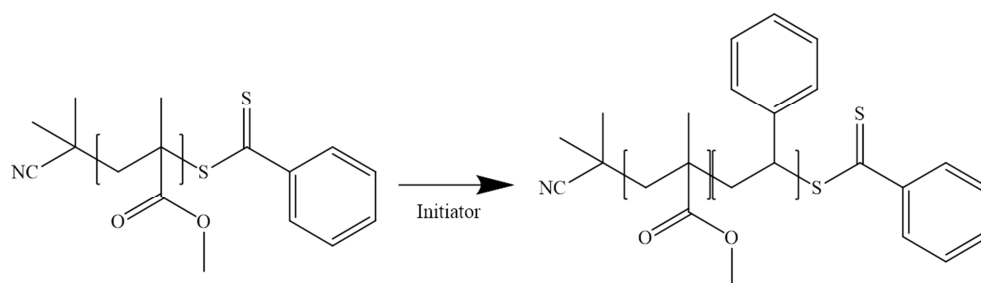


**Figure 3-22. Chain extension of PMMA-CPDB with styrene**

### 3.3.5. Supercritical Fluid Extraction of Residual Monomer

In all reactions above the polymers were dissolved in THF and precipitated into an anti-solvent to ensure good yield calculations could be made. A one-pot synthesis would be more beneficial on an industrial scale and also would totally remove the need for organic solvents. This can be achieved using supercritical fluid extraction to remove unreacted monomer post-synthesis.  $\text{ScCO}_2$  is continuously flowed through the autoclave at conditions which the monomer will dissolve into the  $\text{CO}_2$  and be removed, whilst the insoluble polymer remaining in the vessel.

MMA was polymerised in the  $\text{CO}_2$  expanded phase with CPDT and AIBN as the control agent and initiator respectively (Table 3-13. Entry 1),

unreacted monomer was then removed using scCO<sub>2</sub> followed by chain extension with styrene (Table 3-13, Entry 2).

**Table 3-13. Block copolymer synthesis with supercritical fluid extraction <sup>a</sup>**

Entry	Monomer	Duration	Yield	M <sub>n</sub> <sup>theo</sup>	M <sub>n</sub>	Đ <sup>f</sup>
		/ h	/ %	/ Da	/ Da <sup>f</sup>	
1	MMA <sup>b</sup>	24	- <sup>d</sup>	5000	5400	1.21
2	S <sup>c</sup>	48	64 <sup>c</sup>	21000	11800	1.40

<sup>a</sup> All reactions were carried out in a 20 mL autoclave at 65 °C and 276 bar; <sup>b</sup> 14 mL MMA; <sup>c</sup> 10 mL styrene, 4.49 g PMMA; <sup>d</sup> Flushed at 35 °C, 276 bar; <sup>e</sup> Determined gravimetrically after precipitation into excess hexane and dried in-vacuo at room temperature for 72 h; <sup>f</sup> Determined by GPC in THF relative to PMMA standards.

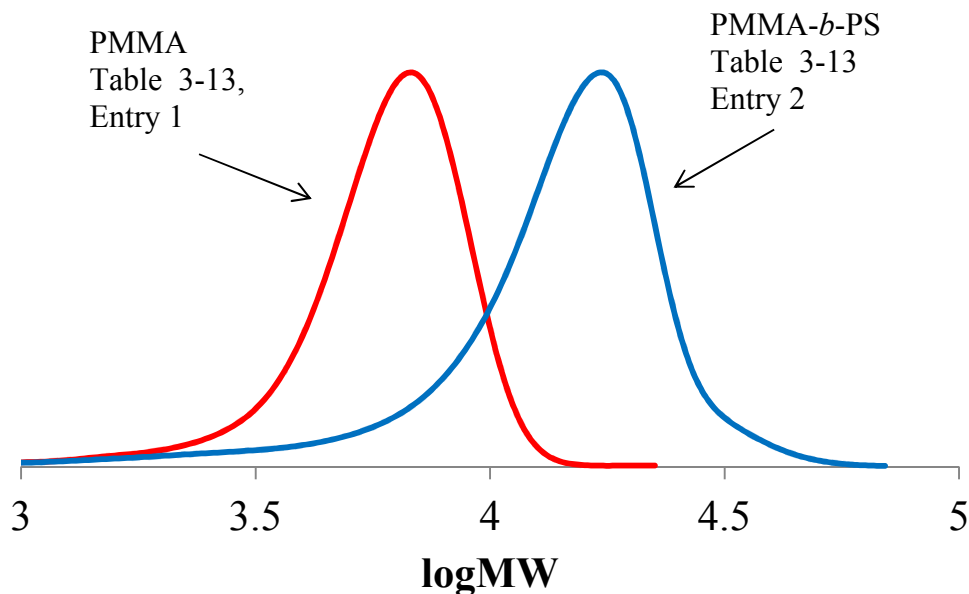


**Figure 3-23. Normalised GPC traces illustrating the data from Table 3-13. The PMMA first block, which was subsequently purified by supercritical fluid extraction, has been chain extended with PS.**

The GPC data obtained for the PMMA matched well with those in Table 3-10 indicating the same level of control is reproducible. The decline in the monomer concentration after flushing with  $\text{scCO}_2$  was quantified by  $^1\text{H}$  NMR. The product taken directly from the autoclave contained 5% of unreacted monomer and 95% polymer. This does not necessarily equate to a reaction conversion of 95% as unreacted monomer may be lost during the venting process. After 15 minutes of flushing the polymer was around 97% pure, with the second flush extracting further monomer to leave a 98 % pure product. A third extraction was able leave a >99% pure product. Through the use of extraction, a near perfectly pure polymer product remains, removing the need for using vast quantities of VOCs needed for precipitation and providing a huge environmental benefit.

The chain extension was successfully performed with a clear molecular weight shift (Figure 3-23), albeit also with a slight broadening of the dispersity which was not previously seen in for the chain extensions in Table 3-12. One explanation is related to ‘dead’ low molecular weight chains which would have been removed by precipitation but remain in the reaction mixture in this case. Upon addition of further monomer, these do not undergo further growth, thus leaving lower molecular weight chains, and as a consequence broadening the dispersity.

The regrowth presented here shows a viable route to low molecular weight block copolymers in two steps (Figure 3-24); however, through further optimisation and advances in RAFT polymerisation techniques, the living character could be improved. For example, Gody *et al.* recently published an optimised synthetic route to creating decablock copolymers (degree of polymerisation of 10 per block) using RAFT at near complete conversions (>99%).<sup>47</sup> By utilising initiators with very short half-lives they were able to have fast initiation, so all the chains began to grow at the same time. This enabled the dispersity to remain low (1.15), whilst retaining a high degree of living character (>93%). They further exploited this technique to create a dodecablock (12 blocks) copolymer from four acrylamide monomers, displaying the versatility of the technique.

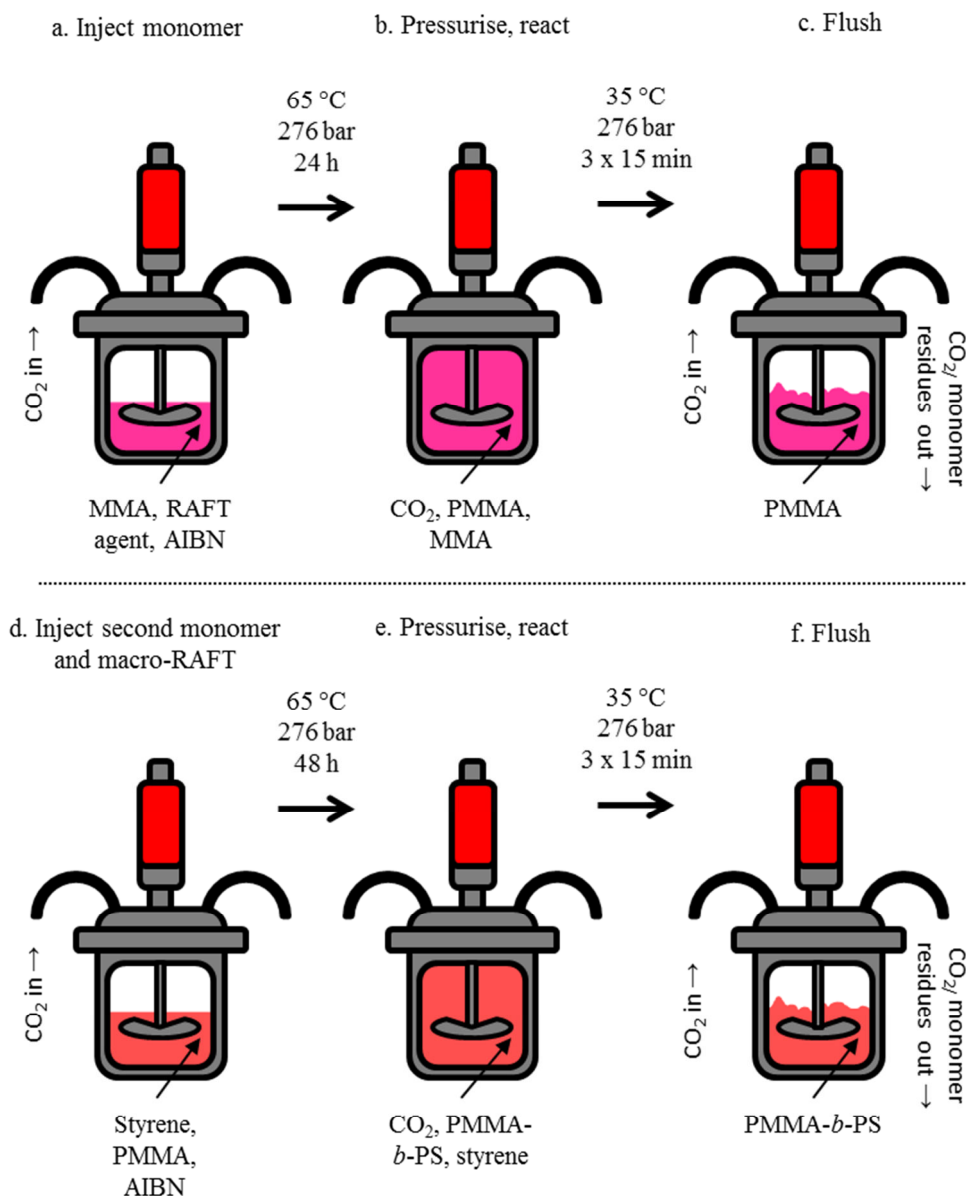


**Figure 3-24. Schematic representation of a complete block copolymer synthesis in a two-step process, without the need for complete purification and dry in between monomer additions**

### 3.4. Conclusions

CO<sub>2</sub> expanded phase offers a viable route to use supercritical fluids for polymerisations on an industrially relevant scale. The advantages of this method include using less CO<sub>2</sub> relative to dispersion and precipitation process,

which increases the amount of product per batch. No stabiliser is required to solubilise the polymer, which again presents a significant cost reduction. Finally it can be considered an environmentally friendly, “green” process; a pure, powder product remains without the need for further purification, therefore no volatile organic solvents are required for work up. The RAFT controlled polymerisation of styrene has been successfully carried out in a CO<sub>2</sub> expanded phase process generating polymer of controlled molecular weight and narrow dispersity at high yields. Most importantly however, it has been shown that time-consuming purification processes can be avoided through the use of supercritical fluid extraction. Earlier work in our group with PMMA indicated a molecular weight limit related to the critical entanglement chain length, restricting potential applications. By ensuring efficient agitation of the reaction mixture high molecular weight PMMA and PS have been synthesised in a controlled manner. A relationship with viscosity has been proposed in order to explain the impact of whether the viscosity can be reduced sufficiently by using CO<sub>2</sub> as a plasticiser, the reaction can proceed efficiently. If the viscosity becomes too high, the magnetically coupled stirrer inside the autoclave stops working efficiently, creating two phases of polymerisation and a poor overall product. The top layer proceeds through a free radical polymerisation mechanism leading to broad and uncontrolled molecular weights, whereas the lower layer remains controlled by the RAFT agent.

Taking these limitations into account the controlled synthesis of low molecular weight block copolymers consisting of PMMA-*b*-PS has been successfully shown. Solubility and viscosity again play an important role with minimum amounts of second monomer required to solubilise the first polymer

block to ensure good chain extension. Finally, two-step synthesis has been performed by incorporating supercritical fluid extraction in between monomer additions yielding dry, powdered PMMA-*b*-PS block copolymer.

It is envisaged that this could be extended to other more industrially relevant oligomeric block copolymers in the future, for example one with a hydrophilic block and a hydrophobic block such as PAAc-*b*-PS have applications as non-ionic surfactants.<sup>48</sup>

### 3.5. References

1. J. L. Kendall, D. A. Canelas, J. L. Young and J. M. DeSimone, *Chemical Reviews*, 1999, **99**, 543-563.
2. T. Arita, S. Beuermann, M. Buback and P. Vana, *E-Polymers*, 2004.
3. F. Aldabbagh, P. B. Zetterlund and M. Okubo, *European Polymer Journal*, 2008, **44**, 4037-4046.
4. K. Adlington, A. Green, W. X. Wang, S. M. Howdle and D. J. Irvine, *Dalton Transactions*, 2013, **42**, 127-136.
5. F. Picchioni, *Polymer International*, 2014, **63**, 1394-1399.
6. G. R. Akiel and M. Poliakoff, *Green Chemistry*, 2009, **11**, 1083-1100.
7. P. G. Jessop and B. Subramaniam, *Chemical Reviews*, 2007, **107**, 2666-2694.
8. D. W. Pu, M. P. Devitt, S. C. Thickett, F. P. Lucien and P. B. Zetterlund, *Polymer*, 2013, **54**, 6689-6694.
9. R. McHale, F. Aldabbagh, P. B. Zetterlund and M. Okubo, *Macromolecular Chemistry and Physics*, 2007, **208**, 1813-1822.

10. F. Aldabbagh, P. B. Zetterlund and M. Okubo, *Macromolecules*, 2008, **41**, 2732-2734.
11. J. Liu, B. X. Han, Z. M. Liu, J. Wang and Q. Huo, *Journal of Supercritical Fluids*, 2001, **20**, 171-176.
12. Q. Xu, B. X. Han and H. K. Yan, *Polymer*, 2001, **42**, 1369-1373.
13. Q. Xu, B. X. Han and H. Yan, *Journal of Applied Polymer Science*, 2003, **88**, 1876-1880.
14. J. Liu, B. X. Han, R. Zhang, Z. M. Liu, T. Jiang and G. Y. Yang, *Journal of Supercritical Fluids*, 2003, **25**, 91-97.
15. Z. B. Guan, J. R. Combes, Y. Z. Menciloglu and J. M. Desimone, *Macromolecules*, 1993, **26**, 2663-2669.
16. G. Zwolak, N. S. Jayasinghe and F. P. Lucien, *Journal of Supercritical Fluids*, 2006, **38**, 420-426.
17. G. Zwolak and F. P. Lucien, *Macromolecules*, 2006, **39**, 8669-8673.
18. G. Zwolak and F. P. Lucien, *Macromolecules*, 2008, **41**, 5141-5147.
19. P. O'Connor, P. B. Zetterlund and F. Aldabbagh, *Macromolecules*, 2010, **43**, 914-919.
20. T. Arita, M. Buback and P. Vana, *Macromolecules*, 2005, **38**, 7935-7943.
21. J. Li, *Free radical polymerisation in supercritical carbon dioxide expanded phase*, 2012, **The University of Nottingham**, 1-205.
22. J. T. Lai, D. Filla and R. Shea, *Macromolecules*, 2002, **35**, 6754-6756.
23. J. Jennings, M. Beija, A. P. Richez, S. D. Cooper, P. E. Mignot, K. J. Thurecht, K. S. Jack and S. M. Howdle, *Journal of the American Chemical Society*, 2012, **134**, 4772-4781.

24. L. J. Fetters, D. J. Lohse, S. T. Milner and W. W. Graessley, *Macromolecules*, 1999, **32**, 6847-6851.
25. U. W. Gedde, *Polymer Physics*, Springer, Chapman and Hall, London, 1995.
26. J. Li, University of Nottingham, 2012.
27. K. J. Thurecht, A. M. Gregory, W. Wang and S. M. Howdle, *Macromolecules*, 2007, **40**, 2965-2967.
28. P. B. Zetterlund, F. Aldabbagh and M. Okubo, *Journal of Polymer Science Part a-Polymer Chemistry*, 2009, **47**, 3711-3728.
29. J. Chiefari, R. T. A. Mayadunne, C. L. Moad, G. Moad, E. Rizzardo, A. Postma, M. A. Skidmore and S. H. Thang, *Macromolecules*, 2003, **36**, 2273-2283.
30. Y. K. Chong, J. Krstina, T. P. T. Le, G. Moad, A. Postma, E. Rizzardo and S. H. Thang, *Macromolecules*, 2003, **36**, 2256-2272.
31. J. R. Royer, J. M. DeSimone and S. A. Khan, *Journal of Polymer Science Part B-Polymer Physics*, 2001, **39**, 3055-3066.
32. M. D. Elkovitch, L. J. Lee and D. L. Tomasko, *Polymer Engineering and Science*, 2001, **41**, 2108-2125.
33. M. D. Elkovitch, D. L. Tomasko and L. J. Lee, *Polymer Engineering and Science*, 1999, **39**, 2075-2084.
34. J. R. Royer, Y. J. Gay, M. Adam, J. M. DeSimone and S. A. Khan, *Polymer*, 2002, **43**, 2375-2383.
35. L. Yu, H. Liu and L. Chen, *Polymer Engineering and Science*, 2009, **49**, 1800-1805.

36. P. D. Condo, D. R. Paul and K. P. Johnston, *Macromolecules*, 1994, **27**, 365-371.
37. C. Gutierrez, J. F. Rodriguez, I. Gracia, A. de Lucas and M. T. Garcia, *Journal of Supercritical Fluids*, 2013, **76**, 126-134.
38. P. Alessi, A. Cortesi, I. Kikic and F. Vecchione, *Journal of Applied Polymer Science*, 2003, **88**, 2189-2193.
39. C. A. Kelly, S. M. Howdle, K. M. Shakesheff, M. J. Jenkins and G. A. Leeke, *Journal of Polymer Science Part B-Polymer Physics*, 2012, **50**, 1383-1393.
40. D. Gourgouillon, H. Avelino, J. Fareleira and M. N. da Ponte, *Journal of Supercritical Fluids*, 1998, **13**, 177-185.
41. C. A. Kelly, A. Naylor, L. Illum, K. M. Shakesheff and S. M. Howdle, *Advanced Functional Materials*, 2012, **22**, 1684-1691.
42. M. Siau, B. S. Hawkett and S. Perrier, *Journal of Polymer Science Part a-Polymer Chemistry*, 2012, **50**, 187-198.
43. J. C. Brendel, H. Burchardt and M. Thelakkat, *Journal of Materials Chemistry*, 2012, **22**, 24386-24393.
44. G. Moad, E. Rizzardo and S. H. Thang, *Australian Journal of Chemistry*, 2006, **59**, 669-692.
45. G. Moad, E. Rizzardo and S. H. Thang, *Polymer*, 2008, **49**, 1079-1131.
46. G. Moad, E. Rizzardo and S. H. Thang, in *Fundamentals of Controlled/Living Radical Polymerization*, eds. B. Z. Tang, N. V. Tsarevsky and B. S. Sumerlin, Royal Soc Chemistry, Cambridge, Editon edn., 2013, pp. 205-249.

47. G. Gody, T. Maschmeyer, P. B. Zetterlund and S. Perrier, *Macromolecules*, 2014, **47**, 3451-3460.
48. J. M. Heinen, A. C. M. Blom, B. S. Hawkett and G. G. Warr, *Journal of Physical Chemistry B*, 2013, **117**, 3005-3018.

## Chapter 4 – Dispersion polymerisation in scCO<sub>2</sub>

---

### 4. Overview

Polymer particles with a variety of internal ordered structures are being developed to fulfil a number of applications, such as data arrays<sup>1</sup> and biomedical delivery vehicles.<sup>2</sup> Time-consuming methods are required to produce good quality block copolymers, with lengthy procedures needed to create the phase separated micro-particles. Recently, self-assembly of block copolymers synthesised by controlled radical polymerisations have gained much interest as these techniques become more developed and industrially viable. These block copolymers can be produced *via* dispersion polymerisations in organic solvents such as hexane or alcohols, which still require purification steps to yield dry, phase separated micro-particles.<sup>3</sup>

One pot dispersion polymerisations in scCO<sub>2</sub> offer an alternative route to producing dry polymer micro-particles, with block copolymers synthesised by this method showing internally ordered structures.<sup>4</sup> Specific CO<sub>2</sub>:polymer swelling interactions are responsible for altering the phase behaviour, with different morphologies observed compared to theory. This Chapter will describe the design and implementation a novel high pressure cell for measuring small angle x-ray scattering patterns of the particles *in situ* during a scCO<sub>2</sub> dispersion polymerisation.

A disadvantage of block copolymer micro-particles synthesised in scCO<sub>2</sub> is the loss of structure upon dissolving in aqueous or organic solvents. The second half of this Chapter will investigate the addition of a cross-linker during the synthesis to trap the phase separated structures.

## 4.1. Introduction

### 4.1.1. Block copolymer phase separation

Macroscopic phase separation occurs when two immiscible polymers are blended leaving domains of each individual polymer.<sup>5</sup> Since the advent of controlled radical polymerisation, block copolymers been synthesised more readily allowing systems where two immiscible blocks are chemically bound to one another. This has led to studies into microphase separation with diblock copolymers being the focus for the remainder of this Chapter.

The Flory-Huggins interaction parameter ( $\chi$ ) refers to the immiscibility of the two blocks which drives the phase separation. Unfavourable segment-segment interactions are minimised by the phase separation, in turn reducing the enthalpy. The degree of polymerisation (N) also must be taken into account when determining if two blocks will phase separate (Equation 4-1); the product of  $\chi$  and N having to exceed the theoretically derived value of 10.5.<sup>6</sup>

$$\chi N > 10.5$$

**Equation 4-1.**

The interaction parameter is temperature (T) dependent (Equation 4-2) with  $\alpha$  and  $\beta$  related to the copolymer composition and volume fraction (f). Thus temperature is heavily involved in determining the observed morphology for block copolymers.

$$\chi \approx \alpha T^{-1} + \beta$$

**Equation 4-2.**

Not all block copolymers will therefore phase separate and miscible diblock copolymers can form disordered domains. To induce phase separation for a block copolymer where  $\chi N$  does not exceed 10.5, the chains must be mobile to enable rearrangement of the structures, with two methods existing for this; heating above the glass transition temperatures of both blocks, or dissolving in a suitable solvent. A disorder-order transition (DOT) is where the polymers initially form a homogeneous mixture and upon changing conditions self-assemble. Alternatively an order-disorder transition (ODT) is the reverse, with a self-assembled structure reverting back to a homogeneous mixture. Order-order transitions (OOTs) occur when an already phase separated structure moves across the phase diagram and a change in morphology is observed.

The inverse temperature dependence means segment-segment interactions tend to decrease at higher temperatures, increasing miscibility. Upon cooling the phase separated structures form, known as an upper order-disorder transition (UODT). The opposite case, phase separation induced by heating, is known as a lower disorder-order transition (LDOT).

Figure 4-1 details the common morphologies that diblock copolymers can self-assemble into.<sup>7</sup> The morphology is dictated by the relative volume fraction of the two blocks, usually referred to as the volume fraction of one block, for example  $f_A$  is the volume fraction of block A in an A-B copolymer. To reduce the enthalpic interactions as much as possible the blocks will arrange themselves to minimise the interfacial area. This is denoted as the thermodynamic morphology. In general if  $f_A = 0.5$  a lamellar structure is formed. As  $f_A$  increases or decreases the morphology will shift through

gyroidal, cylindrical to spherical structures with the smaller block phase held in a matrix of the majority block.

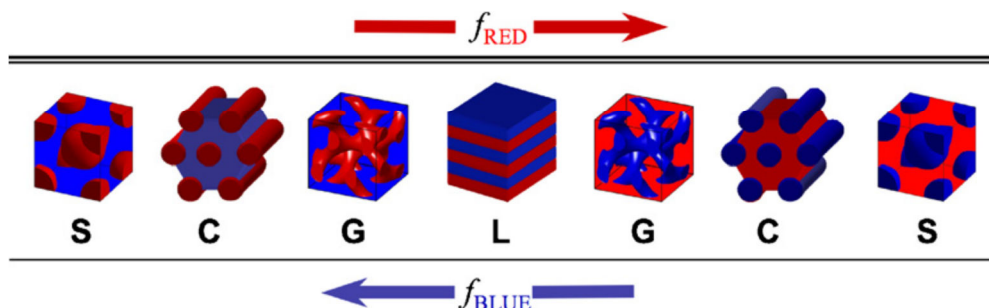


**Figure 4-1. Common morphologies for A-B type diblock copolymers upon increasing volume fraction of block A ( $f_A$ ). S = spherical, C = cylindrical, G = gyroidal, L = lamellar.<sup>7</sup>**

#### 4.1.2. Phase separation in $scCO_2$

The effect of polymers in  $CO_2$  has been well studied with regards to synthetic benefits discussed earlier in this Thesis, moreover there are influences on polymer properties, specifically, lowering of glass transition temperatures in Chapter 3 where  $CO_2$  was able to easily penetrate in between polymer chains.<sup>8, 9</sup> Zhang *et al.* have studied swelling of block copolymers with  $CO_2$ , finding each individual block behaved the same as its respective homopolymer.<sup>10</sup>

Literature on phase behaviour of block copolymers in  $scCO_2$  is generally composed of studies involving treatment of polymer films at elevated temperatures in the presence of  $CO_2$  followed by offline analysis<sup>11-13</sup> with selected examples below.

Many articles focus on polymers which have a  $CO_2$ -philic block, such as siloxanes and fluorinated polymers, with a  $CO_2$ -phobic block.<sup>14</sup> For example,

Li *et al.* studied thin films of poly(ethylene oxide)-*b*-poly(1,1'-dihydroperfluorooctyl methacrylate) (PEO-*b*-PFOMA).<sup>15</sup> Whilst disordered up to 180 °C in a vacuum, under  $scCO_2$  at 139 bar an ODT was noted between 116 – 145 °C with spherical domains of PEO embedded in the PFOMA matrix between 60 - 116 °C. Selective swelling of the PFOMA block at lower temperatures caused an increase in  $\chi$  inducing the phase separation, whereas at higher temperatures the selectivity of  $CO_2$  for one block was reduced leading to the disordered state once again.

Shi *et al.* investigated a poly(dimethyl siloxane)-*b*-poly(2,5-bis[(4-methoxyphenyl)oxycarbonyl]styrene) (PDMS-*b*-PMPCS) under  $CO_2$ .<sup>16</sup>  $CO_2$  treatments were above the estimated  $T_g$ 's of both polymers, the higher of which was the PMPCS estimated as between 61-67 °C. An OOT occurred from hexagonal cylinders to lamellae at 110 bar, attributed to a preferential swelling of the PDMS (increased  $f_{PDMS}$ ) and higher  $\chi_{eff}$ . Interestingly, thermal annealing post treatment enabled a transition back to the original cylindrical morphology.

Plasticising polymers with  $CO_2$  increases the mobility of polymer chains facilitating self-assembly at lower temperatures. In examples where polymer degradation is likely at temperatures required for phase separation to occur this is particularly beneficial.<sup>13</sup> Also, specific segment swelling of block copolymers by  $CO_2$  follows a similar pattern to that seen for conventional solvents where preferential absorption for one block can alter the phase separation. In general, the volume fraction of the more solvent-philic block is increased, affecting the interaction parameter thus inducing transitions. As seen

in the examples above this includes generating nanostructures not seen under conventional conditions.

#### 4.1.3. Phase separation in $scCO_2$ – *in situ* studies

The effect of  $CO_2$  on poly(styrene)-*b*-poly(isoprene) (PS-*b*-PIp) copolymers was investigated by Vogt *et al.* via *in situ* SANS.<sup>17</sup> No specific interactions dominated owing to the similar solubility of  $CO_2$  in both blocks; it behaved as a neutral solvent. However, the ODT temperature was lowered as the miscibility of the two blocks increased; attributed to screening of unfavourable enthalpic interactions. Further evidence of the  $CO_2$  acting as a neutral solvent was gathered with a relationship between the depression in the ODT temperature and the amount of absorbed gas noted. This study has been extended by measuring the swelling of the respective PS and PIp blocks with  $CO_2$ .<sup>18</sup> The same group have since studied transitions for both poly(styrene)-*b*-poly(*n*-hexyl methacrylate) (PS-*b*-PnHMA) and poly(styrene)-*b*-poly(*n*-butyl methacrylate) (PS-*b*-PnBMA).<sup>19</sup> Firstly the PS-*b*-PnHMA acted similarly to PS-*b*-PIp with absorbed  $CO_2$  able to screen the unfavourable enthalpic interactions lowering the temperature at which the two blocks became miscible, leading to an ODT 7 °C lower at a  $CO_2$  density of 0.25 g mL<sup>-1</sup>. With PS-*b*-PnBMA a more dramatic decrease in the LDOT was observed (>60 °C depression at 0.058 g mL<sup>-1</sup>  $CO_2$ ) owing to the more disfavoured entropic contribution from polymer chains being compressed, increasing the likelihood of phase separation.

In the previous example,<sup>19, 20</sup> and elsewhere<sup>21</sup>, the high penetration power of neutrons in SANS enables the use of sapphire windows, in a similar way to

the view cells introduced in Chapter 2. For x-rays however, the sapphire would weaken the transmission of the x-rays to an unacceptably low level, thus diamond windows must be employed. Although the photon energy of the beam can be increased to penetrate the windows it can affect the sample, for example inducing crystallisation.<sup>22</sup> A number of other groups have used high pressure cells for studying SAXS in high pressure environments.<sup>23-25</sup>

Shinkai *et al.* have since used *in situ* SAXS analysis to observe the OOT from hexagonal cylinders to lamellar morphology for a poly(styrene)-*b*-poly(perfluorooctylethyl methacrylate) (PS-*b*-PFMA copolymer at 60 °C and pressures exceeding 100 bar.<sup>26</sup> Upon depressurisation the newly formed structures retained the lamellar morphology. This is consistent with their earlier offline studies where OOT were observed after CO<sub>2</sub> treatment at 60 °C and 80 bar.

The same group have since investigated a PMMA-*b*-PFMA copolymer *in situ* also.<sup>27</sup> The interaction parameter between two blocks usually increases with selective swelling by CO<sub>2</sub> although in this paper the opposite occurred. An ODT was observed at around 200 bar at 90 °C initially, with further experiments concluding that a CO<sub>2</sub> density of 0.6 g ml<sup>-1</sup> was necessary for an ODT to occur. With no ODT noted for the pristine block copolymer ruling out temperature based effects a specific CO<sub>2</sub> effect must be present, masking the repulsive interactions between the respective blocks. This has been denoted as a retrograde ODT.

#### 4.1.4. Internally ordered block copolymer particles – indirect synthesis

A number of methods exist for creating internally phase separated block copolymer particles, most commonly exploiting solvent evaporation-induced self-assembly. These include self-organised reprecipitation (SORP), solvent-absorbing/solvent-releasing (SARM), evaporation-induced self-assembly *via* emulsion or aerosol, and evaporation-induced self-assembly *via* mini-emulsion.

The SARM method requires a two-step method. Firstly particles are prepared as an emulsion in water with the help of surfactants, followed by addition of an organic solvent to swell the particles. This gives the block copolymer enough mobility to phase separate and during the evaporation of this solvent the internal structures are trapped. Examples in the literature include poly(methyl methacrylate)-*b*-poly(styrene),<sup>28-30</sup> and poly(styrene)-*b*-poly(butadiene).<sup>31,32</sup>

For SORP, particles are prepared by evaporation of a good solvent from a solution containing the block copolymer in a mixture of both good and bad solvents, which themselves must be miscible. A key advantage over SARM is no extra surfactant is needed to produce the particles. In general, as solvent quality decreases nucleation of the particles increases, with slow evaporation required to ensure a narrow particle size distribution as shown by Yabu *et al.* in 2005.<sup>33</sup> Increasing the concentration of polymer caused an increase in particle size also. A number of internally phase-separated block copolymer particles of varying morphologies have been prepared by this method including poly(styrene)-*b*-poly(isoprene),<sup>33-35</sup> poly(styrene)-*b*-poly(2-vinylpyridine),<sup>36</sup> and poly(allyl glycidyl ether)-*b*-poly(lactide).<sup>37</sup>

All of these methods have severe disadvantages with respect to industrial scalability. Multiple steps are required, expensive anionic polymerisations are typically used to synthesise the copolymers (see Chapter 1), and they use volatile organic compounds as solvents. An alternative route is the use heterogeneous polymerisation techniques including emulsion, mini-emulsion and dispersion polymerisations in which block copolymers are synthesised and self-assembly occurs *in situ*.

#### 4.1.5. Internally ordered block copolymers particles – direct synthesis

Tausendfreund *et al.* reported the dispersion polymerisation of poly(styrene)-*b*-poly(butadiene) (PS-*b*-PBd) copolymers in a range of alkanes *via* anionic methods.<sup>38</sup> Several phase separated morphologies were observed for di and triblock copolymers, in all cases a low volume fraction of PBd was maintained.

Nicolas *et al.* first used CRP methods to create ordered block copolymer particles, synthesising di and triblock copolymers consisting of poly(*n*-butyl acrylate) as the first/central block and poly(styrene) or poly(methyl methacrylate) as the second/outer blocks.<sup>3</sup> Onion-like morphologies were observed, with the lamellar structure maintained upon thermal annealing and solvent casting.

Okubo *et al.* have utilised ATRP to synthesise poly(*i*-butyl methacrylate)-*b*-poly(styrene) in various seeded mini-emulsion processes.<sup>39-41</sup> Control over the internal morphologies were dictated by the polymerisation temperature, affecting the homopolymer content and subsequent blocking efficiency.

Several RAFT controlled dispersion polymerisations have generated internally ordered block copolymer particles.<sup>4, 42</sup> Wei *et al.* produced PS-*b*-PBd, building on the work of Tausendfreund *et al.*, and were able to tune the internal morphology by varying the volume fraction of the respective blocks.

Recently in our group, block copolymer particles containing internal micro-phase separation were synthesised in a one-pot  $scCO_2$  dispersion polymerisation.<sup>4, 43</sup> MMA was first polymerised to make the PMMA particles, with the second monomer added *via* an HPLC pump, growing from the living end group to create the block copolymer. SEM showed discrete spherical micro-particles, with cross-sections of these particles displaying the internal phase separation (Figure 4-2).

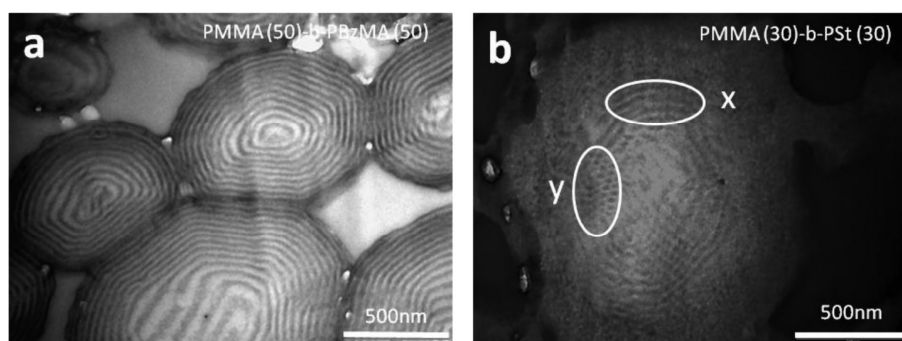


**Figure 4-2. TEM images from Jennings *et al.* showing internal phase separation inside block copolymer particles synthesised in a RAFT controlled  $scCO_2$  dispersion polymerisation.<sup>4</sup>**

For PMMA-*b*-p(benzyl methacrylate) showed well defined lamellar morphologies as expected for this block copolymer. However, in certain systems, such as PMMA-*b*-PS the observed phase separation was different to that seen for conventionally prepared films. This led to the conclusion that specific  $CO_2$  interactions were influencing the phase behaviour. The more

CO<sub>2</sub>-philic segment (PMMA) swelled in the presence of CO<sub>2</sub> relative to the less CO<sub>2</sub>-philic block (PS) which changed the relative volume fraction, changing the morphology. Upon thermal annealing or solvent casting the block copolymers reverted back to the theoretically expected morphology. The ability to physically trap these structures would offer a green route to phase separated micro-particles, with cross-linking a potential route.

#### 4.1.6. Cross-linking

Polymers can be cross-linked through chemical and physical means, but it is chemical cross-links where individual polymer chains are chemically bound to one another which are most relevant for this work. Typically this is done by the addition of a multi-vinyl co-monomer, which has two or more reactive double bonds which are susceptible to radical attack. Other methods include using disulfide linkages, most commonly known for the vulcanisation processes for example in car tyres.<sup>44</sup> Cross-linking polymers changes a variety of their properties, mainly physical ones such as glass transition temperatures, thermal stability and viscosity. Examples of applications include microgels and superabsorbents, as the cross-linked networks absorb solvent and swell, but the chains do not dissolve.<sup>45</sup> Other applications lie in separations science, resins and controlled release of drugs.<sup>46</sup>

The incorporation of a cross-linker in a FRP can occur at any point; therefore a random network is formed. Perfectly branched structures, such as dendrimers, exist but require expensive and time-consuming multiple step syntheses. Using CTAs and CRP methods the amount of branching and cross-linking can be influenced, with examples seen for ATRP,<sup>47</sup> CCTP,<sup>48</sup> as well as

RAFT.<sup>49-51</sup> The typical effect is a delay in the gelation point compared to FRP, allowing highly branched networks to be formed, and more even distribution of cross-linking points. Functionality can also be added, with pendent double bonds available to react with a second aliquot of monomer to create star polymers with cross-linked cores.<sup>47</sup>

#### 4.1.7. Cross-linking in *scCO*<sub>2</sub>

There have been several reports of synthesising cross-linking polymers in *scCO*<sub>2</sub>. The first of these were from Cooper in the late 1990s studying the polymerisation of divinyl benzene (DVB) with ethylvinylbenzene (EVB).<sup>46</sup> The commercial grades of DVB are either 55 wt% DVB with 45 wt% EVB, or 80 wt% DVB with 20 wt% EVB, therefore these two ratios were studied, at conditions of 65 °C and 310 bar. High yields (90%) were obtained with and in the absence of a fluorinated stabiliser, with well-defined spherical particles observed by SEM. This was rationalised by the rigid cross-linked surfaces being unable to aggregate when collisions occurred. In a following paper two other divinyl monomers were studied, ethylene glycol dimethacrylate (EGDMA) and trimethylolpropane trimethacrylate (TRM) although neither produced defined spherical particles in their limited investigations.<sup>52</sup>

Polymerisations in *scCO*<sub>2</sub> offer a clean route to synthesising cross-linked polymers for applications as hydrogels or superabsorbents. Poly(acrylic acid) (PAAc) has been synthesised in *scCO*<sub>2</sub>, with a multi-vinyl cross-linker triallyl pentaerythritol ether or tetraallyl pentaerythritol ether.<sup>53</sup> Highly agglomerated particles were observed in the SEM, although the polymer was able to be dispersed in water to create gels.

Cross-linked poly(N-isopropylacrylamide) (PNIPAAm) has been synthesised by several groups in scCO<sub>2</sub> precipitation polymerisation.<sup>54-56</sup> The first by Temtem *et al.* used N,N-methylenebisacrylamide (MBAM) as the cross-linker up to 4.5 wt%. As with Cooper *et al.* the higher cross-linker concentrations led to the more discrete particles, with the rigid surfaces less able to agglomerate. Cao *et al.* also used MBAM at concentrations up to 20 wt% achieving similar results, as did Hu and co-workers utilising EGDMA at 26.4 wt%.

Vivaldo-Lima *et al.* polymerised a number of ratios of styrene/DVB by FRP in a scCO<sub>2</sub> dispersion polymerisation.<sup>57</sup> They chose two surfactants, PS-*b*-PDMS and Krytox 257 FSL, with typical conditions between 172 - 310 bar and 65 - 80 °C using AIBN as the radical initiator. Good conversions were achieved with particles sizes between 1 – 2 µm, although agglomeration was observed for all samples; this was the least severe with the fluorinated surfactant. The authors attributed the agglomeration to poor mixing.

The same group have since published a study of a similar system controlled using RAFT polymerisation; in bulk,<sup>58</sup> and scCO<sub>2</sub>.<sup>59</sup> In bulk it was found that the addition of the RAFT agent delayed the onset of gelation allowing a more homogeneous cross-link density distribution. The same conclusions were made in scCO<sub>2</sub>. The SEM images however show heavily agglomerated structures, with the slower polymerisation rate causing the polymer particles to be tacky for longer and able to merge together.

Li *et al.* polymerised 80 wt% DVB (20 wt% EVB) in scCO<sub>2</sub> with acetone as a co-solvent.<sup>60</sup> In pure CO<sub>2</sub> the particles were highly agglomerated, but with increasing acetone concentration the particles became more discrete

and also more uniform in size. This, and the methods described have shown a number of viable routes to creating cross-linked, discrete, spherical micro-particles in scCO<sub>2</sub>.

#### 4.1.8. Aims and objectives

*In situ* investigations of the complex systems in scCO<sub>2</sub> are critical to gain an insight to the structural changes that occur due to absorbed CO<sub>2</sub>. The one pot scCO<sub>2</sub> dispersion syntheses in particular would benefit, where understanding when the phase separation occurs could enable targeting of specific morphologies and tuning by CO<sub>2</sub> pressure for example.

This Chapter details the design and construction of a new high pressure cell for measuring X-ray scattering in scCO<sub>2</sub>. A number of criteria were chosen to fulfil; a large volume relevant for industrial applications, the ability to measure both SAXS and WAXS simultaneously, a flexible design to accommodate different path lengths, all whilst maintaining a safe vessel. *In situ* monitoring of dispersion polymerisations in scCO<sub>2</sub> were then required to elucidate information concerning the internal phase separation of the block copolymer particles.

Secondly, through the addition of a cross-linker, is it possible to harden the particles and prevent their dissolution when placed in solvents post-reaction. The first aim is to maintain the spherical nature of the polymer particle. Finally, can the phase separated structures be retained when incorporating the cross-linker, potentially cross-linking only one phase.

## 4.2. Experimental

### 4.2.1. Materials

Methyl Methacrylate (MMA, 99%) and Styrene (St, 99%) were obtained from Acros. Benzyl methacrylate (BzMA, 98%) was purchased from Alfa Aesar. Inhibitors were removed from both monomers prior to use by passing through a column of neutral aluminium oxide. Monomers were then degassed by bubbling with argon for 45 minutes and stored in the freezer. 2,2'-Azobis(2-methylpropionitrile) (AIBN, 98%) was purchased from Sigma-Aldrich and purified by recrystallizing twice in methanol. 2-(Dodecylthiocarbonothioylthio)-2-methylpropionic acid (DDMAT) was synthesised following literature procedure or purchased from Sigma-Aldrich (97% purity) and used as received. Poly(dimethyl siloxane monomethyl methacrylate) (PDMS-MA,  $M_n = 10$  kDa) was purchased from ABCR. Dry  $CO_2$  (SFC grade, 99.99%) was purchased from BOC.

### 4.2.2. *In-situ* SAXS measurements

Simultaneous SAXS-WAXS experiments have been conducted at the Dutch-Belgian Beamline (DUBBLE) station BM26-B of the European Synchrotron Radiation Facility (ESRF) in Grenoble (France). Two sample-detector distances have been used which covered a scattering angle range of 0.03-1.9  $nm^{-1}$  and 0.07-3.65  $nm^{-1}$  respectively. The scattering vector  $q$  is defined as  $q = 4\pi/\lambda \sin\theta$  with  $2\theta$  being the scattering angle. Experiments were performed using a wavelength of 0.6526 Å (15 Kev). A Dectris-Pilatus 1M detector with a resolution of  $981 \times 1043$  pixels and a pixel size of  $172 \times 172$   $\mu m$  has been employed to record the 2D SAXS scattering patterns. The data

were normalized to the incident beam intensity and were corrected for absorption and background scattering. Silver Behenate patterns were used for the wave-vector calibration. WAXS patterns have been acquired by a 300K linear Pilatus detector (254 mm x 33.5 mm active area). The maximum diffraction angle recordable is about  $2\theta = 40^\circ$  and a pixel size of  $172 \times 172 \mu\text{m}$ . The wavenumber  $q = 4\pi/\lambda \sin\theta$  scale for WAXS experiments was calibrated using the diffraction pattern of alpha alumina as a reference.

#### 4.2.3. MMA homopolymerisation

Poly(dimethylsiloxane monomethyl methacrylate) (PDMS-MA, 0.5616 g) was weighed into a 100 mL round bottom flask. DDMAT (0.0410 g, 0.1123 mmol) and AIBN (0.0184 g, 0.1123 mmol) were weighed into glass vials and transferred into the same round bottom flask containing the PDMS-MA. This was sealed with a septum and degassed for 30 minutes to remove the oxygen. Once degassed, MMA (6 mL, 56 mmol) was transferred *via* a glass syringe into the flask with PDMS-MA, DDMAT and AIBN. Once homogeneous, this was transferred *via* a glass syringe into the autoclave through the key hole. The autoclave was then sealed and  $CO_2$  added until a pressure of around 48 bar (700 psi) was reached. The overhead stirrer was set to 300 rpm and the solution agitated for 10 minutes to ensure efficient mixing had taken place. The vessel was heated to  $65^\circ\text{C}$ , this related to around  $80^\circ\text{C}$  on the external heating controller, and once at the reaction temperature the pressure was raised to 210 bar (3000 psi). The reaction was left for 18 hours at which time the heating and stirring was stopped. Once at ambient temperature the  $CO_2$  was slowly vented, the vessel opened and the product collected.

4.2.4. *One pot synthesis of block copolymers*

The PMMA block was begun as in the previous section and left to react for 18 hours. CO<sub>2</sub> was vented until a pressure of 138 bar (2000 psi) was reached to allow addition of the second monomer. AIBN (0.0552 g, 0.3369 mmol) was weighed into a 100 mL round bottom flask and degassed with argon for 30 minutes. BzMA (16.2 mL, 95.61 mmol) was transferred to the AIBN *via* a glass syringe to make a stock solution. In total BzMA (5.4 mL, 31.87 mmol) and AIBN (0.01844 g, 0.1123 mmol) was then added to the reaction *via* the attached HPLC pump. This was left for a further 24 hours, the temperature lowered to ambient and the autoclave vented over around 30 minutes. The product was then collected and analysed.

### 4.3. Results and Discussion

#### 4.3.1. New High Pressure Cell

The details of the new high pressure cell have been described in Chapter 2, along with the rig diagrams and standard operating procedures. Figure 4-3 shows the engineering drawing of the vessel, illustrating the components required and position of the diamond windows, with a more detailed window schematic in Figure 4-4.

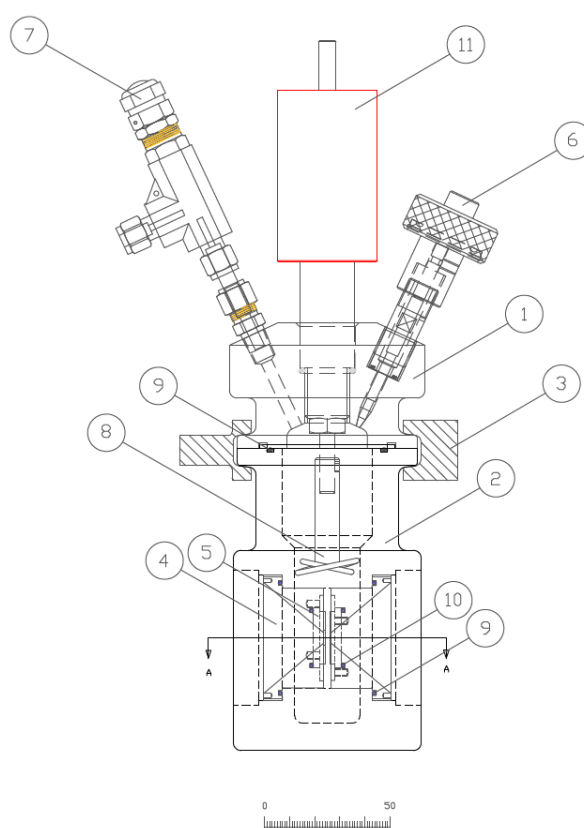


**Figure 4-3. Engineering drawing showing details of the high pressure X-ray scattering cell consisting of (1) Head, (2) Cell Body, (3) Clamp, (4) Screwed Window Holder, (5) Carbide Window Holder, (6) Safety Needle Assembly, (7) Swagelok Blow Off Valve, (8) Paddle Stirrer, (9) O-ring (EPDM 42 mm x 2 mm), (10) O-ring (BS019 EPDM 35 mm x 1.78 mm) and (11) Overhead Magnetic Stirrer. Scale bar in mm.**

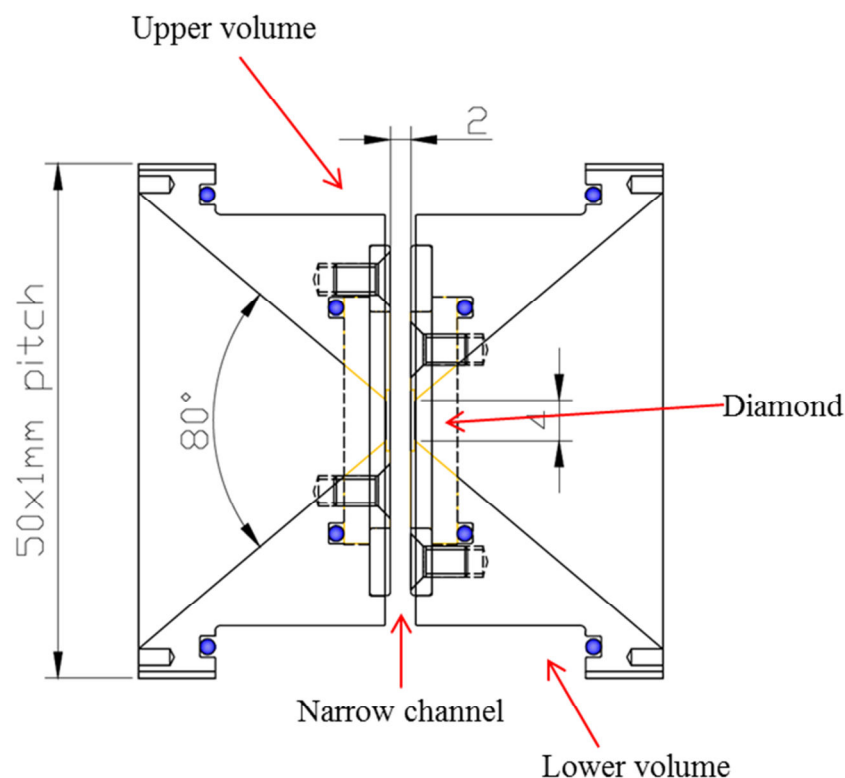


**Figure 4-4. Diamond window inserts showing the 80° clear optical aperture for collecting simultaneous SAXS-WAXS. The free window diameter is 4 mm and the exit opening angle is 40°. All lengths on the diagram are in mm**

Briefly, the cell is constructed from AISI 316/316L EN1.4401/4404 certified stainless steel. It is composed of a head containing the stirrer, thermocouple, safety devices and CO<sub>2</sub> inlet and outlet pipes, which is clamped to the heated bottom section housing the threaded mounts for the diamond windows. The windows themselves are made from a synthetic single crystal diamond type III (Element 6), with a thickness of 0.4 mm ± 0.05 mm, and an optical path length between them of 2 - 2.5 mm. The cell is suitable to be operated at a maximum pressure of 210 bar and maximum temperature of 120 °C, with over pressure devices and electrical trips protecting the integrity of

the cell. The cell was pressure tested to ensure safe operation prior to use, and that all of the new features associated with the diamond windows were suitable.

The first experiments were to determine if the same product from polymerisation could be obtained in both a standard 60 mL MKIII autoclave and the new vessel. One key requirement of the system chosen was that the polymerisation would reach completion in as quick a time as possible to efficiently utilise the time at the beamline. All previous studies have begun with a first block of PMMA followed by either benzyl methacrylate (BzMA), styrene (S), dimethylaminoethyl methacrylate (DMAEMA) or dimethyl acrylamide (DMA). A PMMA-*b*-PBzMA copolymer was therefore selected, as it would give both a relatively short reaction duration as well as the benzyl groups offering some electron density difference compared to the MMA side group for contrast in the SAXS.

#### 4.3.2. Reproducibility

With any new autoclave design the reproducibility must be tested to ensure the same product is being formed. This was tested by synthesising PMMA particles in a RAFT controlled  $scCO_2$  dispersion polymerisation. PDMS-MA was used as the stabiliser at 5 wt% relative to monomer, DDMAT as the RAFT agent, with AIBN as the initiator at a [RAFT]:[I] ratio of 2:1.<sup>4, 43</sup>

In a standard 60 mL autoclave the reaction proceeds in a controlled manner (Table 4-1, Entry 1), give an  $M_n$  very close to the  $M_n^{\text{theo}}$ , and narrow dispersity. The first attempt in the x-ray cell (Table 4-1, Entry 2) gave a much higher  $M_n$  and broader molecular weight distribution. Upon opening the cell,

the polymer product was not obtained as a powder, but as a large agglomerated piece in the base of the autoclave. Due to the narrow channel between the main volume of the cell and the lower section (Figure 4-4, Figure 4-5), the mixing will not be as efficient, therefore if the polymer is poorly stabilised then it will precipitate and remain in the base. A magnetic flea was added, with a magnetic stirrer built into the autoclave stand to allow dual stirring (Table 4-1, Entry 3).

**Table 4-1. PMMA homopolymer synthesis <sup>a</sup>**

Entry	Autoclave	P / bar	M <sub>n</sub> / Da <sup>b</sup>	Đ <sup>b</sup>	Appearance <sup>c</sup>	Notes
1	Standard	276	49400	1.27	Powder	-
2	X-ray	200	71200	1.74	Solid	Single Stirring <sup>d</sup>
3	X-ray	200	64000/26900 <sup>e</sup>	1.43/1.73	Powder	Dual Stirring <sup>f</sup>

<sup>a</sup> All reactions were carried out at 65 °C bar for 18 hours, with M<sub>n</sub><sup>theo</sup> of 50 kDa at 100% conversion, [DDMAT]:[AIBN] molar ratio of 2:1, 5 wt% PDMS-MA as stabiliser; <sup>b</sup> Determined by GPC in THF relative to PMMA standards; <sup>c</sup> Visual appearance of product; <sup>d</sup> Overhead stirrer only; <sup>e</sup> Samples taken from the top/bottom of the cell; <sup>f</sup> Overhead stirrer and magnetic flea in the base.

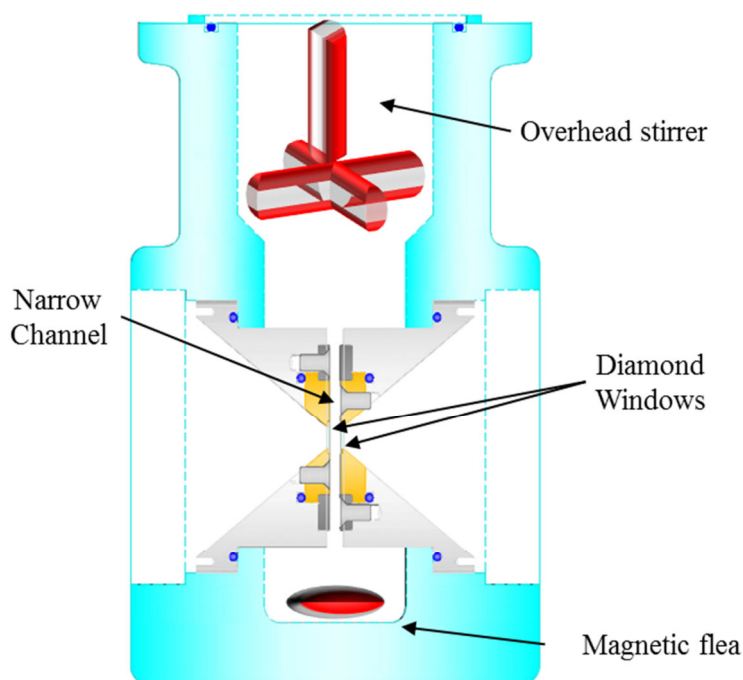
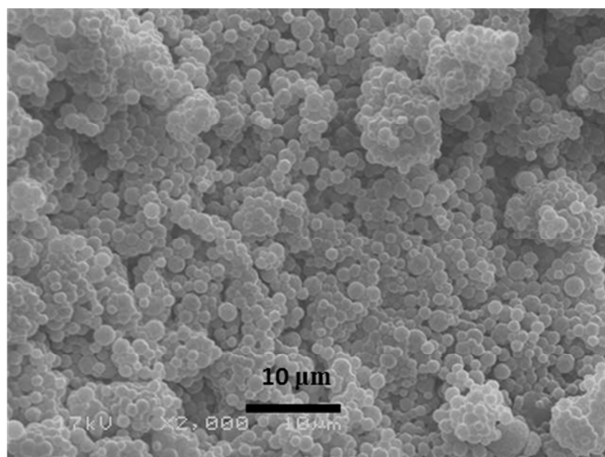


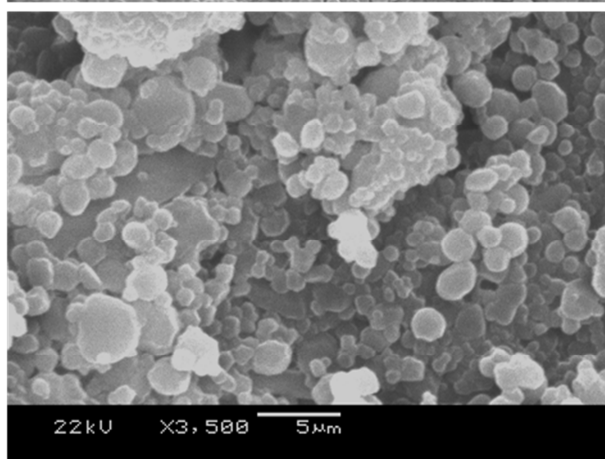
**Figure 4-5. Schematic of the x-ray autoclave base. The overhead stirrer is in the main volume of the cell (around 40 mL), and the magnetic flea in the base (around 15 mL).**

An improvement in the product appearance was gained, with a free flowing powder produced. The  $M_n$  values, however, were vastly different between the top and bottom. Controlling the  $M_n$  is important in this RAFT polymerisation, as this indicates if the RAFT mechanism is working effectively, thus allowing good chain extension upon addition of further monomer. The product morphology is also extremely important to show a stable dispersion is maintained (Figure 4-6).

Entry 1  
Standard autoclave  
PMMA



Entry 2,  
X-ray autoclave,  
PMMA  
single stirring



Entry 3  
X-ray autoclave  
PMMA  
dual stirring

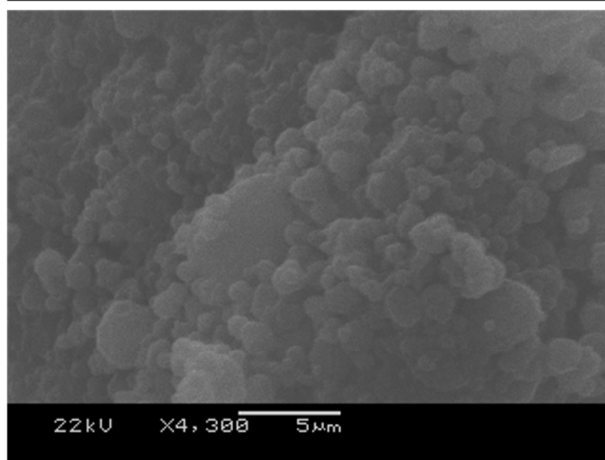


**Figure 4-6. SEM images of the polymers from Table 4-1. (top) In a standard autoclave discrete spherical particles are obtained, (bottom) Both polymerisations in the X-ray cell were highly agglomerated and poor stabilised.**

There is a clear difference in the quality of the particles produced in a standard autoclave, and those produced in the x-ray cell. PMMA synthesised in

the standard autoclave (Figure 4-6, top) gave discrete, uniform, spherical micro-particles. The samples from the x-ray cell had a wide range of morphologies, with some spherical particles, but most of these were highly agglomerated.

These results indicated that the cell itself would not produce the same polymers as the current standard autoclave. This has been attributed to poor mixing, owing to the narrow path length in the centre of the cell needed to acquire good SAXS data. The opportunity to spend some time at the ESRF beamline was presented at short notice, therefore to check if adding the second monomer could produce any block copolymer, the one-pot, two-step synthesis was first attempted offline. This also served as a test of the new high pressure setup.

#### 4.3.3. *Block copolymer synthesis in the x-ray cell*

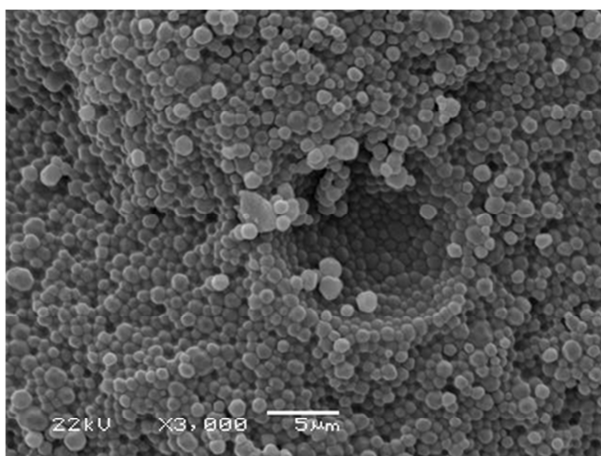
Following the procedure from Jennings *et al.*,<sup>4, 43</sup> the synthesis of a PMMA-*b*-PBzMA block copolymer was attempted (Table 4-2, Figure 4-7). The key difference was the pressure at which the second monomer was added. In a standard autoclave at the maximum operating pressure is 300 bar, therefore to safely add the second amount of BzMA the pressure is reduced to around 200 bar prior to injection. However, the x-ray cell has a maximum operating pressure of 206 bar, therefore the autoclave pressure had to be reduced to around 140 bar before injection. At the lower pressure the solubility of the stabilisers is greatly reduced, potentially causing precipitation of polymer instead of remaining well dispersed. Two syntheses in the x-ray cell are shown (Entries 2 and 3) for highlight the differences between samples.

**Table 4-2. PMMA-*b*-PBzMA block copolymer synthesis <sup>a</sup>**

Entry	Autoclave	P / bar	$M_n$ / Da <sup>b</sup>	$\bar{D}$ <sup>b</sup>	Appearance <sup>c</sup>
1	Standard	276	68500	1.56	Powder
2	X-ray	200	41900	2.52	Powder, solid in base
3	X-ray	200	17100	1.80	Powder, solid in base

<sup>a</sup> All reactions were carried out at 65 °C bar for 18 hours, with  $M_n^{theo}$  of 50 kDa at 100% conversion, [DDMAT]:[AIBN] molar ratio of 2:1, BzMA added and reacted for a further 24 hours to produce an overall  $M_n^{theo}$  of 100 kDa, 5 wt% PDMS-MA stabiliser with respect to total monomer weight; <sup>b</sup> Determined by GPC in THF relative to PMMA standards; <sup>c</sup> Visual appearance of product.

Entry 1  
standard autoclave  
PMMA<sub>50</sub>-*b*-PBzMA<sub>50</sub>



Entry 3,  
X-ray autoclave  
PMMA<sub>50</sub>-*b*-PBzMA<sub>50</sub>

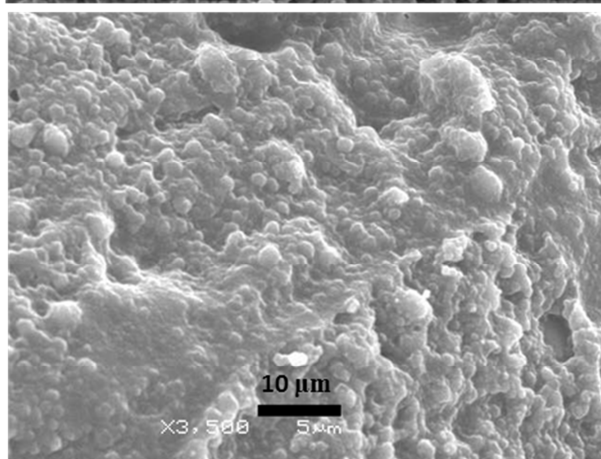


**Figure 4-7. SEM images of the polymers from Table 4-2, (top) Standard autoclave again shows discrete spherical particles, (bottom) Both the block copolymerisation in the X-ray cell had highly agglomerated particles.**

As with the homopolymer PMMA the standard autoclave produced polymer of narrow dispersity (Table 4-2, Entry 1), with defined spherical particles (Figure 4-7, top). Both repeats in the x-ray cell were less successful (Table 4-2, Entries 2 and 3), with broad dispersities and lower than targeted  $M_n$  values. The SEM confirmed a poor dispersion (Figure 4-7, bottom images), with highly agglomerated particles. The large differences between the two syntheses in the x-ray cell highlight how irreproducible the results are, for example the dispersities are 2.52 and 1.80, which will greatly affect the polymer quality. The mixing issue has been discussed, however, the maximum operating pressure is also a key problem, especially when lowering the pressure to add the second monomer. At 140 bar, the density of  $CO_2$  is only  $0.5057 \text{ g mL}^{-1}$  compared to  $0.6917 \text{ g mL}^{-1}$  at 200 bar, therefore the PDMS-MA will have poorer solubility in the medium, and is less able to stabilise the dispersion.

#### 4.3.4. *CO*<sub>2</sub> Backgrounds

Although the syntheses in the new cell were unsuccessful, certain features were required to be tested on line in order to evaluate their suitability, in particular the diamond windows. All SAXS data was produced and analysed with the help of Daniel Hermida-Merino and Guiseppe Portale at BM-26 @ ESRF. Another greatly important experiment was to understand the scattering behaviour of pure  $CO_2$ . The tuneable density of  $CO_2$  is one key advantage for controlling its solvation power, especially in separations science. The density

is particularly sensitive near the critical point (31.1 °C, 73.8 bar), with small changes in pressure able to drastically alter the density (Figure 4-8).

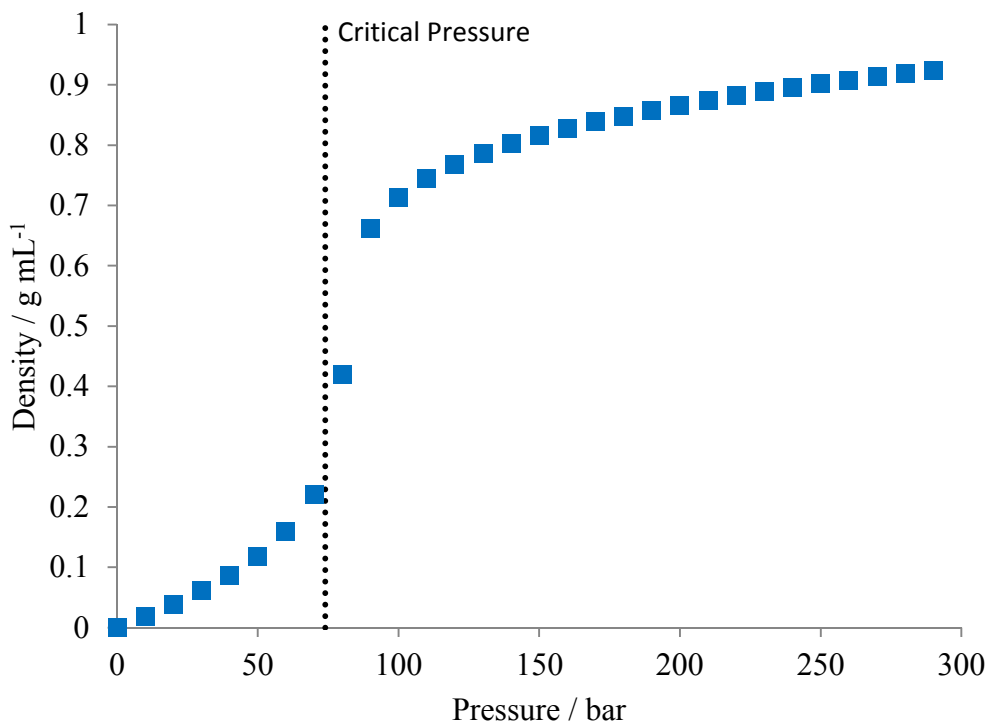


**Figure 4-8. Isothermal change in density with pressure for CO<sub>2</sub> at 35 °C. The critical pressure of 73.8 bar is marked. All values taken from the NIST webbook.<sup>61</sup>**

These density fluctuations are capable of producing a measurable SAXS background, therefore measurements of  $scCO_2$  under isothermal conditions above the critical temperature (35 °C) and over a range of pressures (100-200 bar) were collected (Figure 4-9).

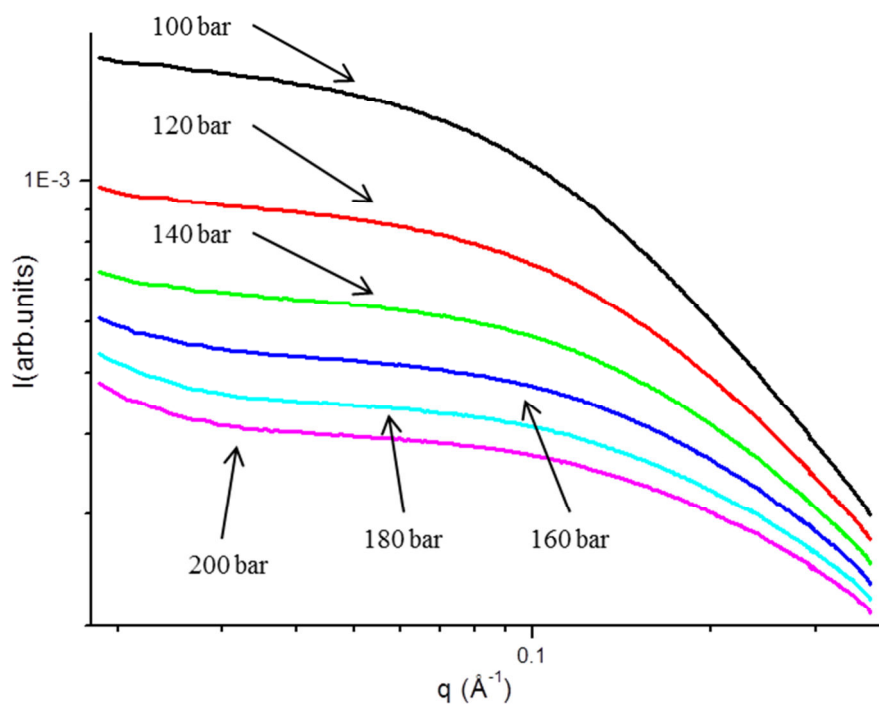


**Figure 4-9. SAXS profiles of pure CO<sub>2</sub> at isothermal conditions above the critical temperature (35 °C) over a range of pressures, always above the critical pressure (73.8 bar).**

The Ornstein-Zernike expression (Equation 4-3) can be used to monitor the density fluctuations with the change in pressure as shown previously by Nishikawa and Tanaka.<sup>62, 63</sup> Where  $I(q)$  is the scattering intensity measured by SAXS,  $q$  is the scattering vector,  $\xi$  is the Ornstein-Zernike correlation length,  $I(0)$  is the scattering intensity at  $q = 0$ .

$$I(q) = I(0)/(1 + \xi^2 q^2)$$

**Equation 4-3.**

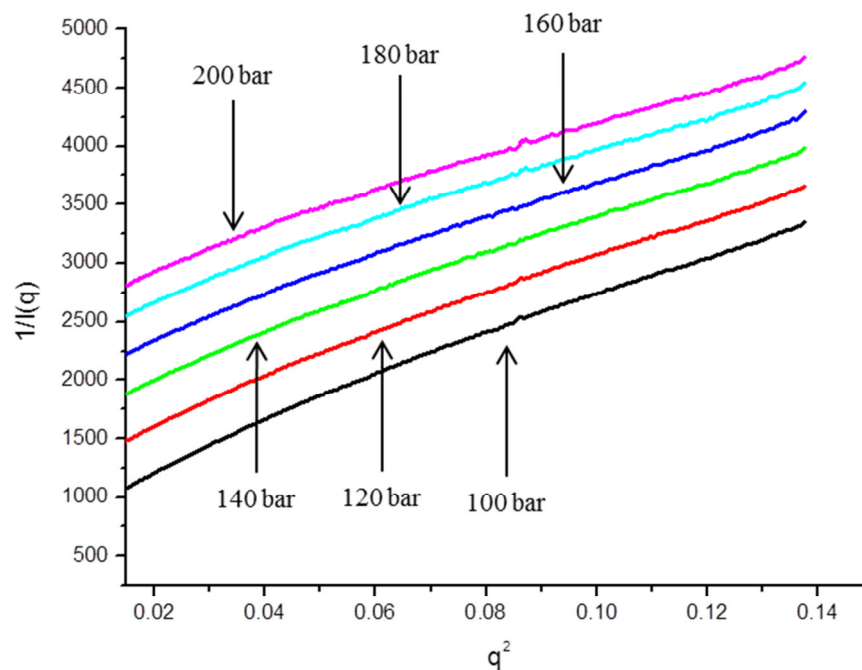


**Figure 4-10. Ornstein-Zernike plots at 35 °C and varying pressures between 100 and 200 bar. The decrease in intensity as function of pressure is due to the decrease in density fluctuations**

In this case the correlation length and density fluctuations near the critical point are in good agreement with previous studies (7 Å at 100 bar).<sup>62, 63</sup> The background from the diamond windows is negligible compared to these density fluctuations indicating the suitability of the single crystal diamonds employed. The determination of the intensity scattering fluctuations is relevant for future experiments as they will be superimposed as a background upon the scattering intensity that result from structural changes in a sample.

4.3.5. *Initial synthesis in situ*

To further understand the suitability of the new cell, the synthesis of a block copolymer in a *scCO*<sub>2</sub> dispersion polymerisation was attempted. It was not expected to produce well-defined polymer particles owing to the poor mixing, but was utilised as a test to see if any changes were noted over the duration of the reaction. PMMA-*b*-PBzMA was again synthesised in a one-pot, two-step manner.

MMA was polymerised for 18 hours off-line to ensure good conversion based on earlier results. BzMA and further AIBN were then injected using an HPLC pump; this was synchronised with the start of the SAXS data collection (Figure 4-11). The rapid increase of intensity and the shift to lower  $q$  of the scattering maximum around  $q = 0.1 \text{ nm}^{-1}$  indicates a change in the structure or morphology of the polymer.

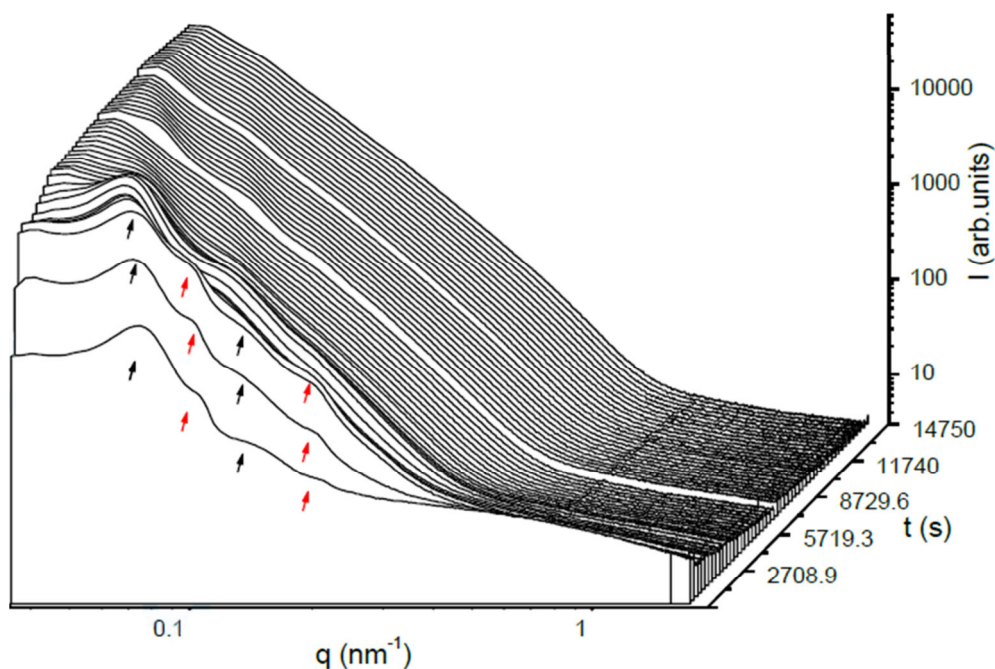


**Figure 4-11. Time-resolved SAXS profiles acquired during the RAFT polymerisation synthesis of PMMA-*b*-PBzMA. The data were collected with a frame rate of 60 s/frame, at a pressure of 200 bar and temperature of 65 °C. The start of the data collection coincides with the addition of BzMA to the PMMA- $CO_2$  dispersion. A photon energy of 15 keV was used which allowed a transmission of 83% of the direct beam through the empty cell. The arrows indicate where structure develops, attributed to a change in size of the micro-particles.**

The SEM images of the polymer (Figure 4-12) again show poor control over the dispersion mechanism with some highly agglomerated particles, as well as areas with no discernible structure. The product itself was a mixture of larger pieces of polymer as well as a solid that filled the lower section of the cell and was unable to be removed without the use of solvents to dissolve the polymer. The GPC data also displays a very broad dispersity for a RAFT controlled polymerisation ( $\mathcal{D} = 1.89$ ) and the  $M_n$  is far lower than the theoretical value ( $M_n = 35,800$  Da compared with  $M_n^{\text{theo}} = 100,000$  Da).

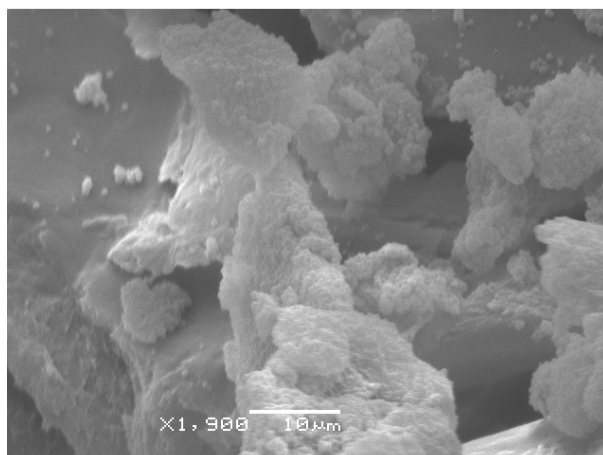


**Figure 4-12. SEM images of the PMMA-*b*-PBzMA synthesised during the *in situ* SAXS measurements.  $M_n = 35900$  Da,  $D = 1.89$  (relative to PMMA standards).**

However, the changes in the scattering meant some structure was being probed. A more detailed description of the evolution of the total scattering intensity ( $Q$ ) or Porod invariant can be found by comparing the electron density difference between the two phases ( $n_e$ ), and the volume fractions of these two phases ( $\phi_1$  and  $\phi_2$ ) (Equation 4-4). It is a particularly useful measurement to make, as when the relative volume fractions of the two phases are equal,  $Q$  reaches a maximum. The data are plotted in Figure 4-13.

$$Q = \int_0^{\infty} I(q)q^2 dq \propto \langle n_e \rangle^2 \phi_1 \phi_2$$

**Equation 4-4.**

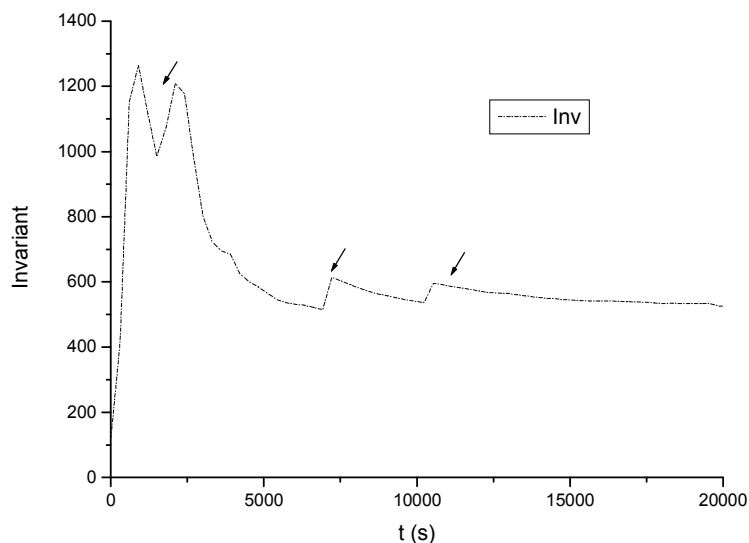


**Figure 4-13. Porod Invariant evolution with time during the polymerisation reaction of PMMA with BzMA. A rapid increase was observed in total scattered intensity which is followed by a slower decrease. The discontinuities in the curve (marked with arrows) can be attributed to the increase in pressure due to the addition of  $CO_2$ . This shows how important a proper determination of the pressure, and thus the background scattering, is.**

Some initial observations can be made. Initially a rapid increase is seen, followed by a slower decrease in the total scattered intensity. The discontinuities in the curve are associated with the addition of  $CO_2$  and thus pressure changes of the system. As discussed the second monomer is added at a pressure of around 140 bar and slowly topped up with  $CO_2$  until the reaction conditions of 200 bar are reached. This had to be manually added in three separate occurrences, leaving time between additions for the cell to equilibrate. This shows that the experiments are rather sensitive to the pressure and the scattered background that it introduced. This is an important point to note for future experiments, with drastic pressure changes needed to be minimised.

Disregarding the discontinuities we can explain the occurrence of a maximum in the data around 2500 seconds (41 minutes) by the fact that in a two phase system the Porod invariant exhibits a maximum when the volume fractions of both phases are equal. Usually this is related to the volume fractions of the respective blocks in a block copolymer. After this short reaction duration, any particles are expected to be mainly PMMA swollen with  $CO_2$  and BzMA monomer. In the early stages after the BzMA addition, two distinct phases are observed from the SAXS data (Figure 4-11, black and red arrows). As the polymerisation proceeds, the two phases evolve into a single phase, displayed by a dramatic decrease in the invariant. This can be attributed to a decrease in the electron density contrast term of Equation 4-4, due to an increased miscibility of the two phases. A number of reasons can potentially explain this. The presence of the  $scCO_2$  can reduce the interaction parameter between the two phases (Equation 4-1),<sup>6</sup> as explained in section 4.1.3. The degree of polymerisation is low for this sample also, which will also reduce the chance of  $\chi N > 10.5$  and inducing phase separation. This effect was seen by Jennings *et al.* for PMMA-*b*-PBzMA, where at low relative volume fractions of PBzMA the blocks became miscible and no phase separation was observed.<sup>4</sup>

#### 4.3.6. X-ray cell MKII

A second autoclave is now in development to address the problems encountered with the synthesis in the MKI cell. The maximum operating pressure is to be increased to at least 300 bar, equivalent to the standard autoclaves used for the original block copolymer synthesis. This should

increase the solubility of the PDMS-MA stabiliser, helping to maintain a stable dispersion when adding the second monomer *in situ*.

Secondly, to improve both the stirring efficiency and ease of cleaning post-reaction, a new internal design has been proposed (Figure 4-14), whilst preserving the short path length between the diamond windows.

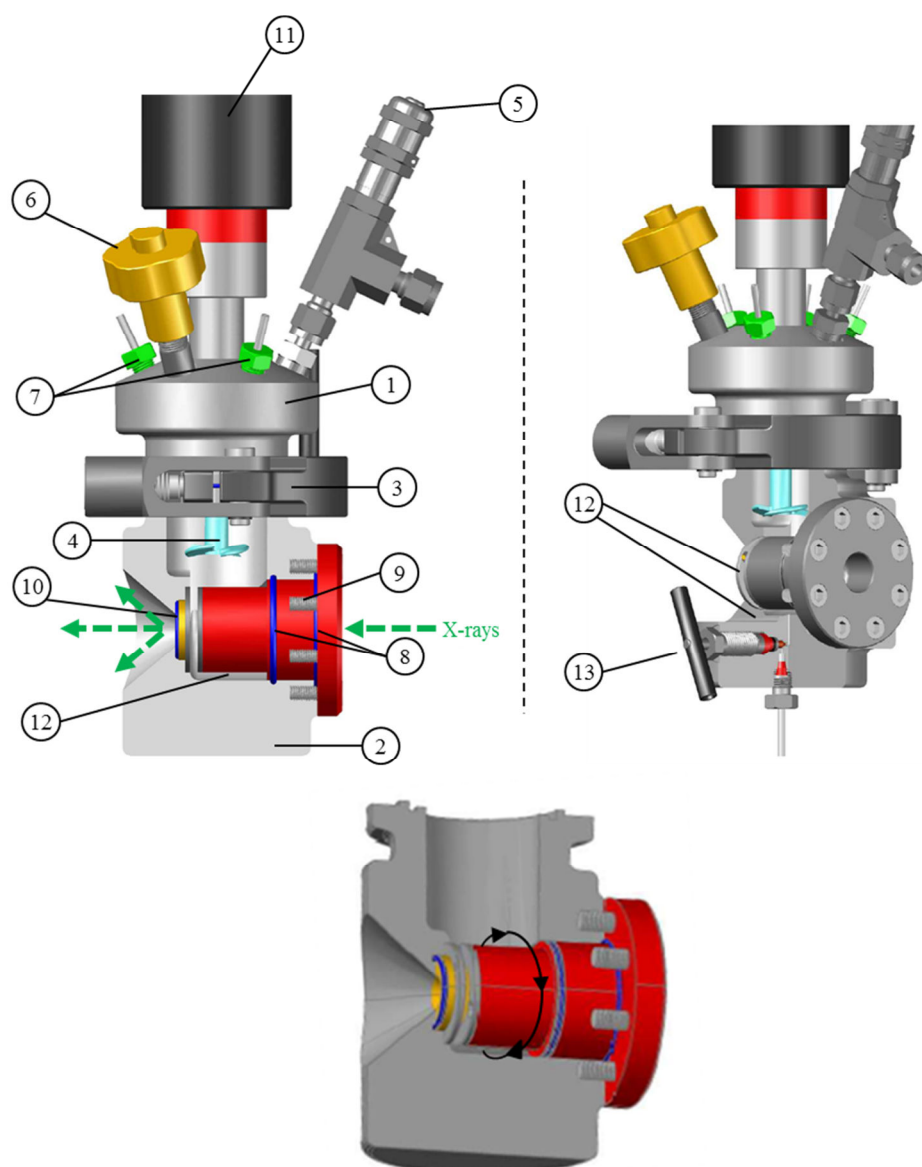


**Figure 4-14. (top) Representation of the MKII x-ray cell. (1) Head, (2) Cell Body, (3) Clamp, (4) Stirrer Blade, (5) Spring Loaded Pressure Relief Valve, (6) Torque Thumbwheel, (7) Inlet and outlet pipes, (8) O-rings, (9) Screws to secure new window holder into the cell body, (10) Diamond windows, (11) Magnetically Coupled Overhead Stirrer, (12) Gap between the window holder to allow polymer to be mixed efficiently, (13) HIP Tap for sampling. (Bottom) Simplified cut-out view of the window holder and main reactor volume, the arrows shows how the CO<sub>2</sub>/reactants can flow around the window holder.**

By creating a curved interior the polymer particles should be forced around and the smooth surface should prevent them building up at edges where the mixing is the least efficient. The bottom image in Figure 4-14 shows a simplified cross-section, with the channel around the window holder for the polymer to flow around. A number of stirrer blade angles and heights will be studied to probe the most successful design also.

The threaded mounts on the MKI were liable to becoming stuck in the body as monomer was able to reach the threads and polymerise. For the MKII, the window holder will be secured in place using screws into the body which are not open to the reactor volume (Figure 4-14, (9)). This removes the possibility of monomer polymerising around the screws, which should enable far easier removal of the insert and facilitate product collection and cleaning post-reaction.

Finally, modifications to the head will create extra ports for building in an HIP tap for adding the second monomer *in situ* (similar to the modified MKIII standard cell introduced in Chapter 2). An HIP tap will also be housed at the base of the body to allow samples to be taken during reaction, although this will have to be performed offline as users are unable to enter the beamline with the x-rays active. This will allow GPC data to be collected, then correlated with the time resolved SAXS traces to deduce the kinetic behaviour during the polymerisation and when the growth of internal microphase separation occurs.

This autoclave is currently under construction, with the first off-line intended to take place early 2015. If these are successful then the synthesis will be tested at the ESRF beamline.

## 4.3.7. Modifications of copolymer particles

Novel block copolymer products synthesised in the dispersion polymerisations have potential applications in optical electronics, separations science, and as coatings.<sup>64</sup> The advantages of using  $scCO_2$  as the continuous phase have been thoroughly described in Chapter 1; with a key benefit being clean, dry polymer powders are produced. However, if these powders are dissolved in organic solvents or thermally annealed, their particulate nature is lost. The aim was that through the addition of a cross-linking agent, can polymer particles synthesised in a  $scCO_2$  dispersion polymerisation be modified. A number of potential structures could be made (Figure 4-15), with benefits from each.

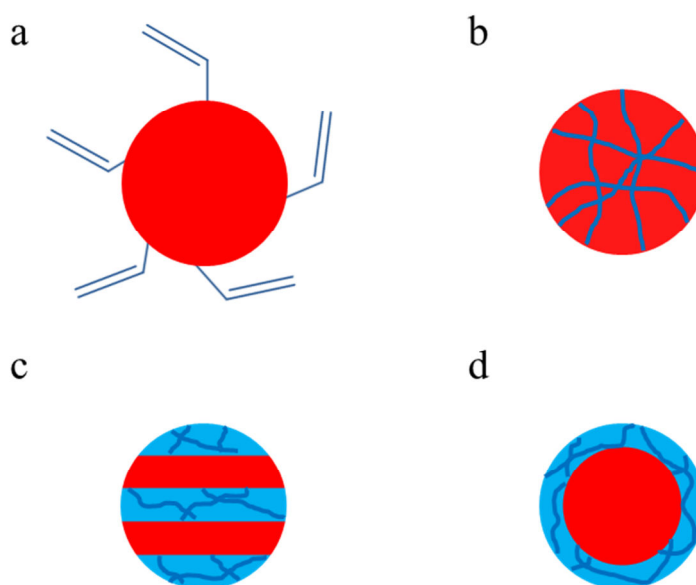


**Figure 4-15. Potential structures that could be synthesised by adding a cross-linker to a  $scCO_2$  dispersion polymerisation, (a) Spherical particles with pendant vinyl group, (b) Statistical arrangement with cross-linking throughout, (c) Internally phase separated structure with one layer cross-linked, (d) Core-shell particles with cross-linked outer layer.**

The possibility of having unreacted vinyl groups for post-synthesis modification would widen the range of potential industrial uses (Figure 4-15, a). Cross-linked micro-particles have uses in separations science as packing materials; for example, in GPC columns (Figure 4-15, b). If the phase separated structures shown by Jennings *et al.* could be selectively cross-linked to give them better mechanical strength, then through etching of one block, porous materials could be made (Figure 4-15, c).<sup>65</sup> The final example is of a core-shell particle with a cross-linked exterior to enable swelling and collapsing upon different stimuli.<sup>66</sup> The first system to be studied was PMMA-*b*-PS, with the addition of DVB as the cross-linker (Figure 4-16).

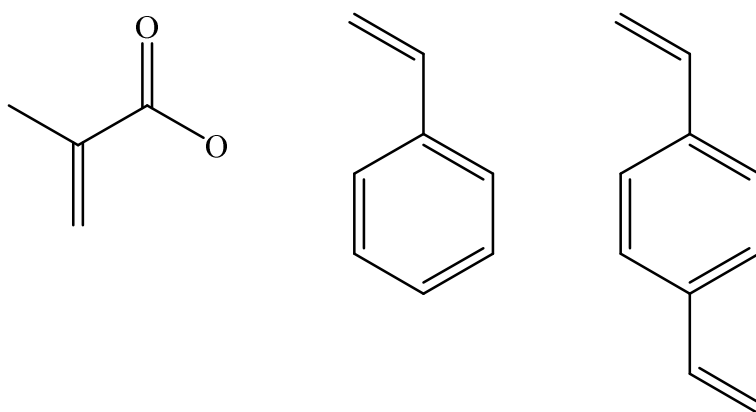


**Figure 4-16. Structures of the monomers used (left) MMA, (centre) styrene, (right) DVB**

#### 4.3.8. Addition Order

In a standard block copolymerisation, MMA is first polymerised for 18 hours, at which time styrene monomer is added and polymerised for a further 72 hours. The point at which the DVB is added will be crucial to when the

cross-linking occurs, in turn affecting the particle size, stabilisation in scCO<sub>2</sub>, and phase separation.

In all cases MMA was polymerised for 18 hours with DDMAT as the RAFT agent, and AIBN as the initiator at a 2:1 molar ratio. At this point, a solution of styrene and DVB, with further initiator, was added using an HPLC pump. For nomenclature the polymers are labelled with a subscript of the percentage by mass of the monomer relative to total monomer mass that was injected into the autoclave. The cross-linking meant the polymers were not soluble in THF or chloroform therefore no GPC analysis was performed, with SEMs and gravimetric yields given (Figure 4-17).

All reactions were carried out at 65 °C and 276 bar, DDMAT:AIBN molar ratio of 2:1. PMMA block duration of 18 hours, then S/DVB injected and reacted for a further 72 hours. Yields were determined gravimetrically after drying *in-vacuo* at room temperature for 72 hours. For sample Figure 4-17, (a), styrene monomer was added after 18 h, reacted for 48 h, then DVB added and reacted for a further 24 h.

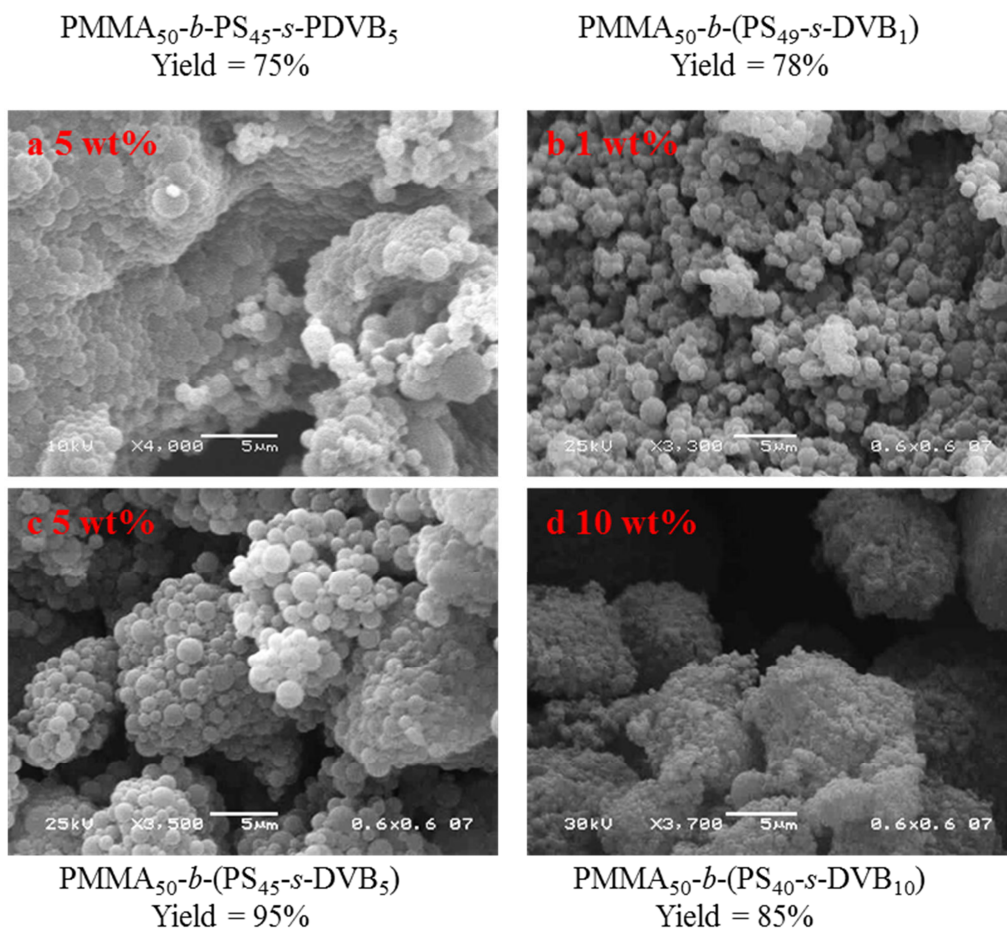


**Figure 4-17. SEM images of homopolymer PMMA that is synthesised in the first step and the PMMA-P(S-*s*-DVB) copolymers, (a) three step synthesis produced agglomerated spheres which were soluble in THF, (b) 1% cross-linker gave discrete spheres, (c) 5% cross-linker produced discrete spheres, (d) 10% cross-linker gave highly agglomerated particles.**

For the first sample (Figure 4-17, a), MMA was polymerised for 18 hours, followed by injection of styrene, the reaction left to proceed for 48 hours, before addition of DVB, then left for a final 24 hours. Some agglomeration of the particles was seen (Figure 4-17, a), but the main problem was this polymer was soluble in THF meaning not enough cross-links had been formed. This enabled GPC analysis to be performed (Figure 4-18) A shift in molecular weight to higher values indicates that the polymer is growing with

increasing conversion. It would be expected with high conversion of the DVB that cross-links would form and if not making the polymer insoluble, would at least create branch points and see a significant increase in molecular weight.

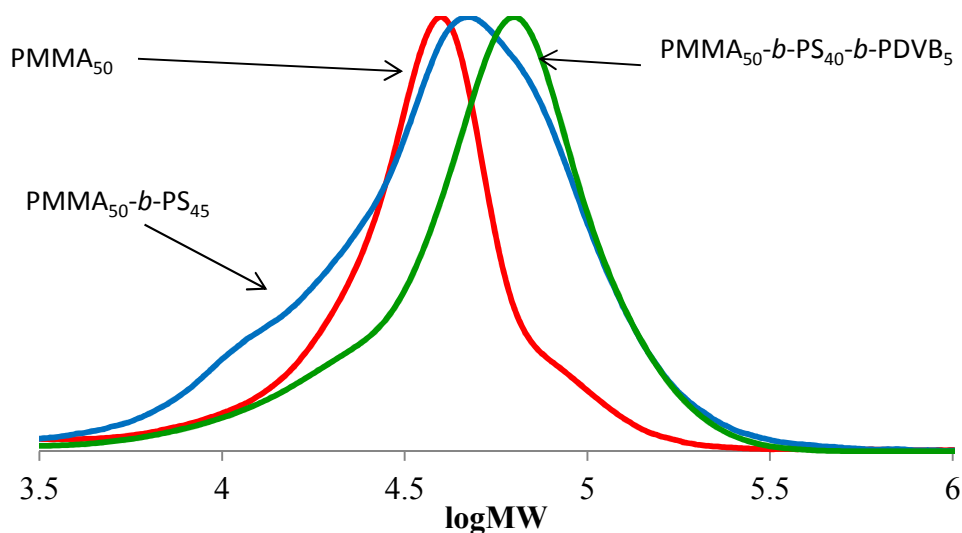


**Figure 4-18. GPC overlay for the addition of each monomer from Figure 4-17, a.**

To allow the cross-linking to take place at an earlier stage, the PMMA block was synthesised, then a solution of styrene/DVB was injected in one step. All samples produced using this method (Figure 4-17, b-d) were insoluble in THF. At cross-linker concentrations of 1% and 5% (Figure 4-17, images b and c respectively), spherical particles could be maintained. At 10% much more agglomeration is observed. At this concentration there may be pendant double bonds which form cross-links between the particles, so although fine powder products are produced, their morphologies are not well defined.

The results at 1 and 5 wt% are in contrast with Vivaldo-Lima *et al.*, who saw with a P(S-*s*-DVB) polymer synthesised by RAFT that maintaining the spherical nature of the particles was difficult, and highly agglomerated

monoliths were obtained.<sup>59</sup> The key difference is the presence of the living PMMA particles in the system before the styrene/DVB is added, so this was probed further.

#### *4.3.9. Solubility Studies*

RAFT polymerisation has been exploited in this Chapter and Chapter 3 to produce block copolymers, owing to the living end group. A potential explanation for the ability of this system to produce spherical micro-particles is that the styrene/DVB swells the PMMA particles, aided by the increased diffusivity in scCO<sub>2</sub>, and chain extends the polymer. The low initiator concentration will also limit the number of initiator derived polymers of PS being formed. However, if the initiator level is increased then some PMMA particles will be terminated (Figure 4-19), thus some styrene/DVB will polymerise as new particles, which as seen in the literature produces agglomerated structures.<sup>59</sup>

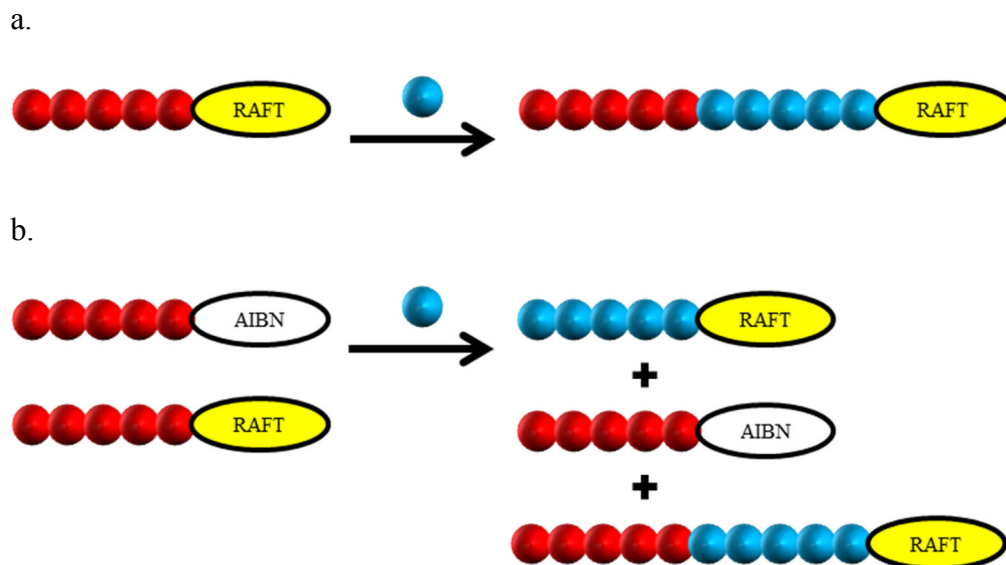


**Figure 4-19. (a) Ideal block copolymer synthesis, low [RAFT]:[Initiator] ratio reduces chance of termination, thus high degree of living character, (b) High [RAFT]:[Initiator] concentration for PMMA synthesis creates ‘dead’ chains, therefore limited block copolymer formation, with homopolymer contamination.**

Usually a [DDMAT]:[AIBN] ratio of 2:1 is used, but to purposefully terminate the PMMA a 1:4 ratio was chosen, which in theory would give 80% terminated chains. A cross-linker concentration of 5 wt% was used also (Figure 4-20).

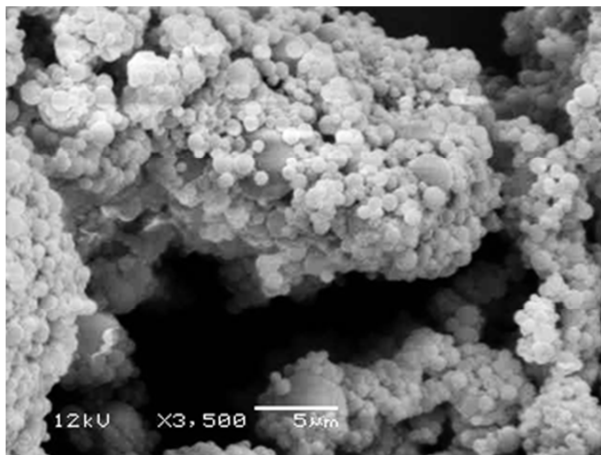


**Figure 4-20. SEM image of ‘dead’ PMMA<sub>50</sub>-*b*-P(S<sub>45</sub>-*s*-DVB<sub>5</sub>), showing high amounts of agglomeration. Produced with a yield of 89%.**

For the sample of ‘dead’ PMMA there is a less uniform structure (Figure 4-20Error! Reference source not found.). Comparing this to the 5 wt% DVB sample earlier (Figure 4-17, c), a slight loss of control is observed. With RAFT chemistry, it is difficult to chain extend 100% of the polymer, with termination processes always going to occur, so a proportion of the samples earlier will have some soluble ‘dead’ PMMA, but to a much lesser extent.

To quantify the amount of soluble polymer several filtering experiments were performed. Half a gram of each polymer studied was suspended in 10 mL THF (a good solvent for both PMMA and PS) and shaken for at least an hour, before being allowed to settle. The solution was passed through a 0.2 µm filter, and the solvent removed from the filtrate. The residue was weighed and the percentage of soluble polymer calculated using Equation 4-5.

$$\% \text{ Soluble Fraction} = \frac{\text{mass of residues}}{\text{mass of polymer dispersed in THF}} \times 100$$

**Equation 4-5.**

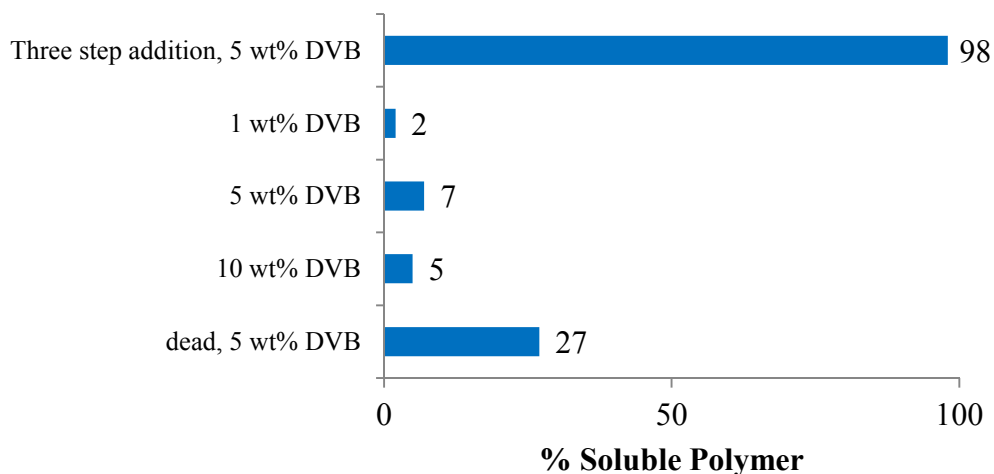


**Figure 4-21. Percentage of soluble polymer for five samples, from top to bottom: Figure 4-17 a, b, c, d, Figure 4-20.**

The first sample (Figure 4-17, a) was when the DVB was added in a third step, showing a lack of cross-linking with 98% of the polymer soluble. This was expected, based upon the ability to perform GPC analysis of this sample (Figure 4-18). All of the other samples prepared by adding styrene/DVB in one step, at different cross-linker amounts (Figure 4-17), showed a small proportion of soluble polymer (<7 %), and by  $^1H$  NMR this was shown to be mainly PMMA. The ‘dead’ PMMA sample (Figure 4-20) showed a much higher proportion of soluble polymer (27%), indicating a high amount of termination had occurred. Alongside the SEM showing poorer particle structure (Figure 4-20) this indicates that it is beneficial, although not vital, for the styrene/DVB to chain extend from the PMMA to retain good particulate structure and prevent agglomeration. Although the RAFT chemistry is not being used for its conventional benefits (control over  $M_n$  and dispersity), its ability to have a living end group allows a high proportion of the polymer to be cross-linked, enabling a high yield of cross-linked polymer to be produced.

This is advantageous for future applications, as if the polymer is placed in a solvent, such as THF, and a high amount of polymer solubilised, then it could hinder performance.

A successful method for incorporating cross-linker into a RAFT controlled *scCO*<sub>2</sub> dispersion polymerisation whilst producing uniform spherical particles has been shown. The next step was to investigate some of the properties of the copolymers to see if any of the suggested structures in Figure 4-15 had been formed.

#### 4.3.10. Internal phase separation

Seo and Hillmyer have used a combined ROP-RAFT process to polymerise block copolymers comprised of a PLA segment and a P(S-*co*-DVB) cross-linked segment.<sup>65</sup> As the mechanisms do not interfere with each other, the cross-linker remains in the styrenic block, with a second paper performing the synthesis in one-pot.<sup>67</sup> The large Flory-Huggins interaction parameter between PLA and PS causes phase separation between the two blocks. The PLA domains were removed by etching with 0.5 M methanol (40% by volume)/water solution of NaOH, leaving a cross-linked, porous P(S-*co*-DVB) monolith.

As these types of polymer particles have shown internal microstructures (Figure 4-2), TEM was performed on two of the cross-linked polymers synthesised here; PMMA<sub>50</sub>-b-P(S<sub>45</sub>-s-DVB<sub>5</sub>) with 5 wt% cross-linker (Figure 4-17, c) and the same polymer where the PMMA block was intentionally overloaded with initiator (Figure 4-20).

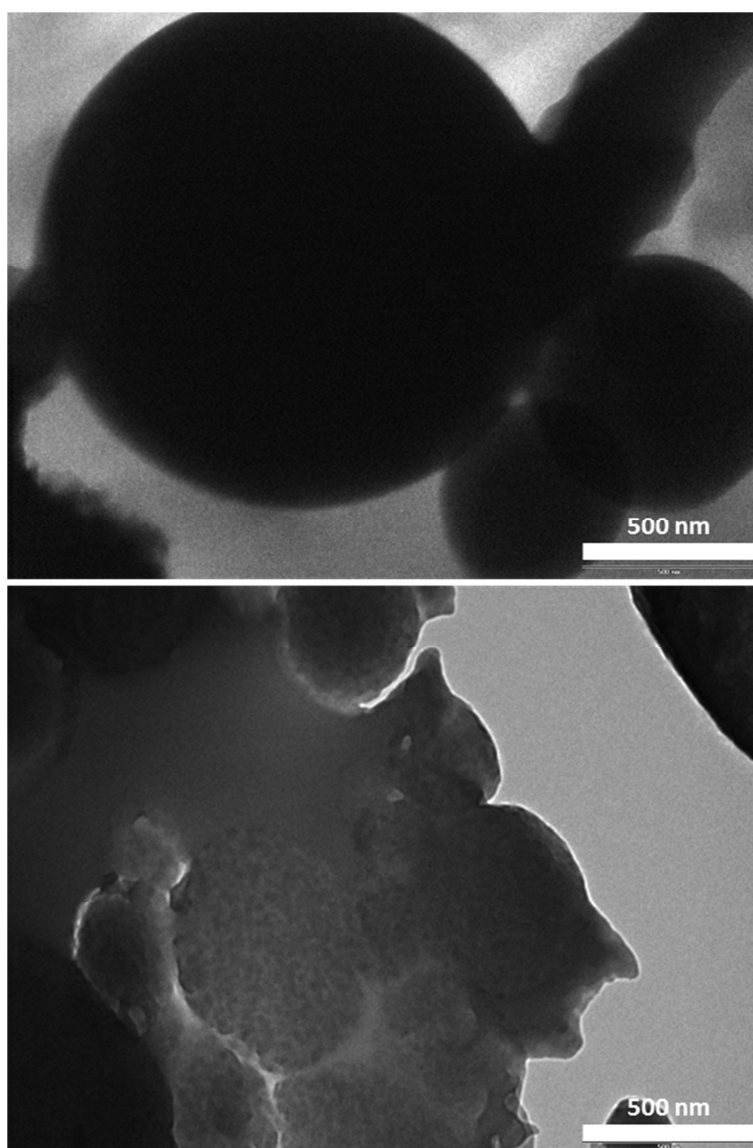


**Figure 4-22. TEM images of (top)  $PMMA_{50}\text{-}b\text{-}P(S_{45}\text{-}s\text{-}DVB_5)$  and (bottom) dead  $PMMA_{50}\text{-}b\text{-}P(S_{45}\text{-}s\text{-}DVB_5)$  Both at magnifications  $\times 43000$ , with scale bars at 500 nm.**

At 5 wt% DVB no phase separation was observed in any of the particles. By adding the cross-linker, the synthesis will have become less controlled, as branching points will be randomly distributed along the polymer chains. As the cross-linked network is formed the chain mobility will be greatly reduced,

even with the plasticising effect of the scCO<sub>2</sub>, which will most likely prevent phase separation.

Interestingly there appears to be some slight phase separation for the sample where the PMMA was purposefully terminated before addition of the styrene/DVB mixture. This is not fully clear from the TEM, with other techniques such as SAXS necessary to confirm in the future. From the filtering experiments it is understood that there is a high proportion of dead PMMA remaining in this sample, which will not be fully miscible with the cross-linked polymer. It is most likely therefore that the different phases are more like a polymer blend.

#### 4.3.11. Thermal Properties

DMA analysis of three of the cross-linked copolymers synthesised here was performed, with a non-cross-linked PMMA-*b*-PS copolymer also studied for comparison. This was to investigate if the addition of the cross-linker had any thermal or mechanical benefit compared to the linear copolymer. The sample (around 40 mg) was placed into an aluminium powder pocket, and clamped into the sample holder. The sample was then rapidly heated above the observed T<sub>g</sub> (around 200 °C) in order to create an even contact in the powder pocket. Once allowed to cool to room temperature, the sample was heated slowly at 2 °C min<sup>-1</sup> whilst applying an axial stress (Figure 4-23).

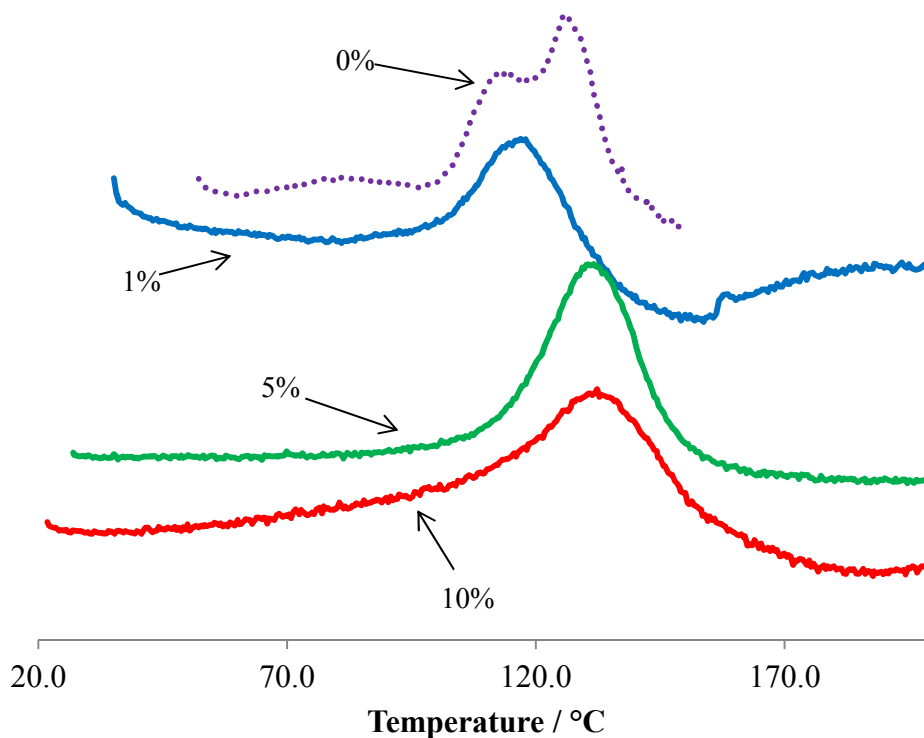


**Figure 4-23. Normalised  $\tan\delta$  as a function of temperature of four copolymers. Samples held in aluminium powder pockets, in single cantilever bending mode at a frequency of 1 Hz. Samples were rapidly heated at a rate of  $10\text{ }^\circ\text{C min}^{-1}$  and tightened to ensure good contact between the sample and powder pocket. Once cooled the measurements were taken at a ramp rate of  $2\text{ }^\circ\text{C min}^{-1}$ .**

The non-cross-linked copolymer displayed two glass transition temperatures (a peak in  $\tan\delta$ ), at around  $112\text{ }^\circ\text{C}$  and  $125\text{ }^\circ\text{C}$ . This indicates that the two blocks are separate to each other, and also are immiscible.

The polymer containing 1 wt% cross-linker,  $\text{PMMA}_{50}\text{-}b\text{-}(\text{PS}_{49}\text{-}s\text{-}\text{DVB}_1)$ , only displayed one T<sub>g</sub> at around  $115\text{ }^\circ\text{C}$ . Two routes could lead to this. Either, the polymers are miscible and an average T<sub>g</sub> is being observed, but more likely, during the polymerisation itself distinct blocks of PMMA and cross-linked PS are not being formed. Instead, the cross-linker will be

distributed randomly throughout the particles, creating more statistical copolymer. As the percentage of cross-linker increases to 5 wt%, the T<sub>g</sub> shifts to a higher value (130 °C), therefore improving the thermal properties. By increasing the cross-linker amount further to 10 wt%, the T<sub>g</sub> remains roughly the same as the 5 wt%, but inspection of the tanδ trace shows a much broader transition. Torron *et al.* saw a broadening of the T<sub>g</sub> measured by DMA for a polymer cross-linked through three methods, with the most cross-linked polymer showing the broadest T<sub>g</sub>.<sup>68</sup> Therefore the structure from Figure 4-15 (b) is the most likely in these cases, with cross-linking throughout the particles.

Storage and loss modulus data are not reported here, owing to the measurement method. The aluminium powder pockets will influence the mechanical response in the DMA, therefore the absolute values will not be representative of the polymer, but a mix of the aluminium and polymer combined.

#### 4.3.12. Other monomers

The ability to produce spherical particles in *scCO*<sub>2</sub> dispersion polymerisations can be limited to higher T<sub>g</sub> monomers. Wang *et al.* found when polymerising dimethylaminoethyl methacrylate (DMAEMA), which has a T<sub>g</sub> of 19 °C, high levels of agglomeration were seen.<sup>69</sup> High levels (95%) of MMA were needed to be incorporated to produce defined particles.

Through the addition of a cross-linker can spherical micro-particles of DMAEMA, and ultimately other low T<sub>g</sub> polymers, be synthesised in a *scCO*<sub>2</sub> dispersion polymerisation. Two other methacrylate monomers were chosen,

BzMA, and diethylene glycol methacrylate (DEGMA), with the cross-linker EGDMA used with all for better compatibility (Figure 4-24).

All reactions were carried out at 65 °C and 276 bar, DDMAT:AIBN molar ratio of 2:1. PMMA block duration of 18 hours, then the second monomer feed injected and reacted for a further 72 hours. Yields were determined gravimetrically after drying *in-vacuo* at room temperature for 72 hours post reaction.

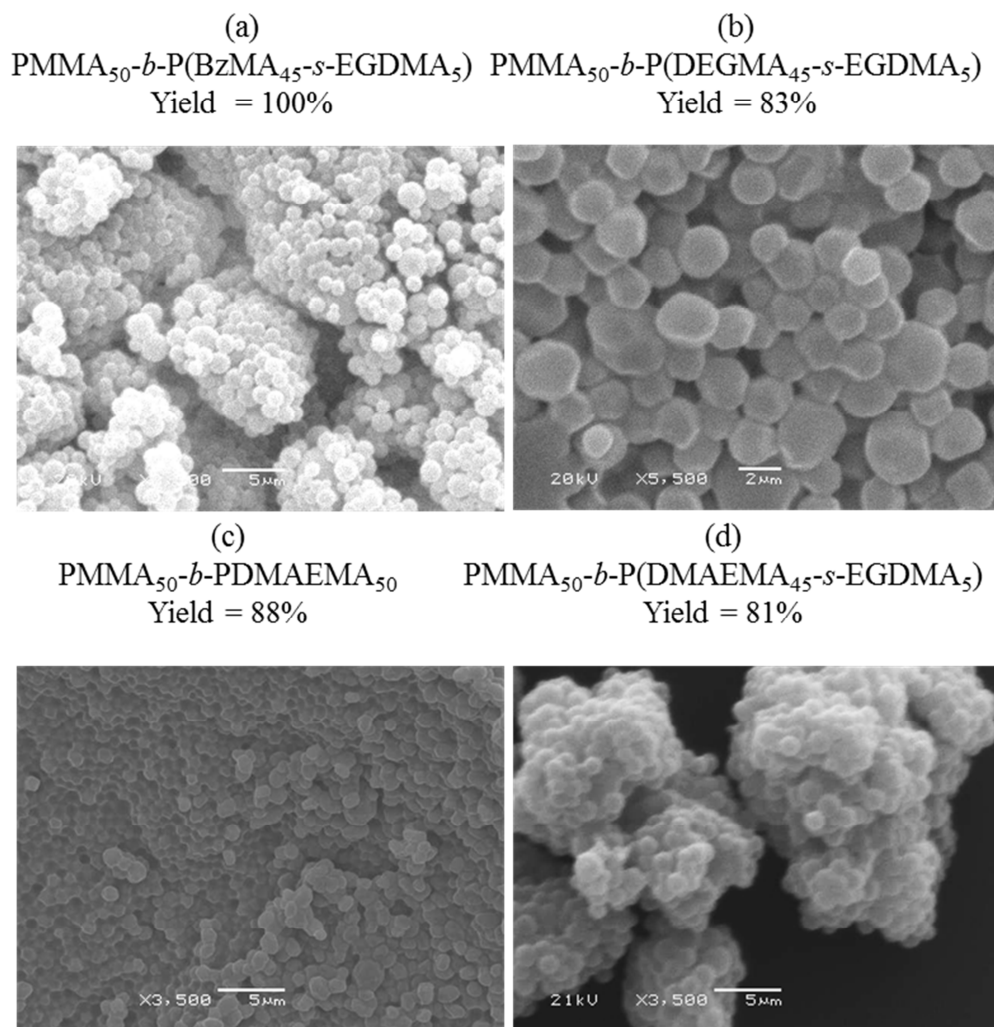


**Figure 4-24. SEM images of polymers with lower glass transition temperatures, (a) Spherical morphology, (b) Deformed particles, (c) Highly agglomerated particles, (d) Aggregated spheres.**

In section 4.3.2, PMMA<sub>50</sub>-*b*-PBzMA<sub>50</sub> formed spherical particles in a *scCO*<sub>2</sub> dispersion polymerisation. With addition of 5 wt% EGDMA the spherical nature of the particles was maintained with no visible cross-linking between the particles (Figure 4-24, a).

PDEGMA usually has a T<sub>g</sub> below 0 °C, so highly agglomerated particles would be expected. PMMA<sub>50</sub>-*b*-P(DEGMA<sub>45</sub>-*co*-EGDMA<sub>5</sub>) was synthesised with a high yield of 83%, with the SEM image showing mainly discrete particles (Figure 4-24, b). They were not as spherical as the PS or PBzMA, most likely due to the flexible PDEGMA portions of the polymer allowing some mobility.

Finally PDMAEMA is a polymer that is known for being both thermo and pH responsive, with applications in the pharmaceutical industry.<sup>66, 70</sup> Previous syntheses in *scCO*<sub>2</sub> dispersion polymerisation have made agglomerated particles, attributed to the low T<sub>g</sub> of PDMAEMA (16 °C in this case), requiring copolymerisation with MMA to improve the thermal properties.<sup>69</sup> The 50:50 block copolymer without cross-linker was highly agglomerated as expected (Figure 4-24, c). However, by adding cross-linker the particles became more spherical, although they did partially aggregate (Figure 4-24, d). Although it would be expected that the T<sub>g</sub> would be shifted to a higher value, in the presence of CO<sub>2</sub> polymer is likely plasticised enough that if particles collide they are still soft enough to agglomerate.

With optimisation and further understanding of the thermal behaviour of the copolymers with and without CO<sub>2</sub>, this shows that the system could be applicable to other monomer types and different cross-linkers, with potential for synthesising functional cross-linked micro-particles.

#### 4.4. Conclusions

A new high pressure cell suitable for the study of chemical and physical processes in  $scCO_2$  using X-ray or neutrons has been developed. The versatile design allows for the addition of other techniques in the future as well as interchangeable windows for varying the path length between the diamond windows. The window apertures are able to cover a large X-ray scattering vector range allowing studies of the necessary length scales for polymer systems.

Although the vessel is able to successfully make measurements, issues with the polymerisation process itself have limited the ability to monitor the internal phase separation in a block copolymer micro-particle. Initial studies have observed a failure in the dispersion polymerisation mechanism upon addition of the second monomer causing particle agglomeration and poor growth confirmed by GPC and SEM. This has been attributed to inefficient stabilisation and mixing through the narrow internal channel of the vessel. *In situ* SAXS measurements have however shown growth of the micro-particles themselves after the addition of the second monomer. A second vessel is currently under construction to address the mixing issues.

Applications of these block copolymer micro-particles are limited as the particulate structure is lost upon dissolution in organic solvents. By addition of a divinyl co-monomer several of these block copolymers have been cross-linked to make them insoluble and improve the thermal properties. Discrete spherical particles were produced at cross-linker concentrations of 5 wt% with respect to total monomer mass for PMMA-*b*-P(S-*s*-DVB). DMA analysis of a non-cross-linked PMMA-*b*-PS copolymer showed two T<sub>g</sub> peaks, but with the

addition of only 1 wt% DVB only a single T<sub>g</sub> was shown. This indicates that instead of a block copolymer of PMMA and cross-linked PS being formed, a more statistical copolymer is produced with random cross-linking throughout. However, an increase in T<sub>g</sub> with increasing cross-linker concentration showed that the thermal properties could be improved. Two other monomers with lower T<sub>g</sub> values were briefly investigated, PMMA-*b*-P(BzMA-*s*-EGDMA) and PMMA-*b*-P(DMAEMA-*s*-EGDMA), with spherical particles produced for both polymers.

#### 4.5. References

1. I. W. Hamley, *Nanotechnology*, 2003, **14**, R39-R54.
2. D. Schmaljohann, *Advanced Drug Delivery Reviews*, 2006, **58**, 1655-1670.
3. J. Nicolas, A.-V. Ruzette, C. Farcet, P. Gérard, S. Magnet and B. Charleux, *Polymer*, 2007, **48**, 7029-7040.
4. J. Jennings, M. Beija, A. P. Richez, S. D. Cooper, P. E. Mignot, K. J. Thurecht, K. S. Jack and S. M. Howdle, *Journal of the American Chemical Society*, 2012, **134**, 4772-4781.
5. I. W. Hamley, *The Physics of Block Copolymers*, Oxford University Press, 1998.
6. F. S. Bates and G. H. Fredrickson, *Annual Review of Physical Chemistry*, 1990, **41**, 525-557.
7. N. A. Lynd, A. J. Meuler and M. A. Hillmyer, *Progress in Polymer Science*, 2008, **33**, 875-893.

8. P. Alessi, A. Cortesi, I. Kikic and F. Vecchione, *Journal of Applied Polymer Science*, 2003, **88**, 2189-2193.
9. I. Kikic, F. Vecchione, P. Alessi, A. Cortesi, F. Eva and N. Elvassore, *Industrial & Engineering Chemistry Research*, 2003, **42**, 3022-3029.
10. Y. Zhang, K. K. Gangwani and R. M. Lemert, *Journal of Supercritical Fluids*, 1997, **11**, 115-134.
11. K. A. Lavery, J. D. Sievert, J. J. Watkins, T. P. Russell, D. Y. Ryu and J. K. Kim, *Macromolecules*, 2006, **39**, 6580-6583.
12. V. S. RamachandraRao and J. J. Watkins, *Macromolecules*, 2000, **33**, 5143-5152.
13. V. S. RamachandraRao, R. R. Gupta, T. P. Russell and J. J. Watkins, *Macromolecules*, 2001, **34**, 7923-7925.
14. Y. Li, L. Meli, K. T. Lim, K. P. Johnston and P. F. Green, *Macromolecules*, 2006, **39**, 7044-7054.
15. Y. Li, X. Wang, I. C. Sanchez, K. P. Johnston and P. F. Green, *The Journal of Physical Chemistry B*, 2006, **111**, 16-25.
16. L. Y. Shi, Z. H. Shen and X. H. Fan, *Macromolecules*, 2011, **44**, 2900-2907.
17. B. D. Vogt, G. D. Brown, V. S. RamachandraRao and J. J. Watkins, *Macromolecules*, 1999, **32**, 7907-7912.
18. C. M. Chandler, B. D. Vogt, T. J. Francis and J. J. Watkins, *Macromolecules*, 2009, **42**, 4867-4873.
19. B. D. Vogt, V. S. RamachandraRao, R. R. Gupta, K. A. Lavery, T. J. Francis, T. P. Russell and J. J. Watkins, *Macromolecules*, 2003, **36**, 4029-4036.

20. J. J. Watkins, G. D. Brown, V. S. RamachandraRao, M. A. Pollard and T. P. Russell, *Macromolecules*, 1999, **32**, 7737-7740.
21. T. J. Francis, B. D. Vogt, M. X. Wang and J. J. Watkins, *Macromolecules*, 2007, **40**, 2515-2519.
22. V. Martis, S. Nikitenko, S. Sen, G. Sankar, W. van Beek, Y. Filinchuk, I. Snigireva and W. Bras, *Crystal Growth & Design*, 2011, **11**, 2858-2865.
23. J. L. Fulton, D. M. Pfund, J. B. McClain, T. J. Romack, E. E. Maury, J. R. Combes, E. T. Samulski, J. M. DeSimone and M. Capel, *Langmuir*, 1995, **11**, 4241-4249.
24. J. D. Londono, R. Dharmapurikar, H. D. Cochran, G. D. Wignall, J. B. McClain, D. E. Betts, D. A. Canelas, J. M. DeSimone, E. T. Samulski, D. Chillura-Martino and R. Triolo, *Journal of Applied Crystallography*, 1997, **30**, 690-695.
25. N. F. Carnahan, L. Quintero, D. M. Pfund, J. L. Fulton, R. D. Smith, M. Capel and K. Leontaritis, *Langmuir*, 1993, **9**, 2035-2044.
26. T. Shinkai, M. Ito, K. Sugiyama, K. Ito and H. Yokoyama, *Soft Matter*, 2012, **8**, 5811-5817.
27. T. Shinkai, M. Ito, K. Sugiyama, K. Ito and H. Yokoyama, *Soft Matter*, 2013, **9**, 10689-10693.
28. M. Okubo, R. Takekoh and J. Izumi, *Colloid and Polymer Science*, 2001, **279**, 513-518.
29. M. Okubo, R. Takekoh and N. Saito, *Colloid and Polymer Science*, 2004, **282**, 1192-1197.

30. M. Okubo, R. Takekoh and N. Saito, *Colloid and Polymer Science*, 2003, **281**, 945-950.
31. S. J. Jeon, G. R. Yi, C. M. Koo and S. M. Yang, *Macromolecules*, 2007, **40**, 8430-8439.
32. S. J. Jeon, G. R. Yi and S. M. Yang, *Advanced Materials*, 2008, **20**, 4103-4108.
33. H. Yabu, T. Higuchi, K. Ijiro and M. Shimomura, *Chaos*, 2005, **15**, 7.
34. T. Higuchi, A. Tajima, K. Motoyoshi, H. Yabu and M. Shimomura, *Angewandte Chemie-International Edition*, 2008, **47**, 8044-8046.
35. T. Higuchi, A. Tajima, H. Yabu and M. Shimomura, *Soft Matter*, 2008, **4**, 1302-1305.
36. D. Klinger, M. J. Robb, J. M. Spruell, N. A. Lynd, C. J. Hawker and L. A. Connal, *Polymer Chemistry*, 2013, **4**, 5038-5042.
37. M. J. Robb, L. A. Connal, B. F. Lee, N. A. Lynd and C. J. Hawker, *Polymer Chemistry*, 2012, **3**, 1618-1628.
38. I. Tausendfreund, F. Bandermann, H. W. Siesler and M. Kleimann, *Polymer*, 2002, **43**, 7085-7091.
39. Y. Kagawa, H. Minami, M. Okubo and J. Zhou, *Polymer*, 2005, **46**, 1045-1049.
40. Y. Kitayama, M. Yorizane, Y. Kagawa, H. Minami, P. B. Zetterlund and M. Okubo, *Polymer*, 2009, **50**, 3182-3187.
41. Y. Kitayama, Y. Kagawa, H. Minami and M. Okubo, *Langmuir*, 2010, **26**, 7029-7034.
42. R. Wei, Y. Luo and Z. Li, *Polymer*, 2010, **51**, 3879-3886.

43. J. Jennings, M. Beija, J. T. Kennon, H. Willcock, R. K. O'Reilly, S. Rimmer and S. M. Howdle, *Macromolecules*, 2013, **46**, 6843-6851.
44. C. E. Carraher, *Carraher's Polymer Chemistry*, Ninth edn., CRC Press, Taylor & Francis Group, 2014.
45. T. J. Romack, E. E. Maury and J. M. DeSimone, *Macromolecules*, 1995, **28**, 912-915.
46. A. I. Cooper, W. P. Hems and A. B. Holmes, *Macromolecular Rapid Communications*, 1998, **19**, 353-357.
47. H. F. Gao and K. Matyjaszewski, *Progress in Polymer Science*, 2009, **34**, 317-350.
48. I. A. Barker, J. El Harfi, K. Adlington, S. M. Howdle and D. J. Irvine, *Macromolecules*, 2012, **45**, 9258-9266.
49. B. L. Liu, A. Kazlauciusas, J. T. Guthrie and S. Perrier, *Macromolecules*, 2005, **38**, 2131-2136.
50. L. Barner, C. Li, X. J. Hao, M. H. Stenzel, C. Barner-Kowollik and T. P. Davis, *Journal of Polymer Science Part a-Polymer Chemistry*, 2004, **42**, 5067-5076.
51. M. L. Koh, D. Konkolewicz and S. Perrier, *Macromolecules*, 2011, **44**, 2715-2724.
52. A. I. Cooper, W. P. Hems and A. B. Holmes, *Macromolecules*, 1999, **32**, 2156-2166.
53. T. Liu, J. M. DeSimone and G. W. Roberts, *Polymer*, 2006, **47**, 4276-4281.
54. L.-q. Cao, L.-p. Chen, J.-q. Jiao, S.-y. Zhang and W. Gao, *Colloid and Polymer Science*, 2007, **285**, 1229-1236.

55. M. Temtem, T. Casimiro, J. F. Mano and A. Aguiar-Ricardo, *Green Chemistry*, 2007, **9**, 75-79.
56. Y. D. Hu, L. Q. Cao, F. Xiao and J. D. Wang, *Polymers for Advanced Technologies*, 2010, **21**, 386-391.
57. P. R. Garcia-Moran, G. Jaramillo-Soto, M. E. Albores-Velasco and E. Vivaldo-Lima, *Macromolecular Reaction Engineering*, 2009, **3**, 58-70.
58. M. Roa-Luna, G. Jaramillo-Soto, P. V. Castaneda-Flores and E. Vivaldo-Lima, *Chemical Engineering & Technology*, 2010, **33**, 1893-1899.
59. G. Jaramillo-Soto and E. Vivaldo-Lima, *Australian Journal of Chemistry*, 2012, **65**, 1177-1185.
60. C. S. Li, J. C. Liang, X. L. Zhu and X. Z. Kong, *Colloid and Polymer Science*, 2010, **288**, 1571-1580.
61. <http://webbook.nist.gov/chemistry/fluid/>.
62. K. Nishikawa and I. Tanaka, *Chemical Physics Letters*, 1995, **244**, 149-152.
63. K. Nishikawa, I. Tanaka and Y. Amemiya, *Journal of Physical Chemistry*, 1996, **100**, 418-421.
64. A. P. Richez, H. N. Yow, S. Biggs and O. J. Cayre, *Progress in Polymer Science*, 2013, **38**, 897-931.
65. M. Seo and M. A. Hillmyer, *Science*, 2012, **336**, 1422-1425.
66. A. Car, P. Baumann, J. T. Duskey, M. Cham, N. Bruns and W. Meier, *Biomacromolecules*, 2014, **15**, 3235-3245.
67. M. Seo, C. J. Murphy and M. A. Hillmyer, *Acs Macro Letters*, 2013, **2**, 617-620.

68. S. Torron, S. Semlitsch, M. Martinelle and M. Johansson, *Macromolecular Chemistry and Physics*, 2014, doi: 10.1002/macp.201400192.
69. W. X. Wang, M. R. Giles, D. Bratton, D. J. Irvine, S. P. Armes, J. V. W. Weaver and S. M. Howdle, *Polymer*, 2003, **44**, 3803-3809.
70. X. Han, X. X. Zhang, H. F. Zhu, Q. Y. Yin, H. L. Liu and Y. Hu, *Langmuir*, 2013, **29**, 1024-1034.

# Chapter 5 - ROP of Renewable Monomers in scCO<sub>2</sub>

---

## 5. Overview

The work in this Chapter was performed in collaboration with the groups of Professor Matthew Davidson and Dr Matthew Jones at the University of Bath.

Worldwide plastic production is close to 300 million tonnes annually, with a vast proportion still synthesised *via* petrochemical routes.<sup>1</sup> Producing polymers from renewable feedstocks is therefore of major importance.<sup>2</sup> A key issue is maintaining the physical and chemical properties from these new polymers compared with traditional materials. Poly(lactic acid) (PLA) and poly( $\epsilon$ -caprolactone) (PCL) are two polymers which are viable replacements, being produced from biorenewable sources as well as being biodegradable and biocompatible.<sup>3</sup>

On a commercial scale, PLA is synthesised *via* melt polymerisations at extremely high temperatures, often in excess of 160 °C. This makes the processes very energy intensive, and can lead to product degradation. One option to reduce the reaction temperature is through using solution polymerisations, for example in toluene or chloroform. Utilising volatile organic solvents such as these have inherent disadvantages also; notably a negative environmental impact, as well as requiring lengthy purification steps to ensure complete solvent removal.

Supercritical carbon dioxide is an efficient plasticiser for both PLA and PCL, enabling the processing of these polymers to occur at much lower temperatures than typically required, often below 37 °C, which allows blending with thermally labile drugs. By using scCO<sub>2</sub> as a reaction medium, the melting temperatures of the monomers and polymers can be depressed, alongside a reduction in viscosity to aid mixing. The objective therefore, is to produce PLA *via* a melt-type polymerisation at lower temperatures than currently employed.

Another key development in ring-opening polymerisation of PLA is the design and implementation of novel catalysts/initiators, typically metal complexes, for imparting control over stereoselectivity. Issues have been encountered where catalyst degradation or loss of activity is seen at the elevated temperatures of melt polymerisations. Although these problems are overcome by utilising organic solvents at lower reaction temperatures, greener methods are necessary, in particular for medical applications where purity is highly important.

This Chapter first reviews the current literature concerning the synthesis of PLA and PCL with scCO<sub>2</sub> as a reaction medium. The experimental data mainly focusses on PLA, with the phase behaviour of the monomers and polymers studied in scCO<sub>2</sub>. Furthermore, investigations into the synthesis of PLA using a novel stereoselective zirconium-based catalyst in scCO<sub>2</sub> are described, with initial results extending the synthetic procedure to synthesising PCL also presented.

## 5.1. Introduction

### 5.1.1. Poly(lactic acid)

PLA is derived from the biorenewable monomer lactic acid, which is readily obtained from the fermentation of agricultural sources such as corn or cane sugar.<sup>4, 5</sup> It has a number of applications ranging from packaging and insulation foams,<sup>6</sup> to more specialised biomedical scaffolds<sup>7, 8</sup> and drug delivery systems<sup>9, 10</sup>. A key property is the biodegradability of the polymer, owing to the ester linkages in the backbone.<sup>11</sup>

There are two approaches by which PLA can be synthesised, either directly from the condensation of lactic acid or *via* formation of a di-lactic acid (lactide) ring and subsequent ring-opening polymerisation (ROP); this study will concentrate on the latter. There are three forms of the lactide dimer which can be successfully polymerised *via* ROP (Figure 5-1); this all depends on the enantiomer of lactic acid used. They are: L-lactide (LLA) with *S,S* stereocenters, D-lactide (DLA) with *R,R* stereocenters, and meso-lactide with *R,S* stereocenters. DL-lactide (DLLA), the 1:1 racemic mixture of LLA and DLA, is commonly polymerised on an industrial scale. PLA can therefore exist with a variety of different tacticities, dependent on the arrangement of the different monomers.

If meso-lactide is polymerised then syndiotactic PLA can be formed, with alternating  $-(RS)_n$  stereochemistry. Atactic PLA has no repeating structure, with random insertions of LLA or DLA in the backbone. This is the typical PLA synthesised commercially as it does not require specialised initiators to impart any stereo-control. Isotactic PLA is characterised by the presence of distinct blocks of either PLLA,  $-(SS)_n$ , or PDLA,  $-(RR)_n$ ; this can

be produced *via* two methods. If the enantiopure monomer is polymerised then an isotactic product must be formed (assuming no epimerisation occurs). Alternatively a racemic mixture can be used, with novel stereoselective initiators developed to preferentially polymerise one of the enantiomers first; for example the chiral Schiff's base/aluminium alkoxides developed by Spassky *et al.*<sup>12</sup> Finally, heterotactic PLA is produced by alternating insertions of LLA and DLA, giving rise to a polymer with  $-(SSRR)-_n$  stereochemistry. Again, stereoselective initiators are required to do this,<sup>13</sup> with further details concerning these in subsequent sections.

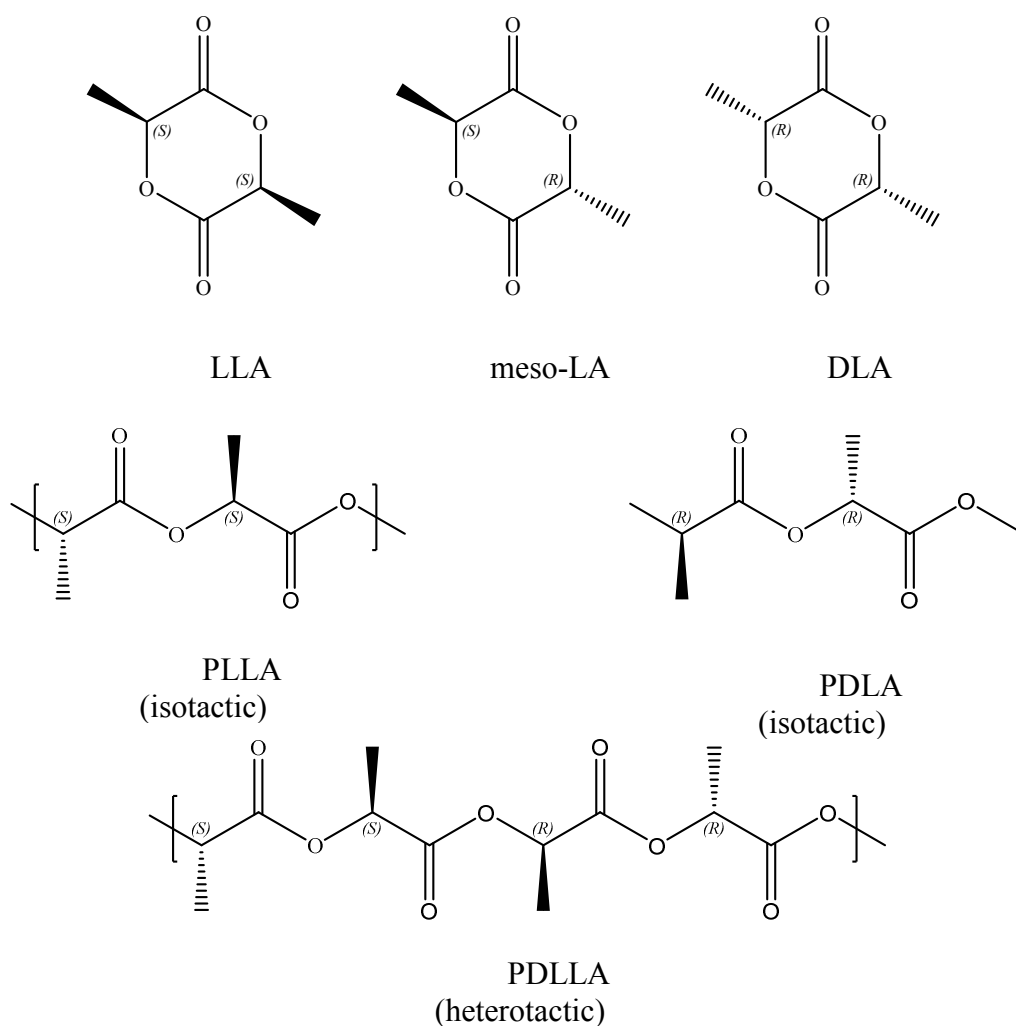


**Figure 5-1. Structures of the lactide enantiomers and PLA**

### 5.1.2. Thermal properties of PLA

The thermal and mechanical properties of PLA are influenced heavily by the tacticity, which enables the properties to be tuned by varying the polymer structure.

Poly(DL-lactide) (PDLA) is an amorphous polymer with a  $T_g$  of around 50-60 °C;<sup>15</sup> with similar thermal properties for the atactic and heterotactic microstructures. Isotactic poly(L-lactide) (PLLA) is semi-crystalline, exhibiting a melt point around 170 °C and  $T_g$  around 67 °C,<sup>16</sup> with PDLA having similar properties. Ikada *et al.* found that by blending PLLA and PDLA a stereocomplex (s-PLA) can be created which vastly increases the melting temperature to around 220 °C.<sup>17-19</sup> A number of methods exist to form s-PLA including melt blending, solution casting or using supercritical fluids.

For melt blending, a mixture of PLLA and PDLA, usually in a 1:1 ratio, is heated above the expected melting point of the stereocomplex, typically above 230 °C, with the two polymers co-crystallising upon cooling. The exceedingly high temperatures used for this are not only expensive to maintain, but also risk thermally degrading the polymers themselves.<sup>20</sup>

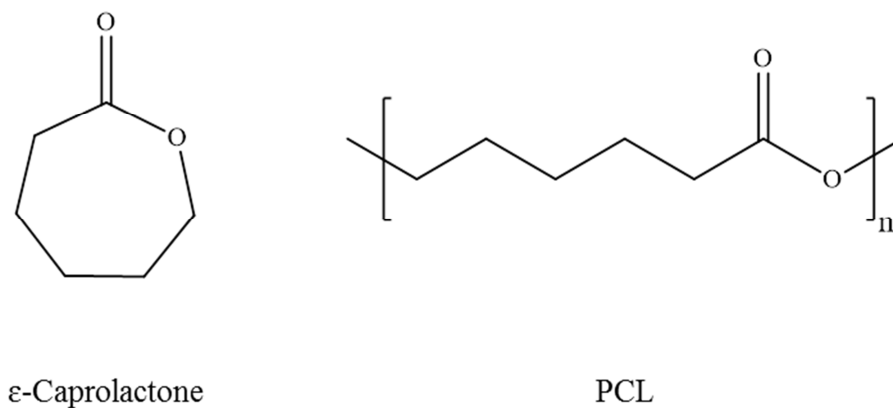
Solution casting involves mixing a dilute solution of PLLA, for example in chloroform, with an equally dilute solution of PDLA. The solvent is allowed to slowly evaporate, typically over a number of days, during which time the polymers stereocomplex.<sup>21</sup> This solvent evaporation step is an extremely time-consuming and expensive process, requiring high vacuum for complete removal, particularly necessary for medical applications where no toxic organic solvent residues can remain.

Purnama and Kim have developed a route combining scCO<sub>2</sub> and dichloromethane to yield a dry s-PLA with a high degree of stereocomplexation (around 97%).<sup>22</sup> This has been extended to a continuous process allowing rapid s-PLA formation in minutes at conditions of 65 °C and 350 bar.<sup>23</sup>

The thermal and mechanical properties of PLA can also be modified using additives such as hydroxyapatite,<sup>8</sup> or through copolymerisation with other monomers.<sup>4</sup> PCL has been extensively studied owing to its biocompatibility and biodegradability, as well as being polymerised *via* the same mechanism of ring opening.<sup>24, 25</sup> For example, Hiljanen-Vainio and co-workers showed that by incorporating more flexible  $\epsilon$ -caprolactone units into the PLA backbone, the T<sub>g</sub> could be depressed from 49.1 °C for pure PDLA, to -50.9 °C for a P(CL<sub>80-c</sub>-LA<sub>20</sub>) copolymer.<sup>26</sup>

### 5.1.3. Poly( $\epsilon$ -caprolactone)

PCL is formed from  $\epsilon$ -caprolactone ( $\epsilon$ -CL) units which usually obtained from crude oil sources,<sup>11</sup> although renewable sources exist.<sup>27</sup> It has similar applications to PLA owing to its biodegradability and biocompatibility, including packaging,<sup>6</sup> and biomedical devices.<sup>10, 28</sup> The synthesis of PCL has been recently reviewed by Labet *et al.* detailing a number of methods including anionic and cationic ROP, enzyme controlled ROP, as well as the coordination/insertion mechanism (section 5.1.4).<sup>24</sup>



ε-Caprolactone

PCL

**Figure 5-2. Structures of ε-caprolactone monomer and PCL**

PCL is a semi-crystalline polymer (up to 69% crystallinity) with a  $T_g$  around  $-60\text{ }^\circ\text{C}$  and a melting temperature around  $60\text{ }^\circ\text{C}$ .<sup>24, 29</sup> Like PLA the ester linkages in the backbone are susceptible to hydrolysis; enzymatically in soil but non-enzymatically in the body. Homopolymer blending or copolymerisation of PCL with PLA enables the production of biorenewable, biocompatible and biodegradable polymers with tuneable properties.<sup>30-32</sup> Depending on the monomer feeds, either random or block copolymers can be synthesised.<sup>26, 33</sup> Examples of benefits include stress crack resistance, difference degradation rates, change in permeability for drug delivery systems and modification of mechanical properties.<sup>29, 34, 35</sup>

#### 5.1.4. Commercial ROP catalysts

Tin (II) octanoate ( $\text{Sn}(\text{Oct})_2$ ) is by far the most common ROP catalyst owing to its high solubility in organic solvents, ease of use, commercial availability and it is FDA approved.<sup>4, 36</sup> It follows a coordination/insertion mechanism with the help of an initiating species, typically an alcohol, with a pre-initiation step forming a tin alkoxide (Figure 5-3). A generic

coordination/insertion mechanism is detailed in Figure 5-4. In general, the carbonyl oxygen coordinates to the metal (M) and a four-membered ring transition state is formed. The alkoxy group attached to the metal attacks the carbonyl carbon through a nucleophilic addition, followed by ring opening. This propagates through the same mechanism to yield a polymer chain.<sup>37-39</sup>

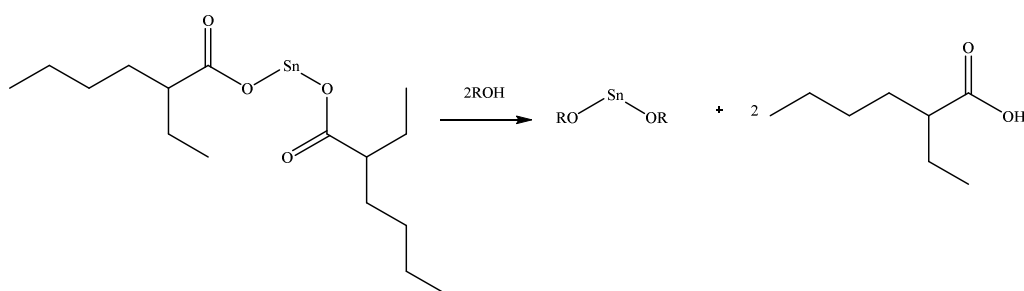


**Figure 5-3. Pre-initiation step converting  $Sn(Oct)_2$  to the activated Sn**

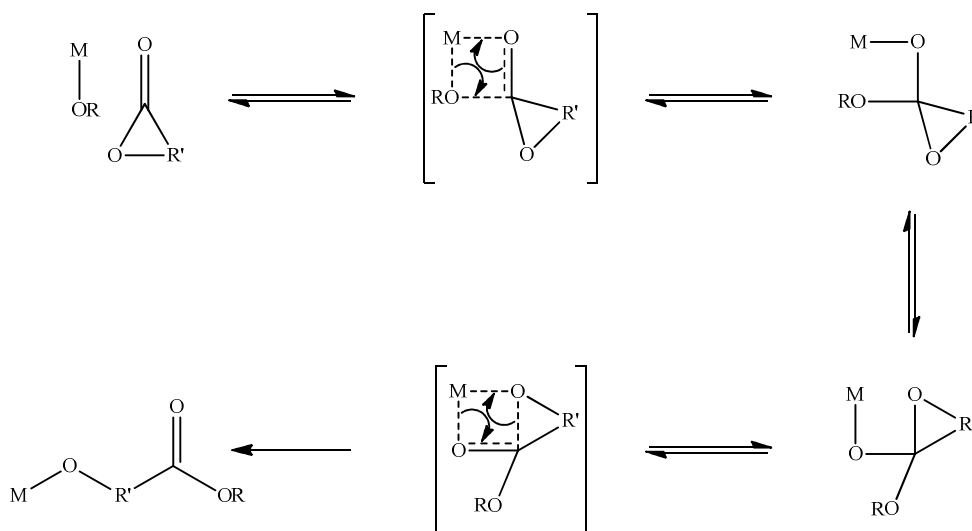


**Figure 5-4 Generic coordination/insertion mechanism for the metal (M) alkoxide catalyzed ROP on cyclic ester**

#### 5.1.5. Novel ROP catalysts

A number of metal alkoxide initiators for ROP have been developed, based upon aluminium, zinc and yttrium. Such initiators are able to create

isotactic PLA from a racemic mixture, including stereo-block copolymers, as well as standard atactic PLA.<sup>40</sup> Stanford and Dove have recently reviewed the current range of initiators available.<sup>14</sup>

The work in this Chapter will focus on zirconium-based alkoxides developed by Davidson *et al.* at the University of Bath (Figure 5-5).<sup>41, 42</sup> From a racemic lactide mixture, their initiators were able to control the alternating insertion of LLA and DLA monomer to produce heterotactic PLA (repeat unit  $-(SSRR)_n$ ). The probability of heterotactic enchainment,  $P_r$ , determines the degree of selectivity imparted by the initiators, with perfectly heterotactic polymer having a  $P_r$  of 1.

This work focusses on a zirconium trisphenolate complex ( $Zr-^{tBu}C_3$ ), with the following two examples using this initiator, although other ligands were investigated and found to be less successful.<sup>13, 43</sup> At room temperature in toluene, at a [monomer]:[initiator] ratio of 100:1, an isolated yield of only 50% was reached in 48 hours, although a  $P_r$  value of 0.98 was achieved indicating the high activity of the initiator. Most importantly, the activity of the catalyst was retained at 130 °C in the melt ([M]:[I] = 300:1), with 78% conversion in only 6 minutes, and a  $P_r$  value of 0.96. In both cases, the living characteristics of lactide ROP were maintained, with a linear increase of molecular weight with conversion, and narrow molecular weight distributions. This offers a route to producing well-defined PLA, at industrially relevant conditions. Copolymerisation with other monomers have shown the versatility of trisphenolate based catalysts also, although different ligands were employed.<sup>44</sup>

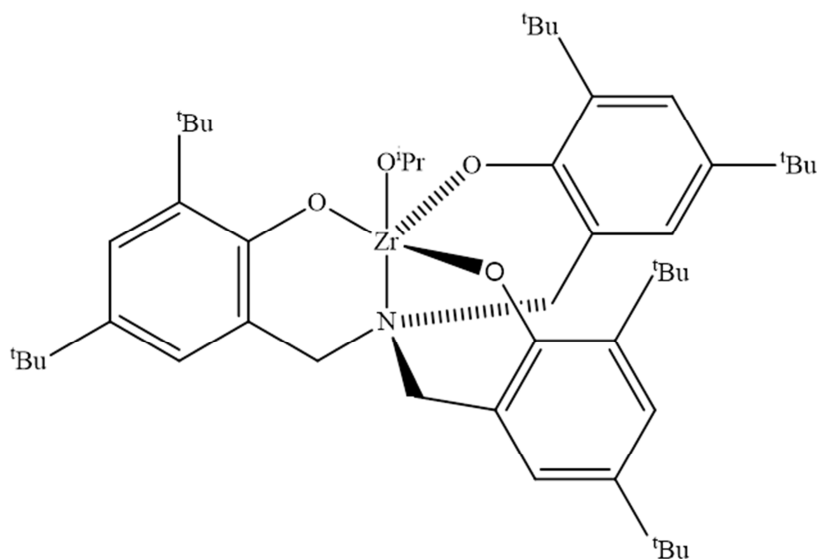


**Figure 5-5. Zirconium trisphenolate ( $Zr-tBu_3C_3$ )**

#### 5.1.6. PLA and PCL properties in supercritical carbon dioxide

Gregorowicz has investigated the solubility of lactide monomer in  $CO_2$  at a range of temperatures and pressures.<sup>45</sup> At lactide mole fractions of 0.0092 the monomer appears to be soluble at modest temperatures and pressures (<80 °C and <300 bar). As the lactide concentration is increased the conditions required increase, with pressures in excess of 300 bar required (this is higher than the limit of the equipment in this Thesis).  $\epsilon$ -Caprolactone has been shown to exhibit good solubility at typical reaction temperatures and pressures in  $scCO_2$ . Bratton *et al.* determined that a 14%  $\epsilon$ -CL loading required a  $CO_2$  density of  $0.56 \text{ g mL}^{-1}$  (80 °C, 195 bar).<sup>46</sup>

Both PLA and PCL are insoluble in  $CO_2$ , although  $CO_2$  has a relatively high solubility in the respective polymers owing to the carbonyl groups in the backbone.<sup>47</sup> This lowers the  $T_g$ , liquefying the polymers, allowing blending at lower than normal temperatures. This has been exploited for various foaming and mixing processes for biomedical devices whereby the polymer is initially

liquefied in scCO<sub>2</sub> and as the CO<sub>2</sub> is released the polymer foams and solidifies.<sup>7, 8, 28</sup> As most polymers are insoluble, heterogeneous polymerisations are the most common methods of synthesising PLA and PCL in scCO<sub>2</sub>.

#### 5.1.7. ROP in supercritical carbon dioxide

The insolubility of LLA makes it ideal for suspension type processes as shown by Bratton *et al.*<sup>48</sup> Without stabiliser an aggregated product was obtained, whereas in the presence of a PCL-perfluoropolyether-PCL stabiliser, fine free flowing powders were formed. The same group also developed triblock hydrocarbon stabilisers composed of PPG-PEG-PPG for ROP in scCO<sub>2</sub>, although in this case poly(glycolide) was the polymer synthesised.<sup>49</sup>

Several other groups have investigated the effect of changing the CO<sub>2</sub>-philic portion of the stabiliser, with all the syntheses employing Sn(Oct)<sub>2</sub> at temperatures of 80 °C or higher and pressures of at least 100 bar. Yilmaz and co-workers performed reactions using fully hydrocarbon stabilisers based on PCL-PEG-PCL copolymers,<sup>50</sup> whereas Zhang *et al.* used a PCL-PDMS-PCL triblock copolymer.<sup>51</sup> In all cases free flowing powder products were obtained.

Diblock copolymers composed of a CO<sub>2</sub>-philic PDMS block, with polymer-philic blocks of either poly(acrylic acid) or poly(methacrylic acid), have been successfully implemented as stabilisers for the suspension ROP of LLA in scCO<sub>2</sub>, producing discrete PLA micro-particles.<sup>52</sup> In the same publication however, PDMS-g-pyrrolidonecarboxylic acid graft copolymers were shown to be less effective, with the short polymer-philic side chains unable to anchor to the polymer particles.

It is not solely Sn(Oct)<sub>2</sub> that has been used for ROP of DLLA in scCO<sub>2</sub>. Blakey *et al.* used an organo-catalytic system with 1,8-diazabicyclo[5.4.0]undec-7-ene (DBU) and benzyl alcohol as the initiator.<sup>53</sup> At temperatures of 80 °C and pressures of 250 bar, high conversions could be attained with narrow dispersity polymers produced, significantly below the 130 °C usually employed.

Recently, scCO<sub>2</sub> has been shown to remove lactide monomer post-polymerisation by Dehghani *et al.*<sup>54</sup> Employing Sn(Oct)<sub>2</sub> and diethylene glycol, PLLA was synthesised in a precipitation polymerisation without stabilisers with conversions consistently above 80%. Supercritical fluid extraction from a crude mixture of monomer, polymer, catalyst and initiator at 80 °C and 200 bar for one hour enabled complete removal of the monomer. Encouragingly, only 4% of the polymer was removed, indicating that scCO<sub>2</sub> is suitable as a separation technique for removing lactide monomer. This potentially provides an improved green synthetic route to an industrially important polymer.

In all of the above cases, no data specifying the tacticity of the resulting polymers was given. It is expected that only isotactic PLLA or atactic PDLLA would have been synthesised, as the initiators chosen are not known for exhibiting control over the stereochemistry.

Stassin *et al.* first investigated the ROP of ε-CL in 2001 showing a linear increase of molecular weight with conversion<sup>55</sup>. However, an increase in transesterification compared to bulk and solution polymerisations was observed, reducing the living character. Their following paper further investigated the effect of reaction conditions upon kinetics.<sup>56</sup> A higher activation energy, thus

slower rate of polymerisation, was observed in scCO<sub>2</sub> (91 kJ mol<sup>-1</sup>) when compared to the analogous reaction in toluene (65 kJ mol<sup>-1</sup>). Carbonation of the tin alkoxide initiating species led to its deactivation, resulting in the rate depression.

Bergeot *et al.* also observed a reduction in rate compared to conventional solvents for several other metal alkoxide initiators; Y(O<sup>i</sup>Pr)<sub>3</sub>, La(O<sup>i</sup>Pr)<sub>3</sub>, and Al(O<sup>i</sup>Pr)<sub>3</sub>.<sup>57</sup> Reversible reactions between the initiators and CO<sub>2</sub> formed dormant species, preventing the initiation of new chains, thus slowing the rate of polymerisation. For example, polymerisation with Y(O<sup>i</sup>Pr)<sub>3</sub> is slowed down by a factor of around 50 when compared to the same reaction in solvent, and by a factor of 400 for the La(O<sup>i</sup>Pr)<sub>3</sub>. Reducing the ability of the initiator to coordinate with CO<sub>2</sub> is therefore an area of importance for controlling the polymerisation of ε-CL for these systems.

A number of other groups have since studied ε-CL in scCO<sub>2</sub>, reviewed by Jérôme and Lecomte in 2008, with Sn(Oct)<sub>2</sub> generally the most favoured catalyst.<sup>58</sup>

Howdle and co-workers investigated the ROP of ε-CL using both Sn(Oct)<sub>2</sub> as the catalyst or *via* enzymatic routes in scCO<sub>2</sub> precipitation and dispersion polymerisations.<sup>46, 59-61</sup> The same group also combined ROP with ATRP and RAFT to produce block copolymers of PCL and either PMMA or PS.<sup>62, 63</sup>

In all cases control over molecular weight was exhibited for both the ring-opening and controlled radical polymerisation mechanisms. A key point from these syntheses was the ε-CL acted as a co-solvent, allowing the reaction mixture to remain homogenous for longer; this is beneficial for controlling the polymerisations.

### 5.1.8. Aims and Objectives

A disadvantage of the zirconium catalysts discussed is the high temperatures required for a melt polymerisation of lactide on an industrial scale can lead to a loss of control over tacticity. These high temperatures, often in excess of 160 °C, still remain an economical issue for large scale PLA production, as well as causing degradation of the product. Lower temperature solution polymerisations require lengthy syntheses, and utilise toxic volatile organic solvents, such as toluene. The aim is to depress the melting and/or glass transition temperatures of the monomers and polymers by exploiting the plasticising ability of  $scCO_2$ . This will hopefully enable the melt polymerisation to be performed at lower than conventional temperatures, whilst still retaining the same rate of polymerisation and catalytic activity. This has potential to produce controlled, biorenewable polymers using an almost entirely green process.

## 5.2. Experimental

### 5.2.1. Materials

The  $Zr-^{tBu}C_3$  catalyst was synthesised by Thomas Forder and Paul McKeown at the University of Bath. L-lactide and D-lactide (Corbion formerly Purac) were recrystallised from hot toluene and dried prior to use, also provided by the University of Bath. DL-lactide was formed by recrystallising a 1:1 mixture of L- and D-lactide.  $\epsilon$ -Caprolactone (99%) was obtained from Sigma-Aldrich and dried in a room temperature vacuum oven. Tetrahydrofuran

(THF, HPLC grade, 99.9%) was purchased from Fisher. Dry CO<sub>2</sub> (SFC grade, 99.99%) was purchased from BOC.

Homonuclear decoupled <sup>1</sup>H NMR was performed at the University of Bath on a Bruker 400 MHz spectrometer for determination of *P<sub>r</sub>* (*P<sub>r</sub>* = the probability of heterotactic linkages) values of *rac*-lactide polymers. This was found through analysis of the decoupled methine region of the spectra by Bernoulli statistics discussed by Chamberlain *et al.*<sup>64</sup>

### 5.2.2. View cell procedure

The behaviour of all reagents was observed using a variable-volume view cell introduced in Chapter 2.<sup>65</sup> A typical measurement was taken as follows. A small amount of material in an open glass vial was placed into the autoclave which was then assembled. CO<sub>2</sub> was first charged into a high pressure bomb (Swagelok), and then transferred from this into the view cell until the pressure reached around 60 bar (870 psi). The autoclave was then heated to 40 °C, which also raised the pressure to ensure the CO<sub>2</sub> was supercritical. Using the piston assembly the pressure was raised to 240 bar (for low temperature measurements this was not possible due to the limitations of the equipment as described in Chapter 2). A visual observation was made to determine if the material was liquefied. The temperature was then raised in 10 °C increments whilst varying the volume to maintain a pressure close to 240 bar. Once all observations had been made the autoclave was cooled and depressurised whilst observing any changes in material morphology.

### 5.2.3. Homopolymerisation procedure

A typical lactide polymerisation in scCO<sub>2</sub> was conducted in an in-house designed 20 mL stainless steel autoclave as introduced in Chapter 2 (section 2.1). The reactor was sealed and leak tested up to 138 bar (2000 psi) with CO<sub>2</sub>. The key was removed and the clamp opened to allow lactide (1 g) to be added into the autoclave with required initiator. For the 100:1 [M]:[I] ratio this related to 60 mg of Zr-<sup>t</sup>BuC<sub>3</sub>, and for the 300:1 ratio 20 mg was used. The clamp was resealed and the vessel purged by allowing a flow of CO<sub>2</sub> through the open key hole at 2 bar (30 psi) for 10 minutes, at room temperature. The autoclave was then sealed, pressurised to 55 bar (800 psi) and heated to 80 °C (this process took approximately 20 minutes). The pressure was topped up to 240 bar (3500 psi) through addition of more CO<sub>2</sub> and the reaction left for the desired time, typically 1 hour. Upon completion the heater and stirrer were turned off and the autoclave left to cool to room temperature (approximately 45 minutes). The vessel was slowly depressurised over 10 minutes, opened and samples taken for <sup>1</sup>H NMR, GPC and DSC.

### 5.2.4. Block copolymerisation procedure

The same procedure was followed as for the homopolymerisation (section 5.2.3). This was performed in two ways: either the zirconium complex was replaced by a macro-initiator previously synthesised and charged into a clean autoclave. Alternatively, upon completion of the first block, the autoclave was opened samples were taken for analysis, and the second loading of monomer added (total 2 g monomer per autoclave in these cases). The vessel was then reassembled, and purged by allowing a flow of CO<sub>2</sub> through

the open key hole at 2 bar (30 psi) for 10 minutes, at room temperature. The same heating and pressurising procedure as in section 5.2.3 was then followed, with reactions performed at 80 °C and 240 bar (3500 psi).

### 5.3. Results and Discussion

#### 5.3.1. View cell experiments

Solubility tests in scCO<sub>2</sub> were carried out in a high-pressure variable volume view cell, with a maximum operating temperature of 100 °C and maximum pressure of 300 bar. These were used to determine if the reactants/products were either soluble or the temperature at which they were liquified, as previously performed by Bratton *et al.*<sup>46</sup> These visual observations were compared to thermal data obtained for the monomers and polymers from DSC, and are presented in Table 5-1, with the DSC traces for the monomers displayed in Figure 5-6.

**Table 5-1. Melting temperatures with and without scCO<sub>2</sub>**

Entry	Sample	Mpt / °C <sup>a</sup>	Tg / °C <sup>a</sup>	Mpt in scCO <sub>2</sub> / °C <sup>b</sup>
1	LLA	99	-	55
2	DLA	99	-	55
3	DLLA	127	-	100
4	LLA/DLA <sup>c</sup>	97, recrys, 127 <sup>d</sup>	-	55, recrys, 100 <sup>d</sup>
5	PDLLA	-	43	20 <sup>f</sup>
6	PDLA	172	51	N/A <sup>e</sup>
7	PLLA	171	57	N/A <sup>e</sup>
8	PLLA/PDLA <sup>c</sup>	207	-	N/A <sup>e</sup>
9	s-PLA <sup>c</sup>	225	-	N/A <sup>e</sup>

<sup>a</sup> Determined by DSC at 10 °C min<sup>-1</sup> in a nitrogen atmosphere; <sup>b</sup> By visual inspection at approximately 240 bar; <sup>c</sup> 1:1 ratios; <sup>d</sup> See Figure 5-6; <sup>e</sup> Remained solid until 100 °C, 240 bar; <sup>f</sup> Liquified upon increasing pressure to 60 bar

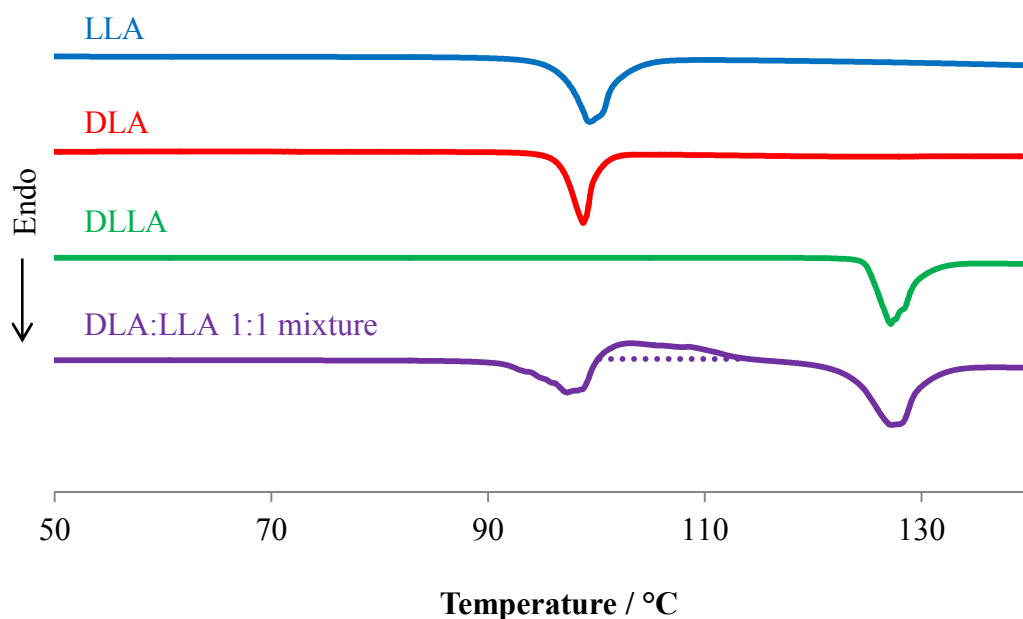


**Figure 5-6. DSC traces for the different enantiomers, racemic mixture and physical blend (endothermic down)**

Pristine LLA and DLA have similar melting points with the racemic mixture showing an increase of almost 30 °C owing to the co-crystallisation of the two enantiomers (Table 5-1, Entries 1-3). This difference in melting temperatures is also observed in  $CO_2$ . The monomers themselves do not appear to be soluble, consistent with the literature where lactide is only sparingly soluble.<sup>45</sup> However, recent extraction studies discussed in section 5.1.6 indicate the  $CO_2$  is able to solubilise the monomers enough to remove them post-polymerisation. In total 250 mL of  $CO_2$  was required at conditions of 80 °C and 200 bar to remove 0.2 g of LLA.<sup>54</sup> Melting point depressions of around 40 °C were observed for the individual enantiomers with only around a 30 °C depression shown for the DLLA (Figure 5-7). This is contrary to a publication by Hile and Pishko<sup>66</sup>, who stated that DL-lactide was liquified at 50 °C,

although the monomer melting temperature at atmospheric pressure was quoted as between 96-104 °C, lower than observed for this sample in the DSC. Melt-type reactions are therefore possible using scCO<sub>2</sub> as a melt point depressant at lower than conventional temperatures (< 160 °C).

A mixture of the two enantiomers led to interesting observations in both the DSC and view cell (Table 5-1, Entry 4). First an endothermic peak in the DSC indicated melting, followed by a recrystallisation immediately after, then by another melting equal to the racemic mixture (Figure 5-6, bottom trace). In scCO<sub>2</sub> the same behaviour is seen with liquefaction at 55 °C, followed by a recrystallisation and foaming of the mixture as the monomers are able to align themselves and re-solidify. The material then liquefies again at 100 °C as for the DLLA. This is therefore a potential solvent-free route for blending the two monomers to make DLLA at lower than conventional temperatures and in the absence of solvents such as toluene.



**Figure 5-7. Images from view cell experiments at 80 °C and 240 bar.**

**(left) LLA, (middle) DLLA, (right) Zr-<sup>t</sup>BuC<sub>3</sub>**

Many applications exploit the ability of scCO<sub>2</sub> to plasticise atactic, amorphous PLA, especially for blending thermally labile materials with the polymer at temperatures below 37 °C (the temperature of the human body).<sup>7, 8</sup>

The same effect was observed in the view cell, with a sample of heterotactic PDLA requiring only 60 bar of CO<sub>2</sub> at 20 °C to plasticise the polymer, liquifying it fully.

For the isotactic PLLA and PDLA no depression is seen within the limits of the equipment (maximum operating temperature 100 °C, maximum operating pressure 300 bar). This is not surprising considering the high degree of crystallinity contained within these polymers, which can be calculated using Equation 5-1.

$$X_c = \frac{\Delta H_f(T_m)}{\Delta H_f^0(T_m^0)}$$

**Equation 5-1. Weight fraction degree of crystallinity ( $X_c$ ) where  $\Delta H_f(T_m)$  is the enthalpy of fusion at the melting point by DSC and  $\Delta H_f^0(T_m^0)$  is the enthalpy of fusion for a 100% crystalline polymer; equal to 93 J g<sup>-1</sup> for PLLA and 125 J g<sup>-1</sup> for s-PLA.<sup>67</sup>**

CO<sub>2</sub> is known to be an efficient plasticiser for amorphous polymers but is unable to disrupt highly ordered crystalline domains. Although the polymers here are semi-crystalline, exhibiting glass transition temperatures between 50-60 °C, they have high degrees of crystallinity; 76% for PLLA and 61% for PDLA respectively. This prevents plasticisation within the limits of the equipment, although that is not to say a depression from 170 °C would not be observed at all.

These measurements provided information for choosing reaction temperatures with the zirconium catalysts (the catalyst was found to be insoluble in the temperature and pressure range, see Figure 5-7). In the case of

enantiopure reactions the presence of CO<sub>2</sub> will ensure the monomers are liquid-like above 50 °C but will solidify during the polymerisation. For the racemic mixture the reactions must be performed above 100 °C to ensure that CO<sub>2</sub> liquefies monomer. The polymer however, will be liquid-like at room temperature if the pressure is above 60 bar, potentially acting as a co-solvent for the monomer.

### 5.3.2. ROP of DLLA using Zr-<sup>t</sup>BuC<sub>3</sub> in scCO<sub>2</sub>

Most reports of synthesising PLA in scCO<sub>2</sub> have used Sn(Oct)<sub>2</sub> with an alcohol as a co-initiator,<sup>48, 54</sup> with an example of using an organo-catalyst also reported.<sup>53</sup> The majority of these studies use a single monomer enantiomer, LLA, presumably forming isotactic PLLA. For studies using the racemic the product tacticity was not investigated, although atactic PLA is most likely produced as the initiating systems used are not known to be able to control the stereochemistry. The implementation of a zirconium trisphenolate (Zr-<sup>t</sup>BuC<sub>3</sub>) initiator capable of producing highly heterotactic PLA is described. To investigate if the activity of this complex could be retained in scCO<sub>2</sub>, DLLA was polymerised for one hour at three temperatures at a [M]:[I] ratio of 100:1, with results shown in Table 5-2.

**Table 5-2. ROP of DLLA at [M]:[I] of 100:1 with Zr-<sup>t</sup>BuC<sub>3</sub><sup>a</sup>**

Entry	Media <sup>b</sup>	Temp / °C	Conversion / % <sup>c</sup>	P <sub>r</sub> <sup>d</sup>	M <sub>n</sub> <sup>theo</sup> / Da <sup>e</sup>	M <sub>n</sub> / D <sup>f</sup>	D <sup>f</sup>
1	scCO <sub>2</sub>	50	14	-	2000	- <sup>i</sup>	- <sup>i</sup>
2	Toluene	80	32	-	4600	- <sup>i</sup>	- <sup>i</sup>
3	scCO <sub>2</sub>	80	86	0.83	12400	12800	1.29
4	Melt <sup>g</sup>	130	98	0.74	14100	9800	1.10
5	scCO <sub>2</sub> <sup>h</sup>	130	93	0.78	13400	18000	1.32

<sup>a</sup> DLLA (1 g) polymerised for 1 hour; <sup>b</sup> 20 mL autoclave at 240 bar for CO<sub>2</sub> reactions, in 20 mL toluene or in bulk; <sup>c</sup> Determined by <sup>1</sup>H NMR; <sup>d</sup> Probability of heterotactic PLA formation determined by <sup>1</sup>H homonuclear decoupled NMR at the University of Bath; <sup>e</sup>  $M_n^{theo} = (144 \times [M] \times \frac{conversion}{100}) + 59$ ; <sup>f</sup> Determined by GPC in THF relative to PS standards (Bath); <sup>g</sup> Reaction duration 0.1 hours; <sup>h</sup> Reaction duration of 0.5 hours; <sup>i</sup> Below the low limit of the GPC columns.

Three temperatures were studied using the Zr-<sup>t</sup>BuC<sub>3</sub> initiator. This catalyst and derivatives have been shown to successfully work at room temperature with a P<sub>r</sub> value of 0.98, although this reaction required 48 hours in toluene at the same 100:1 [M]:[I] ratio used here to reach conversions > 90%.<sup>41</sup> A temperature of 50 °C was chosen to ensure supercritical conditions were maintained (T<sub>c</sub> = 31.1 °C), although only a 14% conversion was reached after one hour (Table 5-2, Entry 1). This was to be expected as the monomer would remain solid at these conditions and would be unable to polymerise, therefore higher temperatures were required.

Although data are published utilising zirconium catalysts for the polymerisation of DLLA at elevated temperatures at the 100:1 ratio, none

employed the same ligand system as used here. It was reported that the ligand had little effect on the activity or selectivity of the zirconium initiators, with typical  $P_r$  values around 0.7 and conversions greater than 80%.<sup>43</sup> To confirm the activity of this specific initiator, a melt polymerisation at 130 °C was performed (Table 5-2, Entry 4), with a conversion of 98% reached in only 6 minutes. The same reaction was performed in scCO<sub>2</sub> at 130 °C and 240 bar, achieving a similarly high conversion of 93% (Table 5-2, Entry 5). A small improvement was seen in the  $P_r$  value when performing the reaction in scCO<sub>2</sub> compared with the melt, although not sufficient enough to justify the cost of the CO<sub>2</sub> and high pressure equipment.

A polymerisation temperature of 80 °C is often used as a compromise between rate and polymer quality, although organic solvents are required to solubilise the reactants. Toluene is commonly used, although as with many volatile organic solvents it has a number of disadvantages. It is highly flammable and toxic, specifically it is a skin irritant and can potentially cause harm to the unborn child. Its relatively high boiling point of 110 °C makes removal difficult, so for medical applications it is not a good solvent to use. The extensive advantages of CO<sub>2</sub> with regards to this have been comprehensively discussed in this Thesis, therefore reactions in scCO<sub>2</sub> at 80 °C were studied (Table 5-2, Entry 3). In one hour, a high conversion of 86% was achieved, compared with 32% for a polymerisation in toluene for the same duration (Table 5-2, Entry 2). This is a significant improvement in both reducing the temperature compared to the melt, as well as improving the rate compared to the 50 °C reactions discussed above (14% conversion in 1 hour). The stereo-control imparted by the zirconium catalyst was also maintained

with a  $P_r$  value of 0.83. Whilst this is lower than the 0.98 value obtained for the room temperature reaction in toluene, it is an improvement compared to the melt polymerisation at 130 °C.

The reaction at 80 °C in scCO<sub>2</sub> is therefore more similar to the melt polymerisation at 130 °C than the solution reaction in toluene also at 80 °C; this has been attributed to the proximity of the reactants. In solution the DLLA is evenly dissolved throughout the medium, and it is well known that performing reactions in solution slows down the rate of polymerisation compared to melt reactions. Clearly the reaction is much quicker in scCO<sub>2</sub>, with the rate at 80 °C more comparable to a melt polymerisation at 130 °C (Table 5-2, Entry 3 versus 4). As seen earlier, the reactants are not soluble, because of this CO<sub>2</sub> should not be thought of as a reaction solvent, but simply a method for lowering the melting/glass transition temperatures. This means the benefits of an increased rate associated with a melt polymerisation can be maintained at lower reaction temperatures, although a slight retardation is observed compared to the melt owing to the lower temperature.

Another observed benefit is the ease of product recovery. In a typical melt polymerisation, as the polymer is solid at room temperature, dichloromethane must be added to solubilise the polymer and enable it to be collected. The polymer is then extracted in excess methanol to obtain a powdered product suitable for further use. In scCO<sub>2</sub> however, a foamed polymer product remains, which with gentle force can be easily broken into a crystalline powder (Figure 5-8). This is then ready for use immediately, however, this would depend on the application owing to residual zirconium in the polymer. Potentially this could be combined with a supercritical fluid

extraction (Lee *et al.*<sup>54</sup>) to ensure unreacted monomer is removed, creating a biodegradable polymer that has not been in contact with any toxic volatile organic solvents.



**Figure 5-8. Foamed PDLLA product directly from the autoclave**

These results are particularly significant for industrial scale-up and offer good processing advantages as well as the reduction in toxic organic solvents required. Although the initial capital costs of setting up a high pressure reactor can be high, the energy gain from a 50 °C reaction temperature reduction is substantial, combined with the ease of production extraction, mean this could be a viable industrial route for synthesising PLA.

For the previous literature and Table 5-2, Entries 2 and 4, all the conventional toluene and melt polymerisations were undertaken in a glove box to minimise the effect of air on the catalyst. These air sensitive conditions were unable to be mimicked with the high pressure equipment, although steps were taken to reduce the effect. The monomer and catalyst were stored under argon and once charged into the autoclave *CO*<sub>2</sub> was added to purge the cell of oxygen. Even under these less stringent conditions, heterotactic PLA was obtained showing the robust nature of the catalyst. To further confirm the success of the polymerisations in *scCO*<sub>2</sub>, several repeats were performed using the most successful synthetic conditions (Table 5-3).

**Table 5-3. Reproducibility of DLLA polymerisation with Zr-<sup>t</sup>BuC<sub>3</sub><sup>a</sup>**

Entry	Conversion / % <sup>b</sup>	P <sub>r</sub> <sup>c</sup>	M <sub>n</sub> / Da <sup>d</sup>	D <sup>d</sup>
1	86	0.83	12800	1.29
2	86	0.85	10400	1.18
3	92	0.83	20000	1.16
4	90	0.83	20200	1.17

<sup>a</sup> DLLA (1 g) polymerised for 1 hour at a [M]:[I] of 100:1, in 20 mL autoclave at 240 bar; <sup>b</sup> Determined by <sup>1</sup>H NMR; <sup>c</sup> Probability of heterotactic PLA formation determined by <sup>1</sup>H homonuclear decoupled NMR at the University of Bath; <sup>d</sup> Determined by GPC in THF relative to PS standards (Bath).

The results in Table 5-3 were based upon reactions using two separate batches of monomer, as well as two different batches of the zirconium complex. For all of the entries, the conversions were consistently high, all reaching around 90% after one hour. Encouragingly, the P<sub>r</sub> values are almost identical in each case also, all 0.83 or above. This demonstrates that not only is the process highly reproducible, but also that the activity and stereoselectivity of the initiator is able to be retained. The only issue encountered was the inconsistency in the M<sub>n</sub> values, with Entries 1 and 2 from a different batch of monomer compared to Entries 3 and 4. Impurities in the different batches, although recrystallised, will poison the catalyst and lead to lower than expected M<sub>n</sub> values. This must be addressed in the future to ensure a completely reproducible synthesis.

One question that arose from the success at 80 °C and 240 bar, is that in the view cell experiments, it was observed that the DLLA monomer remained solid at these conditions. The amorphous PDLA product however, was efficiently plasticised by the CO<sub>2</sub>, with the polymer liquefying at room

temperature and a pressure of only 60 bar. One potential explanation is that the polymer is acting as a co-solvent for the monomer. In the racemic mixture, if there are portions of enantiopure LLA or DLA, these should liquefy around 50 °C, and will be able to polymerise. The resulting polymer chains will be plasticised by the CO<sub>2</sub> and liquefied. The remaining monomer can then be dissolved into this, allowing a homogenous melt phase to be created, in which further polymer growth can occur similarly to a conventional melt polymerisation. Two methods were used to investigate this.

Firstly, a 9:1 mixture by weight of DLLA:PDLLA was treated at 80 °C and 240 bar in the view cell. The contents of the vial appeared to be liquefied, although as with the other samples this was still not CO<sub>2</sub> soluble. This indicated that even at such a low polymer concentration a homogenous monomer/polymer mixture can be formed, aided by the plasticisation of the polymer by CO<sub>2</sub>.

Secondly a polymerisation was attempted in the 100 mL static view cell with DLLA. To keep the concentrations the same, 5 g of monomer was used, at the same 100:1 [M]:[I] ratio, again at 80 °C and 240 bar. Once reaction conditions were reached the white crystalline monomer remained solid. After approximately 15 minutes some liquefaction was observed with areas of white crystalline monomer still visible. It was expected that the liquefied portions were amorphous PLA, with some monomer dissolved into the liquefied polymer. The agitation is far more inefficient in the static view cell compared with a MKIII autoclave owing to the internal shape of the reactor and the stirrer design. This would prevent good mixing and the production of an

overall molten monomer/polymer blend, therefore this reaction was not representative of polymerisations in the standard autoclave.

### 5.3.3. [M]:[I] ratio of 300:1

Industrially the molecular weight of PLA is often far higher than conventionally studied in the literature, typically employing [M]:[I] ratios of 5000:1. The Zr-<sup>t</sup>BuC<sub>3</sub> catalyst studied here has not been fully tested at these concentrations as the reaction times will be vastly increased and achieving high conversions is difficult. A [M]:[I] ratio of 300:1 has been studied in the melt at 130 °C previously, producing an isolated yield of 78% in only 6 minutes, whilst also having a high degree of heterotacticity (P<sub>r</sub> = 0.96). Polymerising DLLA at a 300:1 ratio in scCO<sub>2</sub> to similarly high conversions, whilst retaining the stereoselectivity, is necessary to display the industrial applicability of this process (Table 5-4).

**Table 5-4. ROP of DLLA at [M]:[I] of 300:1**

Entry	Media <sup>a</sup>	Temp / °C	Duration / h	Conversion / % <sup>b</sup>	P <sub>r</sub> <sup>c</sup>	M <sub>n</sub> <sup>theo</sup> / Da <sup>d</sup>	M <sub>n</sub> / Da <sup>e</sup>	Đ <sup>e</sup>
1 <sup>f</sup>	Melt	130	0.1	78	0.96	33700	32300	1.22
2	Melt	130	1	95	0.67	41000	10900	1.11
3	scCO <sub>2</sub>	80	1	27	-	11700	4200	1.15
4	scCO <sub>2</sub>	130	0.5	83	0.73	35900	17000	1.21

<sup>a</sup> 20 mL autoclave at 240 bar for CO<sub>2</sub> reactions; <sup>b</sup> Determined by <sup>1</sup>H NMR; <sup>d</sup>

Probability of heterotactic PLA formation determined by <sup>1</sup>H homonuclear

decoupled NMR at the University of Bath; <sup>d</sup>  $M_n^{theo} = (144 \times [M] \times \frac{conversion}{100}) +$

59; <sup>e</sup> Determined by GPC in THF relative to PS standards (Bath); <sup>f</sup> Chmura et

al.

Entry 1 in Table 5-4 details the results obtained by Chmura *et al.* for the melt polymerisation of DLLA at the 300:1 ratio. As differences in molecular weight have been observed between batches of monomer and initiator, this was repeated using the current batch (Table 5-4, Entry 2). Near complete conversion was obtained, although in this case the  $P_r$  value decreased, indicating less stereoselective control. The degree of heterotacticity was however, similar to those using this batch of monomer at 100:1 in the melt (Table 5-4, Entry 4,  $P_r = 0.74$ ), thus the initiator selectivity remained constant. The living characteristics of the polymerisation were questioned however, with the  $M_n$  of the product much lower than the theoretical value at the given conversion. Chmura *et al.* saw a similar observation when using unsublimed monomer in their previous studies at this ratio owing to impurities in the monomer, such as residual lactic acid or water.<sup>43</sup> For example, one zirconium initiator produced PDLLA with an  $M_n$  of 59000 Da and  $\bar{D}$  of 1.77 from sublimed monomer, but an  $M_n$  of only 24350 Da with a  $\bar{D}$  of 1.19 using unsublimed monomer. It was felt that using unsublimed monomer for the syntheses in  $scCO_2$  would assess the activity and selectivity of the initiators under more industrially relevant conditions.

The most successful conditions used at a  $[M]:[I]$  ratio of 100:1 were a temperature of 80 °C, a pressure of 240 bar, with a reaction duration of one hour (86% conversion,  $P_r = 0.83$ ). A DLLA polymerisation was performed at these conditions for the 300:1 ratio (Table 5-4, Entry 3). This was less successful with only a 27% conversion reached in the same time period of one hour, with the  $M_n$  again far lower than  $M_n^{\text{theo}}$ . This was significantly lower than the melt polymerisation (95% conversion), contrary to the 100:1 ratio. A lower

concentration of initiator is expected to slow the polymerisation rate, although it was seen at the 100:1 ratio that the 80 °C reaction in scCO<sub>2</sub> should proceed more similarly to the melt at ambient pressure.

Raising the reaction temperature to 130 °C in scCO<sub>2</sub> (Table 5-4, Entry 4), had a large influence on the conversion, reaching 83% in only 30 minutes. A small improvement in the selectivity was observed compared to the melt reaction, as well as a higher  $M_n$ . This indicated that the scCO<sub>2</sub> may be more tolerant to the impurities, with any residual lactic acid dissolving throughout the volume of the autoclave, reducing the chance of meeting a polymer chain and reacting. The kinetics profiles of the reactions were therefore necessary to understand the rate of polymerisation in scCO<sub>2</sub>.

#### 5.3.4. Reaction Duration

A reaction time of one hour was used for the previous syntheses to enable a fair comparison between the different reaction media. The scCO<sub>2</sub> reactions at 80 °C produced similar results to the melt reactions at 130 °C, which itself is known to approach completion in around 10 minutes. To probe the rate of the reaction in CO<sub>2</sub> multiple reactions were performed for different times to generate kinetic data (Table 5-5).

**Table 5-5. Varying reaction time for the ROP of DLLA at [M]:[I] of 100:1<sup>a</sup>**

Entry	Duration / h	Conversion / % <sup>b</sup>	$M_n^{theo} / Da$ <sup>c</sup>	$M_n / Da$ <sup>d</sup>	$\bar{D}$ <sup>d</sup>
1	0	44	6300	6000	1.42
2	0.25	91	13100	11400	1.40
3	0.5	83	12000	8700	1.43
4	1	74	10700	10100	1.47
5	1.5	89	12800	15700	1.60

<sup>a</sup> DLLA (1 g) polymerised in a 20 mL autoclave at 80 °C and 240 bar; <sup>b</sup>

Determined by <sup>1</sup>H NMR; <sup>c</sup>  $M_n^{theo} = (144 \times [M] \times \frac{conversion}{100}) + 59$ ; <sup>d</sup>

Determined by GPC in THF relative to PS standards (Nottingham).

For each polymerisation, the duration is taken as the time from which the autoclave reached the reaction conditions of 80 °C and 240 bar, to when the heating jacket was switched off and the reactor left to cool to ambient temperature. Typically the heating took 20 minutes, with the autoclaves left to cool for 20 minutes, followed by a 5-10 minute venting step. The reproducibility of this proved difficult, as can be seen by the variation in the conversions. Entry 1 was allowed to heat to 80 °C, then the heating jacket was immediately turned off and the autoclave cooled and depressurised. Even when only at the elevated temperatures for such a short period of time, the conversion was already at 44%. From Entry 2, the polymerisation is almost complete within 15 minutes, which is consistent with the melt polymerisations at 130 °C (Table 5-2). Increasing the reaction time did not improve this, with high conversions achieved throughout. The variability between reactions has been attributed to the different heating and cooling rates for the autoclaves as shown in Figure 5-9.

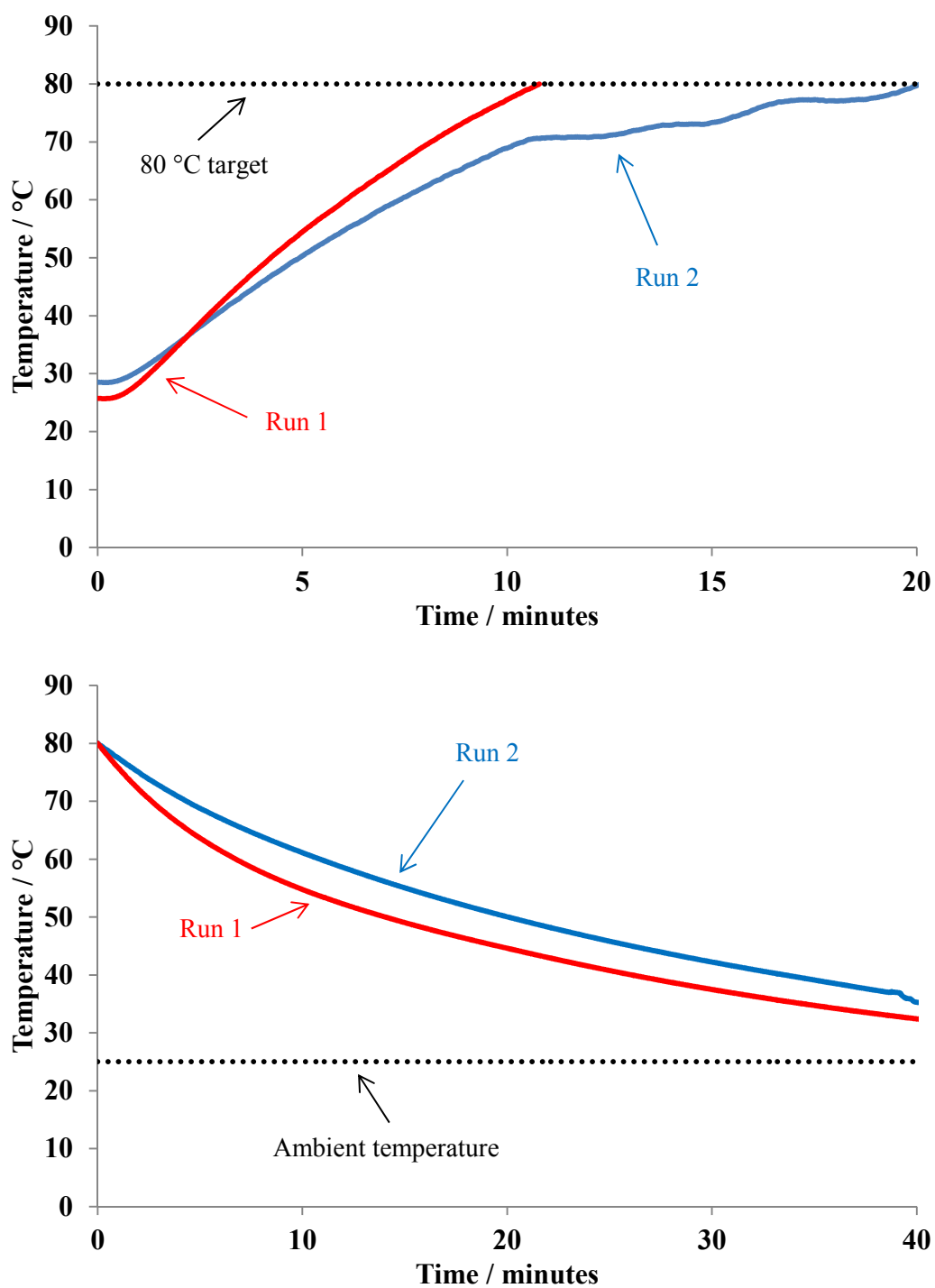


Figure 5-9. Temperature profile for a 20 mL autoclave, (top) heating from ambient to 80 °C, (bottom) cooling from 80 °C over a 40 minute period.

The data in Figure 5-9 has been measured on a 20 mL autoclave with an extra internal thermocouple installed to log the temperature during the heating and cooling ramps. The autoclave was filled with 60 bar of CO<sub>2</sub>, with no reactants present, and heated to 80 °C. The heater was then switched off, and the cooling period monitored in the second graph. This was repeated on same autoclave, with the same heating jacket and electronics to check the reproducibility of the system.

On the heating ramp there is a difference of around ten minutes between the two runs, which was not taken into account as part of the reaction duration. Run 1 reached 80 °C in only ten minutes, whereas run 2 was only at 70 °C in the same time, taking a further ten minutes to reach 80 °C. During this extra time the reaction will most likely have started, giving rise to the varied conversions observed in Table 5-5, including the apparent 44% conversions for a zero hour reaction. Therefore the kinetic data at a ratio of 100:1 with DLLA was unable to be obtained accurately. A number of methods have been suggested to facilitate this, notably the release of the initiator once the reactions conditions are reached and stable. This is not possible in the current autoclaves currently, due to their small size and the difficulty in modifying the head section. One idea is to load the catalyst in a breakable container, such as a sealed glass capillary tube, and once at 80 °C, the action of switching the stirrer on will release the catalyst and begin the reaction. One attempt was made with this, but a poor conversion was observed (18%), indicating not all of the catalyst was available for the polymerisation. This is owing to the poor solubility of the catalyst in scCO<sub>2</sub>, thus it remains in the glass capillary.

The rate of polymerisation for enantiopure LLA is known to be around seven times slower than for the racemic mixture with this Zr-<sup>t</sup>Bu<sub>3</sub>C<sub>3</sub> catalyst ( $k_{app}^{DLLA} = 4.2 \times 10^{-3} \text{ min}^{-1}$  and  $k_{app}^{LLA} = 0.6 \times 10^{-3} \text{ min}^{-1}$  for polymerisations at 25 °C).<sup>41</sup> In the solubility studies LLA was shown to liquefy at around 50 °C in scCO<sub>2</sub>, with the polymer remaining solid up to 100 °C and 240 bar. Synthesising PLLA at 80 °C and 240 bar should therefore proceed in the same manner as a conventional melt polymerisation, with the monomer acting as the reactant and solvent (Table 5-6).

**Table 5-6. Varying reaction time for the ROP of LLA at [M]:[I] of 100:1<sup>a</sup>**

Entry	Duration / h	Conversion / % <sup>b</sup>	M <sub>n</sub> <sup>theo</sup> / Da <sup>c</sup>	M <sub>n</sub> / Da <sup>d</sup>	M <sub>p</sub> / Da <sup>d</sup>	Đ <sup>d</sup>
1	1	31	4500	2200	2300	1.12
2	3	68	9800	5500	8100	1.36
3	5	95	13700	5900	9500	1.39

<sup>a</sup> LLA (1 g) polymerised in a 20 mL autoclave at 80 °C and 240 bar; <sup>b</sup>

Determined by <sup>1</sup>H NMR; <sup>c</sup>  $M_n^{theo} = (144 \times [M] \times \frac{conversion}{100}) + 59$ ; <sup>d</sup>

Determined by GPC in THF relative to PS standards (Nottingham).

After polymerising for one hour the conversion was considerably lower for LLA (Table 5-6, Entry 1, 31%) compared to DLLA (Table 5-2, Entry 4, 86%). Increasing the reaction time saw a much better growth, reaching 68% conversion in three hours, with a further increase to five hours leading to almost complete conversion. This follows similar behaviour to the solution analogues with LLA polymerising much slower than DLLA.

The same issues were encountered with the M<sub>n</sub> values consistently being lower than the expected. The main problem lies in the GPC traces themselves (Figure 5-10), and the difficulty in integrating accurately, as the catalyst peak

overlaps the main polymer peak. However, the  $M_p$  was far closer to the  $M_n^{\text{theo}}$  for each of the samples, with the traces displaying an overall shift in the main polymer peak (right hand side of the traces).

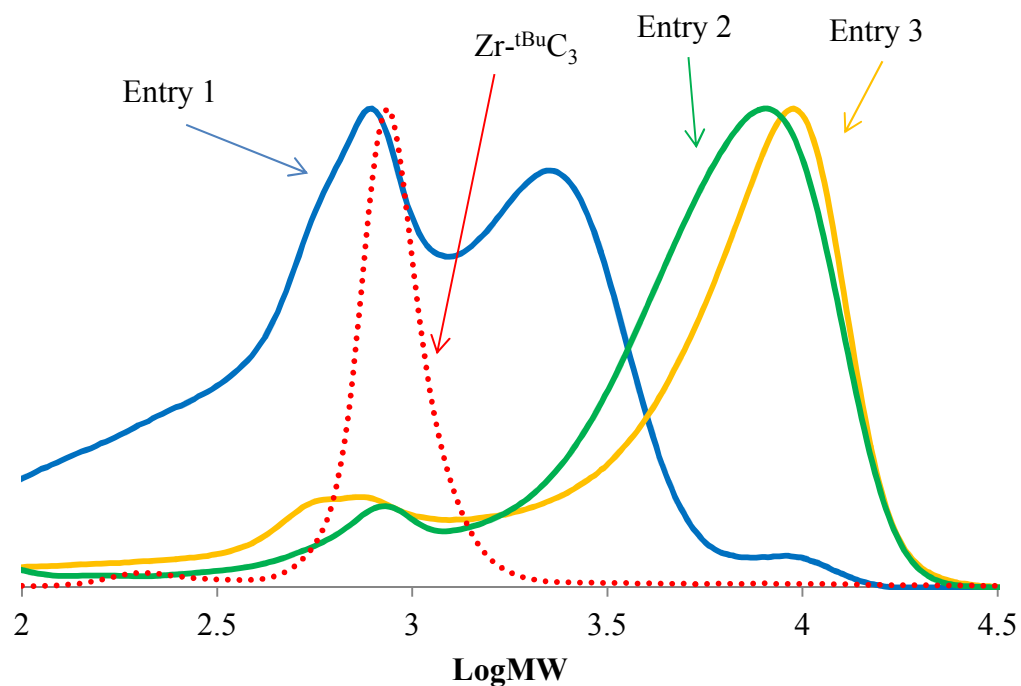


**Figure 5-10. GPC traces for the polymerisation of LLA in  $scCO_2$ . Data is from the samples detailed in Table 5-6, including a trace of the pristine  $Zr-tBuC_3$  catalyst.**

From the PLLA data, the main point to note is that high conversion of monomer to polymer is possible, and that isotactic PLA can be synthesised using this catalyst also. The inherent problems associated with GPC calibrations, in particular with PLA having such a different structure compared to PS, means the actual values cannot be used to judge the success of the polymerisation, but the shift observed in the traces is indicative that the molecular weight does indeed grow with conversion. To understand further the

living character of these polymerisations, chain extension reactions were performed.

#### 5.3.5. Chain Extensions

Synthesising heterotactic PLA ensures a well-defined structure is created, ensuring the polymer is highly amorphous. Perhaps more important aspect of controlling the synthesis is the living end group, which retains the ability to be chain extended once all the monomer is consumed. Production of block copolymers, including enantiopure blocks, influences the thermal properties, ultimately leading to stereocomplexed PLA with a melting point in excess of 220 °C.

The synthesis of such block copolymers can prove difficult under melt conditions, owing to the high melting point (around 170 °C) of the highly crystalline enantiopure PLLA or PDLA. Degradation of both the catalyst and/or the polymer itself becomes more likely at these very high temperatures; therefore solution reactions are often necessary. The work in this Chapter in *scCO*<sub>2</sub> has shown a solvent-free route for synthesising amorphous PDLLA, as well as semi-crystalline PLLA at reduced temperatures, whilst retaining a faster polymerisation rate relative to the solution reactions at similar temperatures. Several reactions were performed to investigate if block copolymers can be produced *via* a one-pot, two-step process in the absence of organic solvents (Table 5-7), all at 80 °C and 240 bar.

**Table 5-7. Chain extension via a one pot, two step process<sup>a</sup>**

Entry	M <sup>b</sup>	Duration / h	Conversion / % <sup>c</sup>	P <sub>r</sub> <sup>d</sup>	M <sub>n</sub> / Da <sup>e</sup>	Đ <sup>e</sup>
1a	DLLA	1	92	0.83	20000	1.16
1b	DLLA	1	65 (38) <sup>f</sup>	0.83	25800	1.01
2a	DLLA	1	90	0.83	20200	1.17
2b	LLA	14	85 (80) <sup>f</sup>	0.65	29700	1.08

<sup>a</sup> In a 20 mL autoclave at 240 bar; <sup>b</sup> Initial [M]:[I] of 100:1, with a further 100 equivalents of second monomer added to give an overall ratio of 200:1; <sup>c</sup> Determined by <sup>1</sup>H NMR; <sup>d</sup> Probability of heterotactic PLA formation determined by <sup>1</sup>H homonuclear decoupled NMR at the University of Bath; <sup>e</sup> Determined by GPC in THF relative to PS standards (Bath); <sup>f</sup> Value in brackets is the estimated conversion of the second block.

The living character of the polymerisation was first investigated by synthesising PDLLA, then chain extending with the addition of further DLLA. The first block followed the same behaviour as expected (Table 5-7, Entry 1a), reaching 92% conversion, with highly heterotactic polymer produced. After reacting for one hour, a further 1 g of DLLA was added into the autoclave (2 g in total, minus around 50 mg taken for analysis). A far lower conversion was seen for the second block (Table 5-7, Entry 1b), with 38% of the remaining monomer polymerising. There is however, a shift in molecular weight, as seen from the GPC trace (Figure 5-11) and the M<sub>n</sub> values, showing an indication that the polymer has been chain extended and possesses living character. As explained earlier, the conditions used meant oxygen and water could be contaminating the sample, which has been seen to retard the reactions. The overall [M]:[I] will change from 100:1 for the first polymerisation, to 200:1 for the second polymerisation. At lower catalyst loadings the rate of polymerisation

slowed (section 5.3.3.), therefore the lower conversion is to be expected. The results were encouraging as the  $P_r$  value remained constant, indicating the initiator was able to retain the heterotactic selectivity upon the addition of further monomer.

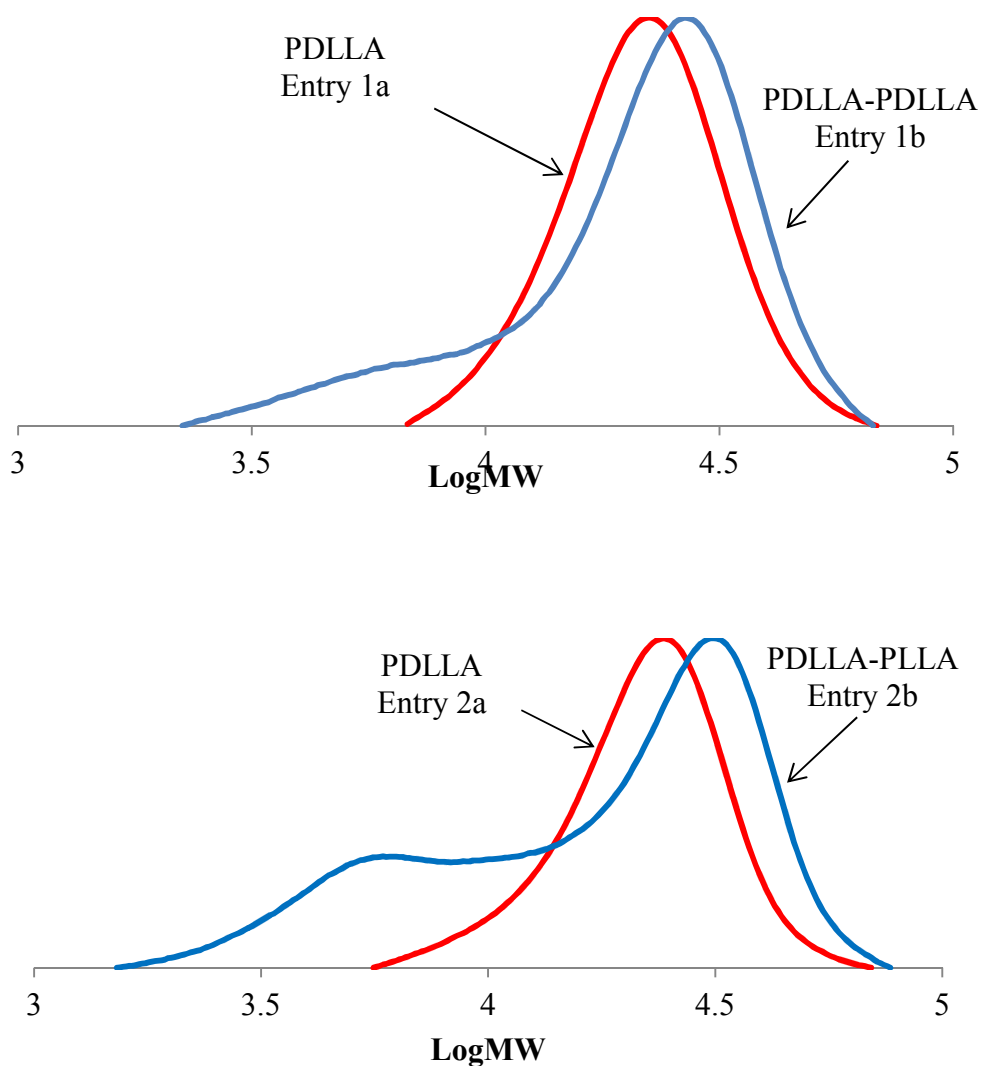


**Figure 5-11. GPC traces indicating the growth in  $M_n$  for (left) Table 5-7, Entry 1a and 1b, (right) Table 5-7, Entry 2a and 2b.**

The next targeted block copolymer was PDLLA-*b*-PLLA (Table 5-7, Entries 2a and 2b), produced in an identical way to the first example, with the exception that enantiopure LLA was added in the second step. The PDLLA

first block followed the previous samples, with good conversion,  $M_n$  and narrow dispersity. As seen earlier, LLA polymerised at a much slower rate, therefore the second block was left to react overnight to ensure as high a conversion as possible was attained. In this case the conversion was 80%, with good growth in  $M_n$  observed also (Figure 5-11). Further evidence of block copolymerisation is seen in the  $P_r$  values. The  $P_r$  value was high for the PDLLA, at 0.83, signifying a high degree of stereoselective control. A decrease in the  $P_r$  to 0.65, indicated the formation of either atactic or isotactic polymer, in this case it would be isotactic PLLA.

For both of the above chain extensions a lower molecular weight shoulder appeared in both GPC traces. This indicated that not only are the already formed polymers growing further, but also new chains are being initiated. If impurities are present, for example water, then this would be able to cleave the initiating group from a polymer chain and re-initiate new monomer. Monomer purity and air sensitive conditions are needed to check that this is an effect of impurities, as opposed to the  $CO_2$  conditions. Further work is needed to increase the monomer conversion for the second step, with in-depth characterisation of the product required to confirm if a block copolymer is indeed formed.

#### 5.3.6. ROP of $\epsilon$ -caprolactone using $Zr-^{tBu}C_3$ in $scCO_2$

Copolymerisations of other monomers with PLA can also help to modify the thermal and mechanical properties; in particular  $\epsilon$ -caprolactone has been used as it can be obtained from biorenewable sources, as well as being biodegradable and biocompatible. The versatility of this system was therefore

studied by the ROP of  $\epsilon$ -caprolactone using the same catalyst and polymerisation conditions (Table 5-8). The key difference in the procedure was the lack of flushing prior to the polymerisation as  $\epsilon$ -CL is known to be more soluble in CO<sub>2</sub> than lactide, therefore this reduced the risk of extracting the monomer.

**Table 5-8. ROP of  $\epsilon$ -caprolactone<sup>a</sup>**

Entry	Duration / h	Conversion / % <sup>b</sup>	$M_n^{theo}$ / Da <sup>c</sup>	$M_n$ / Da <sup>d</sup>	$\bar{D}$ <sup>d</sup>
1	1	44	5000	4600	1.19
2	3	91	10400	7600	1.22
3	6	99	11300	6700	1.44
4	15	99	11300	9500	1.50

<sup>a</sup>  $\epsilon$ -CL (1 g) polymerised with Zr-<sup>t</sup>BuC<sub>3</sub> catalyst in a 20 mL autoclave at 240 bar, stirring at 300 rpm, [M]:[I] ratio of 100:1;<sup>b</sup> Determined by <sup>1</sup>H NMR; <sup>c</sup>  $M_n^{theo} = (114 \times [M] \times \frac{conversion}{100})$ ; <sup>d</sup> Determined by GPC in THF relative to PS standards (Nottingham).

Initially a time of 1 hour was set (Table 5-8, Entry 1), with a slower rate of polymerisation exhibited with  $\epsilon$ -CL compared with DLLA. The product molecular weight itself was in good agreement with the theoretical at that conversion, also displaying a narrow dispersity.

Tripling the reaction time to 3 hours (Table 5-8, Entry 2) allowed a conversion of 91% to be attained which was further increased to >99% when polymerising for 6 and 15 hours. A broadening of the molecular weight distribution was observed upon increasing reaction time however, most likely as trans-esterification side reactions occur. The molecular weights were slightly lower than the calculated value although the structure of PCL is quite

different to that of the PS standards which will account for some discrepancies. Comparing with previous work in scCO<sub>2</sub> using Sn(Oct)<sub>2</sub> a vast increase in rate is observed under the same conditions, with over 48 hours required for >90% conversion.<sup>46</sup> This shows a considerable improvement solely by changing the catalyst/initiator system.

The synthesis of copolymers of ε-CL and lactide is a potential application for creating biorenewable and biodegradable polymers with tuneable properties. The other advantage of the ε-CL monomer is its form as a liquid allowing it to be added *via* an HPLC pump, in a similar system to Chapter 4, for the production of block copolymers, although this is beyond the scope of this Thesis.

#### 5.4. Conclusions

Zirconium-alkoxide initiators have been successfully used for the ROP of DLLA in scCO<sub>2</sub>. High conversions could be reached at high catalyst loadings ([M]:[I] of 100:1), with polymer molecular weights in fairly good agreement with calculated values, as well as possessing narrow molecular weight distributions, indicating good control over the polymerisation. Compared with the analogous solution reactions at 80 °C in toluene, the polymerisation rate in scCO<sub>2</sub> was much faster. In fact, the reactions progressed more similarly to melt polymerisations at 130 °C. It is proposed that the CO<sub>2</sub> aids liquefaction of the monomer/polymer mixture, allowing a melt-type polymerisation to occur at only 80 °C.

The influence of the zirconium catalyst on the tacticity of the final polymer was improved also. At 80 °C in scCO<sub>2</sub>, the P<sub>r</sub> values were consistently

above 0.8, whereas for melt polymerisations at 130 °C they were closer to 0.7. The lower reaction temperature reduces the amount of trans-esterification and other side reactions, enabling the polymerisation to proceed in a more controlled manner.

Finally, the synthetic procedure has been extended to the homopolymerisation of  $\epsilon$ -CL. Again good control was maintained, offering a potential solvent-free route to the formation of copolymers with tuneable properties.

Overall, this process fulfils several of the twelve principles of green chemistry. Although the toxicity of the catalyst is unknown, the polymer itself is biocompatible and biodegradable, as well as being synthesised from biorenewable sources. ScCO<sub>2</sub> is classed as a green solvent, with the added benefit of lowering the reaction temperature considerably, which has an energy gain. Finally, the product is obtained as a crystalline powder, removing the need for extra processes steps in order to create a product ready for market.

### 5.5. References

1. R. Muelhaupt, *Macromolecular Chemistry and Physics*, 2013, **214**, 159-174.
2. L. T. Lim, R. Auras and M. Rubino, *Progress in Polymer Science*, 2008, **33**, 820-852.
3. R. Chandra and R. Rustgi, *Progress in Polymer Science*, 1998, **23**, 1273-1335.
4. O. Dechy-Cabaret, B. Martin-Vaca and D. Bourissou, *Chemical Reviews*, 2004, **104**, 6147-6176.
5. R. E. Drumright, P. R. Gruber and D. E. Henton, *Advanced Materials*, 2000, **12**, 1841-1846.
6. R. Auras, B. Harte and S. Selke, *Macromolecular Bioscience*, 2004, **4**, 835-864.
7. E. Tayton, S. Fahmy, M. Purcell, A. Aarvold, J. O. Smith, S. Kalra, A. Briscoe, S. Lanham, S. Howdle, K. Shakesheff, D. G. Dunlop and R. O. C. Oreffo, *Journal of Biomedical Materials Research Part A*, 2012, **100A**, 3211-3219.
8. E. Tayton, M. Purcell, A. Aarvold, J. O. Smith, S. Kalra, A. Briscoe, K. Shakesheff, S. M. Howdle, D. G. Dunlop and R. O. C. Oreffo, *Acta Biomaterialia*, 2012, **8**, 1918-1927.
9. F. Jordan, A. Naylor, C. A. Kelly, S. M. Howdle, A. Lewis and L. Illum, *Journal of Controlled Release*, 2010, **141**, 153-160.
10. Y. Ikada and H. Tsuji, *Macromolecular Rapid Communications*, 2000, **21**, 117-132.
11. R. A. Gross and B. Kalra, *Science*, 2002, **297**, 803-807.

12. N. Spassky, M. Wisniewski, C. Pluta and A. LeBorgne, *Macromolecular Chemistry and Physics*, 1996, **197**, 2627-2637.
13. A. J. Chmura, M. G. Davidson, C. J. Frankis, M. D. Jones and M. D. Lunn, *Chemical Communications*, 2008, 6611-6611.
14. M. J. Stanford and A. P. Dove, *Chemical Society Reviews*, 2010, **39**, 486-494.
15. H. R. Kricheldorf and I. KreiserSaunders, *Macromolecular Symposia*, 1996, **103**, 85-102.
16. C. P. Radano, G. L. Baker and M. R. Smith, *Journal of the American Chemical Society*, 2000, **122**, 1552-1553.
17. Y. Ikada, K. Jamshidi, H. Tsuji and S. H. Hyon, *Macromolecules*, 1987, **20**, 904-906.
18. H. Tsuji, *Macromolecular Bioscience*, 2005, **5**, 569-597.
19. H. Tsuji and Y. Ikada, *Macromolecules*, 1993, **26**, 6918-6926.
20. D. Garlotta, *Journal of Polymers and the Environment*, 2001, **9**, 63-84.
21. Y. He, Y. Xu, J. Wei, Z. Y. Fan and S. M. Li, *Polymer*, 2008, **49**, 5670-5675.
22. P. Purnama and S. H. Kim, *Macromolecules*, 2010, **43**, 1137-1142.
23. P. Purnama and S. H. Kim, *Polymer International*, 2012, **61**, 939-942.
24. M. Labet and W. Thielemans, *Chemical Society Reviews*, 2009, **38**, 3484-3504.
25. M. K. Kang, Y. Jung and S. H. Kim, *Macromolecular Research*, 2013, **21**, 1036-1041.
26. M. HiljanenVainio, T. Karjalainen and J. Seppala, *Journal of Applied Polymer Science*, 1996, **59**, 1281-1288.

27. T. Buntara, S. Noel, P. H. Phua, I. Melian-Cabrera, J. G. de Vries and H. J. Heeres, *Angewandte Chemie-International Edition*, 2011, **50**, 7083-7087.
28. M. Tang, M. Purcell, J. A. M. Steele, K. Y. Lee, S. McCullen, K. M. Shakesheff, A. Bismarck, M. M. Stevens, S. M. Howdle and C. K. Williams, *Macromolecules*, 2013, **46**, 8136-8143.
29. V. R. Sinha, K. Bansal, R. Kaushik, R. Kumria and A. Trehan, *International Journal of Pharmaceutics*, 2004, **278**, 1-23.
30. H. Tsuji and Y. Ikada, *Journal of Applied Polymer Science*, 1996, **60**, 2367-2375.
31. H. Tsuji and Y. Ikada, *Journal of Applied Polymer Science*, 1998, **67**, 405-415.
32. H. Tsuji, A. Mizuno and Y. Ikada, *Journal of Applied Polymer Science*, 1998, **70**, 2259-2268.
33. M. H. Huang, S. M. Li and M. Vert, *Polymer*, 2004, **45**, 8675-8681.
34. M. Martina and D. W. Hutmacher, *Polymer International*, 2007, **56**, 145-157.
35. L. Yu, K. Dean and L. Li, *Progress in Polymer Science*, 2006, **31**, 576-602.
36. H. R. Kricheldorf, I. Kreiseraunders and C. Boettcher, *Polymer*, 1995, **36**, 1253-1259.
37. A. Kowalski, A. Duda and S. Penczek, *Macromolecular Rapid Communications*, 1998, **19**, 567-572.
38. A. Duda, S. Penczek, A. Kowalski and J. Libiszowski, *Macromolecular Symposia*, 2000, **153**, 41-53.

39. P. Dubois, O. Coulembier and J.-M. Raquez, *Handbook of Ring-Opening Polymerization*, Wiley-VHC, Weinheim, 2009.
40. A. Arbaoui and C. Redshaw, *Polymer Chemistry*, 2010, **1**, 801-826.
41. A. J. Chmura, M. G. Davidson, C. J. Frankis, M. D. Jones and M. D. Lunn, *Chemical Communications*, 2008, 1293-1295.
42. M. D. Jones, M. G. Davidson and G. Kociok-Kohn, *Polyhedron*, 2010, **29**, 697-700.
43. A. J. Chmura, D. M. Cousins, M. G. Davidson, M. D. Jones, M. D. Lunn and M. F. Mahon, *Dalton Transactions*, 2008, 1437-1443.
44. B. J. Jeffery, E. L. Whitelaw, D. Garcia-Vivo, J. A. Stewart, M. F. Mahon, M. G. Davidson and M. D. Jones, *Chemical Communications*, 2011, **47**, 12328-12330.
45. J. Gregorowicz and P. Bernatowicz, *Journal of Supercritical Fluids*, 2009, **51**, 270-277.
46. D. Bratton, M. Brown and S. M. Howdle, *Macromolecules*, 2005, **38**, 1190-1195.
47. Y. T. Shieh and K. H. Liu, *Journal of Supercritical Fluids*, 2003, **25**, 261-268.
48. D. Bratton, M. Brown and S. M. Howdle, *Macromolecules*, 2003, **36**, 5908-5911.
49. D. Bratton, M. Brown and S. M. Howdle, *Chemical Communications*, 2004, 808-809.
50. M. Yilmaz, S. Egri, N. Yildiz, A. Calimli and E. Piskin, *Journal of Polymer Research*, 2011, **18**, 975-982.

51. S. Zhang, S. P. Zhan, Q. C. Zhao, S. H. Chen, Z. J. Liu and J. J. Deng, *Journal of Polymer Research*, 2013, **20**, 1-9.
52. H. S. Ganapathy, H. S. Hwang, Y. T. Jeong, W. K. Lee and K. T. Lim, *European Polymer Journal*, 2007, **43**, 119-126.
53. I. Blakey, A. G. Yu, S. M. Howdle, A. K. Whittaker and K. J. Thurecht, *Green Chemistry*, 2011, **13**, 2032-2037.
54. S. Y. Lee, P. Valtchev and F. Dehghani, *Green Chemistry*, 2012, **14**, 1357-1366.
55. F. Stassin, O. Halleux and R. Jerome, *Macromolecules*, 2001, **34**, 775-781.
56. F. Stassin and R. Jerome, *Chemical Communications*, 2003, 232-233.
57. V. Bergeot, T. Tassaing, M. Besnard, F. Cansell and A. F. Mingotaud, *Journal of Supercritical Fluids*, 2004, **28**, 249-261.
58. C. Jerome and P. Lecomte, *Advanced Drug Delivery Reviews*, 2008, **60**, 1056-1076.
59. K. J. Thurecht, A. Heise, M. deGeus, S. Villarroya, J. Zhou, M. F. Wyatt and S. M. Howdle, *Macromolecules*, 2006, **39**, 7967-7972.
60. F. C. Loeker, C. J. Duxbury, R. Kumar, W. Gao, R. A. Gross and S. M. Howdle, *Macromolecules*, 2004, **37**, 2450-2453.
61. D. Bratton, M. Brown and S. M. Howdle, *Journal of Polymer Science Part a-Polymer Chemistry*, 2005, **43**, 6573-6585.
62. K. J. Thurecht, A. M. Gregory, S. Villarroya, J. Zhou, A. Heise and S. M. Howdle, *Chemical Communications*, 2006, 4383-4385.
63. C. J. Duxbury, W. X. Wang, M. de Geus, A. Heise and S. M. Howdle, *Journal of the American Chemical Society*, 2005, **127**, 2384-2385.

64. B. M. Chamberlain, M. Cheng, D. R. Moore, T. M. Ovitt, E. B. Lobkovsky and G. W. Coates, *Journal of the American Chemical Society*, 2001, **123**, 3229-3238.
65. P. Licence, M. P. Dellar, R. G. M. Wilson, P. A. Fields, D. Litchfield, H. M. Woods, M. Poliakoff and S. M. Howdle, *Review of Scientific Instruments*, 2004, **75**, 3233-3236.
66. D. D. Hile and M. V. Pishko, *Journal of Polymer Science Part a-Polymer Chemistry*, 2001, **39**, 562-570.
67. C. A. Kelly, S. M. Howdle, K. M. Shakesheff, M. J. Jenkins and G. A. Leeke, *Journal of Polymer Science Part B-Polymer Physics*, 2012, **50**, 1383-1393.

## Chapter 6 –Conclusions and Future Work

---

### 6. Overview

This Chapter will summarise the synthetic procedures developed in this Thesis and discuss the work concerning the novel high pressure cell for measuring SAXS *in situ*. Potential future work that could be undertaken is then described.

#### 6.1. Conclusions

The effect of using a small amount of scCO<sub>2</sub> to expand RAFT controlled bulk polymerisations of either MMA or styrene was investigated in Chapter 3. The viscosity of the polymers could be heavily reduced, by up to 98% with 120 bar CO<sub>2</sub>, reducing the Trommsdorff Effect significantly. This enabled controlled polymers to be synthesised in high yields with narrow molecular weight distributions. This was extended to the synthesis of a low molecular weight PMMA-*b*-PS block copolymer, using supercritical fluid extraction to purify the first block prior to the addition of the second monomer in a two-step process.

Block copolymer micro-particles synthesised in a scCO<sub>2</sub> dispersion polymerisation by Jennings *et al.* showed internally phase separated structures. To understand when the phase separation occurs a new high pressure cell for measuring *in situ* SAXS during a scCO<sub>2</sub> dispersion polymerisation was designed and constructed. A modified autoclave base containing two diamond

windows and an exit opening aperture of 40 ° allows simultaneous collection of both SAXS and WAXS data. Unfortunately it was not possible to reproduce the block copolymer micro-particles in the new cell. The design requires a narrow path length between the windows to obtain good scattering data, which has detrimental effects on the mixing. The threaded window mounts also reduced the maximum operating temperature to 200 bar, lowering the solubility of the PDMS-MA stabiliser required for a successful dispersion. The combination of these two problems meant highly agglomerated particles were produced. However, initial scattering data was obtained during a polymerisation in scCO<sub>2</sub>, indicating this could be a viable method of monitoring polymerisations *in situ*.

Preliminary investigations into modifying particles produced in scCO<sub>2</sub> dispersion polymerisations through cross-linking showed that a stable dispersion could be maintained at levels up to 5 wt%. By using RAFT chemistry, nearly 100% of the product could incorporate cross-linking and remain insoluble with dynamic mechanical analysis showing an increase in the T<sub>g</sub> with increasing cross-linker concentration. Lower T<sub>g</sub> polymers often need high amounts of co-monomer to produce solid particles, but at cross-linking concentrations of 5 wt% improvements were made to the morphology.

In the final Chapter, scCO<sub>2</sub> was used as a reaction solvent in the polymerisation of lactide using a novel zirconium catalyst. Through this method the standard melt reaction temperature of 130 °C was able to be reduced to 80 °C, offering a large energy (and therefore cost) saving. The catalyst enables control over the polymer tacticity, specifically producing

heterotactic PLA from a racemic monomer mixture. The catalytic activity is retained in scCO<sub>2</sub>, with the degree of heterotactic polymer,  $P_r$ , >0.8 ( $P_r = 1$  for perfect control). PCL was also synthesised using the same method, with copolymerisation a future objectives.

## 6.2. Future Work

The scCO<sub>2</sub> expanded phase work has shown that oligomeric block copolymers can be synthesised in the absence of volatile organic solvents, using scCO<sub>2</sub> as both a reaction medium and as a purification method. This was shown for a simple PMMA-*b*-PS block copolymer; however, RAFT chemistry is applicable to many commercial monomers which opens up a range of possibilities.<sup>1</sup> This method is probably most suited to polymers with low glass transition temperatures, which will be liquefied at lower temperatures. Alternatively, polymers in which CO<sub>2</sub> has good solubility and can plasticise well would be suitable as their viscosity could be easily lowered. PVAc/PVPi copolymers are one potential choice, with applications as fully hydrocarbon stabilisers for scCO<sub>2</sub> dispersion polymerisations.<sup>2-4</sup>

Details of a second version of the high pressure cell for measuring *in situ* SAXS were described in Chapter 4. A number of issues have been addressed, notably the design of the internal reactor volume to improve mixing, an increase in the maximum allowable working pressure, plus addition/sampling ports. This cell is currently under construction with initial tests expected to take place at the end of 2014, with beam time allocated at the ESRF for early 2015. With the modifications it is hoped that the synthesis from a standard

autoclave can be reproduced,<sup>5</sup> and the SAXS measurements will be able to generate information on when/how internal microphase separation occurs.

Dynamic mechanical analysis of the cross-linked micro-particles showed an increase in the T<sub>g</sub> of the copolymers. This technique can also be used to measure the mechanical strength of a polymer. The powder pocket method employed in Chapter 4 does not allow this as the aluminium has its own temperature dependent response. Through moulding into uniform polymer bars the absolute mechanical properties can be studied, which could allow materials with targeted properties to be synthesised (by changing monomer feed, functional groups, etc).

One of the requirements for making polymers from renewable sources, as opposed to crude oil derivatives, is that they must have comparable or improved properties for specific applications. Amorphous PLA has found uses in high value medical applications as it fulfils many key properties, for example it degrades into lactic acid which can be excreted by the body. However, it would be desirable to use PLA in more commodity applications. Stereocomplexed PLA, which can be synthesised from the same renewable monomer, offers a solution, having a high melting temperature above 200 °C. As many suitable catalysts lose activity at the high temperatures required for the melt synthesis, scCO<sub>2</sub> could be used to lower the reaction temperature. This reduction in temperature would have a huge energy saving, which would lower the price of the materials, enabling PLA to become a viable replacement for polymer such as PS.

**6.3. References**

1. G. Moad, E. Rizzardo and S. H. Thang, *Chemistry-an Asian Journal*, 2013, **8**, 1634-1644.
2. N. A. Birkin, N. J. Arrowsmith, E. J. Park, A. P. Richez and S. M. Howdle, *Polymer Chemistry*, 2011, **2**, 1293-1299.
3. E. J. Park, A. P. Richez, N. A. Birkin, H. Lee, N. Arrowsmith, K. J. Thurecht and S. M. Howdle, *Polymer*, 2011, **52**, 5403-5409.
4. S. Harrisson, X. Liu, J. N. Ollagnier, O. Coutelier, J. D. Marty and M. Destarac, *Polymers*, 2014, **6**, 1437-1488.
5. J. Jennings, M. Beija, A. P. Richez, S. D. Cooper, P. E. Mignot, K. J. Thurecht, K. S. Jack and S. M. Howdle, *Journal of the American Chemical Society*, 2012, **134**, 4772-4781.